
Electronic Thesis and Dissertation Repository

4-21-2017 12:00 AM

Metalation and Structural Properties of apo-Metallothioneins

Gordon W. Irvine

The University of Western Ontario

Supervisor

Martin Stillman


The University of Western Ontario

Graduate Program in Chemistry

A thesis submitted in partial fulfillment of the requirements for the degree in Doctor of Philosophy

© Gordon W. Irvine 2017

Follow this and additional works at: <https://ir.lib.uwo.ca/etd>

 Part of the [Analytical Chemistry Commons](#), [Biochemistry Commons](#), and the [Inorganic Chemistry Commons](#)

Recommended Citation

Irvine, Gordon W., "Metalation and Structural Properties of apo-Metallothioneins" (2017). *Electronic Thesis and Dissertation Repository*. 4527.

<https://ir.lib.uwo.ca/etd/4527>

This Dissertation/Thesis is brought to you for free and open access by Scholarship@Western. It has been accepted for inclusion in Electronic Thesis and Dissertation Repository by an authorized administrator of Scholarship@Western. For more information, please contact wlsadmin@uwo.ca.

Abstract

Metals are required by a quarter of all proteins to achieve their biological function, whether in an active site involved in catalytic chemistry or in a structural capacity. Metals are tightly regulated at the cellular level due to their propensity to cause unwanted side reactions and to be scavenged for use by pathogens. One of the proteins involved in this regulation of metal homeostasis is metallothionein (MT) which is a small, cysteine rich protein primarily involved in the regulation of zinc and copper homeostasis and heavy metal detoxification. MT is unique in its high cysteine content (~30% of the residues), its high capacity for metal binding and its highly dynamic structure in the absence of metals. This fluxionality has made the structure of apo- and partially-metalated MTs difficult to study and as a result, the binding pathway of MT for various metals remains unclear.

This thesis describes the hard-to-characterize structure of apo- and partially-metalated MTs, their binding pathways and potential applications. Using electrospray ionization mass spectrometry (ESI-MS) and covalent labeling, the structure of apo- and partially metalated MTs was probed. Modeling techniques that generate simulated ESI-MS data were used to recreate the covalent labeling spectra and aid in the interpretation of this complicated reaction. These experiments showed that apo-MT adopts a compact, globular conformation that is resistant to initial modification by alkylating reagents. Furthermore, this compact conformation is essential to the fast kinetics of cadmium binding and cluster formation. This cluster formation was found to be pH dependent and this insight was essential in the design of an MT-based biosensor for the detection of As(III) and Hg(II). Altogether, these results reconcile previously conflicting reports about the metal binding mechanisms of MTs, provide evidence of compact conformations of apo-MT and its role in binding kinetics and begin to demonstrate potential application of this fundamental knowledge in the design and testing of an electrochemical, MT-based biosensor.

Keywords

Metallothionein, electrospray ionization mass spectrometry, cysteine modification, covalent labeling, cluster formation, metal-thiolate cluster, cadmium, zinc, arsenic, binding constants, chemical kinetics

Co-Authorship Statement

This thesis contains material from manuscripts published previously. Dr. Martin Stillman is a co-author on all of these papers and was the supervisor of Gordon Irvine. Dr. Swee Ngim Tan supervised Gordon Irvine during a research exchange in Singapore and had a major role in training on the electrochemical equipment and design and testing of the biosensor. Dr. Tan was involved in the preparation of the biosensor manuscript (Chapter 7). Dr. Stillman was involved in all levels of publication including the editing and revising of published papers.

Ms. Kelly Summers is acknowledged for providing MT models in chapter 4 and is listed as a co-author on the published manuscript. Ms. Summers was guided by Dr. Stillman and Gordon Irvine as to the modifications related to the models that were required. Gordon Irvine was responsible for all protein preparation and execution of ESI-MS experiments as well as preparation of figures and writing and editing of the paper.

Dr. Kelly Rigby-Duncan is kindly acknowledged for her contribution to Chapter 6 which included the stopped-flow kinetics experiment, preparation of figures related to that experiment and a preliminary draft with regard to the kinetic section of the published manuscript. Gordon Irvine contributed the covalent modification and modeling data, preparation of those figures and wrote and revised the manuscript. For her contribution, Dr. Rigby-Duncan is listed as a co-author. Ms. Meredith Gullons is also listed as a co-author as she repeated the kinetic experiments and calculated statistics associated with the additional tests.

Ms. Melissa Santolini is gratefully acknowledged for her contribution to Chapter 5 which included the experiments related to the modification of the isolated β -domain of MT-1a with p-benzoquinone and N-ethylmaleimide, measurement of the ESI-MS data and preparation of associated figures. Ms. Santolini was directly supervised by Gordon Irvine from September-December 2015 during her 4th year thesis project. Ms. Santolini appears as a co-author on the published manuscript.

Acknowledgments

I first and foremost thank my supervisor Dr. Martin Stillman for his warm welcome when I came to visit the lab during my 4th year at Brock University and for convincing me to join the lab for what has been a productive, enlightening and fun 5 years in the pursuit of my PhD. I thank him for his close guidance, supervision and support allowing me to attend international conferences to present my work and enjoy great traveling experiences I will never forget.

I'd also like to thank group members past and present but I must mention a few in particular. Special thanks to Dr. Mike Tiedemann for initial training on most of the equipment in the lab and to Dr. Tyler Pinter for his magic touch in the troubleshooting and maintenance of equipment, for additional training, use of his modeling spreadsheet (original thanks to Dr. Duncan Sutherland), helpful discussions and needed distractions for time to time. Thanks to Mr. Evan Walters for his many insightful discussions, his unique perspective and for making the Stillman lab great again. Thanks to Ms. Judith Scheller for subletting my apartment, leaving it better than she found it and for her hard work while executing experiments that led to our publication.

Many thanks to the members of the electronic shop that kept all of the equipment running, regardless of age. Also to the department of Chemistry which has always been generous with their support and has fostered a collegial environment for many wonderful people to come together to do great research.

I'd like to thank Drs. Swee Ngim Tan and Ka Lun Wong for hosting me at NTU-NIE in Singapore first, on a quick visit after a conference and second, on a research exchange. Special thanks also have to be given to my dad, Dr. Kim Irvine, for introducing me to the people in the Chemistry Department at NTU-NIE and for supporting me and my research, especially during my time in South-East Asia.

Lastly, I acknowledge the support of my friends and family. My friends for sharing ride-along experiences and the great meals that served to refresh and recharge during school

breaks. My mom for her immeasurable amount of support and my brother for challenging me to finish my PhD thesis before he finished his Master's degree.

Table of Contents

Abstract.....	i
Co-Authorship Statement.....	iii
Acknowledgments.....	iv
Table of Contents.....	vi
List of Tables.....	xii
List of Figures.....	xiii
List of abbreviations and definitions.....	xvii
Chapter 1.....	1
1 Introduction.....	1
1.1 Metals in biology.....	2
1.2 Cadmium toxicity and MT.....	4
1.3 Arsenic and MT.....	5
1.4 Structural characterization of MT.....	7
1.5 Metalation pathways of MT and structural intermediates.....	9
1.5.1 Cooperative vs. non-cooperative metal binding.....	9
1.6 Methods for structural characterization of MT.....	12
1.6.1 Ultraviolet (UV) absorption spectroscopy.....	12
1.6.2 Circular dichroism spectroscopy.....	13
1.6.3 Emission spectroscopy.....	13
1.7 Mass spectrometry.....	14
1.7.1 ESI-MS for analysis of MT structure and metalation.....	16
1.7.2 Covalent modification coupled with ESI-MS.....	17
1.8 Scope of the thesis.....	20

1.9 References.....	21
Chapter 2.....	29
2 Defining the metal binding pathways of human metallothionein 1a: balancing zinc availability and cadmium exclusion.....	29
2.1 Introduction.....	29
2.2 Methods.....	32
2.2.1 Protein preparation.....	32
2.2.2 ESI-MS and circular dichroism pH titrations	33
2.3 Results.....	35
2.3.1 pH dependence of cadmium binding to apo-MT1a	35
2.3.2 pH dependence of zinc binding to apo-MT1a.....	39
2.4 Discussion	41
2.4.1 pH dependency of cadmium binding	41
2.4.2 pH dependency of the zinc binding pathway	44
2.4.3 The divergent metalation pathway preferences for zinc and cadmium binding	45
2.4.4 The origin of proton sensitivity of the beaded and clustered binding constants.....	49
2.4.5 Understanding the multitude of biological functions of MT1a	49
2.4.6 Importance of pH control during experimental measurements.....	50
2.5 Conclusions.....	51
2.6 References.....	52
Chapter 3.....	59
3 Cadmium binding mechanisms of the isolated domains of human MT1a: non-cooperative terminal sites and cooperative clusters	59
3.1 Introductions	59
3.2 Methods.....	61

3.2.1	Protein preparation.....	61
3.2.2	ESI-MS pH titrations	63
3.2.3	Circular dichroism pH titrations	64
3.3	Results.....	64
3.3.1	The pH dependence of cadmium metalation of the α MT fragment.....	64
3.3.2	pH dependence of the cadmium metalation of the β MT fragment	67
3.3.3	Circular dichroism spectra of the pH titration of partially metalated α and β MT fragments.....	69
3.3.4	pH titration curves of the partially metalated α and β -domains.....	71
3.4	Discussion.....	74
3.4.1	Historical conflict on the binding mechanism of MTs	74
3.4.2	Bridging the gap between apparent discrepancies	76
3.4.3	Isolated domains give insight into the full-length MT binding mechanism	77
3.4.4	Biological context of low pH studies.....	77
3.5	Conclusions.....	78
3.6	References.....	79
Chapter 4.....		83
4	Structural changes of MT1a during the arsenic metalation reaction: folding under typically denaturing conditions	83
4.1	Introduction.....	83
4.2	Methods.....	85
4.2.1	Protein preparation.....	85
4.2.2	Solution preparation and titrations.....	85
4.3	Results.....	86
4.3.1	Metalation of α and β MT with As^{3+}	86

4.3.2	Cysteine modification of As _n -αMT with Bq.....	91
4.3.3	Modeling the As-MT metalation reaction.....	96
4.4	Discussion.....	97
4.5	Conclusions.....	99
4.6	References.....	100
Chapter 5.....		102
5	Selective cysteine modification of metal-free human metallothionein 1a and its isolated domain fragments: Solution structural properties revealed via ESI-MS.....	102
5.1	Introduction.....	102
5.2	Methods.....	104
5.2.1	Protein preparation.....	104
5.2.2	ESI-mass spectra collection.....	106
5.2.3	Molecular models.....	106
5.3	Results.....	106
5.3.1	Modification of the isolated α- and β-domain fragments of metallothionein.....	106
5.3.2	Modification of the full-length protein (βαMT).....	113
5.4	Discussion.....	117
5.5	Conclusion.....	125
5.6	References.....	125
Chapter 6.....		129
6	Metalation kinetics of the human α-metallothionein 1a Fragment is dependent on the fluxional structure of the apo-protein.....	129
6.1	Introduction.....	129
6.2	Methods.....	133
6.2.1	Metallothionein preparation.....	133

6.2.2	ESI-MS of proteins with modified cysteines	134
6.2.3	ESI-MS data analysis and reaction modeling	134
6.2.4	Molecular modeling of apo- α MT and cysteine modifications.....	134
6.2.5	Kinetic measurements of cadmium binding to α MT	135
6.3	Results.....	136
6.3.1	Metallothionein cysteine modification using p-benzoquinone (Bq).....	136
6.3.2	Determination of relative rate constants	138
6.3.3	Comparison of the k_n Values Used in Generating the Model Reaction Profile.....	142
6.3.4	Molecular dynamics models	143
6.3.5	Cadmium metalation kinetics of α MT in the presence of a chemical denaturant.....	144
6.4	Discussion	149
6.4.1	Metalation of the α -domain with Cd^{2+} : Testing the Two Conformational Classes	152
6.5	Conclusions.....	154
6.6	References.....	155
Chapter 7.....		160
7	A Simple Metallothionein-Based Biosensor for Enhanced Detection of Arsenic and Mercury	160
7.1	Introduction.....	160
7.2	Methods.....	161
7.2.1	Reagents and instrumentation	161
7.2.2	Recombinant protein preparation.....	162
7.2.3	Disc preparation and electrochemical measurements	163
7.3	Results.....	163
7.3.1	Biosensor preparation	163

7.3.2	Arsenic detection using anodic stripping voltammetry (ASV).....	166
7.3.3	Mercury detection using ASV	168
7.4	Discussion.....	171
7.4.1	MT biosensors.....	171
7.5	Conclusions.....	173
7.6	References.....	173
Chapter 8	176
8	Conclusion	176
8.1	Metal binding mechanisms of MT.....	176
8.1.1	A non-cooperative mechanism?.....	177
8.2	Cysteine alkylation.....	179
8.3	Importance of the structure of apo-MT.....	180
8.4	Insight into potential metal sensing applications	182
8.5	Biological relevance of MT structure and metalation.....	183
8.6	Final word.....	184
8.7	References.....	185
Curriculum Vitae	188

List of Tables

Table 3-1: Summary of results from selected groups using a variety of methods and pH conditions to study the M(II) metalation mechanism of metallothioneins	75
Table 5-1: Summary of reaction profiles following reaction of three cysteine modifiers with the full protein and the two isolated fragments under native and denaturing conditions	124
Table 7-1: Summary of MT incorporated biosensors	172

List of Figures

Figure 1-1: Representation of the ``dumbbell`` structure of MT	2
Figure 1-2: Clustal Omega sequence alignment of the major human metallothionein isoforms with conserved amino acids highlighted in black.	7
Figure 1-3: ESI-mass spectral data for the metalation of apo- β MT 1a with Zn^{2+}	11
Figure 1-4: Schematic of an electrospray ionization mass spectrometer.....	15
Figure 1-5: Possible reaction profiles of a cysteine alkylating reagent with a peptide containing 9 reaction sites.....	19
Figure 2-1: Cartoon ribbon representation of proposed MT1a metalation intermediates	Error! Bookmark not defined.
Figure 2-2: Representative ESI-MS data showing the relative abundances of Cd_xMT species ($x=0-4$) as a function of pH	36
Figure 2-3: Circular dichroism spectra of apoMT1a with 2.5 mol. eq. of Cd(II) added as a function of increasing pH.....	37
Figure 2-4: Change in cadmium binding pathway as a function of pH	38
Figure 2-5: Representative ESI-MS spectra recorded during the pH titration of Zn_xMT ($x=0-5$) after approximately 2.5 equivalents of Zn(II) had been added.....	40
Figure 2-6: Simulated (hatched) and experimental (solid) ESI-MS data for binding of 2.5 mol. equivalent of Cd(II) to apo-MT1a at pH 5.0. (A), 6.7 (B) and 7.9(C).....	43
Figure 2-7: Simulated (hatched) and experimental (solid) ESI-MS data for MT metalation with 2.5 mol. equivalents of Zn(II) at pH 4.5 (A) and 7.4 (B).	45
Figure 2-8: Representation of two possible pathways for MT1a metalation with Zn(II) or Cd(II).....	47

Figure 2-9: Change in Zn(II) metalation pathway as a function of pH (grey line) compared to Cd (orange line).	48
Figure 3-1: Representative deconvoluted ESI-mass spectra showing the trend in speciation as a function of pH for 4 steps in the Cd(II) metalation of apo- α MT.....	66
Figure 3-2: Representative deconvoluted ESI-MS spectra of the metalation of apo- β MT with Cd(II) at various stages in the titration	68
Figure 3-3: Circular dichroism spectra of Cd _{1.5} - α MT at pH 5.2-7.8	69
Figure 3-4: : Circular dichroism spectra of Cd _{1.5} β MT at various pH values.....	70
Figure 3-5: The pH dependence of the binding mechanism of the α MT fragment.	72
Figure 3-6: The pH dependence of the binding mechanism of the β MT fragment.	73
Figure 4-1: ESI mass spectra of α MT1a with increasing As ³⁺ loading and cysteine modifications to form As _n - α MT (n = 1-3).....	88
Figure 4-2: ESI mass spectra of β MT1a showing As ³⁺ binding and cysteine modification with Bq to form As _n - β MT (n=1-2) using Bq.	90
Figure 4-3: Deconvoluted ESI-MS data showing the binding of As ³⁺ to apo- α MT and the subsequent titration of the protein solution with Bq.....	91
Figure 4-4: Deconvoluted ESI-MS data showing the 27 individual species of intermediate and fully modified MT (A)	93
Figure 4-5: Scigress models (MM3/MMD) of the structure of Apo- α MT (A), As ₁ - α MT (B), As ₂ - α MT(C) and As ₃ - α MT (D) using space filling models to visualize the extent of folding in each species	96
Figure 5-1: Representative deconvoluted ESI-MS spectra from the modification of the β -domain fragment of MT1a with p-benzoquinone (Bq).....	107

Figure 5-2: Representative deconvoluted ESI-MS spectra from the stepwise modification of the β MT fragment by NEM.....	108
Figure 5-3: Representative ESI-MS charge state manifolds measured during cysteine modification of $\beta\alpha$ MT1a and its isolated fragments.....	110
Figure 5-4: Representative deconvoluted ESI-MS spectra of the modification of α MT fragment with NEM.....	112
Figure 5-5: Deconvoluted mass spectra of NEM modifications of $\beta\alpha$ MT under native (pH 7.4, right) and denaturing (pH 2.8, left) conditions.....	114
Figure 5-6: Deconvoluted mass spectra of the $\beta\alpha$ MT modification with IAM under denaturing conditions at pH 3.0 (A) and native conditions at pH 7.4 (B).....	116
Figure 5-7: Comparison of the reaction profiles shown by the relative abundances of each modified $\beta\alpha$ MT-species at approximately the half way point, for the three cysteine modifiers used.....	119
Figure 5-8: Molecular dynamics simulated structures of apoMT under native conditions.....	120
Figure 5-9: Extracted ESI-MS reaction profiles for all three cysteine modifiers used...	122
Figure 6-1: The structure of the α -fragment of hMT1a.....	132
Figure 6-2: ESI mass spectral data recorded for the stepwise modification of the 11 Cys in apo- α MT1a with para-benzoquinone (Bq).....	137
Figure 6-3: Simulations of the protein speciation when 11 mol eq Bq react over time with apo- α MT at (A) pH 2.8 and (B) pH 6.7.....	140
Figure 6-4: Comparison between the experimental data (black) and the simulated model data (red) for stepwise modification of apo- α -MT by Bq at low pH (Left) and neutral pH (Right).....	141

Figure 6-5: Normalized relative rate constants (k_n) for each of the 11 cysteine modification reactions at each pH (2.8 and 6.7)	142
Figure 6-6: Molecular dynamics (MM3/MD) calculated structures at the energy minima for each of the key structures.	144
Figure 6-7: Circular dichroism spectra of Cd ₄ α-MT in 10mM ammonium formate (black lines).....	146
Figure 6-8: Time dependence of the metalation reaction of apo- αMT with Cd ²⁺ as a function of an increasing concentration of GdmCl.....	148
Figure 6-9: The observed rate constant (k_{obs}) for the metalation of apo- α-MT with Cd ²⁺ as a function of GdmCl concentration.	149
Figure 7-1: Far UV spectra of metallothionein (MT) used to monitor oxidation of thiols.	164
Figure 7-2: Influence of paper disc MT-loading on the peak heights of the SH(Cys) responses at +0.22 V in the electrochemical scans.	165
Figure 7-4: Typical ASV scans using blank paper discs on screen-printed carbon electrodes (SPCEs) with 25 μL of arsenic solutions of varying concentration added.	167
Figure 7-5: Representative ASV scans of MT-adsorbed paper discs with 25 μL droplets of varying arsenic concentrations added.....	168
Figure 7-6: Representative ASV scans of blank paper discs on SPCEs with 25 μL aliquots of Hg ²⁺ solutions of concentrations 20, 50 and 200 ppb.....	169
Figure 7-7: Representative ASV scans for MT-loaded discs with 25 μL drops of diluted Hg ²⁺ standards with concentrations of 20, 50 and 200 ppb.	170
Figure 8-1: Potential metalation pathways and subsequent deconvoluted mass spectra.	178

Figure 8-2: Cysteine alkylating reagent accessibility to the compact and open conformers of apo-MT	180
Figure 8-3: Schematic of the MT-biosensor preparation	183

List of abbreviations and definitions

α -MT	α domain of human metallothionein isoform 1a
β -MT	β domain of human metallothionein isoform 1a
$\beta\alpha$ -MT	Full-length human metallothionein isoform 1a
apo-MT	Metal-free metallothionein
CD	Circular dichorism
CRM	Charged residue model
DNA	Deoxyribonucleic acid
ϵ	Molar absorptivity or molar extinction coefficient
<i>E. coli</i>	Escherichia coli
ESI	Electrospray ionization
IPTG	Isopropyl- β -D-thiogalactoside
K_n	Relative binding constant
LMCT	Ligand-to-metal charge transfer
m/z	Mass-to-charge ratio
MD	Molecular dynamics

MM	Molecular modeling
MM3/MD	Molecular dynamics with energy minimization by molecular mechanics with Allinger's MM3 force field
MS	Mass spectrometry
MT	Metallothionein
MT1a	Metallothionein isoform 1a
MT2a	Metallothionein isoform 2a
NMR	Nuclear magnetic resonance
pET	Plasmid for expression by T7 RNA polymerase
TOF	Time of flight
Tris	tris(hydroxymethyl)aminomethane buffer

Chapter 1

1 Introduction

Metallothioneins (MTs) are a ubiquitous family of small, cysteine-rich proteins that are primarily involved with metal homeostasis, heavy metal detoxification and cellular redox chemistry.¹⁻⁴ Metal saturated mammalian MTs consist of two metal binding domains, the C-terminus α -domain which contains 11 cysteine residues and the N-terminus β -domain which contains 9 cysteines.⁵ These MTs bind up to seven divalent metals, for a maximum of 4 in α - and 3 in the β -domain to form a dumbbell shape (Figure 1-1) under saturative conditions.⁶ The stoichiometries and coordination geometry of divalent metals such as zinc and cadmium are well defined and have been studied for many years.^{5, 7-10} However, there still remains controversy over the specific binding mechanisms for these two metals.¹¹⁻¹³ MTs are also known to promiscuously bind soft metals and metalloids such as: Uranium¹⁴, arsenic¹⁵, mercury¹⁶, copper¹⁷ and lead.¹⁸ This promiscuity is facilitated by the lack of rigid, formal structure in the peptide backbone, keeping it flexible to accommodate metals and metalloids of different sizes and preferred coordination geometries.¹⁹

MTs generally lack formal secondary structural elements, especially in the absence of metals.¹⁶ They also lack aromatic amino acids which limits the usefulness of optical methods in the purification and isolation procedure and to probe structural changes. This property along with the propensity for the reduced cysteine residues to oxidize forming intra-protein covalent linkages, make MTs difficult to work with.

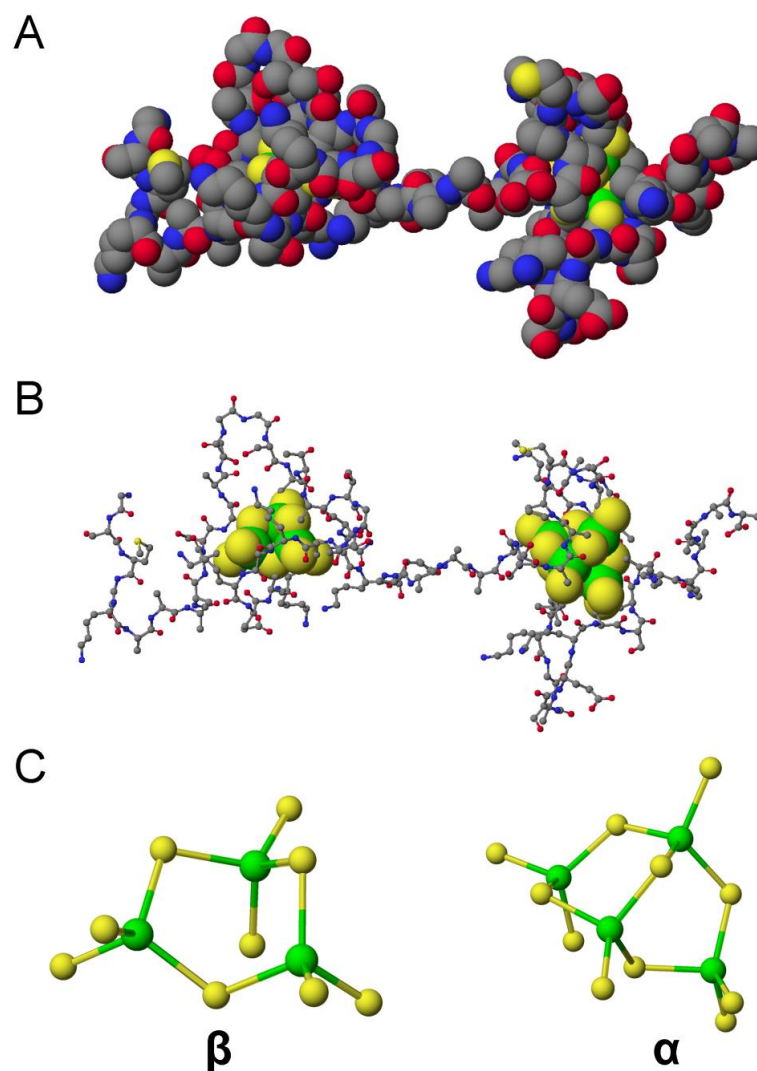


Figure 1-1: Representation of the ``dumbbell`` structure of MT. (A) Space-filling diagram of Cd₇-MT. (B) Ball-and-stick diagram of the fully metalation protein. (C) Ball-and-stick diagram of the isolated metal-thiolate clusters of each domain of MT. Reproduced using data from Chan et al., 2007.²⁰

1.1 Metals in biology

A number of transition metals are required to catalyze the reactions required for life. Nature has selected naturally abundant metals like zinc, copper and iron for their unique abilities to perform redox chemistry, transfer electrons and switch back and forth between oxidation states.²¹⁻²² Redox inactive metals like zinc act more frequently as Lewis acids

that promote reactivity of a substrate²³⁻²⁴ or act in a structural role to stabilize inter-molecular interactions as in the case of zinc-finger proteins.²⁵ While essential for many cellular processes, metals also must be strictly controlled and regulated, shuttling electrons and changing oxidation states is not without consequences and potential unwanted side reactions can occur causing damage to cellular machinery.²⁶⁻²⁷ In addition, pathogens also require metals for their survival and must scavenge them from the host.²⁸ As a result, an evolutionary arms race has ensued to develop ever more effective metal capturing agents for pathogens while being countered by ever more strictly controlled cellular and intra-cellular metal concentrations by the host.²⁹⁻³¹

The strict control of metals in biological environments is achieved through binding affinity gradients that shuttle metal ions from extra to intracellular spaces and from intracellular chaperones to the active sites of metalloenzymes.³² The highest binding affinities for various metals are usually found in structural enzymes that utilize those metals to stabilize a shape to perform a specific function.³³⁻³⁴ Cells must also transport metal ions across the hydrophobic cellular membrane, which requires metal transporter proteins.³⁵ These proteins often contain large stretches of hydrophobic residues to anchor themselves within the lipid bilayer and provide small electrostatic channels specific for certain ions based mostly on size and charge restrictions.³⁶ Thus, during all stages of transport the freedom of movement of metal ions is restricted so that side reactions and potential thefts by pathogens are minimized.

MTs are one of the families of chaperones responsible for this strict control of free metal concentrations, mainly of copper and zinc.^{1,37} Their high capacity for binding these metals allows them to act as a buffer, releasing zinc or copper in times of scarcity and binding excess ions in times of over-abundance. This is the essence of homeostatic control. MTs do not carry out any catalytic function themselves involving metals, although reactions related to the redox state of the cell may be facilitated by the many cysteinyl thiols of MT.³⁸ Instead, MTs ensure a near constant supply of metals to proteins that interact with DNA and catalyze essential reactions, while keeping concentrations of free zinc or copper to a minimum. Free copper, in particular, can be damaging to cells because of the Fenton and Haber-Weiss reactions it can catalyze.²⁶

Interactions of MTs and other metalloproteins have been investigated *in vitro* in order to understand the mechanisms and kinetics involved in biological metal transfer.³⁹ These studies have shown potentially dangerous interactions, including the substitution of cadmium for zinc in carbonic anhydrase, facilitated by Cd-MT.⁴⁰⁻⁴¹ Metal swapping between MTs has also been demonstrated, highlighting the lability required for proper MT function *in vivo*.⁴²

Many metals that are considered toxic derive their toxicity from the substitution of an essential metal, like zinc, with a toxic metal, like cadmium, altering or inhibiting the function of the metalloprotein.^{41, 43} The substitution is possible due to the electronic similarities between the two metals, but size and reactivity differences render the substituted metalloprotein useless.⁴⁴ Two toxic metals we are particularly interested in with relation to MT are cadmium and arsenic.

1.2 Cadmium toxicity and MT

Since its discovery by Margoshes and Vallee while investigating cadmium-bound proteins in horse liver, MT has been known to bind strongly to this toxic metal.⁴⁵ Like many biological processes, the role MT plays in the detoxification of cadmium is complicated.^{3, 46-48} Cadmium toxicity mainly targets the kidneys where significant amounts of MTs are expressed concomitantly.⁴⁸ The first evidence of the detoxifying role of MT came from studies where MT was isolated from human kidney, having both Cd(II) and Hg(II) bound.⁴⁹ The binding affinity for these toxic metals is orders of magnitude higher than that of Zn(II), (zinc binding range K_a 10^{11-12} , cadmium K_a 10^{15-16}) so native Zn-MT is displaced when these metals are present.⁵⁰ MT knockout mice, while not immediately fatal, show greater sensitivity to toxic metal exposure.⁵¹

Occupational exposure to cadmium is the most common source of cadmium poisoning⁵²⁻⁵³, although environmental contamination has historically been a problem as well leading to itai-itai disease in people eating foods grown in cadmium contaminated irrigation water or drinking that contaminated water directly.⁵⁴ This is exemplified in the Jinzu river basin in Japan where industrial contamination led to the poisoning of local inhabitants, the name of the disease “itai-itai” deriving from the expression for pain in Japanese.⁵⁵

This was the first officially recognized case of environmental induced disease in Japan and serves as a warning for industrially developing regions.

1.3 Arsenic and MT

Arsenic is a toxic metalloid known since ancient times as a potent poison and used historically as a pest control agent, whether those pests are rats⁵⁶ or political enemies of Pope Alexander VI or Napoleon Bonaparte.⁵⁷ Today, these sinister uses are much less prevalent and the main concern around arsenic poisoning involves naturally contaminated well-water in poor, rural areas lacking access to centralized water treatment facilities.⁵⁸⁻⁵⁹ In areas such as South and South-East Asia, much of the surface water is highly contaminated with bacteria and is acutely infectious.⁶⁰ In the late 1980s and early 90s, many NGOs began building wells to alleviate the problem of waterborne diseases.⁶¹ The drilling of these wells exposed arsenic-containing rock to oxygen when the well was depleted, solubilizing the arsenic and contaminating the well water.⁶² While levels even at the most contaminated wells do not approach those that could cause acute effects, the long term exposure to arsenic concentrations above 10-20 ppb has serious consequences.⁶³ Arsenicosis is characterized by skin lesions, cancers and multi-system disease that currently lacks effective treatment options.⁶⁴

Drinking water is the main source of hazardous exposure to arsenic, although an increasing amount of evidence points to contaminated irrigation water and uptake by rice crops as another potential exposure route.⁶⁵ Arsenic is thought to interfere with proper DNA methylation through its interaction with S-adenosylmethionine (SAM).⁶⁶ SAM is the source of the methyl group which attaches to DNA via enzymatic coupling by DNA methyltransferase and which detoxifies arsenicals to mono-, di- and tri-methyl arsenic.⁶⁷⁻⁶⁸ DNA methylation controls transcription and either hypo- or hyper-methylation can alter transcription patterns and rates, leading to cancer.⁶⁹ Arsenic also acts as a phosphorous mimic, as they are in the same group in the periodic table sharing many chemical properties.⁷⁰ Arsenic may take the place of phosphorous in ATP molecules, the DNA backbone or even in bone structure.⁷¹ This replacement of long-lived structures in biological systems may contribute to the many effects of chronic arsenic poisoning. In

acute poisoning, replacement of phosphate in ATP and inhibition of proteins essential for energy metabolism essential starves the cell of energy causing death.⁷²⁻⁷³

Arsenical binding to MTs has been studied since the early 2000s,^{15, 74} with seminal work in the determination of kinetic parameters using ESI-MS due to the slow reaction rate of MT with As(III).³⁹ Toxicological studies have shown upregulation of MT genes in response to acute arsenic exposure, indicating *in vivo* interaction with at least the metal responsive elements that regulate MT expression.⁷⁵⁻⁷⁶ Questions remain about the extent to which MTs play a role in defense against arsenicals *in vivo* as isolation of As-MT from biological samples remains elusive.⁷⁷ Despite lack of clear evidence for As-MT formation in biological samples, the interactions *in vitro* have allowed us to gain more understanding of the metal binding pathways of MT, structural determinants and have produced unique binding modes under unusual conditions where MT does not typically coordinate metals.

Arsenical binding to MT is curious in that it binds strongly, albeit slowly, at very low pH, less than 3.0, where most metals do not bind as they are out-competed for thiolates by the wealth of H⁺ ions.⁷⁴ Only Cu(I) and Ag(I) can be able to bind at such a low pH, as Cd- and Zn-MTs demetalate starting at pH 5.0.⁷⁸ This is advantageous for manipulation *in vitro* due to the protective effect of low pH on the inadvertent oxidation of MT thiols during experimental procedures. Low pH also facilitates the complete dissolution of As₂O₃ used for the experiments, and As(OH)₃ tends to precipitate out of solution at physiological pH, confounding stoichiometric calculations.⁴²

The slow binding of As³⁺ to MT requires a long equilibration time for steady-state studies, however this sluggish binding allowed the determination of specific constants from ESI-MS relative abundance data that was both time and temperature resolved. The detailed investigations of Ngu and coworkers revealed important kinetic properties of the MT-1a isoform and its isolated domain fragments.³⁹ The kinetic data show a “kink” in the reaction rate, where the first rate constant is lower than second, followed by a linear decrease in the subsequent rate constants. This phenomenon was observed in the isolated α -domain as well but was absent in the β -domain. These investigations also showed that

transfer of As(III) between MT peptides could not be a dissociative mechanism since at physiological pH stoichiometric transfer would not occur due to precipitation of arsenic species once dissociated from the protein.⁴² These studies were among the first to demonstrate reliably that kinetic parameters can be resolved via ESI-MS. The strengths and limitation of this method will be discussed further in section 1.6.4.

1.4 Structural characterization of MT

The MT family consists of many isoforms and sub-isoforms that can vary in sequence but generally all share Cys-Cys, Cys-X-Cys and Cys-X-X-Cys motifs.⁷⁹ For the purpose of this thesis the discussion will be limited to more generally mammalian MTs and more specifically human isoforms. In humans there are four major MT isoforms: MT-1 which is constitutively expressed, MT-2 which is also constitutively expressed, MT-3 which is expressed in cells of the nervous system including brain cells, and MT-4 which is expressed mainly in epithelial cells.⁸⁰ While differences in sequence of the isoforms exist (Figure 1-2), only minor differences in binding properties occur and MT-1 and MT-2 have been considered to behave in near identical fashion.⁸¹

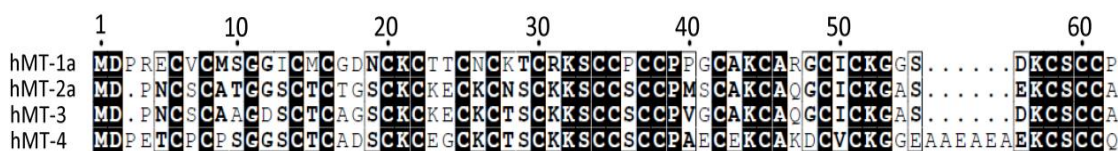


Figure 1-2: Clustal Omega sequence alignment of the major human metallothionein isoforms with conserved amino acids highlighted in black. Generated with ESPript 3.0.

Mammalian MTs consist of 60-70 residues, 20 of them being cysteine which facilitate the coordination of up to seven divalent metals, and twenty monovalent metals such as Cu(I).⁸² The N-terminal β -domain contains 9 cysteine residues that can accommodate up to 3 divalent metals, the C-terminal α -domain contains 11 cysteine residues that can coordinate up to 4 divalent metals.⁸³ In conditions where there is a vast excess of cadmium, these isolated domain fragments and the full-length protein have been shown to super-metalate and coordinate an extra Cd(II) ion.⁸⁴⁻⁸⁵ The β -domain M_3S_9 cluster forms a six member ring like structure of alternating metal (M)-sulfur (S) bonds where all

the sulfurs in the ring are bridging ligands. The remaining coordination sites on the metal are filled by terminal cysteinyl sulfurs. The α -domain forms an adamantane like structure, an M_4S_{11} cluster, with 5 bridging and 6 terminal sulfurs. Taken together, the full protein forms a “dumbbell” shaped structure when both clusters are formed.⁸ The differences in Cys:metal ratios of these domains are thought to give rise to domain specificity observed in some MTs.

While a countless number of MTs exist due to their ubiquitous nature and variety of metal available for coordination, only two x-ray structures have been solved to date. MTs are notoriously difficult to crystallize due to their small size and inherent fluxionality. This high fluxionality has also precluded NMR analysis of many partially metalated species with the possible exception of cooperatively formed Cd_4 -clusters in the α -domain, but these are not complete structures of the full protein.⁸⁶ Full metalation of MT tends to limit the conformational freedom which the peptide can explore, allowing a limited number of fully-metalated structures to be solved by X-ray and NMR analysis.^{7, 83, 86} These structures were determined for divalent species, the only monovalent solved structure being the Cu_8 -MT species from yeast.⁸⁷ The structure of yeast MT is very different from mammalian MTs, and ESI-MS, CD spectroscopy and emission studies have suggested that the Cu_8 -cluster is not formed in mammalian MTs.⁸⁸⁻⁹¹ No X-ray diffraction or NMR structures exist for metal-free MT.

The absence of metals in apo-MT eliminates the ability of researchers to use metal-based probes of its structure and greatly complicates structural determination. Techniques like molecular dynamics (MD) simulations⁹²⁻⁹³ and fluorescence resonance energy transfer (FRET) have indicated that apo-MT exists as a random coil structure with no well-defined secondary structural elements like alpha helices or beta sheets.⁹⁴⁻⁹⁵ The lack of intrinsic optical probes in the peptide adds further complication to studies of apo-MT. Recently, ion-mobility mass spectrometry (IM-MS) has been used to investigate the conformation of apo-MT in the gas phase.⁹⁶ These results show apo-MT adopts both compact and extended conformers depending on the charge state and the variety of conformations converges as metalation occurs.⁹⁶⁻⁹⁷ As the starting point in the metalation

pathway(s) of MT, the determination of apo-MT structure is important in order to fully understand the complicated metalation mechanism.

1.5 Metalation pathways of MT and structural intermediates

To form a metal saturated MT, apo-MT passes through many intermediate metalation states, each adopting distinct structure to facilitate the coordination of an additional metal. Since metal saturation of MTs is unlikely given normal cellular metal concentrations and competition for metals from the binding sites of other metallochaperones and enzymes, these metalation intermediates are among the most biologically relevant MT species.⁹⁸

The flexibility of the peptide backbone allows it to adopt many possible coordination geometries and structures of many metalation intermediates remain ambiguous. For example, Zn₄-MT could exist as a Zn₄S₁₁ cluster in the α -domain or 4 separate ZnS₄ coordinated metal structures spread throughout the protein. Zinc being spectroscopically silent, makes further structural investigation difficult. The proposed ZnS₄ structures are termed “beads” as they would be spread across the protein causing local wrapping of the peptide backbone to orient the cysteine residues in a way amenable for tetrahedral coordination.⁹⁹

There has been significant controversy over the mechanism of metal binding and as a result, the pathway which apo-MT takes to form the fully metalated species. Significant evidence exists for both cooperative and anti- or non-cooperative metal binding.^{11-12, 91, 99-100} In addition to the slight differences in pathway preference between MT isoforms, the identity of the metal being bound also has a substantial effect. Even electronically similar metals like Zn(II) and Cd(II) have radically different pathway preferences as will be demonstrated in Chapter 2 of this thesis.

1.5.1 Cooperative vs. non-cooperative metal binding

When describing the binding properties of proteins and other ligands with multiple binding sites the terms “cooperative” and “non-cooperative” are often used but not

frequently defined. A cooperative binding mechanism is one where there is an effector, a conformation change, for example, which promotes subsequent binding events after the first substrate has bound.¹⁰¹ The manifestations of a cooperative mechanism include an increasing set of equilibrium binding constants and physical presence of mainly the apo-ligand and the saturated ligand simultaneously with little contribution from any intermediate species.¹⁰² A non-cooperative mechanism can be thought of as the “default” mechanism where no effector is present and each subsequent binding after the first is less favoured due to statistical loss of binding sites as the reaction proceeds. This manifests as a series of sequentially decreasing equilibrium constants, significant presence of intermediate species and often the final substrate being bound less tightly to the ligand.¹⁰²

For MTs both types of binding have been observed. Calculations that involved fine-tuning equilibrium constants to simulate mass spectra have shown that these alone can determine the type of reaction mechanism and can be compared with experimental evidence, as seen in Figure 1-3.¹⁰² Experimentally, ESI-MS is the most reliable method for determining binding mechanisms for MTs because of the lack of unique optical signatures for each intermediately metalated species. All species in solution are observed via ESI-MS, whereas in optical spectroscopy an average signal of all species in solution is observed. Metal titrations of apo-MT monitored solely by optical methods result in a steadily increasing peak for the optical spectra with little information about the distribution of species in solution.

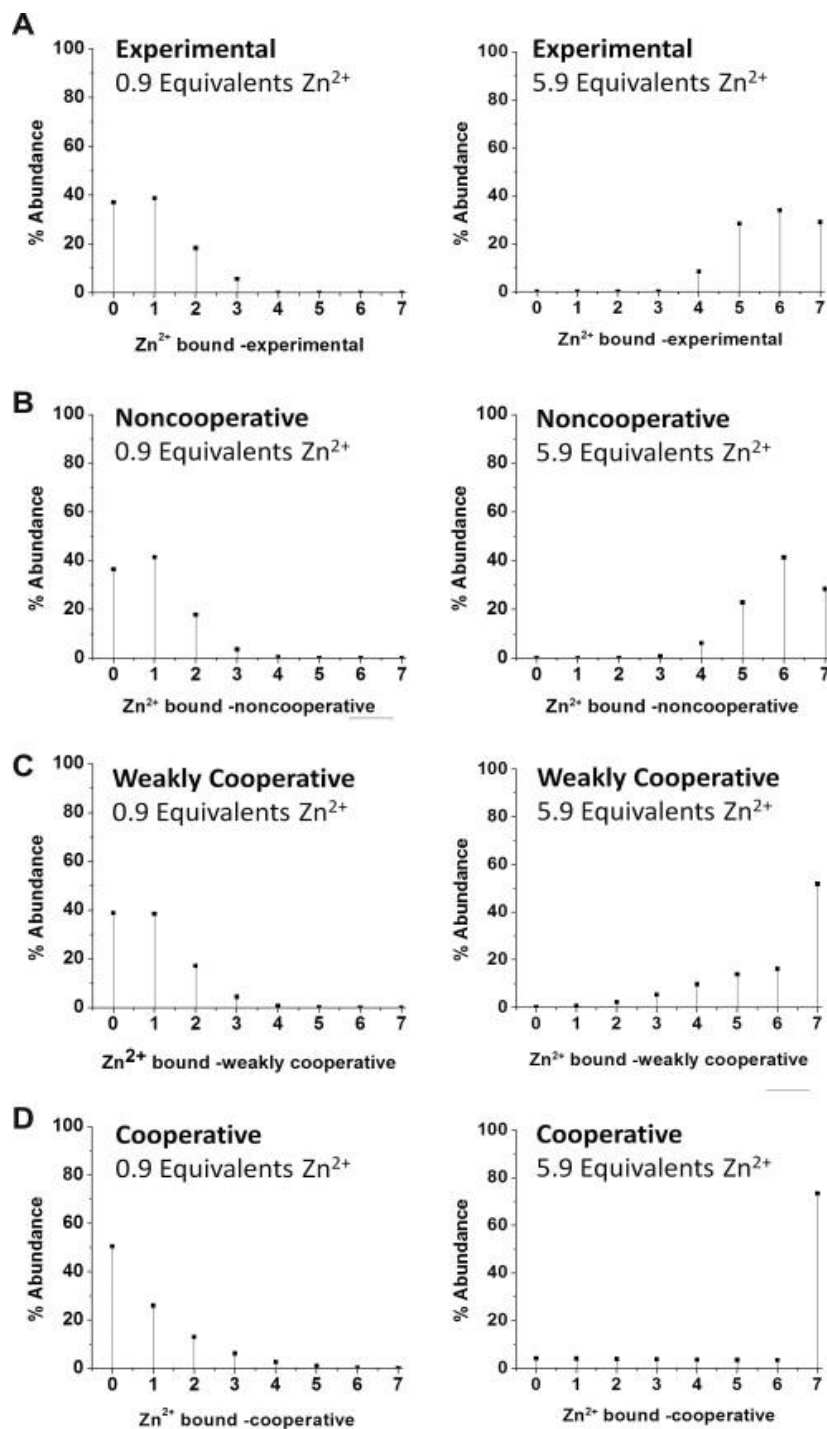


Figure 1-3: ESI-mass spectral data for the metalation of apo- $\beta\alpha$ MT 1a with Zn^{2+} . (A) Experimental ESI-mass spectral data for $\beta\alpha$ MT 1a at the 0.9 and 5.9 equivalents-added steps of the Zn^{2+} metalation reaction. (B) Simulated ESI-mass spectral data based upon a noncooperative mechanism (C) Simulated ESI-mass spectral data based upon a weakly cooperative mechanism. (D) Simulated ESI-mass spectral data based upon a cooperative mechanism. Reproduced with permission from Sutherland et al., 2012.¹⁰²

Results from ESI-MS show that both types of binding are possible and that a mixed mechanism is also possible where certain intermediate species are more abundant than others and clusters still form with a slight preference.³⁴

1.6 Methods for structural characterization of MT

Due to its unique properties, a number of methods are required for proper investigations of MT, each with their own specific strengths and weaknesses. Relying on one method alone gives a limited picture of the complicated processes of metal binding, protein folding and protein-protein interaction that occurs for MTs. The most commonly used techniques to study MTs are: ultraviolet (UV) and X-ray absorption, circular dichroism (CD) spectroscopy, electrospray ionization mass spectrometry (ESI-MS) and nuclear magnetic resonance ($^{111/113}\text{Cd}$ and ^1H NMR). The strengths and limitations of these methods will be discussed in this section with emphasis on those used in this thesis.

1.6.1 Ultraviolet (UV) absorption spectroscopy

Ultraviolet spectroscopy is useful for quick characterization of characteristic ligand-to-metal charge transfer (LMCT) bands for metals such as cadmium and copper in MT. Only the far UV-region contains relevant absorption bands. For zinc binding to MT, the LMCT band overlaps with the absorption from the protein backbone and is not particularly useful for analysis. The 250 nm cysteine-cadmium charge transfer band is frequently used to confirm molar equivalents of metal bound to MTs and also for MT concentration determination using the molar absorptivity constant. The use of this technique primarily occurs during the preparation and purification of recombinant MTs due to the speed and simplicity needed for detecting molecules following chromatographic separation. In addition to its use in purification protocols, absorption spectroscopy is useful in monitoring the fast kinetics of a reaction where measurements must be taken on the order of milliseconds. Other techniques cannot achieve this type of speed.

However, absorption spectroscopy suffers from lack of specific information; only the average metal loading in solution can be probed. MT also lacks aromatic amino acids that typically absorb around the 280 nm region and are frequently used to determine the

presence and concentration of proteins. This renders absorption spectroscopy less useful than for other proteins. As mentioned previously, if optical absorptions overlap there is no way to distinguish between the two using absorption spectroscopy alone. While often considered a crude analytical method, this method finds a niche in providing cheap, quick, easy and non-specific information in situations where time is important and extreme detail is not required.

1.6.2 Circular dichroism spectroscopy

Circular dichroism spectroscopy is a technique often used to probe secondary structural elements of proteins due to their natural chirality. Given the lack of these features in MTs, this is not the primary tool for the measurement of folding but rather to probe the chirality of the environment surrounding metal centers. Like UV absorption, CD spectroscopy has fast time resolution so it is able to monitor events that happen on the ms time scale, like the folding of more typical peptides to form alpha helices and beta sheets.

The basis of CD spectroscopy is the measurement of differences between the absorption of left and right-handed circularly polarized light. Optically active molecules absorb one of the two types of polarized light and a difference spectra is generated. Amino acids, with the exceptions of glycine and proline, are naturally chiral and have a CD signal in the UV region that is sensitive to shifts in the conformation of the protein. The folding of these chiral residues into secondary structural elements gives signature spectral features that can be identified as α -helices, β -sheets or random coils typically in the far UV region, 190-220 nm. In this region, apo-MTs give a strongly negative difference spectra, indicative of random coil structure.

1.6.3 Emission spectroscopy

For emissive MT species, such as Cu(I) MTs, emission spectroscopy can be used to determine and quantify species present in solution. It is known that Cu-thiolate clusters that are exposed to the solvent have reduced emission intensity compared to a counterpart buried within the interior of the protein. Therefore, by measuring the intensity of emission bands, the structure of the Cu-MTs can be determined. Like other optical techniques, emission spectroscopy gives an average of all species in solution, so it is

difficult to assign spectra to specific species when multiple species are present. ESI-MS can confirm the presence of multiple species in solution.

1.7 Mass spectrometry

Mass spectrometry (MS) is a technique that relies on the ionization of chemical entities and subsequent sorting of ions based on their mass-to-charge ratio. Many methods exist for ionization of molecules for analysis by MS, many of which are harsh and cause fragmentation of the analyte in the process of ionization. This is useful in structural determination of small, organic molecules but not for analysis of larger bio-molecules such as proteins when extensive fragmentation occurs. Less harsh fragmentation techniques, however, have proven to be useful in the field of proteomics and structural biology.

Electrospray is a soft ionization technique that is especially well suited for the study of metalation of metallothioneins. A schematic diagram of a typical ESI mass spectrometer is shown in Figure 1-4A. All mass spectrometers contain a sample inlet source that converts analytes into ions in the gas phase (a). The ions are then focused with ion optics and directed into the mass spectrometer (b). Then they are detected by the ion detector (c) and with an analyzer displaying the counts and masses of the detected ions.

The mechanism of ion formation in electrospray is still being investigated. From what we know, a sample solution that is infused through a charged capillary exits as a fine mist of tiny, charged droplets. These droplets quickly evaporate increasing the charge density until the Rayleigh limit is reached where the electrostatic repulsion overcomes the surface tension of the droplet and fission occurs. This process continues until only the gas phase analyte remains, and is known as the charged residue model (CRM). The specific mechanism of this process depends on the nature of the analyte.

In the CRM (Figure 1-4B) a distribution of charges per analyte molecule is possible and is dependent on solution composition, instrumental conditions and the size of the analyte. This results in the formation of a number of "charge states" which have different numbers of adducted protons which form $[M + nH]^{n+}$ species. These proton adducts form more

readily with unfolded proteins, due to increased surface area and exposure of protonatable sites. This phenomenon results in useful information about conformational preferences and folded states to be gained by charge state analysis.

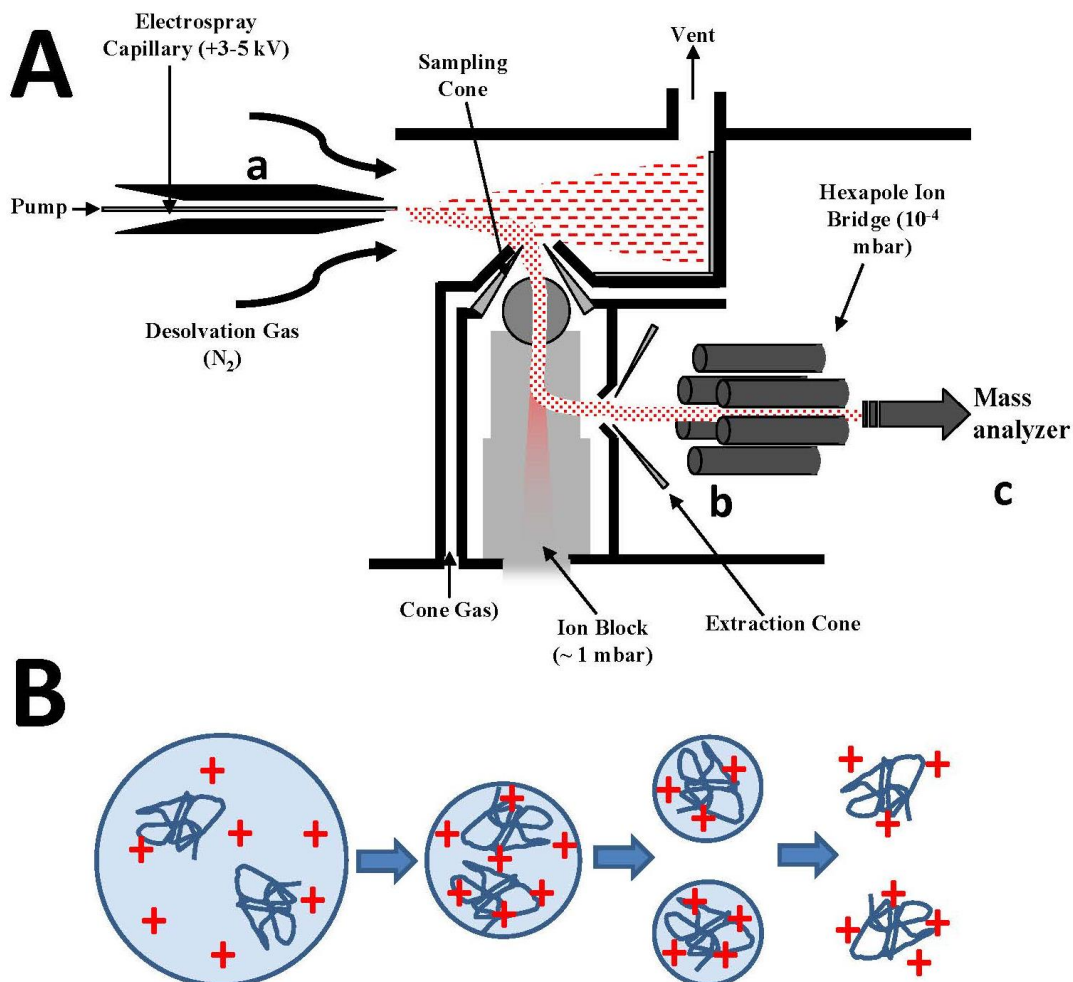


Figure 1-4: Schematic of an electrospray ionization mass spectrometer. (A) Schematic of an ESI- mass spectrometer ionization and ion focusing set-up. (a) ion source, (b) ion focuser and (c) mass analyzer. (B) Simplified diagram of the charged residue model (CRM) of the electrospray ionization mechanism

Since the development of soft ionization techniques like electrospray, the use of mass spectrometry in the field of protein structure and dynamics has grown exponentially.¹⁰³ Unlike optical techniques, which examine global properties and observe an average response of all species present, MS techniques can simultaneously delineate many parameters including: species distribution, relative abundance, protein surface area and conformational changes via charge states and information about specific regions within

the protein and their solvent exposure via hydrogen/deuterium exchange (HDX).¹⁰⁴⁻¹⁰⁵ In addition, protein-ligand interactions or site specific covalent modifications can be measured.¹⁰⁶⁻¹⁰⁷ HDX is suited for larger proteins, with an extensive H-bonding network between backbone amide hydrogens which limits the rate of association/dissociation resulting in a smaller mass change compared with disordered regions and those that are more solvent exposed. These exchange techniques are reviewed in detail elsewhere.¹⁰⁸

1.7.1 ESI-MS for analysis of MT structure and metalation

ESI-MS is particularly well suited for the study of metalation reactions of MTs due to the ease in which metal binding can be detected even for spectroscopically silent ions like zinc. The mass increase upon binding of metals is easily distinguished and metals with similar masses can be identified via isotopic pattern analysis. In addition, ESI-MS offers the ability to: identify individual or many species in solution with unique m/z ratios, use dilute samples of small volumes with direct solution injection, monitor structural changes via charge state analysis and obtain time and temperature resolved metalation data.

A potential limitation, especially for semi-quantitative analysis using ESI-MS, lies in the ionization efficiencies of the protein analytes. Quantitative analysis of relative abundances of species in solution relies on the assumption that all species have the same ionization efficiency; meaning that all species in solution have the same likelihood of successful ionization into the gas phase and detection by the MS. It is known that different isoforms of MT have varying ionization efficiencies and concentrations of domain fragments and the full-length protein must be externally quantified in competition experiments. However, Fenselau and co-workers showed in 1993 that concentrations of M_n -MT species determined via ESI-MS are reliable.¹⁰⁹ Further studies used ESI-MS semi-quantitatively to determine parameters such as binding and kinetic constants.^{34, 39, 97,}¹¹⁰ The equal ionization assumption appears to be valid as long as the analysis only considers one isoform or construct of MT at a time.

Charge state analysis has been applied to MTs in a limited scope due to the small changes observed for the unfolding of such a small protein.¹¹¹ Charge state distributions do not change drastically for MTs unless demetalation is being monitored or apo-MT is

subjected to extreme conditions (pH 1.8) which may introduce signal masking.^{20, 112} For apo-MT, where a multitude of conformers exist, the charge distributions carried by individual conformers likely do not vary enough to be distinguished by ESI-MS.¹¹³ This type of analysis is better suited to larger proteins with more distinct structural features that include tertiary structural elements and dramatic surface area changes when unfolding.¹¹⁴⁻¹¹⁵

1.7.2 Covalent modification coupled with ESI-MS

A common criticism of the use of ESI-MS for the analysis of protein structure and conformation lies in the radically different surroundings the protein finds itself in when being analyzed compared to its native state.¹¹⁶ The native state is one in solution, buffered around neutral pH with an appropriate salt concentration, approximately 37°C and in the absence of chemical denaturants. The conditions of the electrospray process introduce high voltages, evaporating solvents causing a hyper-accumulation of salt ions and finally ionization of the protein itself and transition into a gas phase ion.¹¹⁷ The assumption that the conformations adopted in solution and under ESI conditions may be a tenuous one.

An advantage of covalent modification is that it probes the conformation in solution and changes thereafter during analysis and measurement of the gas phase ions have no effect on the modifications that occur prior to ionization. This is especially important for proteins whose structure is unstable and whose solution stabilized conformation may not reflect those conformers adopted during the electrospray process.

Cysteine is an important amino acid with high reactivity¹¹⁸, an ability to coordinate a variety of soft metals¹¹⁹ and form Cys-Cys covalent linkages that add stability to folded proteins.¹²⁰ Cysteine is also used to attach therapeutic and imaging moieties to proteins *in vivo*.¹²¹ Covalent modification coupled with mass spectrometry can easily identify free cysteinyl thiols vs those that are oxidized to form crosslinks. New proteomic strategies also make use of specific covalent modifiers coupled with LC-MS and tandem MS to identify S-sulfenylation of cysteines and identify the most solvent exposed residues.¹²² The redox chemistry inherent in quinones has been used for on-line tagging of free

cysteines in ESI-MS analysis via a 1,4-Michael addition.¹²³ With the incorporation of a photo-active quinone, the protein backbone can be selectively fragmented with ultraviolet light for analysis of solution structural properties or to monitor biological quinone post-translational modifications.¹²⁴ This technique can also be applied to other amino acids by leveraging thiol chemistry to selectively modify phosphorylated serine or threonine residues.¹²⁵

In the case of MTs, determining the number of free thiols under an assortment of different metal coordination numbers and geometries can help in structural determination. The number of free thiols can be a good indicator of metal-cysteine cluster formation, as clusters involve bridging thiolates and, as a result, more metal ions can be coordinated with a smaller number of cysteine residues. Terminally coordinated metals require more cysteinyl thiols in MT and are theorized to be more labile and primed for donation to other metalloenzymes.¹²⁶ Also when probing potentially new structures formed by coordination of unusual metals and metalloids where the stoichiometry is not defined, the quantification of free thiols by cysteine modification and ESI-MS can establish defined Cys:Metal ratios.¹²⁷ The reaction profile of alkylation reagents with the many cysteines of MT may also be useful in determination of solution structural conformation. Examples of three major types of reaction profiles are given in Figure 1-5.

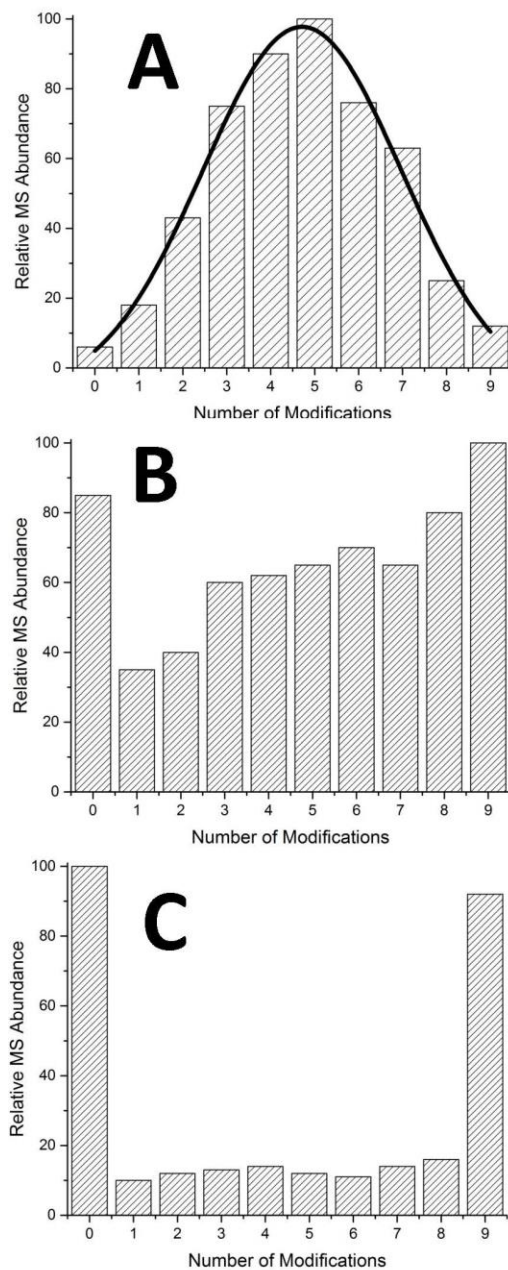


Figure 1-5: Possible reaction profiles of a cysteine alkylating reagent with a peptide containing 9 reaction sites. (A) Normal distribution of modified species. (B) Semi-cooperative pattern with significant amount of all possible modified species. (C) Cooperative pattern with little contribution from intermediate species, unmodified and fully modified species dominate.

1.8 Scope of the thesis

Much of what is known about MTs is based on models and experiments investigating fully metalated and well-defined structures. Apo- and partially metalated MTs pose a unique challenge to investigators but are critical to the biological function. Key to a complete description of MT chemistry and function *in vivo* is structural information about the starting point of the metalation reaction, apo-MT, and the many possible intermediate structures the protein can adopt in the metalation pathway before saturation. The research presented in this thesis primarily concerns the elucidation of the many structures adopted by metal-free and partially metalated MTs along the metalation pathway and their implications for binding kinetics and biological function.

This thesis contains eight Chapters and an Appendix. The first Chapter includes a brief introduction of techniques relevant to MT research and what is known about the structure and metalation mechanisms of MT. The biological context of MTs is also discussed with detailed background information pertaining to the toxicity of arsenic and cadmium and the essentiality of zinc. Chapter 2 describes the pH dependence of the cadmium and zinc binding pathways of $\beta\alpha$ MT using ESI-MS and CD spectroscopy. Chapter 3 investigates the isolated domains of MT to determine their individual properties and compare them to that of the full-length protein. These two chapters reconcile previously conflicting reports on the nature of the metalation mechanism.

Chapter 4 details our use of covalent cysteine modification to determine the stoichiometry of As^{3+} binding to the α - and β MT fragments and the structures adopted during metalation. Furthermore, we probe the configuration of apo- and partially metalation species under denaturing conditions to investigate the role of metal-induced folding and protein-protein interaction of As-MT species.

Chapter 5 further investigates the use of cysteine alkylating reagents to probe the conformations adopted by apo-MTs in a systematic way testing three different reagents with the full-length protein and its isolated domains. Chapter 6 builds on the conformational investigations of chapter five by testing the Cd^{2+} metalation kinetics of MT under native and denaturing conditions.

Chapter 7 chronicles progress in building on knowledge gained by the fundamental research into MT binding affinities and the pH dependence of metal binding through the design and testing of an MT-based biosensor for the electrochemical detection of arsenic and mercury.

Chapter 8 attempts to bring together the results from the previous seven chapters in order to paint a clearer picture of MT structure, metalation mechanisms and possible applications of MTs in biosensors. The results are also discussed in a biological context to connect the *in vitro* studies to MT function *in vivo*.

1.9 References

1. T. Miyayama, Y. Ishizuka, T. Iijima, D. Hiraoka and Y. Ogra, *Metallomics*, 2011, **3**, 693-701.
2. C. A. Blindauer and O. I. Leszczyszyn, *Natural product reports*, 2010, **27**, 720-741.
3. J. Loebus, B. Leitenmaier, D. Meissner, B. Braha, G.-J. Krauss, D. Dobritzsch and E. Freisinger, *Journal of Inorganic Biochemistry*, 2013, **127**, 253-260.
4. W. Maret, *The Journal of nutrition*, 2003, **133**, 1460S-1462S.
5. Y. Boulanger, I. Armitage, K. Miklossy and D. Winge, *Journal of Biological Chemistry*, 1982, **257**, 13717-13719.
6. D. E. Sutherland and M. J. Stillman, *Metallomics*, 2011, **3**, 444-463.
7. W. Braun, M. Vasak, A. Robbins, C. Stout, G. Wagner, J. Kägi and K. Wüthrich, *Proceedings of the National Academy of Sciences of the United States of America*, 1992, **89**, 10124-10128.
8. K. Zangger, G. ÖZ, I. M. Armitage and J. D. Otvos, *Protein Science*, 1999, **8**, 2630-2638.
9. M. Vasak, J. H. Kaegi and H. A. O. Hill, *Biochemistry*, 1981, **20**, 2852-2856.
10. Z. Gui, A. R. Green, M. Kasrai, G. M. Bancroft and M. J. Stillman, *Inorganic chemistry*, 1996, **35**, 6520-6529.

11. D. E. Sutherland and M. J. Stillman, *Biochemical and Biophysical Research Communications*, 2008, **372**, 840-844.
12. M. Vaher, N. Romero-Isart, M. Vašák and P. Palumaa, *Journal of Inorganic Biochemistry*, 2001, **83**, 1-6.
13. P. Palumaa, E. Eriste, O. Njunkova, L. Pokras, H. Jörnvall and R. Sillard, *Biochemistry*, 2002, **41**, 6158-6163.
14. C. Acharya and C. A. Blindauer, *Inorganic chemistry*, 2016, **55**, 1505-1515.
15. G. Jiang, Z. Gong, X.-F. Li, W. R. Cullen and X. C. Le, *Chemical research in toxicology*, 2003, **16**, 873-880.
16. W. Lu and M. J. Stillman, *Journal of the American Chemical Society*, 1993, **115**, 3291-3299.
17. M. J. Stillman, A. S. Zelazowski, J. Szymanska and Z. Gasyna, *Inorganica Chimica Acta*, 1989, **161**, 275-279.
18. M. C. Carpenter, A. S. Shah, S. DeSilva, A. Gleaton, A. Su, B. Goundie, M. L. Croteau, M. J. Stevenson, D. Wilcox and R. N. Austin, *Metallomics*, 2016, **8**, 605-617.
19. J. Ejnik, J. Robinson, J. Zhu, H. Försterling, C. F. Shaw and D. H. Petering, *Journal of inorganic biochemistry*, 2002, **88**, 144-152.
20. J. Chan, Z. Huang, I. Watt, P. Kille and M. J. Stillman, *Canadian Journal of Chemistry*, 2007, **85**, 898-912.
21. P. Gamez, P. G. Aubel, W. L. Driessen and J. Reedijk, *Chemical Society Reviews*, 2001, **30**, 376-385.
22. C. Andreini, I. Bertini, G. Cavallaro, G. L. Holliday and J. M. Thornton, *JBIC Journal of Biological Inorganic Chemistry*, 2008, **13**, 1205-1218.
23. J. McKinley-McKee, J. Winberg and G. Pettersson, *Biochemistry international*, 1991, **25**, 879-885.
24. M. F. Dunn, H. Dietrich, A. K. MacGibbon, S. C. Koerber and M. Zeppezauer, *Biochemistry*, 1982, **21**, 354-363.
25. J. H. Laity, B. M. Lee and P. E. Wright, *Current opinion in structural biology*, 2001, **11**, 39-46.
26. L. Cai, X.-K. Li, Y. Song and M. G. Cherian, *Current medicinal chemistry*, 2005, **12**, 2753-2763.

27. L. E. Laverman and P. C. Ford, *Journal of the American Chemical Society*, 2001, **123**, 11614-11622.
28. K. W. Becker and E. P. Skaar, *FEMS microbiology reviews*, 2014, **38**, 1235-1249.
29. M. Nairz, A. Schroll, T. Sonnweber and G. Weiss, *Cellular microbiology*, 2010, **12**, 1691-1702.
30. T. E. Kehl-Fie, S. Chitayat, M. I. Hood, S. Damo, N. Restrepo, C. Garcia, K. A. Munro, W. J. Chazin and E. P. Skaar, *Cell host & microbe*, 2011, **10**, 158-164.
31. M. T. Tiedemann, D. E. Heinrichs and M. J. Stillman, *Journal of the American Chemical Society*, 2012, **134**, 16578-16585.
32. L. Banci, I. Bertini, S. Ciofi-Baffoni, T. Kozyreva, K. Zovo and P. Palumaa, *Nature*, 2010, **465**, 645-648.
33. K. Raha and K. M. Merz, *Journal of medicinal chemistry*, 2005, **48**, 4558-4575.
34. T. B. Pinter, G. W. Irvine and M. J. Stillman, *Biochemistry*, 2015, **54**, 5006-5016.
35. D. Radisky and J. Kaplan, *Journal of Biological Chemistry*, 1999, **274**, 4481-4484.
36. S. K. Buchanan, B. S. Smith, L. Venkatramani, D. Xia, L. Esser, M. Palnitkar, R. Chakraborty, D. van der Helm and J. Deisenhofer, *Nature Structural & Molecular Biology*, 1999, **6**, 56-63.
37. L. C. Costello, Z. Guan, R. B. Franklin and P. Feng, *Journal of inorganic biochemistry*, 2004, **98**, 664-666.
38. H. Gonzalez-Iglesias, L. Alvarez, M. García, C. Petrash, A. Sanz-Medel and M. Coca-Prados, *Metallomics*, 2014, **6**, 201-208.
39. T. T. Ngu, A. Easton and M. J. Stillman, *Journal of the American Chemical Society*, 2008, **130**, 17016-17028.
40. T. B. Pinter and M. J. Stillman, *Biochemical Journal*, 2015, **471**, 347-356.
41. J. Ejnik, A. Muñoz, T. Gan, C. F. Shaw III and D. Petering, *Journal of Biological Inorganic Chemistry*, 1999, **4**, 784-790.
42. T. T. Ngu, M. D. Dryden and M. J. Stillman, *Biochemical and biophysical research communications*, 2010, **401**, 69-74.
43. E. Kopera, T. Schwerdtle, A. Hartwig and W. Bal, *Chemical research in toxicology*, 2004, **17**, 1452-1458.

44. P. F. Predki and B. Sarkar, *Journal of Biological Chemistry*, 1992, **267**, 5842-5846.
45. M. Margoshes and B. L. Vallee, *Journal of the American Chemical Society*, 1957, **79**, 4813-4814.
46. C. D. Klaassen and J. LIU, *The Journal of toxicological sciences*, 1998, **23**, 97-102.
47. J. D. Park, Y. Liu and C. D. Klaassen, *Toxicology*, 2001, **163**, 93-100.
48. H. Baba, K. Tsuneyama, M. Yazaki, K. Nagata, T. Minamisaka, T. Tsuda, K. Nomoto, S. Hayashi, S. Miwa and T. Nakajima, *Modern Pathology*, 2013, **26**, 1228-1234.
49. D. R. Winge, R. Premakumar and K. Rajagopalan, *Archives of Biochemistry and Biophysics*, 1975, **170**, 242-252.
50. M. P. Waalkes, M. J. Harvey and C. D. Klaassen, *Toxicology letters*, 1984, **20**, 33-39.
51. M. P. Waalkes, J. Liu, R. A. Goyer and B. A. Diwan, *Cancer Research*, 2004, **64**, 7766-7772.
52. M. Thun, A. M. Osorio, S. Schober, W. Hannon, B. Lewis and W. Halperin, *British journal of industrial medicine*, 1989, **46**, 689-697.
53. J. G. Hengstler, U. Bolm-Audorff, A. Faldum, K. Janssen, M. Reifenrath, W. Götte, D. Jung, O. Mayer-Popken, J. Fuchs and S. Gebhard, *Carcinogenesis*, 2003, **24**, 63-73.
54. I. Murata, T. Hirono, Y. Saeki and S. Nakagawa, *Bulletin de la Societe internationale de chirurgie*, 1969, **29**, 34-42.
55. K. Nogawa and A. Ishizaki, *Environmental research*, 1979, **18**, 410-420.
56. L. Goldberg, *Journal of the American Institute for Conservation*, 1996, **35**, 23-43.
57. X. Lin, D. Alber and R. Henkelmann, *Analytical and bioanalytical chemistry*, 2004, **379**, 218-220.
58. M. E. Cebrian, A. Albores, M. Aguilar and E. Blakely, *Human toxicology*, 1983, **2**, 121-133.
59. D. K. Nordstrom, *Science*, 2002, **296**, 2143-2145.
60. A. H. Smith, E. O. Lingas and M. Rahman, *Bulletin of the World Health Organization*, 2000, **78**, 1093-1103.

61. D. Polya, A. Gault, N. Diebe, P. Feldman, J. Rosenboom, E. Gilligan, D. Fredericks, A. Milton, M. Sampson and H. Rowland, *Mineralogical Magazine*, 2005, **69**, 807-823.
62. R. Nickson, J. McArthur, P. Ravenscroft, W. Burgess and K. Ahmed, *Applied Geochemistry*, 2000, **15**, 403-413.
63. S. Kapaj, H. Peterson, K. Liber and P. Bhattacharya, *Journal of Environmental Science and Health Part A*, 2006, **41**, 2399-2428.
64. G. Sun, *Toxicology and applied pharmacology*, 2004, **198**, 268-271.
65. G. Duan, W. Liu, X. Chen, Y. Hu and Y. Zhu, *Metallomics*, 2013, **5**, 784-792.
66. J. F. Reichard, M. Schnekenburger and A. Puga, *Biochemical and biophysical research communications*, 2007, **352**, 188-192.
67. J. Qin, B. P. Rosen, Y. Zhang, G. Wang, S. Franke and C. Rensing, *Proceedings of the National Academy of Sciences of the United States of America*, 2006, **103**, 2075-2080.
68. S. Chanda, U. B. Dasgupta, D. GuhaMazumder, M. Gupta, U. Chaudhuri, S. Lahiri, S. Das, N. Ghosh and D. Chatterjee, *Toxicological Sciences*, 2006, **89**, 431-437.
69. L. Benbrahim-Tallaa, R. A. Waterland, M. Styblo, W. E. Achanzar, M. M. Webber and M. P. Waalkes, *Toxicology and applied pharmacology*, 2005, **206**, 288-298.
70. D. S. Tawfik and R. E. Viola, *Biochemistry*, 2011, **50**, 1128-1134.
71. E. J. Denning and A. D. MacKerell Jr, *Journal of the American Chemical Society*, 2011, **133**, 5770-5772.
72. M. Gresser, *Journal of Biological Chemistry*, 1981, **256**, 5981-5983.
73. M. F. Hughes, *Toxicology letters*, 2002, **133**, 1-16.
74. T. T. Ngu and M. J. Stillman, *Journal of the American Chemical Society*, 2006, **128**, 12473-12483.
75. L. Nejdil, S. Skalickova, J. Kudr, B. Ruttkay-Nedecky, S. Dostalova, M. Kremplova, R. Kensova, A. Moulick, M. Konecna and V. Adam, *International journal of biological macromolecules*, 2015, **72**, 599-605.
76. A. Slusser, Y. Zheng, X. D. Zhou, S. Somji, D. A. Sens, M. A. Sens and S. H. Garrett, *Toxicology letters*, 2015, **232**, 141-148.

77. R. Garla, R. Ganger, B. P. Mohanty, S. Verma, M. P. Bansal and M. L. Garg, *Toxicology*, 2016, **366**, 68-73.
78. J. Chan, Z. Huang, I. Watt, P. Kille and M. Stillman, *Chemistry-A European Journal*, 2008, **14**, 7579-7593.
79. M. Vašák, *Journal of Trace Elements in Medicine and Biology*, 2005, **19**, 13-17.
80. N. Thirumoorthy, A. S. Sunder, K. M. Kumar, G. Ganesh and M. Chatterjee, *World journal of surgical oncology*, 2011, **9**, 54.
81. Y. Li and W. Maret, *Journal of Analytical Atomic Spectrometry*, 2008, **23**, 1055-1062.
82. P. Faller and M. Vašák, *Biochemistry*, 1997, **36**, 13341-13348.
83. W. Furey, A. Robbins, L. Clancy, D. R. Winge, B. Wang and C. Stout, *Science*, 1986, **231**, 704-710.
84. D. E. K. Sutherland, M. J. Willans and M. J. Stillman, *Biochemistry*, 2010, **49**, 3593-3601.
85. D. E. Sutherland, M. J. Willans and M. J. Stillman, *Journal of the American Chemical Society*, 2012, **134**, 3290-3299.
86. M. Good, R. Hollenstein, P. J. Sadler and M. Vasak, *Biochemistry*, 1988, **27**, 7163-7166.
87. V. Calderone, B. Dolderer, H.-J. Hartmann, H. Echner, C. Luchinat, C. Del Bianco, S. Mangani and U. Weser, *Proceedings of the National Academy of Sciences of the United States of America*, 2005, **102**, 51-56.
88. D. W. Hasler, P. Faller and M. Vašák, *Biochemistry*, 1998, **37**, 14966-14973.
89. M. J. Stillman, Z. Gasyna and A. J. Zelazowski, *FEBS letters*, 1989, **257**, 283-286.
90. A. Presta, A. R. Green, A. Zelazowski and M. J. Stillman, *European Journal of Biochemistry*, 1995, **227**, 226-240.
91. P. M. Gehrig, C. You, R. Dallinger, C. Gruber, M. Brouwer, J. H. KÄGI and P. E. Hunziker, *Protein Science*, 2000, **9**, 395-402.
92. K. E. Rigby and M. J. Stillman, *Biochemical and Biophysical Research Communications*, 2004, **325**, 1271-1278.
93. R. Garla, M. P. Bansal and M. L. Garg, *Journal of Proteins & Proteomics*, 2015, **6**.

94. S.-H. Hong, Q. Hao and W. Maret, *Protein Engineering Design and Selection*, 2005, **18**, 255-263.
95. S.-H. Hong and W. Maret, *Proceedings of the National Academy of Sciences*, 2003, **100**, 2255-2260.
96. S.-H. Chen, L. Chen and D. H. Russell, *Journal of the American Chemical Society*, 2014, **136**, 9499-9508.
97. S.-H. Chen, W. K. Russell and D. H. Russell, *Analytical chemistry*, 2013, **85**, 3229-3237.
98. D. H. Petering, J. Zhu, S. Krezoski, J. Meeusen, C. Kiekenbush, S. Krull, T. Specher and M. Dughish, *Experimental Biology and Medicine*, 2006, **231**, 1528-1534.
99. K. L. Summers, D. E. Sutherland and M. J. Stillman, *Biochemistry*, 2013, **52**, 2461-2471.
100. K. E. Duncan and M. J. Stillman, *FEBS Journal*, 2007, **274**, 2253-2261.
101. Y. R. Cho, A. J. Maguire, A. C. Try, M. S. Westwell, P. Groves and D. H. Williams, *Chemistry & biology*, 1996, **3**, 207-215.
102. D. E. Sutherland, K. L. Summers and M. J. Stillman, *Biochemical and biophysical research communications*, 2012, **426**, 601-607.
103. A. El-Aneed, A. Cohen and J. Banoub, *Applied Spectroscopy Reviews*, 2009, **44**, 210-230.
104. R. Grandori, *Journal of mass spectrometry*, 2003, **38**, 11-15.
105. A. D. Rodriguez, S. D. Dunn and L. Konermann, *Biochemistry*, 2014, **53**, 4072-4080.
106. B. Deng, C. Lento and D. J. Wilson, *Analytica Chimica Acta*, 2016, **940**, 8-20.
107. E. S. Witze, W. M. Old, K. A. Resing and N. G. Ahn, *Nature methods*, 2007, **4**, 798-806.
108. L. Konermann, S. Vahidi and M. A. Sowole, *Analytical chemistry*, 2013, **86**, 213-232.
109. X. Yu, M. Wojciechowski and C. Fenselau, *Analytical chemistry*, 1993, **65**, 1355-1359.
110. T. B. Pinter and M. J. Stillman, *Biochemistry*, 2014, **53**, 6276-6285.

111. K. E. Rigby-Duncan and M. J. Stillman, *Journal of Inorganic Biochemistry*, 2006, **100**, 2101-2107.
112. D. R. Gumerov, A. Dobo and I. A. Kaltashov, *European Journal of Mass Spectrometry*, 2002, **8**, 123-130.
113. A. Mohimen, A. Dobo, J. K. Hoerner and I. A. Kaltashov, *Analytical chemistry*, 2003, **75**, 4139-4147.
114. O. O. Sogbein, D. A. Simmons and L. Konermann, *Journal of the American Society for Mass Spectrometry*, 2000, **11**, 312-319.
115. L. Konermann and D. Douglas, *Biochemistry*, 1997, **36**, 12296-12302.
116. D. J. Tobias and C. L. Brooks, *J. Phys. Chem*, 1992, **96**, 3864-3870.
117. I. A. Kaltashov and R. R. Abzalimov, *Journal of the American Society for Mass Spectrometry*, 2008, **19**, 1239-1246.
118. E. Weerapana, C. Wang, G. M. Simon, F. Richter, S. Khare, M. B. Dillon, D. A. Bachovchin, K. Mowen, D. Baker and B. F. Cravatt, *Nature*, 2010, **468**, 790-795.
119. T. V. O'Halloran and V. C. Culotta, *Journal of Biological Chemistry*, 2000, **275**, 25057-25060.
120. N. E. Zhou, C. M. Kay and R. S. Hodges, *Biochemistry*, 1993, **32**, 3178-3187.
121. B. Bernardim, P. M. Cal, M. J. Matos, B. L. Oliveira, N. Martínez-Sáez, I. S. Albuquerque, E. Perkins, F. Corzana, A. C. Burtoloso and G. Jiménez-Osés, *Nature communications*, 2016, **7**.
122. J. Yang, V. Gupta, K. S. Carroll and D. C. Liebler, *Nature communications*, 2014, **5**, 4776.
123. L. Dayon, C. Roussel and H. H. Girault, *CHIMIA International Journal for Chemistry*, 2004, **58**, 204-207.
124. J. K. Diedrich and R. R. Julian, *Analytical chemistry*, 2010, **82**, 4006-4014.
125. J. K. Diedrich and R. R. Julian, *Journal of the American Chemical Society*, 2008, **130**, 12212-12213.
126. G. W. Irvine, T. B. Pinter and M. J. Stillman, *Metallomics*, 2016, **8**, 71-81.
127. G. W. Irvine, K. L. Summers and M. J. Stillman, *Biochemical and biophysical research communications*, 2013, **433**, 477-483.

Chapter 2

2 Defining the metal binding pathways of human metallothionein 1a: balancing zinc availability and cadmium exclusion¹

2.1 Introduction

Mammalian metallothioneins (MTs) are a family of small, cysteine rich metal-binding proteins that are involved in zinc and copper homeostasis,¹⁻⁸ heavy metal detoxification⁹⁻¹⁶ and cellular redox chemistry.¹⁷⁻²¹ When saturated with seven divalent metals, mammalian MTs consist of an N-terminal β -domain and a C-terminal α -domain connected by a flexible linker region.²² The α -domain can accommodate up to 4 divalent metals and the β -domain 3 metals by forming $M^{II}_4S_{cys11}$ and $M^{II}_3S_{cys9}$ clusters, respectively. This domain description is only relevant in the fully metalated structure as there are no true binding domains in the partially-metalated and apo-structures under most conditions.²³⁻²⁷ The more biologically relevant structures of the apo- and partially metalated MTs are considered to be poorly defined.^{23,27-28} Currently, these apo- and partially metalated MT species are thought to adopt a fluxional, globular structure.²⁹⁻³⁰

Metalation of the 20 Cys apo-peptide can take place in a number of different ways.^{24, 31} As there is no pre-existing domain structure in the absence of bound metals, the thermodynamics and kinetics associated with metal binding control the structures adopted at each metalation step.²⁷ For each species (ie. M_1 - $\beta\alpha$ MT, M_2 - $\beta\alpha$ MT, etc) numerous structures are possible and complex rearrangement of the bound metals can occur.³²⁻³³ The mechanism of divalent metal binding to MTs, specifically that of Zn(II) and Cd(II), has been a topic of great interest but the results have generated conflicting reports

¹ A version of this chapter has been published:

Reproduced with permission from: Irvine, Gordon W., Tyler BJ Pinter, and Martin J. Stillman. "Defining the metal binding pathways of human metallothionein 1a: balancing zinc availability and cadmium seclusion." *Metallomics* 8.1 (2016): 71-81.

Copyright 2016 Royal Society of Chemistry

concerning the identity and description of the intermediate structures formed before the complete complement of seven metals has been bound.^{2, 34-38} Because of the spectroscopic accessibility of Cd(II), much of what is currently known about Zn(II) and Cd(II) binding to MT has been based largely on the chemistry of Cd(II) or other spectroscopically active metals, such as Co(II).^{25, 39} Indeed, ¹¹³Cd is often used to probe structural properties of Zn(II) binding sites in proteins other than MTs.⁴⁰

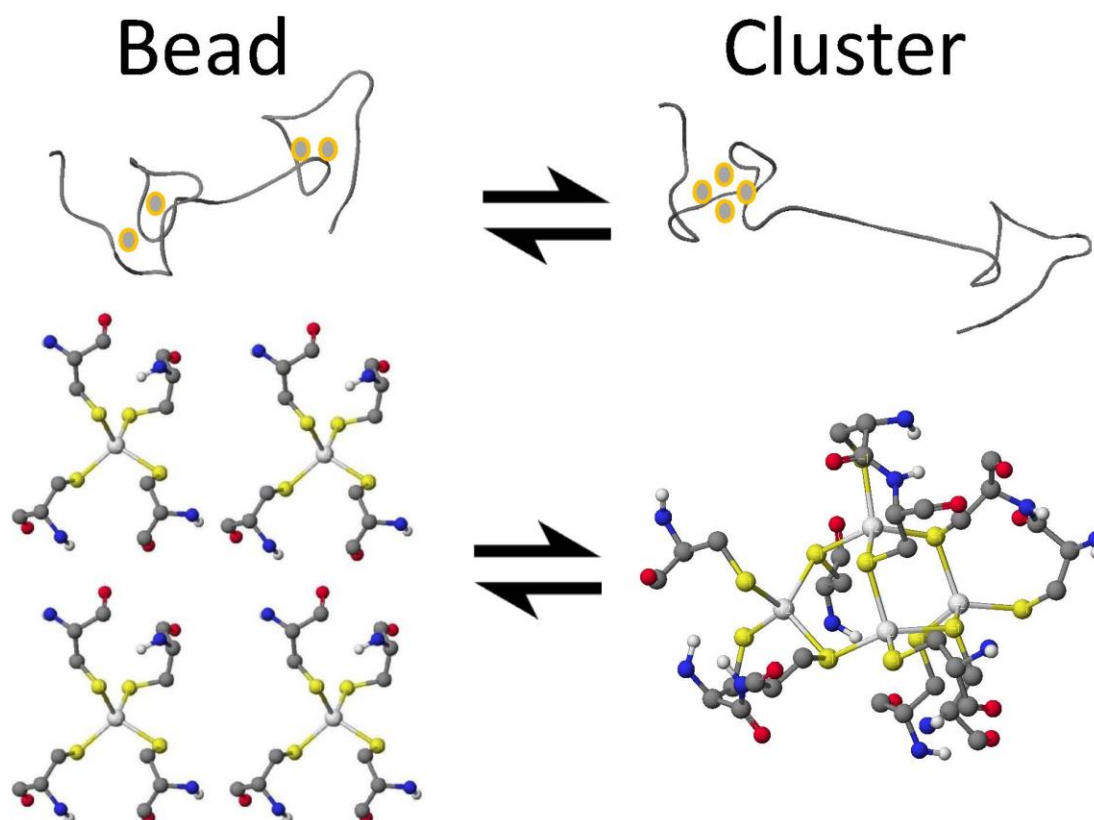


Figure 2-1: Cartoon ribbon representation of proposed MT1a metalation intermediates. The "beaded" intermediate and a ball-and-stick representation of the terminal coordination of the metals with up to 5 $M^{\text{II}}(\text{S}_{\text{Cys}})_4$ "beads" (left; 4 beads shown). The cluster structure $M_4\text{S}_{\text{CYS11}}$ is shown in the α -domain of the ribbon structure and as a ball-and-stick model of the bridged and terminal Cys that make up the cluster (right).

When discussing metal binding mechanisms of MTs, the terms cooperative and noncooperative are often used. In a fully cooperative mechanism, only the apo-MT and end-product should be detected at any point during the reaction. In a non-cooperative mechanism, intermediates can be measured and become the most abundant species during

the early to mid-stages of the metal titration. The kinetic data for As(III) binding to MT-1a clearly follow this noncooperative, stochastic model.³¹

Metalation details from early studies of cadmium binding relied on ^{113}Cd NMR²⁶ or protein modification⁴¹ and reported the formation of cluster dominated products. With the development of new technologies, most notably electrospray ionization mass spectrometry (ESI-MS), the description of a purely cluster dominated mechanism became less convincing. Some groups have reported a cluster dominated mechanism with ESI-MS³⁷ and reported that the Cd-thiolate cluster formation occurs first in the α -domain.³⁰ However, reports by our group and others have shown that the binding pathway involves non-clustered intermediates.^{35-36, 38, 42} It should be noted that these studies used different solution conditions and often different isoforms of human MT, which possess different metalation properties.⁴³ It has also been suggested that differing ESI-MS settings may cause the discrepancy in mechanistic details.³⁰

In this chapter, we report definitive evidence for two parallel, competing pathways that are dependent on metal identity, Zn(II) or Cd(II), and the pH. We have examined the pH dependence of the Zn(II) and Cd(II) metalation pathways of human MT1a using ESI-MS and circular dichroism spectroscopy at the important early stages of metalation where the largest number of conformations are possible. The presence of these two distinct metalation pathways was determined by monitoring the formation of the partially metalated intermediates during the Zn(II) and Cd(II) metalation reactions of the apo-MT-1a. We discuss how significant differences in the intermediates formed during metalation for each metal may explain how MT-1a functions as a multi-purpose protein: regulating zinc levels, providing zinc to other apo-enzymes,⁴⁴ and sequestering toxic heavy metals.⁴⁵⁻⁴⁶ From the data presented here it is clear that metalation can occur via one of two major pathways: a cooperative, α -cluster driven pathway or a non-cooperative, terminally-bound, beaded pathway (Figure 2-1).

2.2 Methods

2.2.1 Protein preparation

Recombinant human metallothionein 1a (MGKAAAACSC ATGGGCTCTG SCKCKECKCN SCKKCC SCCPMSCAKC AQCVCCKGAS EKCSCCK KAA AA) was expressed with an S-tag in BL21 *E. coli* cells which has been described in detail elsewhere.⁴⁷ In brief, cells containing the plasmid for the full protein ($\beta\alpha$ -MT1a) were plated on to growth media containing kanamycin from a stock culture stored at -80°C and grown for 16 hours at 37°C . The grown cells were then inoculated into 4x1L LB broth cultures enriched with 50 μL of 1 M cadmium and incubated in a shaker for 4 hours until OD_{600} absorbance was 0.8. An aliquot of 0.7 mL of 1 M Isopropyl β -D-1-thiogalactopyranoside (IPTG) was then added to induce expression of MT and 30 minutes later 150 μL of 1 M cadmium sulfate solution was added to the broth. The cells were collected 3.5 hours after induction, centrifuged and stored at -80°C .

The recombinant cells were lysed using a cell disruptor (Constant Systems, UK) shot at 20K psi. From there, the cell lysate was centrifuged for 1h to pellet out cellular debris. The supernatant was filtered and loaded on to a GE healthcare SP ion exchange columns with a total volume of 10 mL. The columns were washed with pH 7.4 10 mM Tris(tris-hydroxymethyl-aminomethane) buffer for approximately 2h to remove loosely bound proteins and other organic compounds. MT was eluted using an increasing gradient of 1 M NaCl + 10 mM Tris buffer at pH 7.4. The eluted MT was concentrated down to <20 mL and the S-tag cleaved using a Thrombin Clean-Cleave kit as per the manufacturers' instructions (Sigma-Aldrich). The mixture was then diluted, desalted and placed on another SP ion exchange column. The S-tag does not bind as strongly as MT and thus elutes at low salt concentrations. The protein and S-tag were separated in this fashion. The eluted MT was concentrated to approximately 120 μM and stored at -20°C .

To prepare MT for the pH titration experiments, aliquots were first demetalated and desalted using centrifugal filter tubes with a 3 kDa membrane (Millipore) and a 10 mM pH 2.8 ammonium formate buffer. The low pH solutions contained 1 mM Dithiothreitol (DTT) to prevent oxidation of the free thiols in MT. The pH was raised by buffer

exchange with argon saturated, pH 7.0 10 mM ammonium formate solutions that did not contain reductant. The protein solutions were checked for final concentration by remetalation of a small aliquot with cadmium using the metal-to-ligand charge transfer band at 250 nm ($\epsilon_{250} = 89,000 \text{ L mol}^{-1} \text{ cm}^{-1}$). The solutions were also monitored for oxidation using UV-visible absorption spectroscopy to monitor absorption corresponding to 280 nm from oxidized disulfide. Once demetalated and desalted, the MT concentration was determined, all concentrations were between 40-90 μM to ensure good signal to noise ratios in the ESI-MS experiment. We note that this was a concern because the titration introduced salt into the solution which suppresses the MT signal at high concentrations.

In addition to demetalating MT in the presence of DTT, the solutions were vacuum degassed and bubbled with Argon to displace any dissolved oxygen. This was done for the 10 mM Cd^{2+} and Zn^{2+} and the 0.5% NH_3 and 0.5% formic acid solutions as well to ensure no oxygen was introduced into the system during the titration. Great care was taken to reduce the possibility of oxidation of the protein at neutral pH.

2.2.2 ESI-MS and circular dichroism pH titrations

Mass spectra were collected on a micrOTOF II electrospray-ionization time-of-flight mass spectrometer (Bruker Daltonics) in the positive ion mode. NaI was used as the mass calibrant. The scan conditions for the spectrometer were: end plate offset, -500 V ; capillary, $+4200 \text{ V}$; nebulizer, 2.0 bar; dry gas flow, 8.0 L min^{-1} ; dry temperature, $30 \text{ }^\circ\text{C}$; capillary exit, 180 V; skimmer 1, 22.0 V; hexapole 1, 22.5 V; hexapole RF, 600 Vpp; skimmer 2, 22 V; lens 1 transfer, 88 μs ; lens 1 pre-pulse storage, 23 μs . The mass range was 500.0–3000.0 m/z . Spectra were assembled and deconvoluted using the Bruker Compass data analysis software package. ESI-mass spectrometry was used to monitor all stages of the pH titration of Cd-MT and Zn-MT. First, approximately 2.5 molar equivalents of Cd(II) acetate and Zn(II) acetate were added to the MT solution at pH 5.5. This caused a drop in pH due to the displacement of H^+ from the thiol groups. After the metal solution was added, the ESI-MS spectra were recorded and averaged over 2 minutes. Then aliquots of 0.5% NH_3 were added to raise the pH and the spectra recorded. The pH was confirmed using a micro-pH probe (Accumet). This was repeated in steps

until the salt peaks became more intense than the peaks corresponding to MT species. No change of the M^{2+}/MT ratio was observed meaning no precipitation of $Cd(OH)_2$ or $Zn(OH)_2$ occurred.

The pH titrations of the partially metalated Cd-MT and Zn-MT were performed at least 6 separate times with different protein preparations and starting at slightly different pH values in the region of 4.5-5.5. Thus separate data points were obtained for each pH reported increasing in increments of 0.1 pH units and serve as a statistical check. The separate preparations were run under the same solution and ESI-MS conditions. The error associated with these ESI-MS measurements is estimated to be about $\pm 10\%$.

For the circular dichroism (CD) spectra, 2.5 molar equivalents of cadmium acetate were added to apo-MT in a pH 7.0 10 mM ammonium formate solution in the manner described above for the ESI-MS data. The CD spectra (Jasco J810) were measured over the range of 200-300 nm at various stages in the pH titration. Below 220 nm, the CD spectrum is skewed due to the absorbance of the ammonium formate buffer and is not shown. The significant Cd-dependent CD spectral bands lie in the 240-280 nm region. The CD spectra obtained were compared to spectra of apo-MT and Cd_4 -MT that were obtained previously by our group and have been extensively discussed in other works.⁴⁸⁻⁴⁹ We note that the Zn-S charge transfer band lies at 220-230 nm under the protein bands.

To determine the degree of cluster formation vs terminally bound metal, the ratios of the abundances of the intermediates (Cd_{1-3} - $\beta\alpha$ MT) to the initial apo-MT and final product (Cd_4 - $\beta\alpha$ MT) were determined and normalized for each ESI mass spectrum in the pH titration. The most clustered spectra (at lower pH) had only a minimal fraction of intermediates compared to the spectra recorded at more basic pH. The sigmoidal fit of the set of ratios was generated using a least squares method. The lack of saturation of the sigmoidal fit is likely due to the 100% terminal coordination binding mechanism occurring at the highest pH range of the titration and spectra were not measured above pH 8.2.

The simulated ESI-MS data were calculated using a set of 4 equilibrium constants that correspond to each of the bimolecular metalation reactions up to Cd_4 -MT (Scheme 1).

Each sequential bimolecular reaction was controlled by an individual K_f . The values of the $\log(K_f)$ of the formation constants all average to 14.4 which is within the range reported in the literature for Cd(II) binding to MT.⁵⁰ It should be noted that the binding constants presented in this work and those referenced are conditional binding constants that amongst other parameters, are dependent on pH.

2.3 Results

2.3.1 pH dependence of cadmium binding to apo-MT1a

Figure 2-2 shows a series of deconvoluted ESI mass spectra recorded for a single sample of apo-MT1a metalated with 2.5 equivalents of Cd(II) at increasing pH (A-E). This metal loading of 2.5 molar equivalents (mol. eq.) was chosen to challenge the formation of the ambiguous Cd_4 intermediate. This is the point at which the spectra corresponding to the cooperative and non-cooperative mechanisms appear in stark contrast to each other. Each species present in solution can be identified and the change in its relative abundance monitored. At more acidic pH (<6.0) the relative abundance of the intermediates, Cd_{1-3} -MT1a, is very low and the dominant species is Cd_4 -MT1a. With increasing pH, the appearance of Cd_{1-3} -MT1a can be seen with their relative intensities increasing as the pH is raised. At pH 7.9 the distribution of species present is narrower, now completely dominated by the terminally-bound Cd_{1-3} -MT1a species, which we describe as being comprised of the “beaded” $Cd(S_{CYS})_4$ structures. Our assignment of these species being terminally-bound is supported by the loss of the specific spectral envelope motif in the circular dichroism spectral data seen in Figure 2-3. The change in metalation pathway is apparent from the complete loss of both the initial apo- and Cd_4 -MT1a masses in the ESI-mass spectrum (Figure 2-2A). These two species are replaced by higher intensities of Cd_{1-3} -MT1a species (Figure 2-2E). Figure 2-2 B-D show a blending of these two pathways leading to a mixture of all species.

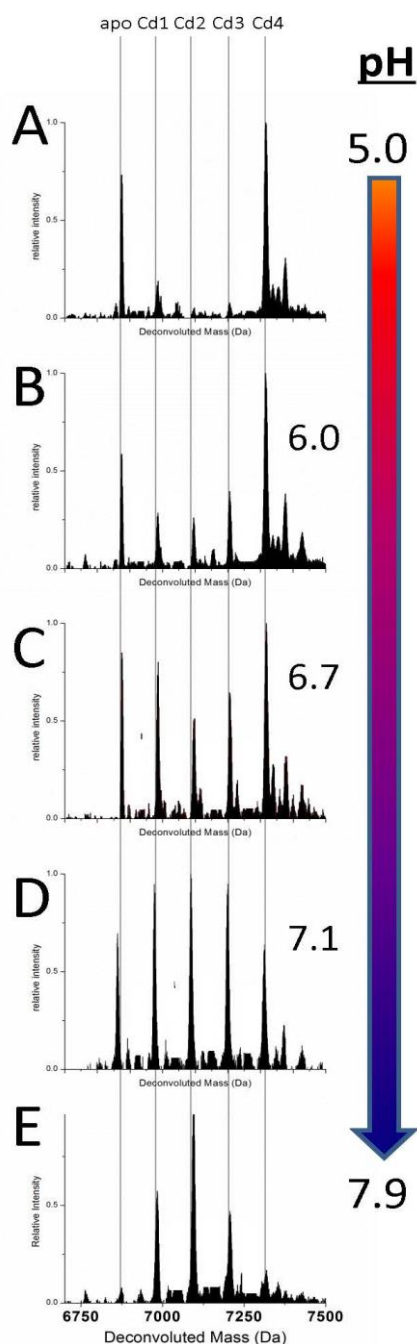


Figure 2-2: Representative ESI-MS data showing the relative abundances of Cd_xMT species ($x=0-4$) as a function of pH. These are representative spectra from pH titrations after an aliquot of approx. 2.5 molar equivalents of Cd(II) was added to the apoMT solution. The species distribution at pH 5.0 (A) and 6.0 (B) represent a mostly cluster-dominated pathway for metal binding. The spectra at pH 6.7 (C) shows a blend of the pathways, and at pH 7.1 (D) and 7.9 (E) a terminal binding pathway dominates. Adduct peaks with a mass of +60 Da were present for each species and were removed for clarity.

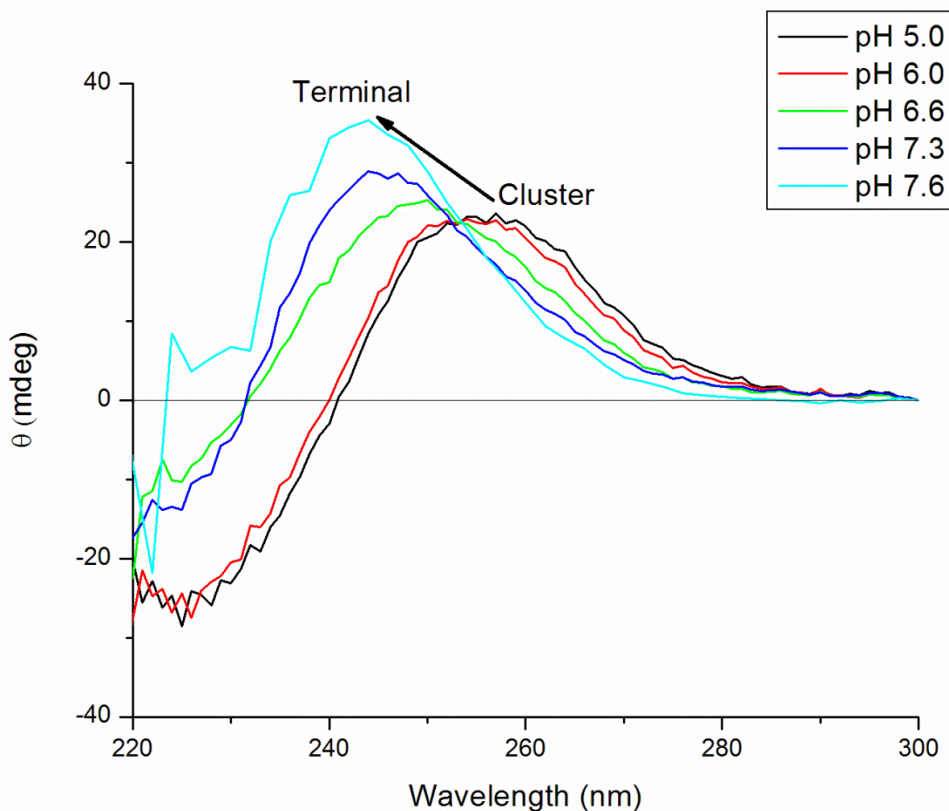


Figure 2-3: Circular dichroism spectra of apoMT1a with 2.5 mol. eq. of Cd(II) added as a function of increasing pH. The derivative envelope with a cross-over near 240 nm is characteristic of the Cd₄-cluster whereas the maximum dichroic intensity near 242 nm is characteristic of partially-metalated species with terminal thiolate coordination or supermetallated species.

The switch from cluster bound Cd(II) to terminally bound Cd(II) was observed in the circular dichroism (CD) spectra, Figure 2-3.⁵⁴⁻⁵⁷ When the Cd(II) are bound only as Cd₄α-clusters the spectra show a characteristic derivative envelope with a crossover point near 240 nm and a maximum near 260 nm. The shape of this CD envelope has been assigned previously as arising from exciton coupling of Cd(II) from the ligand to metal charge transfer band.⁵¹⁻⁵⁴ The spectrum shown here is a combination of contributions from apo-MT1a and the clustered intermediate, Cd₄-MT1a. As the pH is raised, the terminally bound contribution increases and the envelope from the clustered species disappears. This neutral pH spectra matches that of previous work where 1-3 mol. eq. Cd(II) had been added to mouse apo-MT1.⁵¹ When the cluster structure is disrupted by

either excess or insufficient Cd(II), the spectra is blue shifted, which can be observed in Figure 2-3. The CD spectral data correlate closely with the species measured in the ESI-mass spectra. The Cd₄ cluster, dominant at low pH in the ESI-MS data (Figure 2-2) is associated with the derivative envelope in Figure 2-3. The terminally bound Cd(II) at neutral pH exhibit a CD envelope centered on the absorption band of Cd-MT (240-250 nm). The CD data confirm that the gas phase, ESI-MS data are reporting the solution species accurately.

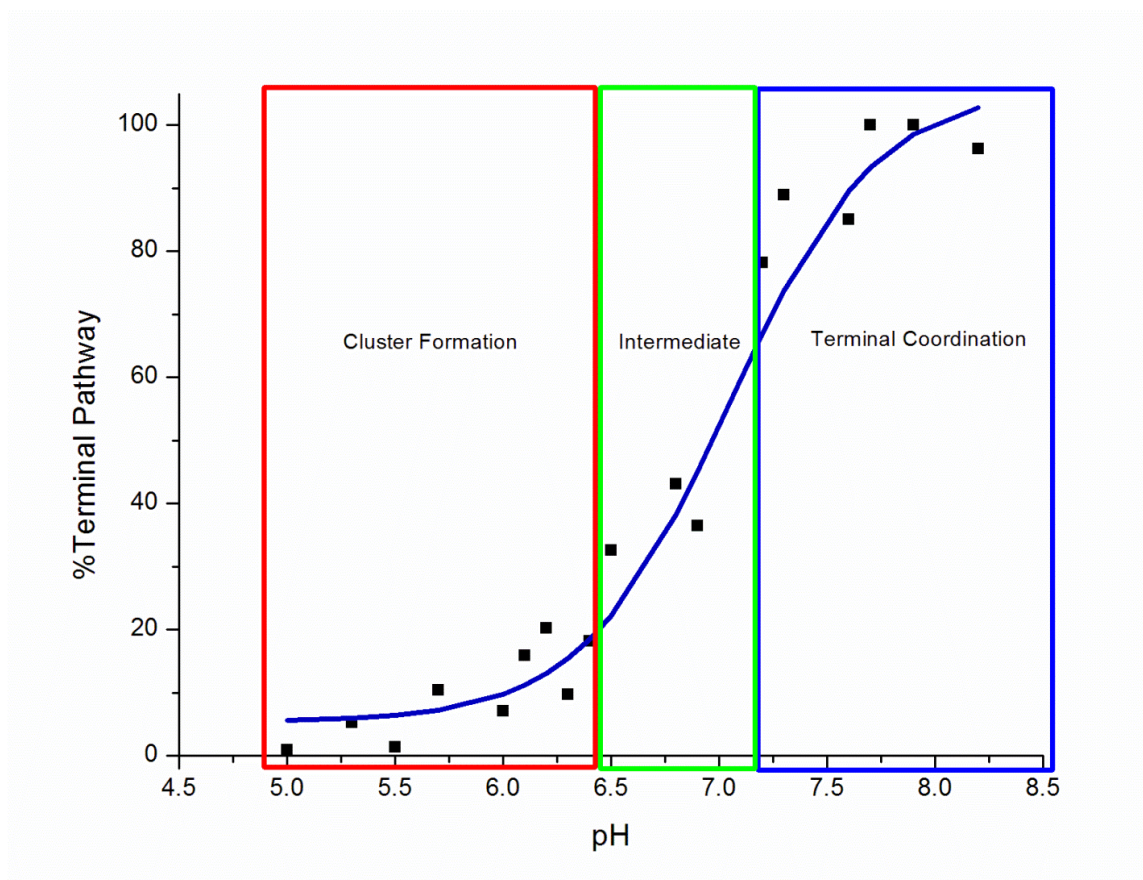


Figure 2-4: Change in cadmium binding pathway as a function of pH. The "% Terminal Pathway" was calculated from the ESI-MS data shown in Figure 2-2. The cluster formation pathway dominates below pH 6.5 (red box), between pH 6.5-7.2 (green) the two pathways compete and the terminal pathway based on "beads" dominates above pH 7.2 (blue).

The pH dependence of the Cd-metalation pathway is plotted in Figure 2-4. The trend is similar to a standard pH titration with a sharp change just before pH 7.0. Between pH 5.0-6.4 the change from cluster to terminal pathway is gradual, then the terminally-bound

fraction increases sharply between 6.5-7.2. The binding mechanism is mostly terminal above pH 7.2, the non-cooperative metalation pathway.

2.3.2 pH dependence of zinc binding to apo-MT1a

MT1a speciation during Zn(II) binding differs drastically from that of Cd(II) at all pH values, Figure 2-5. This is a very significant result when Cd(II) is considered as a model for Zn(II). Clustering does not become dominant to the extent that it does with the Cd(II) metalation at any pH tested here. Only at very low pH, less than 5.0, does some cluster formation (Zn_4S_{CYS11}) become evident. Even at this low pH, the Zn(II) spectra are comparable to the blended pathway shown in Figure 2-2B or C for Cd(II). Such a low pH (≤ 5.0) is not physiologically relevant except for in low pH cellular compartments such as the lysosome.⁵⁵⁻⁵⁶ Therefore, we can conclude that the Zn(II) binding pathway is dominated by the formation of terminally-bound Zn(II) intermediates (Figure 2-5B, C) over a physiologically relevant pH range, in sharp contrast to Cd(II) binding.

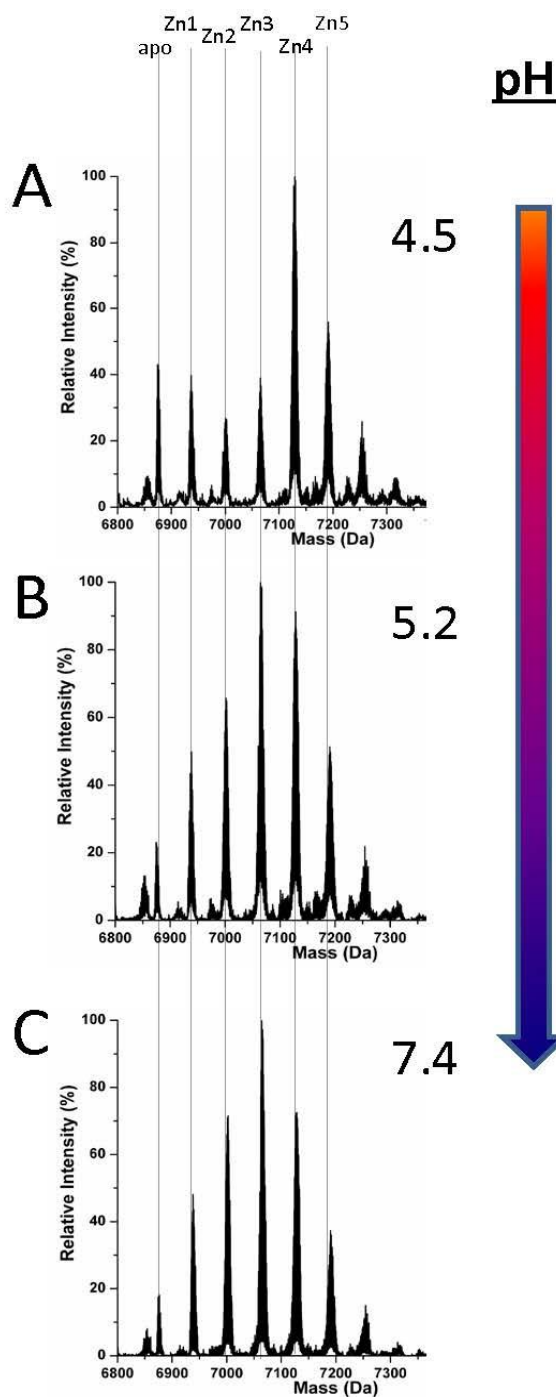


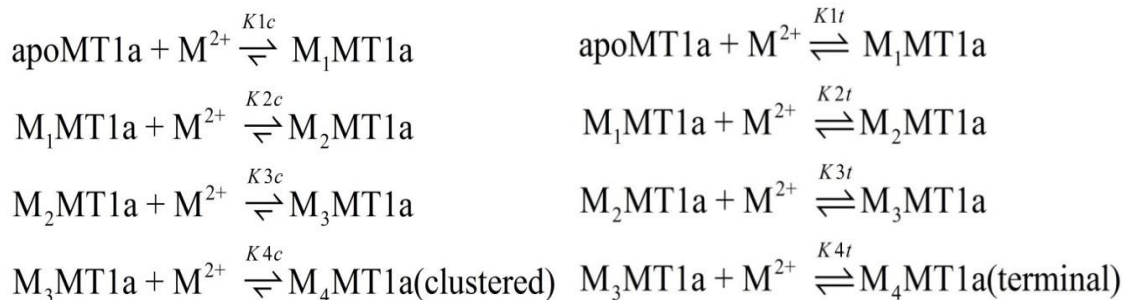
Figure 2-5: Representative deconvoluted ESI-MS spectra recorded during the pH titration of Zn_xMT (x=0-5) after approximately 2.5 equivalents of $Zn(II)$ had been added. The spectra at pH 4.5 (A) shows a mixed binding mechanism whereas by pH 5.2 (B) it is largely distributive and terminally bound remaining unchanged to pH 7.4 (C).

2.4 Discussion

The metalation mechanism of MT1a is critical to our understanding of its *in vivo* function and to the fundamental description of protein based metal-thiolate chemistry. MT1a provides a unique example of a highly flexible metal-binding protein that can coordinate many metals in a number of conformations. This flexibility makes defining a specific binding mechanism difficult as there may be many possible mechanisms and conformations that can be adopted. Adding to this difficulty, metallothioneins lack spectroscopic features common in other proteins like aromatic amino acids or well-defined secondary structural elements.⁵⁷ Thus, spectroscopically active metals like Cd(II) have been used as a model for Zn(II) binding which is more difficult to monitor. From the experiments presented here, we show that MT1a metalation can begin via two main pathways and that Zn(II) and Cd(II) show divergence in their pathway preference and pH sensitivity. The presence of a pH dependent equilibrium between structures of the partially metalated species has fundamental importance in the assessment of the role of MT1a *in vivo*.

2.4.1 The pH dependency of cadmium binding

The data shown in Figures 2-2 and 2-3 demonstrate the pH dependence of the Cd(II) binding pathway. The distributed pattern of the Cd₁₋₃-MT1a species at pH 7.9, and reported for more basic pH,³⁸ shows a stochastic distribution of metals over 7 possible binding sites. Scheme 1 shows the equilibria for the binding of the first four metals to MT with different Ks to indicate that the values of these constants change, depending on conditions, and control pathway selection.



Scheme 2-1: The possible metalation pathways for the first four metals bound to human MT1a. These pathways follow a clustered (cooperative mechanism) or beaded (terminally-bound, noncooperative) structure.

The declining stoichiometric binding constants ($K_1 > K_2 > K_3 > K_4$), calculated to fit the non-cooperative data are shown in Figure 2-6C. From the binding constants, simulated ESI-MS spectra were generated which closely match the experimental data. At pH 5.0, the data do not show a distributed pattern and we sought to replicate the experimental data by modifying the binding constants in the simulation. Figure 2-6A shows that an increasing series of binding constants ($K_1 < K_2 < K_3 < K_4$) generates a close fit to the low pH data. In Figure 2-6B the intermediate or mixed pathway is replicated by binding constants that are approximately equal. These simulations confirm the presence of two major, pH dependent metalation pathways: one leading to a clustered $\text{Cd}_4\text{-MT1a}$ and the other a series of terminally-bound $\text{Cd}_x\text{-MT1a}$ ($x=1-5$) species. The analysis shows that the pH controls pathway selection based on modification of the relative magnitude of the apparent binding constants associated with formation of bead or cluster structures. The important feature is the relative magnitude of the constants and the trend that they follow, not the absolute magnitude, as concentrations of each species were not directly measured through calibration with internal standards.

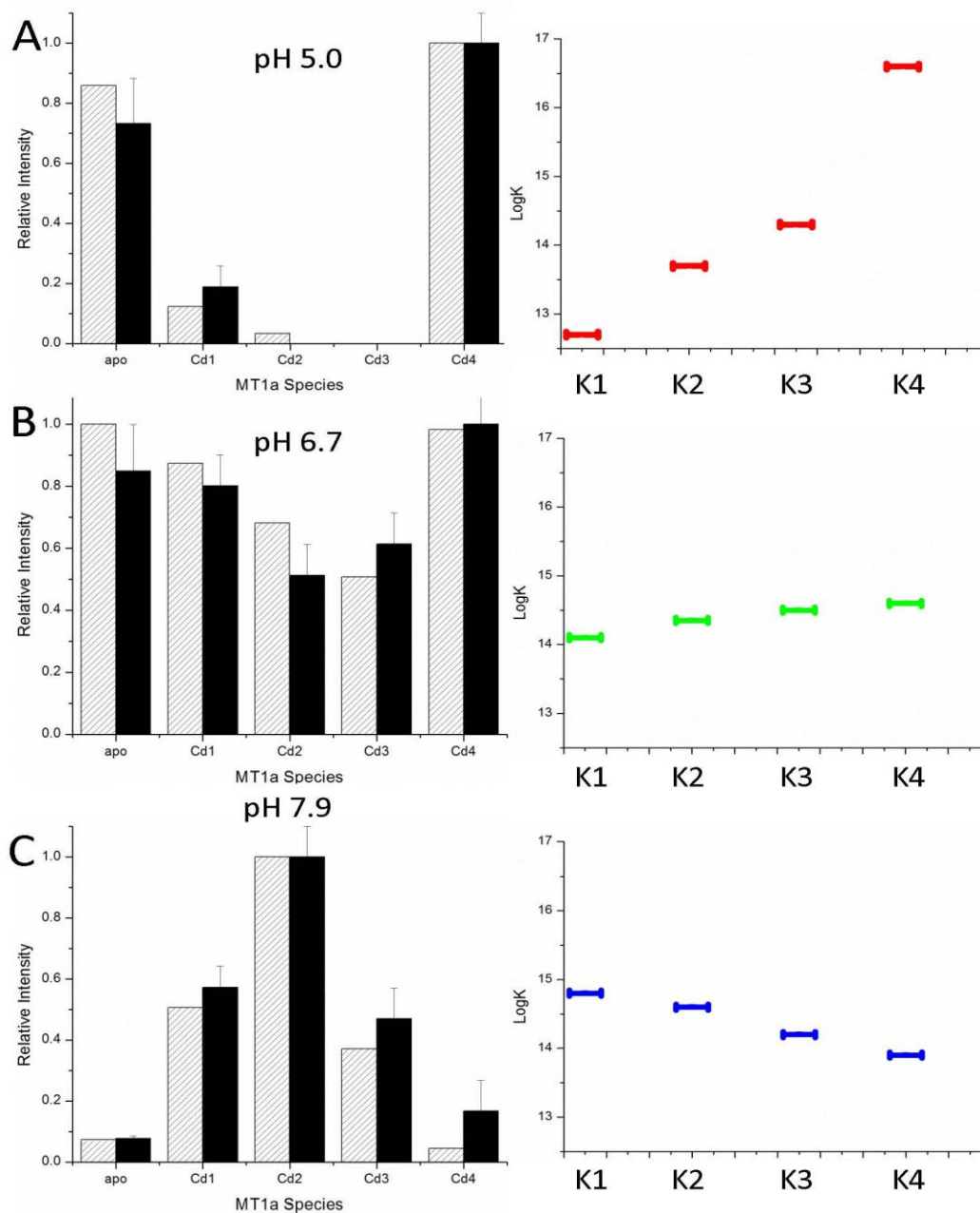


Figure 2-6: Simulated (hatched) and experimental (solid) ESI-MS data for binding of 2.5 mol. equivalent of Cd(II) to apo-MT1a at pH 5.0. (A), 6.7 (B) and 7.9(C). The experimental ESI-MS data are shown by the solid black bars and the simulated data by the hatched bars (left). The simulated data were calculated based on the relative log(K) values for 4 consecutive bimolecular reactions assuming 2.5 mol. eq. Cd(II) had been added. The log(K) values average to 14.4 in A-C, a value similar to that previously reported for the MT Cd-binding affinity.⁵⁰ The trend in the relative log(K) values are shown on the right. K1→K4 are the equilibrium constants for the addition of 1 to 4 Cd(II) to MT1a. It should be noted that these values are relatively correct but not absolute and decrease at lower pH.

2.4.2 pH dependency of the zinc binding pathway

The MT1a-Zn(II) binding pathway always proceeds via terminally-bound, beaded species near physiological pH. The pH sensitivity over a physiologically relevant range, as shown for the Cd(II) data, was not observed for Zn(II). The ESI-MS spectra for Zn(II)-binding (Figure 2-5) are essentially unchanged between pH 5.2 and 7.4. This means that the declining series of formation constants associated with the sequential Zn(II) metalation reactions are much less sensitive to pH and only begin to change below pH 5.2 which is not physiologically relevant. The pathway selection for the Zn(II) metalation is dominated by the non-cooperative, terminally-bound beaded structure. Figure 2-7, specific to Zn(II) binding, was generated in the same way as Figure 2-6 and gives an accurate description of the changes in K_f that are involved in pathway selection. Unlike for the Cd(II) data, the K_f values do not steadily increase for the lowest pH tested, but instead slightly increase then fall. This matches previous work that showed the last Zn(II) atoms are bound weakly by MT1a and are available for donation.⁴⁴

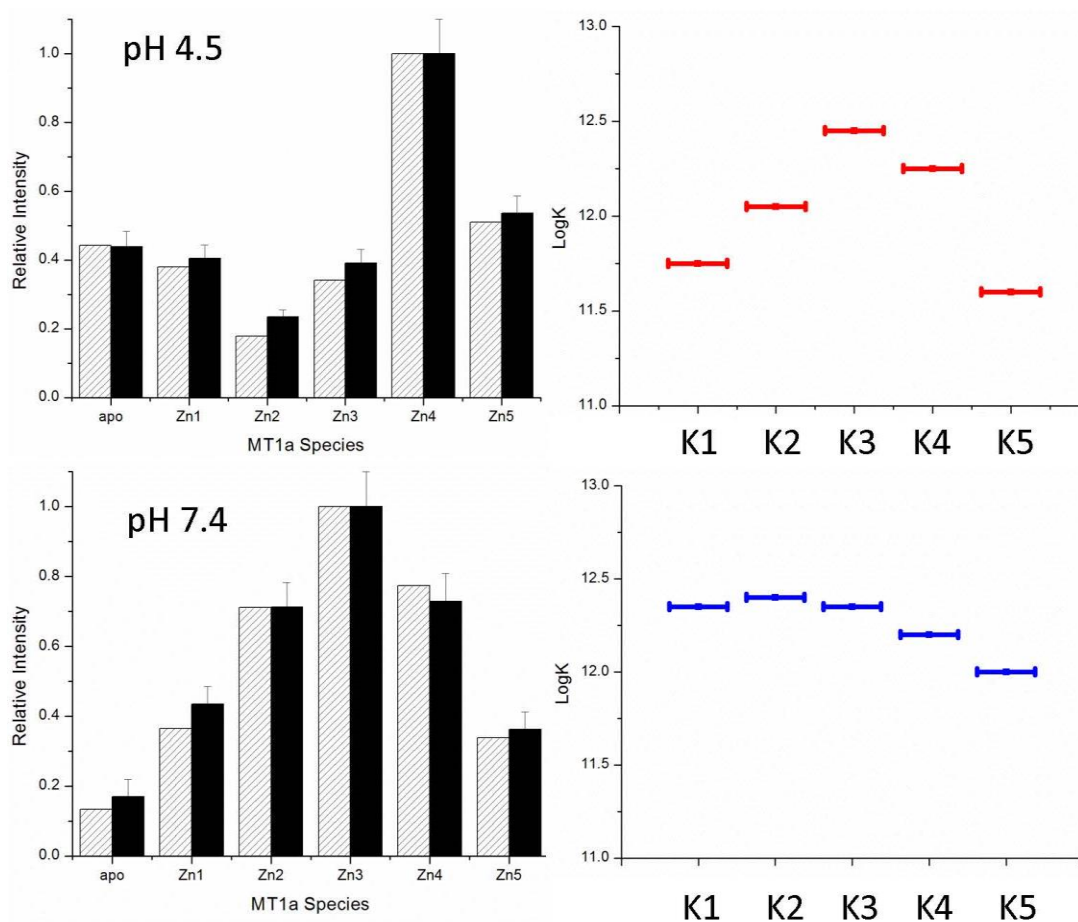


Figure 2-7: Simulated (hatched) and experimental (solid) ESI-MS data for MT metalation with 2.5 mol. equivalents of Zn(II) at pH 4.5 (A) and 7.4 (B). The simulated data were calculated using the relative log(K) values for 5 consecutive bimolecular reactions with relative log(K) values similar to those reported in the literature.⁴⁴

2.4.3 The divergent metalation pathway preferences for zinc and cadmium binding

Critical to the biological functions of MTs are the structures adopted when coordinating various metal ions. The proposed *in vivo* functions of MTs require this family of structurally homogenous proteins to bind essential and toxic metals for different purposes; namely to act as a metallochaperone for Zn(II) and Cu(I) while aiding in the detoxification of heavy metals like Hg(II) and Cd(II). On the surface, this appears to be a difficult task for a protein that lacks defined binding sites and formal secondary structure in the absence of bound metals. This is especially true for Zn(II) and Cd(II) since they

both preferentially adopt tetrahedral coordination geometries and both form $M_4\text{-Cys}_{11}$ and $M_3\text{-Cys}_9$ clusters in the α and β domains of MTs. Critical to the use of Cd(II) as a model for Zn(II) is that the two metals follow the same metalation pathway, form the same intermediates and exhibit similar structural properties. However, our results show that the assumption that the binding pathway is the same for both Zn(II) and Cd(II) is flawed.

Figure 2-8 shows the two competing pathways that account for the metalation of apo-MT1a to the fully metalated species. At slightly basic pH, Cd(II) passes through intermediates to form species similar to those shown in 2-8A and 2-8B before all Cys are involved in coordination and clustering must occur to accommodate further metal binding. At slightly acidic pH, Cd(II) metalation proceeds through the pathway shown by red arrows where the reaction is dominated by the formation of the Cd_4 -cluster structure. The metalation step leading to D may be part of a cooperative pathway that only features a clustered intermediate (2-8C) and a fully metalated, two-domain end-product (2-8E).

The pathway selection for Zn(II) is strongly biased towards the beaded pathway shown by the blue arrows in Figure 2-8. At very low pH, a mixture of the two pathways is seen with some clustering occurring but with a large fraction of $\text{Zn}_5\text{-MT1a}$ being formed, compared to the low pH Cd(II) titration where no $\text{Cd}_5\text{-MT1a}$ was observed. This suggests the presence of both clustered (2-8C) and terminally-bound species (2-8B) in equilibrium at low pH for Zn(II) metalation. The $\text{Zn}_4\text{-MT1a}$ cluster does not have a stability advantage over terminally bound $\text{Zn}_{1-5}\text{-MT1a}$. This supports our previous model where we suggested that Zn(II) binding to apo-MT1a results in a beaded structure with 5 terminally bound zinc.⁵⁸

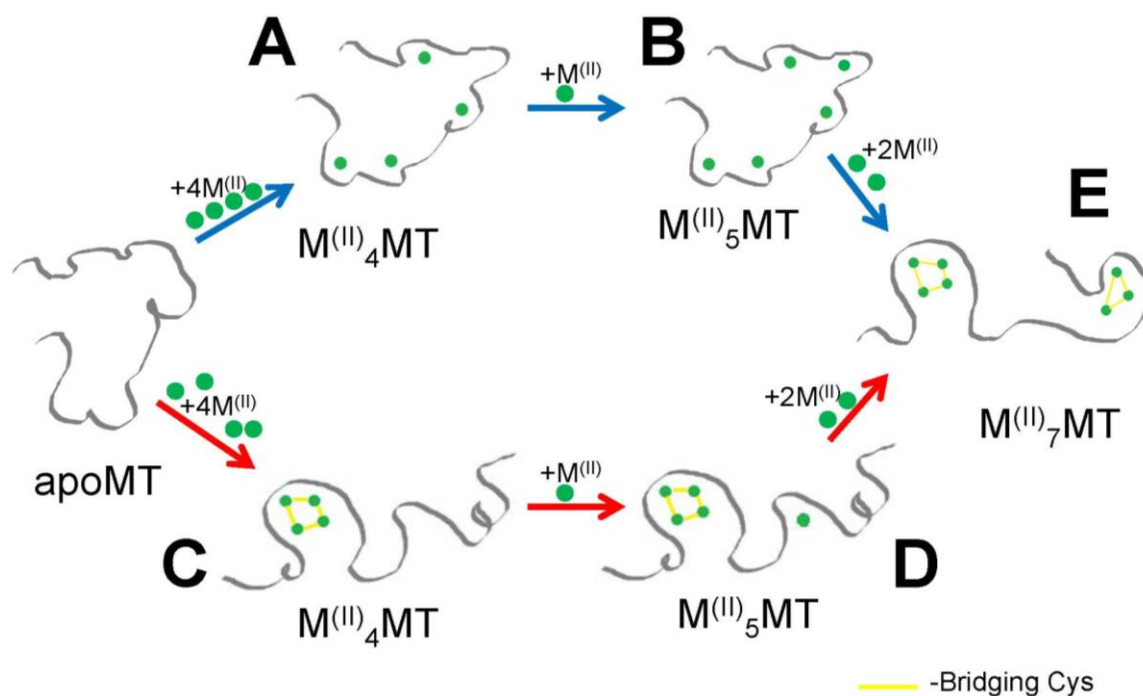


Figure 2-8: Representation of two possible pathways for MT1a metalation with Zn(II) or Cd(II). The cooperative cluster driven pathway (red arrows) and the noncooperative beaded pathway (blue arrows). The terminally-bound, beaded structure (A) is able to coordinate an additional metal terminally, forming (B), which utilizes all twenty Cys residues, after which clusters are formed to accommodate the last two metals and form the stable two-cluster M₇MT (E). The cooperatively formed cluster (C) must coordinate additional metals in the β -domain (D).

Figure 2-9 summarizes the experimental data and compares the pH dependence of the Zn(II) and Cd(II) metalation pathways. Significantly, at neutral pH there is a considerable contribution from the clustered pathway of Cd(II). This suggests that, *in vivo*, MT1a can sequester Cd(II) into clusters with relatively higher binding constants, making it less available for transfer to zinc-dependent enzymes which mostly involve terminal coordination.⁵⁹

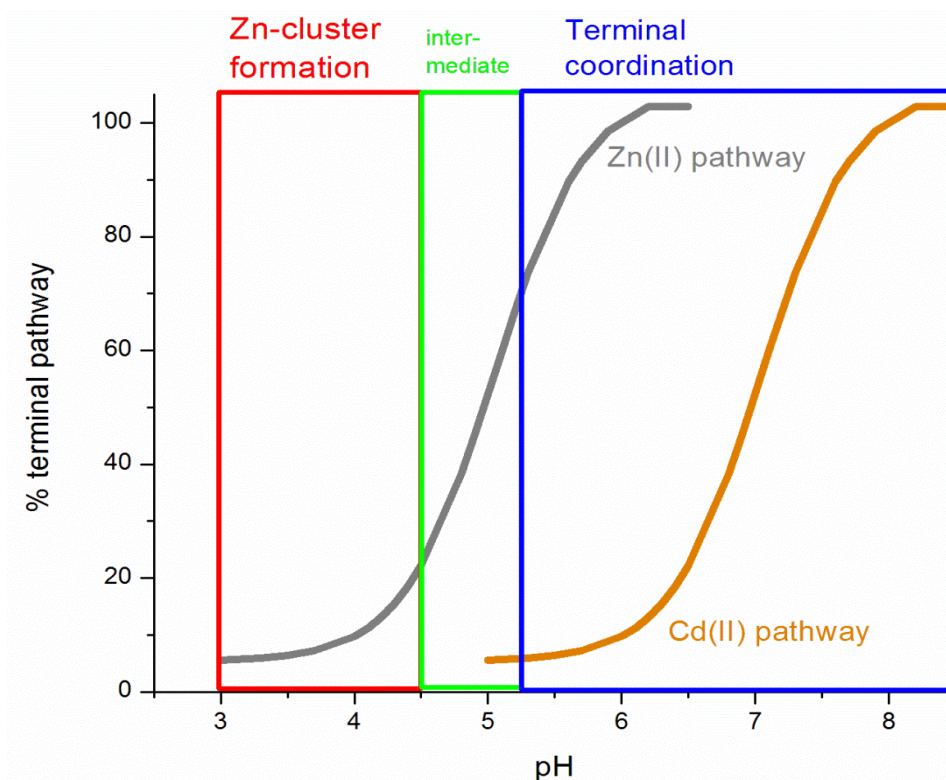


Figure 2-9: Change in Zn(II) metalation pathway as a function of pH (grey line) compared to Cd (orange line). Demetalation begins to occur at $\text{pH} < 4.5$ so the curve was extrapolated to $\text{pH} 3$ based on the Cd metalation data. At the lowest physiologically relevant pH around 5.5 the binding pathway is greater than 80% terminal (blue box) and only forms clusters below $\text{pH} 4.5$ (red box).

Cadmium completely switches pathway preference between $\text{pH} 6.5$ and 7.2 , where cluster formation is favored at lower pH and terminal coordination at higher pH. At lower pH, H^+ ions effectively compete with incoming metals for thiolates and the stability associated with the Cd_4 -thiolate cluster becomes the driving force behind cadmium binding. At higher pH, cadmium is bound terminally as the competition between metal and protons for thiolates is less intense.

In light of the results presented here, the use of exogenous metals as models for zinc and copper binding with respect to cluster formation need to be carried out with caution. Due to its spectroscopic properties, many studies on cluster formation in MT used Co(II) as a spectroscopic probe.^{25, 39, 60} Although Zn(II) and Cd(II) are both d^{10} metals, their Lewis acidities differ, resulting in chemistries that change the mechanism in which they are

bound by thiolates. It is likely that the differences between Zn(II) and Co(II) are even greater.

2.4.4 The origin of proton sensitivity of the beaded and clustered binding constants

The ESI-MS data show that the $[\text{Cd}_4(\text{Cys})_{11}]^{3-}$ cluster dominates as the primary metalation intermediate below pH 6.5 in the metalation of MT1a. DFT calculations of Ohanessian et al.⁶¹ on the proton affinities of thiolates in a wide range of zinc-thiolate compounds, have shown the terminal thiolates in $[\text{Zn}(\text{Cys})_4]^{2-}$ are significantly more basic than in the clustered $[\text{Zn}_4(\text{Cys})_{11}]^{3-}$. In our context, this suggests that the terminally-coordinated, beaded structures will be less stable under acidic conditions. We show the points at which the terminal structures become less stable in MT are approximately pH 5.0 for Zn(II) and 7.0 for Cd(II). The increased nephelauxetic effect or propensity for covalency of Cd(II) compared with Zn(II) supports the stability of the $[\text{Cd}_4(\text{Cys})_{11}\alpha\text{-clusters}]$ over terminally bound Cd(II) below neutral pH and the different speciation observed here by ESI-MS between Zn(II) and Cd(II) for partially metalated MT1a. (The nephelauxetic effect refers to the increased propensity for covalency going down the Zn-Cd-Hg triad.)

2.4.5 Understanding the multitude of biological functions of MT1a

The fact that Zn(II) does not cluster as readily as Cd(II) is relevant to its *in vivo* function. MT1a acts as a zinc-chaperone by delivering Zn(II) to newly synthesized metalloenzymes which requires a constant shuffling of metal ions.^{44, 62} This function is facilitated by terminally bound Zn(II), increasing accessibility for donation compared to the clustered form. On the other hand, the donation of Cd(II) often causes Zn-metalloenzymes to partially or completely lose function.⁶³⁻⁶⁵ By locking most of the Cd(II) in a cluster structure, donation may be discouraged. Only a small change in pH would induce clustering and many biological compartments have a pH well below 7.2 where clustering begins to take over as the preferred Cd-binding pathway.^{55-56, 66} This is especially true in the medulla and proximal tubules of the kidneys which are known to be at low pH.⁶⁷⁻⁶⁸ Cd(II) has also been shown to accumulate in those areas⁶⁹⁻⁷¹ and the

clustered MT1a may promote this accumulation. Wolff et al. have also demonstrated that Cd-MT is localized to lysosomes in proximal tubule cells, which is typically in the pH range that favors cluster formation.⁷² The clustered Cd-MT is also known to be more resistant to proteolysis than apo- or partially metalated MT.⁷³⁻⁷⁵ This resistance to degradation, especially in low pH compartment to which MT1a is localized, may provide a mechanism by which cadmium persists in the kidneys for long periods of time, with a half-life of 10-30 years.⁷⁶ Contrary to the concept of detoxification of heavy metals, this tendency to cluster and persist in the kidneys may cause more damage. It is for this reason that mammalian MTs are not thought of as being "real" cadmium detoxifiers, but bind cadmium as a secondary, intrinsic property which exacerbates the toxicity in mammalian systems.

In addition to specialized cells that are typically found at slightly acidic pH, organelles responsible for protein maturation, such as the golgi, are also slightly acidic (pH 6.4-7.0).⁷⁷ With Zn-MTs being less prone to clustering under acidic conditions, they would still be able to effectively donate zinc ions to maturing metalloproteins. The clustering of Cd-MTs at these pH ranges may provide a mechanism of protection by which the maturing metalloproteins are not improperly metalated with cadmium.

In addition to metal sequestration, MTs play a role in cellular redox chemistry due to its abundance of thiols.⁷⁸ For these thiols to be active they need to be exposed, so only apo- and partially metalated proteins in the MT pool are redox active.⁷⁹ The higher propensity to cluster in slightly acidic environments exposes more thiols which may affect cellular redox balance. This role as a redox active species is not necessarily separate from its main function as a zinc chaperone, and many reports have shown that these functions are intrinsically linked.^{21, 80}

2.4.6 Importance of pH control during experimental measurements

Figures 2-4 and 2-7 highlight the potential complication when determining the metal speciation of MT, particularly when partially metalated, due to the pH effect on intermediate formation. For example, during Cd(II) metalation, a slight change in pH from 7.2 to 7.0 results in a large increase in the cluster pathway contribution.

Experimentally, this small pH change could be caused by the displacement of cysteinyl protons during metalation so it is essential to monitor pH before and after each metal addition. It is also clear that this is much less of a problem during Zn(II) metalation because of the decreased pH sensitivity at physiological pH. MT also binds a number of exogenous heavy metals involved in chemotherapeutics⁸¹⁻⁸³ and water contamination⁸⁴ and the pH considerations raised in this chapter likely apply to other MT-metal binding systems. Similar metalation experiments with human MT2a show a mixed mechanism at pH 7.4³⁰ and rabbit liver MT2a has been shown by NMR to cluster at pH 7.2, with the signal disappearing at higher pH.²⁶ The pH dependence curve can likely be modestly shifted for different isoforms of MT. Indeed small differences in binding properties were found between human MT2 and MT3 isoforms, although the overall trend remained the same.⁸⁵

2.5 Conclusions

The considerable debate in the literature over the mechanisms behind MT metalation can be reconciled by the results presented in this chapter. MT1a can bind Cd(II) and, to a lesser degree, Zn(II) via two distinct pathways that feature either a cooperative (clustered) or non-cooperative (beaded) mechanism. Thus, the discrepancy between experimental results was likely due to small changes in pH conditions and the specific pH at which the cluster pathway dominates for each MT isoform.

Of the two metalation pathways presented here, Zn(II) has a clear preference for the non-cooperative, terminally-coordinated pathway under most pH conditions. The trend in K_f values associated with Zn(II) metalation of MT is largely unchanged over the range of physiologically relevant pH where most experiments are carried out. In contrast, Cd(II) showed a change in pathway preference between pH 6.8-7.2 where clustering became dominant at slightly acidic pH. This highlights the potential pitfalls in using Cd(II) as a model for Zn(II) binding.

The pH dependence of metal binding pathway and the structures adopted in those pathways provide insight into how MT functions as a metallochaperone (for Zn(II)) and sequesters toxic Cd(II). The cluster binds Cd(II) with a high affinity preventing the

donation to lower affinity, terminal sites for Cd(II) coordination. This structure, resistant to degradation, may provide the mechanism by which Cd(II) persists in lower pH compartments in renal cells for many years. For Zn(II), these results strengthen our previously proposed model, where the terminally-coordinated beaded structure is dominant and the Zn₅-MT species is more stable compared to the clustered structures. The last two Zn(II) are bound weakly and can easily be donated to other metalloenzymes.

2.6 References

1. V. Hodgkinson and M. J. Petris, *J. Biol. Chem.*, 2012, 287, 13549-13555.
2. D. E. Sutherland and M. J. Stillman, *Metallomics*, 2011, 3, 444-463.
3. R. A. Festa and D. J. Thiele, *Curr. Biol.*, 2011, 21, R877-R883.
4. K. Balamurugan and W. Schaffner, *Biochim. Biophys. Acta, Mol. Cell Res.*, 2006, 1763, 737-746.
5. T. Miyayama, Y. Ishizuka, T. Iijima, D. Hiraoka and Y. Ogra, *Metallomics*, 2011, 3, 693-701.
6. E. Artells, Ò. Palacios, M. Capdevila and S. Atrian, *FEBS J.*, 2014, 281, 1659-1678.
7. F. Carmona, D. Mendoza, S. Kord, M. Asperti, P. Arosio, S. Atrian, M. Capdevila and J. M. Dominguez- Vera, *Chem.-Eur. J.*, 2015, 21, 808-813.
8. C. A. Blindauer, *Chem. Commun.*, 2015, 51, 4544-4563.
9. J. D. Park, Y. Liu and C. D. Klaassen, *Toxicology*, 2001, 163, 93-100.
10. A. M. Ronco, F. Garrido and M. N. Llanos, *Toxicology*, 2006, 223, 46-53.
11. E. Grill, E.-L. Winnacker and M. H. Zenk, *Proc. Natl. Acad. Sci. U. S. A.*, 1987, 84, 439-443.
12. M. Vašák and D. W. Hasler, *Curr. Opin. Chem. Biol.*, 2000, 4, 177-183.

13. Y. Kondo, S.-M. Kuo, S. C. Watkins and J. S. Lazo, *Cancer Res.*, 1995, 55, 474-477.
14. L. Galluzzi, L. Senovilla, I. Vitale, J. Michels, I. Martins, O. Kepp, M. Castedo and G. Kroemer, *Oncogene*, 2012, 31, 1869-1883.
15. R. J. Person, N. N. O. Ngalame, N. L. Makia, M. W. Bell, M. P. Waalkes and E. J. Tokar, *Toxicol. Appl. Pharmacol.*, 2015, 36-43.
16. D. E. Sutherland, M. J. Willans and M. J. Stillman, *J. Am. Chem. Soc.*, 2012, 134, 3290-3299.
17. W. Maret, *Exp. Gerontol.*, 2008, 43, 363-369.
18. S. G. Bell and B. L. Vallee, *ChemBioChem*, 2009, 10, 55-62.
19. H. Gonzalez-Iglesias, L. Alvarez, M. García, C. Petrash, A. Sanz-Medel and M. Coca-Prados, *Metallomics*, 2014, 6, 201-208.
20. W. Qu and M. P. Waalkes, *Toxicol. Appl. Pharmacol.*, 2015, 282, 267-274.
21. W. Maret, *J. Nutr.*, 2000, 130, 1455S-1458S.
22. W. Braun, M. Vasak, A. Robbins, C. Stout, G. Wagner, J. Kägi and K. Wüthrich, *Proc. Natl. Acad. Sci. U. S. A.*, 1992, 89, 10124-10128.
23. G. W. Irvine, K. E. Duncan, M. Gullons and M. J. Stillman, *Chem.-Eur. J.*, 2015, 21, 1269-1279.
24. J. Ejnik, J. Robinson, J. Zhu, H. Försterling, C. F. Shaw and D. H. Petering, *J. Inorg. Biochem.*, 2002, 88, 144-152.
25. I. Bertini, C. Luchinat, L. Messori and M. Vasak, *J. Am. Chem. Soc.*, 1989, 111, 7296-7300.
26. M. Good, R. Hollenstein, P. J. Sadler and M. Vasak, *Biochemistry*, 1988, 27, 7163-7166.

27. S.-H. Chen, L. Chen and D. H. Russell, *J. Am. Chem. Soc.*, 2014, 136, 9499-9508.
28. G. W. Irvine and M. J. Stillman, *Biochem. Biophys. Res. Commun.*, 2013, 441, 208-213.
29. K. E. Rigby and M. J. Stillman, *Biochem. Biophys. Res. Commun.*, 2004, 325, 1271-1278.
30. S.-H. Chen, W. K. Russell and D. H. Russell, *Anal. Chem.*, 2013, 85, 3229-3237.
31. T. T. Ngu, A. Easton and M. J. Stillman, *J. Am. Chem. Soc.*, 2008, 130, 17016-17028.
32. C. A. Blindauer, *J. Inorg. Biochem.*, 2013, 121, 145-155.
33. C. Afonso, Y. Hathout and C. Fenselau, *Int. J. Mass Spectrom.*, 2004, 231, 207-211.
34. M. Vaheer, N. Romero-Isart, M. Vašák and P. Palumaa, *J. Inorg. Biochem.*, 2001, 83, 1-6.
35. K. E. Duncan and M. J. Stillman, *FEBS J.*, 2007, 274, 2253-2261.
36. P. Palumaa, E. Eriste, O. Njunkova, L. Pokras, H. Jörnvall and R. Sillard, *Biochemistry*, 2002, 41, 6158-6163.
37. P. M. Gehrig, C. You, R. Dallinger, C. Gruber, M. Brouwer, J. H. KÄGI and P. E. Hunziker, *Protein Sci.*, 2000, 9, 395-402.
38. D. E. Sutherland and M. J. Stillman, *Biochem. Biophys. Res. Commun.*, 2008, 372, 840-844.
39. M. Vasak, *J. Am. Chem. Soc.*, 1980, 102, 3953-3955.
40. A. M. M. van Roon, J. C. Yang, D. Mathieu, W. Bermel, K. Nagai and D. Neuhaus, *Angew. Chem.*, 2015, 127, 4943-4946.

41. W. R. Bernhard, M. Vasak and J. H. Kagi, *Biochemistry*, 1986, 25, 1975-1980.
42. A. Krężel and W. Maret, *J. Am. Chem. Soc.*, 2007, 129, 10911-10921.
43. E. Artells, Ò. Palacios, M. Capdevila and S. Atrian, *Metallomics*, 2013, 5, 1397-1410.
44. T. B. Pinter and M. J. Stillman, *Biochemistry*, 2014, 53, 6276-6285.
45. H. Baba, K. Tsuneyama, M. Yazaki, K. Nagata, T. Minamisaka, T. Tsuda, K. Nomoto, S. Hayashi, S. Miwa and T. Nakajima, *Mod. Pathol.*, 2013, 26, 1228-1234.
46. J. Loebus, B. Leitenmaier, D. Meissner, B. Braha, G.-J. Krauss, D. Dobritzsch and E. Freisinger, *J. Inorg. Biochem.*, 2013, 127, 253-260.
47. J. Chan, Z. Huang, I. Watt, P. Kille and M. J. Stillman, *Can. J. Chem.*, 2007, 85, 898-912.
48. M. J. Stillman, *Coord. Chem. Rev.*, 1995, 144, 461-511.
49. K. E. Duncan, C. W. Kirby and M. J. Stillman, *FEBS J.*, 2008, 275, 2227-2239.
50. D. W. Hasler, L. T. Jensen, O. Zerbe, D. R. Winge and M. Vašák, *Biochemistry*, 2000, 39, 14567-14575.
51. N. Cols, N. Romero-Isart, M. Capdevila, B. Oliva, P. González-Duarte, R. González-Duarte and S. Atrian, *J. Inorg. Biochem.*, 1997, 68, 157-166.
52. W. Lu and M. J. Stillman, *J. Am. Chem. Soc.*, 1993, 115, 3291-3299.
53. M. Stillman, W. Cai and A. Zelazowski, *J. Biol. Chem.*, 1987, 262, 4538-4548.
54. J. Pande, C. Pande, D. Gilg, M. Vasak, R. Callender and J. Kägi, *Biochemistry*, 1986, 25, 5526-5532.
55. N. Demarex, *Physiology*, 2002, 17, 1-5.

56. C. Settembre, A. Fraldi, D. L. Medina and A. Ballabio, *Nat. Rev. Mol. Cell Biol.*, 2013, 14, 283-296.
57. S.-H. Hong, Q. Hao and W. Maret, *Prot. Eng. Des. Sel.*, 2005, 18, 255-263.
58. K. L. Summers, D. E. Sutherland and M. J. Stillman, *Biochemistry*, 2013, 52, 2461-2471.
59. W. Maret, *BioMetals*, 2011, 24, 411-418.
60. G. Meloni, K. Zovo, J. Kazantseva, P. Palumaa and M. Vašák, *J. Biol. Chem.*, 2006, 281, 14588-14595.
61. G. Ohanessian, D. Picot and G. Frison, *Int. J. Quantum Chem.*, 2011, 111, 1239-1247.
62. Y. Hathout, D. Fabris and C. Fenselau, *Int. J. Mass Spectrom.*, 2001, 204, 1-6.
63. D. R. Holland, A. C. Hausrath, D. Juers and B. W. Matthews, *Protein Sci.*, 1995, 4, 1955-1965.
64. S. Y. Lo, C. E. Säbel, M. I. Webb, C. J. Walsby and S. Siemann, *J. Inorg. Biochem.*, 2014, 140, 12-22.
65. M. F. Dunn, H. Dietrich, A. K. MacGibbon, S. C. Koerber and M. Zeppezauer, *Biochemistry*, 1982, 21, 354-363.
66. R. Gagescu, N. Demaurex, R. G. Parton, W. Hunziker, L. A. Huber and J. Gruenberg, *Mol. Biol. Cell*, 2000, 11, 2775-2791.
67. J. Kleinman, W. Brown, R. Ware and J. Schwartz, *Am. J. Physiol. Renal. Physiol.*, 1980, 239, F440-F444.
68. N. Raghunand, C. Howison, A. D. Sherry, S. Zhang and R. J. Gillies, *Magn. Reson. Med.*, 2003, 49, 249-257.

69. C. Erfurt, E. Roussa and F. Thévenod, *Am. J. Physiol. Cell. Physiol.*, 2003, 285, C1367-C1376.
70. G. Nordberg, R. Goyer and M. Nordberg, *Arch. Pathol.*, 1975, 99, 192-197.
71. C. Dorian, V. H. Gattone and C. D. Klaasen, *Toxicol. Appl. Pharmacol.*, 1992, 114, 173-181.
72. N. A. Wolff, W.-K. Lee and F. Thévenod, *Toxicol. Lett.*, 2011, 203, 210-218.
73. K. B. Nielson, C. Atkin and D. Winge, *J. Biol. Chem.*, 1985, 260, 5342-5350.
74. K. B. Nielson and D. Winge, *J. Biol. Chem.*, 1985, 260, 8698-8701.
75. D. Winge and K.-A. Miklossy, *J. Biol. Chem.*, 1982, 257, 3471-3476.
76. L. Järup and A. Åkesson, *Toxicol. Appl. Pharmacol.*, 2009, 238, 201-208.
77. J. Llopis, J. M. McCaffery, A. Miyawaki, M. G. Farquhar and R. Y. Tsien, *Proc. Natl. Acad. Sci. U. S. A.*, 1998, 95, 6803-6808.
78. B. Ruttkay-Nedecky, L. Nejdil, J. Gumulec, O. Zitka, M. Masarik, T. Eckschlager, M. Stiborova, V. Adam and R. Kizek, *Int. J. Mol. Sci.*, 2013, 14, 6044-6066.
79. D. H. Petering, J. Zhu, S. Krezoski, J. Meeusen, C. Kiekenbush, S. Krull, T. Specher and M. Dughish, *Exp. Biol. Med.*, 2006, 231, 1528-1534.
80. W. Maret, *J. Nutr.*, 2003, 133, 1460S-1462S.
81. A. Casini, A. Karotki, C. Gabbiani, F. Rugi, M. Vašák, L. Messori and P. J. Dyson, *Metallomics*, 2009, 1, 434-441.
82. J. Lecina, Ò. Palacios, S. Atrian, M. Capdevila and J. Suades, *J. Biol. Inorg. Chem.*, 2014, 465-474.
83. L. Liu, B. E. Rogers, N. Aladyshkina, B. Cheng, S. J. Lokitz, D. T. Curiel and J. M. Mathis, *Mol. Imaging*, 2014, 13, 1-12.

84. A. P. Esser-Kahn, A. T. Iavarone and M. B. Francis, *J. Am. Chem. Soc.*, 2008, 130, 15820-15822.
85. P. Palumaa, I. Tammiste, K. Kruusel, L. Kangur, H. Jörnvall and R. Sillard, *Biochim. Biophys. Acta -Prot. Proteom.*, 2005, 1747, 205-211.

Chapter 3

3 Cadmium binding mechanisms of the isolated domains of human MT1a: non-cooperative terminal sites and cooperative clusters²

3.1 Introductions

Mammalian metallothioneins (MTs) are a family of cysteine-rich proteins associated with essential metal homeostasis and heavy metal detoxification.¹⁻⁵ When fully metalated, the 20 cysteine protein forms two distinct domains, a 9-cysteine N-terminal domain (β) and an 11-cysteine C-terminal domain (α).⁶ When fully metalated with seven divalent metals, the β -domain forms an M_3Cys_9 cluster and the α -domain forms an M_4Cys_{11} cluster.⁷ While structures of the fully metalated species are well-known,⁸ the partially-metalated and apo-structures are fluxional and hard-to-characterize.⁹ Thus, the metalation mechanisms and the factors influencing the metalation pathways of apo-MT1a remain unclear.¹⁰ These mechanisms are essential to our understanding of *in vivo* metalation processes that control the homeostatic role¹, toxic metal responses¹¹ and the resistance to metal-based chemotherapeutics associated with cellular metallothioneins.¹²⁻¹⁵

The well-known description of the clustered domain structure for MT only applies to the metalated structures after cluster formation but is not accurate in describing the structure of apo- and partially-metalated MT species.⁹ To investigate the properties of the

² A version of this chapter has been published.

Reproduced with permission from: Irvine, Gordon W., and Martin J. Stillman. "Cadmium binding mechanisms of isolated domains of human MT isoform 1a: Non-cooperative terminal sites and cooperative cluster sites." *Journal of inorganic biochemistry* 158 (2016): 115-121.

Copyright 2016 Elsevier

individual domains of MT, the isolated domain fragments can be used and metalation studies carried out to determine the behaviour of the individual domains.¹⁶ It should be noted that the isolated domains may have different properties than when joined by the linker sequence due to the possibility of entropic effects in cluster formation and protein folding and also due to inter-domain exchange of metals.¹⁷⁻¹⁹ However, the underlying metal binding structures are the same for the full-length protein and the two isolated domain fragments, namely terminally bound metals at low metal concentrations leading to clustered domains at saturation. For this reason, examining the isolated domains of MT allows separation of the domain specific spectral properties which are blurred in the complete protein.

MT simultaneously functions as a zinc and copper chaperone, a heavy metal chelator and a redox active agent.²⁰⁻²² There have been suggestions that different isoforms bind specific metals and have their own unique functions, despite high sequence similarity.²³ Domain specificity of metal binding also remains a controversial topic in the field.²⁴⁻³⁰ The MT1 and MT2 isoforms are the most widely expressed in human tissues³¹⁻³² and likely most important isoforms for overall metal homeostasis. They have also been implicated in arsenic induced oxidative stress and cancers³³⁻³⁴ and tumor resistance to chemotherapeutics.³⁵ Many chemotherapeutics are metal-based so determining the binding mechanisms operating at all levels of metalation of MT is important for an overall description of its many functions *in vivo*.^{12-13, 15, 36}

Electrospray ionization mass spectrometry (ESI-MS) has emerged as one of the most useful tools for answering questions about MT structure, dynamics and metalation mechanisms.³⁷⁻⁴⁰ This is due to the ability of ESI-MS to distinguish all species in solution

with different masses (ie. different numbers of metals bound) and to give semi-quantitative information on their relative abundances.²⁴ The ionization efficiency of different metal loadings of the same isoform is essentially the same for MTs and thus the relative abundances can be relied upon to accurately reflect solution conditions.⁴¹⁻⁴²

In this chapter we have studied metalation of the isolated α - and β -domains of human MT1a to determine parameters that change the cadmium binding mechanism resulting in either terminally-coordinated or clustered metal binding sites. It is known that the mechanism of the metalation of the full protein is pH-dependent^{24, 43} but little is known about the individual domain responses to changes in pH. Biologically, MT-1a is upregulated in response to cadmium intoxication, due to displacement of Zn from Zn-MT and this newly synthesized apo-MT can be metalated by cadmium.⁴⁴⁻⁴⁵ We also reconcile conflicting reports about MT metalation mechanisms and show significant differences in binding preferences for the individual domains of human MT-1a.

3.2 Methods

3.2.1 Protein preparation

Individual domain fragments of recombinant human metallothionein 1a (β : MGKAAAACSC ATGGCTCTG SCKCKECKCN SCKKAAAA, α : MGKAAAAC CSCCPMSCAK CAQGCVCKGA SEKCSCKKA AAA) were expressed separately with an S-tag in BL21 *E. coli* cells which has been described in detail elsewhere.⁴⁶ In brief, cells containing the plasmid were grown on kanamycin containing media from a stock culture and grown for 16 hours at 37°C. The colonies were then inoculated into 4x1L broth cultures enriched with 50 μ L of 1 M cadmium and incubated in a shaker for

approximately 4 hours until an absorbance of 0.8 at 600 nm was reached. Isopropyl β -D-1-thiogalactopyranoside (IPTG) was then added to induce expression of MT and 30 minutes later 150 μ L of 1 M cadmium sulfate solution was added to the broth. The cells were collected 3.5 hours after induction, centrifuged and stored at -80°C .

The recombinant cells were lysed using a cell disruptor (Constant Systems, UK) at 20,000 psi. Then, the cell lysate was centrifuged for 1 h to remove cellular debris. The supernatant was filtered and loaded on to a GE healthcare SP ion exchange column with a total volume of 10 mL. The columns were washed with 10 mM Tris(tris-hydroxymethyl-aminomethane) buffer at pH 7.4 for approximately 2 h to remove loosely bound proteins and other organic compounds. The MT fragments were eluted using an increasing gradient of 1 M NaCl + 10 mM Tris buffer at pH 7.4. The eluted MT was concentrated down to <20 mL and the S-tag cleaved using a Thrombin Clean-Cleave kit as per the manufacturers' instructions (Sigma-Aldrich). The mixture was then diluted, desalted and placed on another SP ion exchange column. The S-tag was eluted at low salt concentrations with MT eluting at higher concentrations. The isolated MT fragments were concentrated to approximately 100 μ M and stored at -20°C .

To prepare MT for the pH titration experiments, aliquots were first demetalated and desalted using centrifugal filter tubes with a 3 kDa membrane (Millipore) and a 10 mM pH 2.8 ammonium formate buffer. The low pH solutions contained 1 mM dithiothreitol (DTT) to prevent oxidation of the free thiols in MT. The pH was raised by buffer exchange with argon saturated, pH 7.0 10 mM ammonium formate solutions that did not contain DTT. The concentrations of the protein solutions were checked by remetalation of a small aliquot with cadmium using the metal-to-ligand charge transfer band at 250 nm

($\alpha\epsilon_{250} = 45,000 \text{ M}^{-1} \text{ cm}^{-1}$ $\beta\epsilon_{250} = 36,000 \text{ M}^{-1} \text{ cm}^{-1}$). The solutions were also monitored for oxidation using UV-visible absorption spectroscopy at 280 nm. MT concentrations used were 40-90 μM to ensure good signal-to-noise ratios. In addition to demetalating MT in the presence of DTT, the solutions were vacuum degassed and bubbled with argon to displace any dissolved oxygen. This was done for the 10 mM Cd^{2+} , 0.5% NH_3 and 0.5% formic acid solutions as well to ensure no oxygen was introduced into the system during the titration.

3.2.2 ESI-MS pH titrations

Mass spectra were collected on a micrOTOF II electrospray-ionization time-of-flight mass spectrometer (Bruker Daltonics) in the positive ion mode. NaI was used as the mass calibrant. The scan conditions for the spectrometer were: end plate offset, -500 V ; capillary, $+4200 \text{ V}$; nebulizer, 2.0 bar; dry gas flow, 8.0 L min^{-1} ; dry temperature, $30 \text{ }^\circ\text{C}$; capillary exit, 180 V ; skimmer 1, 22.0 V ; hexapole 1, 22.5 V ; hexapole RF, 600 Vpp ; skimmer 2, 22 V ; lens 1 transfer, $88 \mu\text{s}$; lens 1 pre-pulse storage, $23 \mu\text{s}$. The mass range was $500.0\text{--}3000.0 \text{ m/z}$. Spectra were assembled and deconvoluted using the Bruker Compass data analysis software package.

For the metalation experiment, Cd(II) acetate was added sequentially to the MT solution and a spectrum recorded for each step. The metalation caused a drop in pH due to the displacement of H^+ from the thiol groups so the pH was monitored and adjusted as needed throughout the titration. The pH was confirmed using a micro-pH probe (Accumet).

In addition to metal titrations, a pH titration was carried out at the mid-point of the metal titration to monitor the change in metal distribution as a function of pH. Solutions of oxygen-free 0.5% NH_4OH and formic acid were used to adjust the pH. ESI-MS spectra were recorded for each change in pH. In total, 4 replicate pH titrations were taken for each fragment. No change in the overall the M^{2+}/MT ratio was observed meaning no precipitation of $\text{Cd}(\text{OH})_2$ occurred. The error associated with these ESI-MS measurements is estimated to be about $\pm 10\%$ and the error associated with the pH probe is ± 0.1 pH unit.

3.2.3 Circular dichroism pH titrations

For the circular dichroism (CD) spectra 1.5 molar equivalents of cadmium acetate were added to apo- αMT and apo- βMT in a pH 7.0 10 mM ammonium formate solution. The CD spectra (Jasco J810, New Jersey) were measured over the range of 200-310 nm at various pH points. At low pH (<4.0) demetalation occurs and a lowering of signal intensity can be seen in the βMT CD spectra. Below 220 nm, the CD spectra are skewed due to the absorbance of the ammonium formate buffer and are not shown. The significant cadmium-dependent CD spectral bands lie in the 240-280 nm region.^{10, 47-48} The overall CD envelope was monitored for a signal characteristic of a CdS MT cluster, with a crossover point near 250 nm.

3.3 Results

3.3.1 The pH dependence of cadmium metalation of the αMT fragment

The metalation reaction was carried out over a wide pH range and the αMT speciation recorded via ESI-MS and CD spectroscopy. Of particular importance was detecting the

presence or absence of the Cd₄-αMT cluster in both sets of spectral data. Unlike, the situation for the full protein βαMT where there are 20 cys, the formation of the Cd₃- and Cd₄- species in the α-domain fragment must involve bridging cysteinyl thiols due to stoichiometric limitations. The nature of the Cd_x-MT species can be identified from the CD spectral envelope characteristics. The Cd₄-MT cluster species exhibits a characteristic sigmoidal CD band envelope that arises from exciton splitting of pairs of Cd(II) ions in the cluster.⁴⁸

Figure 3-1 shows representative deconvoluted ESI mass spectra of the cadmium metalation of the αMT fragment. The spectra are separated into three distinct binding modes, a cluster-dominated, cooperative binding mechanism at low pH (4.5-6.4), a terminal-thiolate-dominated non-cooperative mechanism at high pH (7.3+) and a mixed mechanism when close to neutral pH (6.5-7.2). This metalation pH dependence is similar to that of the full-length protein where the tendency of the α-domain to cluster dominates the reaction at slightly acidic pH.²⁴ This trend holds true for the isolated domain.

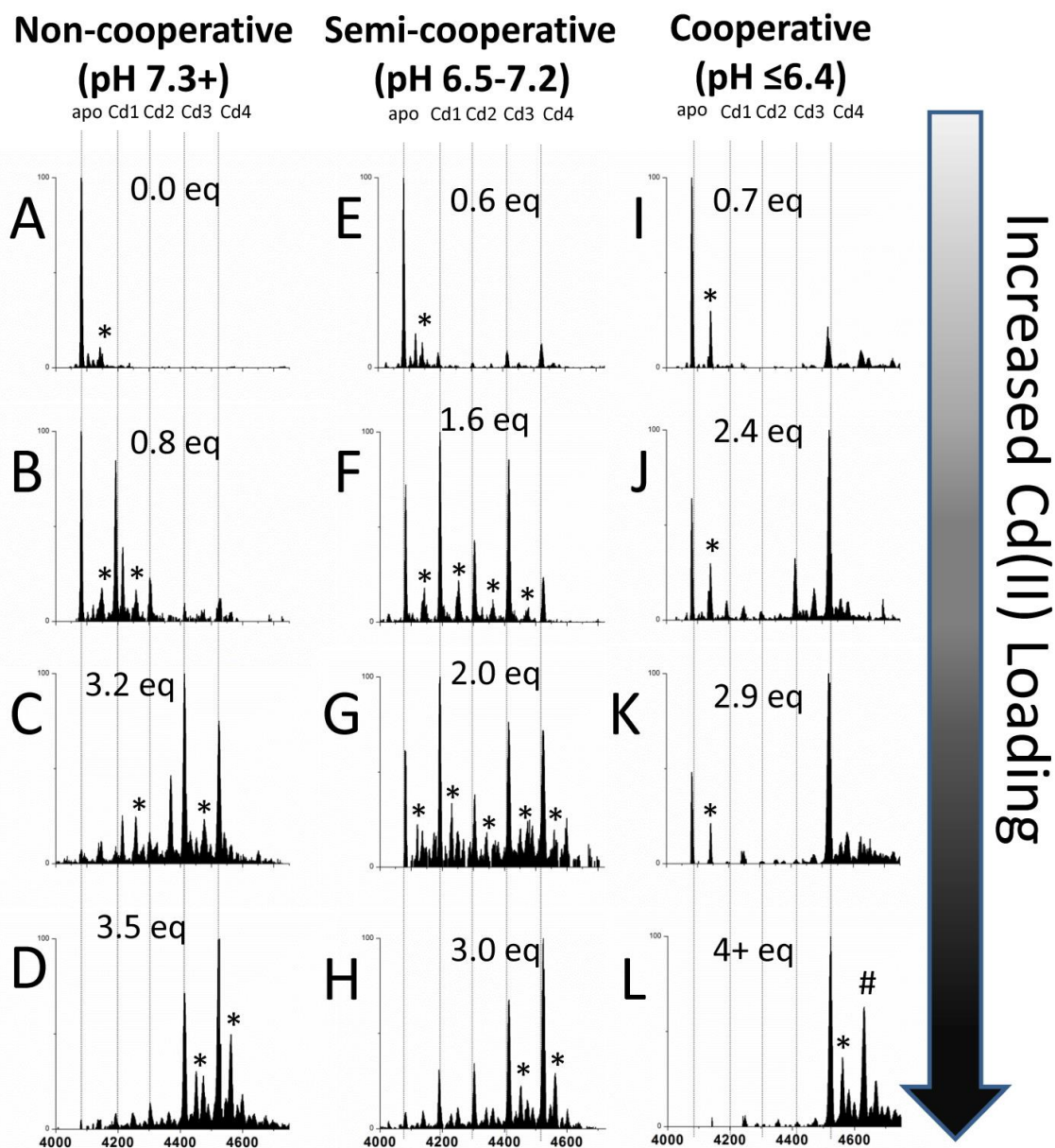


Figure 3-1: Representative deconvoluted ESI-mass spectra showing the trend in speciation as a function of pH for 4 steps in the Cd(II) metalation of apo- α MT. The trend in species formation as the Cd(II) is added in mole equivalent (eq) aliquots can be separated into three: a non-cooperative formation of a distribution of species in spectra (A-D) at the highest pH (7.3 and above: “7.3+”), semi-cooperative formation of both a distribution of species and the Cd₄Cys₁₁ cluster in spectra (E-H) found between pH 6.5-7.2 and the predominant cooperative formation of M₄Cys₁₁ clusters in spectra (I-L) below pH 6.4. *- acetate adducts at +59 Da, #-Cd₅-MT species at +112 Da. Sodium adducts at +22 Da not indicated but are present in some spectra in small quantities.

3.3.2 pH dependence of the cadmium metalation of the β MT fragment

Figure 3-2 shows representative deconvoluted ESI-MS data for the Cd(II) titration of the isolated β -domain fragment. In contrast to the α -domain, the dominant binding mode is the formation of terminally bound metals except at very low pH (<5.8). The spectra are separated into a mixed mechanism at low pH (<5.8) similar to that of the α -domain in Figure 3-1 at pH 6.5-7.2. Even near pH 4.0, there is no strong tendency for the β -fragment to bind the Cd(II) into clusters confirmed by the presence of intermediate metalation products. The non-cooperative, terminal thiolate-bound mechanism becomes dominant above pH 6.0 and representative spectra of this mechanism can be seen in Figure 3-2 E-H.

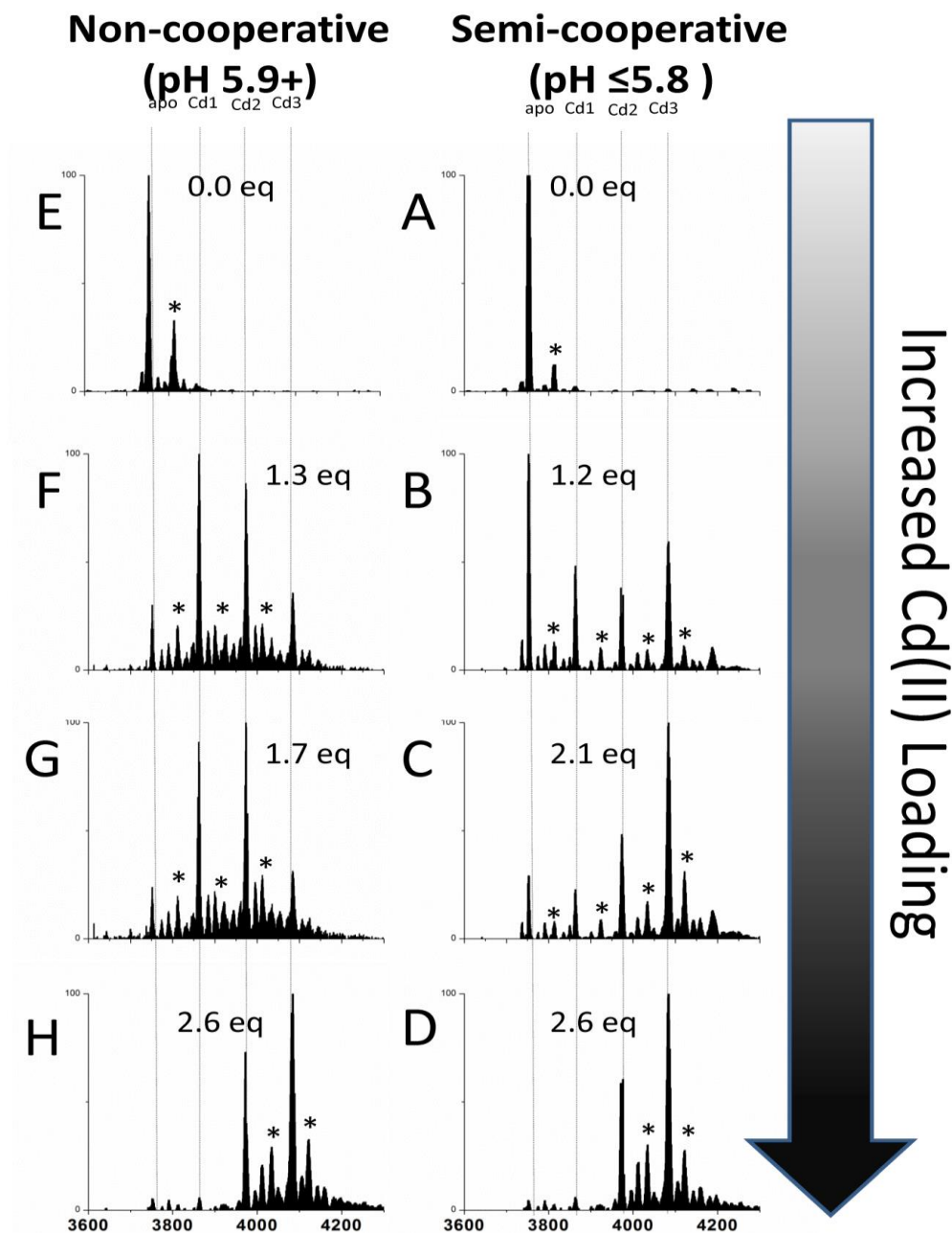


Figure 3-2: Representative deconvoluted ESI-MS spectra of the metalation of apo- β MT with Cd(II) at various stages in the titration. Representative deconvoluted ESI-mass spectra showing the trend in speciation as a function of pH for 4 steps in the Cd(II) metalation of apo- β MT. The trend in species formation as the Cd(II) is added in mole eq aliquots can be separated into two: a semi-cooperative formation of a mixture of a distribution of species and the Cd₃Cys₉ cluster in spectra (A-D) below pH 5.8 and a non-cooperative formation of a distribution of species in spectra (E-H) above pH 5.9 (“5.9+”). *- acetate adducts at +59 Da. Sodium adducts at +22 Da not indicated but are present in some spectra in small quantities.

3.3.3 Circular dichroism spectra of the pH titration of partially metalated α and β MT fragments

Figures 3-3 and 3-4 show the CD spectra of the α - and β -domains of MT under a range of pH conditions. The partially metalated (1.5 eq. of Cd(II)) domains exhibited a change in CD envelope morphology in response to the increasing pH. The bimodal CD envelope with a crossover point near 250 nm and a maximum near 260 nm is characteristic of a $\text{Cd}_4(\text{SCys})_{11}$ cluster.⁴⁸ The slight blue shift is likely due to the simultaneous presence of the apo-fragments and clustered fragments at low pH. The changes in the CD spectra mirror those observed by ESI-MS. This supports the reliability of ESI-MS to report the solution species distribution correctly as both sets of data match closely.

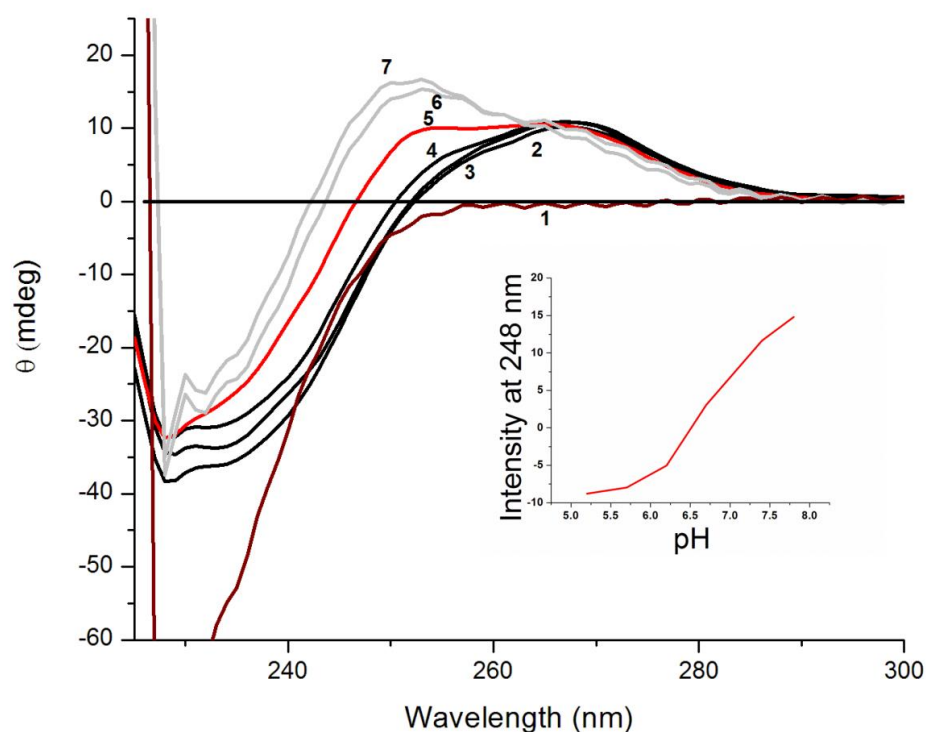


Figure 3-3: Circular dichroism spectra of Cd_{1.5}- α MT at pH 5.2-7.8. Traces 2-4 (black) were measured at pH 5.2, 5.7 and 6.2 respectively. The red line (pH 6.7) shows a mixed spectrum where both clustered and terminally bound Cd-MT are present. The light grey lines 6-7 (pH 7.4 and 7.8) correspond to terminally bound Cd-MT. The apo- α MT spectra (line 1) is shown in burgundy as a reference.

The α -domain shows a clear shift from the $\text{Cd}_4(\text{SCys})_{11}$ cluster signal at low pH with a peak centered near 260 nm and a crossover point near 250 nm to a signal with a maximum near 250 nm and a crossover point closer to 240 nm (Figure 3-3). This new maximum overlaps with the Cd-S ligand-to-metal charge transfer band and is indicative of terminally bound Cd(II) lacking symmetrical structure.

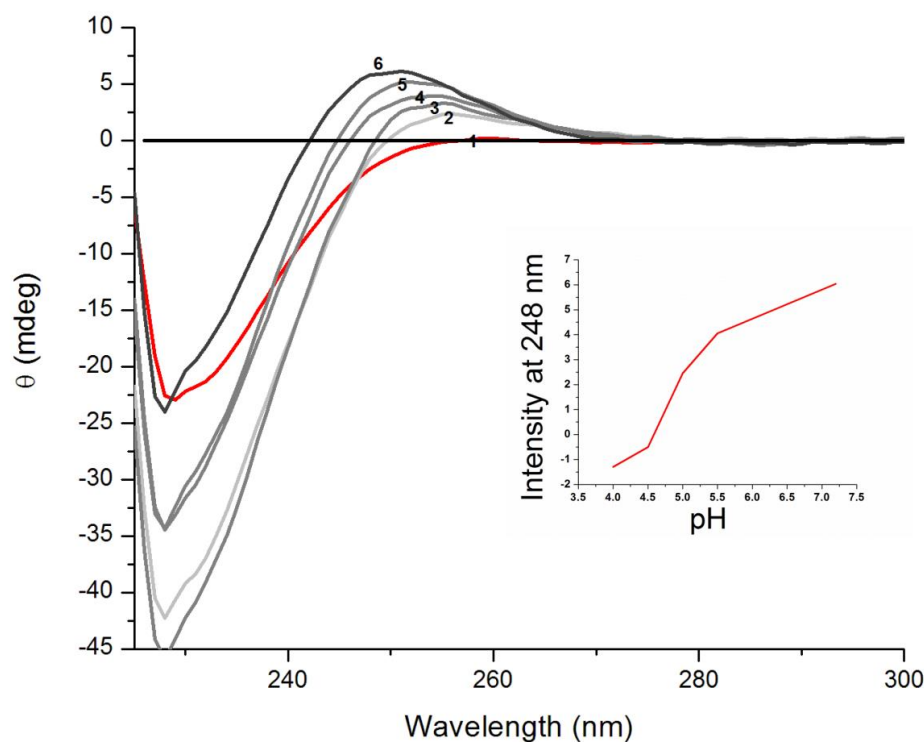


Figure 3-4: Circular dichroism spectra of Cd1.5 β MT at various pH values. Lines 2 and 3 (pH 4.0 and 4.5, respectively) are likely partially demetalated as the intensity is only slightly higher than the apo-trace in red labeled line 1. Lines 4-5 (pH 5.0 and 5.5) and line 6 to a greater extent (pH 7.2) are blue shifted due to cluster collapse and complete binding of free metal, unlike at the lower pH.

The β -domain shows a more subtle shift in its CD spectrum (Figure 3-4) than the α -domain which matches the trend in the ESI-MS data closely. The ESI-MS shows that the cluster structure is not dominant even at low pH so terminally-bound intermediates are present in all CD spectra recorded. The β -fragment spectrum shifts less dramatically from a maximum near 255 nm at low pH to 250 nm at neutral pH. The maximum at 255 nm is

a result of a mixture of the apo, partially-metalated terminal intermediates and the clustered structures. This matches the ESI-MS data in Figure 2 that show a similar mixture of MT species.

3.3.4 pH titration curves of the partially metalated α and β -domains

Figures 3-5 and 3-6 show the change in ESI mass spectral data as a function of pH of the partially metalated domains of MT. The fraction of terminally bound Cd(II) was determined by taking the ratio of intermediates ($Cd_{1-3}\alpha$ MT or $Cd_{1-2}\beta$ MT) to total Cd_x MT species including starting and end products (apo, $Cd_4\alpha$ MT or $Cd_3\beta$ MT) over a wide pH range. All titrations were performed with approximately 1.5-2 eq. of Cd(II) bound to the individual fragments of MT (see Figures 3-1 and 3-2 for representative spectra). Both titrations were fit with a sigmoidal curve using a least-squares fitting method. From this curve it can be seen that the $pK_{a(\text{clustering})}$ of each domain differs greatly with β MT slightly less than 6.0 and α MT at approximately 7.0.

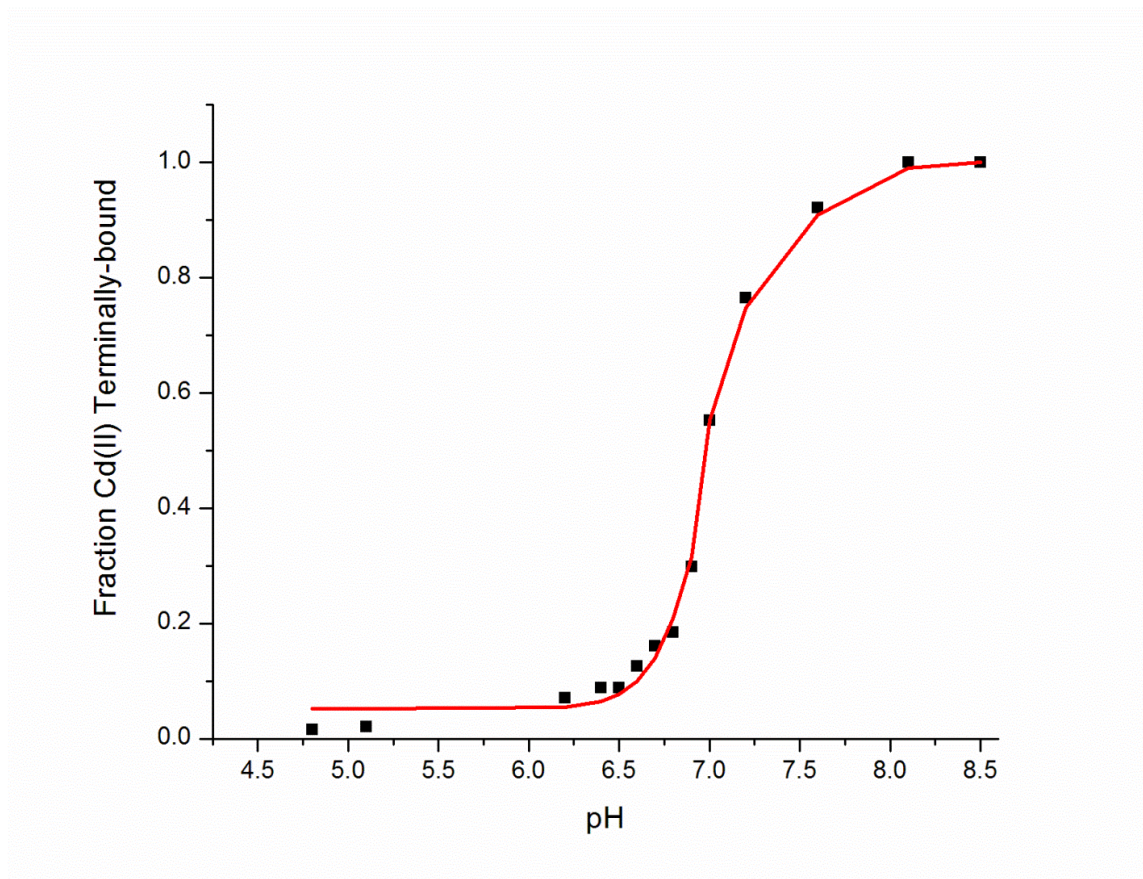


Figure 3-5: The pH dependence of the binding mechanism of the α MT fragment. A sigmoidal fit (red line) was determined by least squares method. The degree of non-cooperativity was determined by the normalized ratio of the intermediates to the initial and end products observed in the ESI mass spectral data. The pH of the 50% mixture was 7.0.

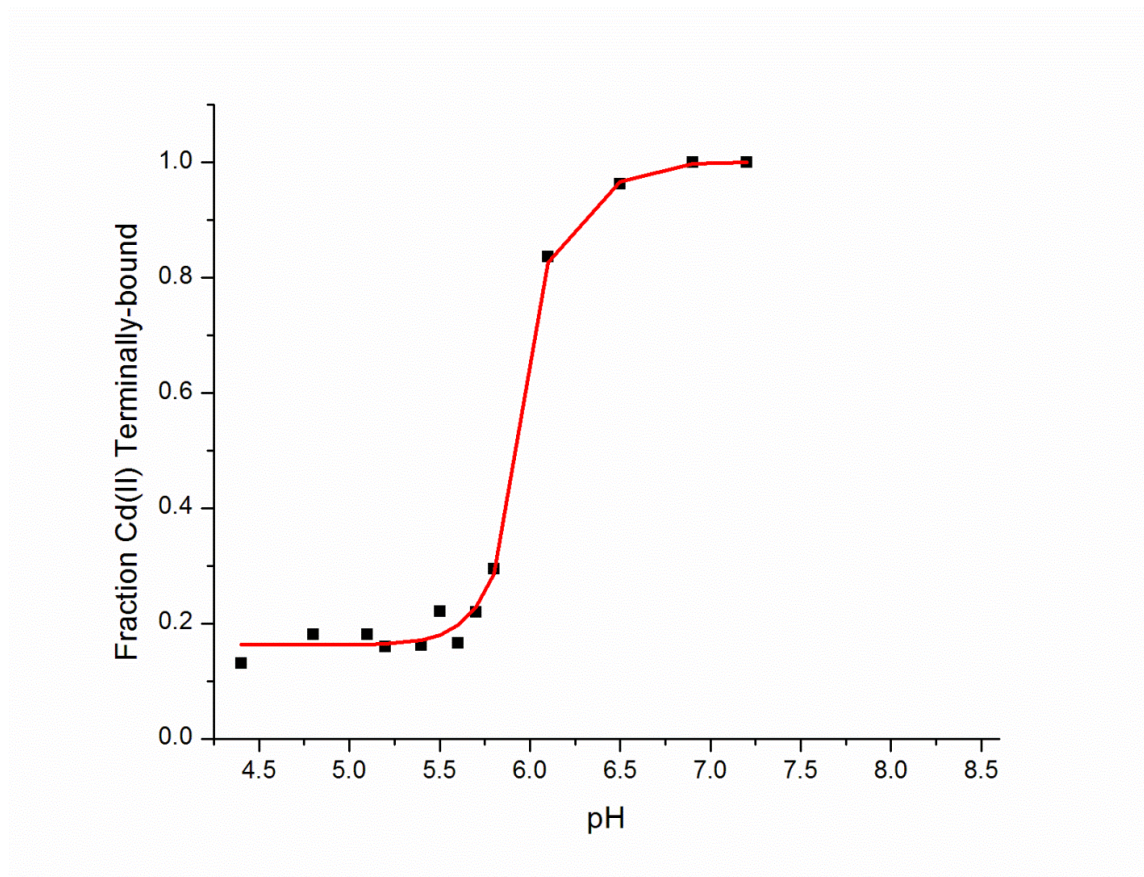


Figure 3-6: The pH dependence of the binding mechanism of the β MT fragment. A sigmoidal fit (red line) was determined by least squares method. The degree of non-cooperativity was determined by the normalized ratio of the intermediates to the initial and end products observed in the ESI mass spectral data. The pH of the 50% mixture was 5.8.

Another significant difference between the two titrations is that the fraction of terminally bound Cd(II) hovers around 0.2 at low pH for β compared to near 0.0 for the α -domain. This indicates an elevated abundance of terminally-bound intermediates in the β -domain metalation mechanism. By using these ratios as an indicator of metalation mechanism, the sensitivity of the binding mode to pH for each domain can be measured. In addition, the pH ranges at which each mechanism dominates can clearly be seen.

3.4 Discussion

3.4.1 Historical conflict on the binding mechanism of MTs

There have been conflicting reports on the metal binding mechanisms of MT for over 30 years.^{20, 39, 49-50} When comparing metals with different electronic properties (ie. Zn(II) vs. Cu(I) vs. As(III)), it is clear that MT would adopt different conformations and likely the metalation reactions would vary greatly in mechanistic detail.⁵¹⁻⁵² However, the metalation mechanism is controversial because the products of the metalation appear to vary for each experiment reported even when focusing only on divalent metals like Zn(II) and Cd(II).^{39, 53-55} For Cd(II) binding, NMR^{26, 43, 56} and CD^{47, 57} spectroscopy have been employed in an attempt to solve the mystery of the divalent metalation mechanism. In addition, metalation with Co(II), a paramagnetic species monitored by visible region absorption and EPR spectroscopy has been used to quantify cluster formation.⁵⁸⁻⁶⁰ With the development of ESI-MS many groups have probed the metal binding reaction and come to a range of conclusions.^{39, 55, 61-64} We have summarized the results of a selection of studies in Table 3-1. The pH dependence of the metalation mechanism presented here allows us to reconcile these conflicting reports and characterize the individual domain binding preferences of Cd(II).

The discrepancy in the mechanisms proposed by the different groups is likely a combination of many factors including isoform differences, sample preparation procedures and ESI-MS settings. However, based on the results we describe here we believe the pH under which the experiments are run is the most important factor in determining the metalation mechanism. From the ESI-MS and CD spectra shown in Figures 3-1 to 3-4 it is clear that the distribution of species in the partially metalated

protein solution is dependent on the solution pH. The exact nature of the species in solution is dependent on the binding mechanism and from the CD spectra we can obtain structural information about the species present. The key to our analysis of the binding mechanism is the presence or absence of intermediate species that involve terminal coordination. For the α -domain this is Cd_{1-3} - α MT and for the β -domain, Cd_{1-2} - β MT.

Table 3-1: Summary of results from selected groups using a variety of methods and pH conditions to study the M(II) metalation mechanism of metallothioneins

Metal	MT isoform	Method	pH	Mechanism	Reference
Cd	rabbit MT2	NMR	7.2	cooperative	41
Cd	rabbit MT2	NMR	8.6	non-cooperative	41
Cd	Blue crab MT1	ESI-MS	7	non-cooperative	18
Cd	hMT1a	CD/UV/ESI-MS	8	non-cooperative	46
Cd	rabbit MT2	NMR	7.5	cooperative	54
Cd	hMT1a	ESI-MS	8.4	non-cooperative	53
Cd	hMT2a	ESI-MS	7.4	cooperative	37
Cd/Zn	hMT3	ESI-MS	7.5	non-cooperative	60
Cd/Zn	hMT2a	ESI-MS	7	cooperative	18
Zn	hMT1a	ESI-MS	9.2	non-cooperative	52
Zn	hMT2a	Zn-sensor fluorescence	7.4	non-cooperative	61
Zn	rabbit MT2	ESI-MS	7.5	cooperative	62
Zn	hMT1a	ESI-MS	7	non-cooperative	14

3.4.2 Bridging the gap between apparent discrepancies

The intermediate species $\text{Cd}_{1-2}\text{-}\beta\text{MT}$ diminish in intensity at lower pH (<5.7) but do not disappear to the extent of the $\text{Cd}_{1-3}\text{-}\alpha\text{MT}$ intermediates. This indicates a fundamental difference in binding mechanism between the two domains. The α -domain mechanism is dominated by cooperative cluster formation at neutral and slightly acidic pH, whereas even at very low pH, the β -domain exhibits a preference for terminal coordination through a mostly non-cooperative mechanism.

We consider the origin of the mechanistic discrepancy between domains to lie in the relative stabilities of the respective metal-thiolate clusters. This is related to the stoichiometry of the domain specific clusters for divalent metals: in the α -domain it is $\text{M}_4(\text{Cys})_{11}$ and in the β -domain $\text{M}_3(\text{Cys})_9$. In the β -domain the Cys-to-M(II) ratio is 3:1 compared to the α -domain where it is 2.75:1. More important is likely the overall charge and proton accessibility of the basic thiolate ligands. The larger extent of bridging in the α -domain reduces the charge-to-metal ratio. The $\text{M}_4(\text{Cys})_{11}$ cluster of αMT has a charge of -3 and is a 3D-almost rigid cage whereas the βMT domain $\text{M}_3(\text{Cys})_9$ cluster structure also has a charge of -3 but the 9 Cys are much more exposed, and offer much less stability than the α -cluster. The terminally coordinated M(II) in $[\text{M}(\text{Cys})_4]^{2-}$ would be more vulnerable to protein attack with a Cys-to-M(II) ratio of 4:1 and an overall charge of -2 for each metal bound. The ability to coordinate 4 metals with a -3 overall charge makes the α -cluster more resistant to proton attack than terminally coordinated metals or the β -cluster.

3.4.3 Isolated domains give insight into the full-length MT binding mechanism

It is important to put these results into context with respect to the binding mechanism of the full protein, $\beta\alpha$ MT. Our results for the domain fragments and the full protein⁶⁵ show that the metalation mechanism, and the intermediates formed before saturation, depend on pH. From previous work on the full-length protein it was inferred that the alpha domain was responsible for the cooperativity of Cd(II) binding since Cd_4 - $\beta\alpha$ MT-1a was the dominant intermediate at lower pH.⁶⁵ We show in this chapter that the α -domain is solely responsible for the cooperative, cluster-driven pathway as the pH dependence matches that of the full-length protein and the isolated β -domain mostly follows the non-cooperative, terminally-bound pathway. This divergence in cluster pH sensitivity must have important biological implications.

3.4.4 Biological context of low pH studies

Many sub-cellular compartments that are involved in protein folding are slightly acidic making the titration curve of the α -domain (Figure 3-5) relevant in a biological context.⁶⁶
⁶⁷ The switch in binding preference near pH 7.0 means that MT could behave differently depending on its cellular localization. In acidic compartments any cadmium present would be bound in a cluster structure in the α -domain, making it less available for donation to other metalloenzymes. These results also imply that in the metalation of the full-length protein, it is the α -domain that clusters at acidic pH when binding cadmium, in agreement with previous work that showed a cooperative binding mechanism for MT-1a⁶⁵ and other isoforms.^{39,43} Taken together, this implies that the α -domain plays a more important role in detoxification, being able to cooperatively bind cadmium in a cluster

structure, leaving the β -domain available to terminally coordinate metals that can be donated to nascent metalloenzymes. Previous studies have indicated that the β -domain is more likely to donate zinc to these newly synthesized proteins because it contains lower affinity binding sites than the α -domain.¹⁶⁻¹⁷

Domain specificity is a topic of interest in the field of metallothionein research that has similarly drawn controversy. Recently, we have shown that pH plays an important role in inducing some domain specificity, specifically in zinc displacement by cadmium.²⁴ At low pH the α -domain shows slight specificity for cadmium but not at neutral pH.²⁴ Together with the results presented in this chapter, we can conclude that the specificity seen in the α -domain is likely due to the strong clustering preference at acidic pH for the α -domain that is not present in the β -domain. The domain specific nature of cadmium binding may have evolved as a mechanism for cadmium sequestration, leaving the β -domain more or less metal-free and able to participate more readily in redox chemistry and the binding of other essential metals like zinc and copper. Indeed, it has been suggested that the β -domain is the copper-binding domain.^{20, 28}

3.5 Conclusions

We have described the pH dependence of the cadmium metalation reaction for each of the isolated domains of human MT-1a. This reconciles previous conflicting reports and demonstrates binding differences between the two domains of MT-1a. We demonstrate that it is possible for α MT to change binding motifs and metalation mechanism within a physiologically relevant pH range and this may help to explain how MTs fulfill their multitude of proposed biological roles. In contrast, the preferred cadmium binding mechanism of the β -domain is non-cooperative metalation by terminal cysteine ligands.

3.6 References

1. C. A. Blindauer, *Chem. Commun.*, 2015, **51**, 4544-4563.
2. J. Loebus, B. Leitenmaier, D. Meissner, B. Braha, G.-J. Krauss, D. Dobritzsch and E. Freisinger, *J. Inorg. Biochem.*, 2013, **127**, 253-260.
3. T. Fukada, S. Yamasaki, K. Nishida, M. Murakami and T. Hirano, *J. Biol. Inorg. Chem.*, 2011, **16**, 1123-1134.
4. W. Maret, *Exp. Gerontol.*, 2008, **43**, 363-369.
5. M. Vašák and D. W. Hasler, *Curr. Opin. Chem. Biol.*, 2000, **4**, 177-183.
6. A. Robbins, D. McRee, M. Williamson, S. Collett, N. Xuong, W. Furey, B. Wang and C. Stout, *J. Mol. Biol.*, 1991, **221**, 1269-1293.
7. W. Braun, M. Vasak, A. Robbins, C. Stout, G. Wagner, J. Kägi and K. Wüthrich, *Proc. Natl. Acad. Sci. U. S. A.*, 1992, **89**, 10124-10128.
8. Y. Boulanger, I. Armitage, K. Miklossy and D. Winge, *J. Biol. Chem.*, 1982, **257**, 13717-13719.
9. G. W. Irvine, K. E. Duncan, M. Gullons and M. J. Stillman, *Chem.--Eur. J.*, 2015, **21**, 1269-1279.
10. M. J. Stillman, *Coord. Chem. Rev.*, 1995, **144**, 461-511.
11. L. Chen, L. Ma, Q. Bai, X. Zhu, J. Zhang, Q. Wei, D. Li, C. Gao, J. Li, Z. Zhang, C. Liu, Z. He, X. Zeng, A. Zhang, W. Qu, Z. Zhuang, W. Chen and Y. Xiao, *J. Biol. Chem.*, 2014, **289**, 22413-22426.
12. A. Pattanaik, G. Bachowski, J. Laib, D. Lemkuil, C. Shaw, D. Petering, A. Hitchcock and L. Saryan, *J. Biol. Chem.*, 1992, **267**, 16121-16128.
13. A. Casini, A. Karotki, C. Gabbiani, F. Rugi, M. Vašák, L. Messori and P. J. Dyson, *Metallomics*, 2009, **1**, 434-441.
14. E. Tuzel, K. Yorukoglu, E. Ozkara and Z. Kirkali, *Central European journal of urology*, 2015, **68**, 45.
15. S. L. Kelley, A. Basu, B. A. Teicher, M. P. Hacker, D. H. Hamer and J. S. Lazo, *Science*, 1988, **241**, 1813-1815.
16. T. B. Pinter and M. Stillman, *Biochem. J.*, 2015, BJ20150676.
17. L.-J. Jiang, M. Vašák, B. L. Vallee and W. Maret, *Proc. Natl. Acad. Sci. U. S. A.*, 2000, **97**, 2503-2508.

18. K. Zangger and I. M. Armitage, *J. Inorg. Biochem.*, 2002, **88**, 135-143.
19. T. T. Ngu, J. A. Lee, M. K. Rushton and M. J. Stillman, *Biochemistry*, 2009, **48**, 8806-8816.
20. P. M. Gehrig, C. You, R. Dallinger, C. Gruber, M. Brouwer, J. H. KÄGI and P. E. Hunziker, *Protein Sci.*, 2000, **9**, 395-402.
21. T. Miyayama, Y. Ishizuka, T. Iijima, D. Hiraoka and Y. Ogra, *Metallomics*, 2011, **3**, 693-701.
22. S. Satarug, J. Baker, P. E. Reilly, M. Moore and D. Williams, *Hum. Exp. Toxicol.*, 2001, **20**, 205-213.
23. E. Artells, Ò. Palacios, M. Capdevila and S. Atrian, *FEBS J.*, 2014, **281**, 1659-1678.
24. T. B. Pinter, G. W. Irvine and M. J. Stillman, *Biochemistry*, 2015, **54**, 5006-5016.
25. M. Stillman, W. Cai and A. Zelazowski, *J. Biol. Chem.*, 1987, **262**, 4538-4548.
26. H. Li and J. D. Otvos, *Biochemistry*, 1996, **35**, 13929-13936.
27. J. D. Otvos, H. R. Engeseth and S. Wehrli, *Biochemistry*, 1985, **24**, 6735-6740.
28. K. B. Nielson and D. Winge, *J. Biol. Chem.*, 1984, **259**, 4941-4946.
29. D. E. Sutherland and M. J. Stillman, *Metallomics*, 2011, **3**, 444-463.
30. D. E. Sutherland and M. J. Stillman, *Metallomics*, 2014, **6**, 702-728.
31. C. J. Schmidt and D. H. Hamer, *Proc. Natl. Acad. Sci. U. S. A.*, 1986, **83**, 3346-3350.
32. A. A. Mehus, W. W. Muhonen, S. H. Garrett, S. Somji, D. A. Sens and J. B. Shabb, *Mol. Cell. Proteomics*, 2014, **13**, 1020-1033.
33. R. J. Person, N. N. O. Ngalame, N. L. Makia, M. W. Bell, M. P. Waalkes and E. J. Tokar, *Toxicol. Appl. Pharmacol.*, 2015, 36-43.
34. W. Qu and M. P. Waalkes, *Toxicol. Appl. Pharmacol.*, 2015, **282**, 267-274.
35. Y. Kondo, S.-M. Kuo, S. C. Watkins and J. S. Lazo, *Cancer Res.*, 1995, **55**, 474-477.
36. X. Yu, Z. Wu and C. Fenselau, *Biochemistry*, 1995, **34**, 3377-3385.
37. G. W. Irvine and M. J. Stillman, *Biochem. Biophys. Res. Commun.*, 2013, **441**, 208-213.

38. S.-H. Chen, L. Chen and D. H. Russell, *J. Am. Chem. Soc.*, 2014, **136**, 9499-9508.
39. S.-H. Chen, W. K. Russell and D. H. Russell, *Anal. Chem.*, 2013, **85**, 3229-3237.
40. C. Afonso, Y. Hathout and C. Fenselau, *Int. J. Mass Spectrom.*, 2004, **231**, 207-211.
41. X. Yu, M. Wojciechowski and C. Fenselau, *Anal. Chem.*, 1993, **65**, 1355-1359.
42. S. Pérez-Rafael, S. Atrian, M. Capdevila and Ò. Palacios, *Talanta*, 2011, **83**, 1057-1061.
43. M. Good, R. Hollenstein, P. J. Sadler and M. Vasak, *Biochemistry*, 1988, **27**, 7163-7166.
44. C. Dorian, V. H. Gattone and C. D. Klaasen, *Toxicol. Appl. Pharmacol.*, 1992, **114**, 173-181.
45. J. D. Park, Y. Liu and C. D. Klaassen, *Toxicology*, 2001, **163**, 93-100.
46. J. Chan, Z. Huang, I. Watt, P. Kille and M. J. Stillman, *Can. J. Chem.*, 2007, **85**, 898-912.
47. N. Cols, N. Romero-Isart, M. Capdevila, B. Oliva, P. González-Duarte, R. González-Duarte and S. Atrian, *J. Inorg. Biochem.*, 1997, **68**, 157-166.
48. K. E. Duncan, C. W. Kirby and M. J. Stillman, *FEBS J.*, 2008, **275**, 2227-2239.
49. M. Vaheer, N. Romero-Isart, M. Vašák and P. Palumaa, *J. Inorg. Biochem.*, 2001, **83**, 1-6.
50. K. E. Duncan and M. J. Stillman, *FEBS J.*, 2007, **274**, 2253-2261.
51. T. T. Ngu and M. J. Stillman, *J. Am. Chem. Soc.*, 2006, **128**, 12473-12483.
52. K. B. Nielson, C. Atkin and D. Winge, *J. Biol. Chem.*, 1985, **260**, 5342-5350.
53. M. Vasak, J. H. Kaegi and H. A. O. Hill, *Biochemistry*, 1981, **20**, 2852-2856.
54. K. L. Summers, D. E. Sutherland and M. J. Stillman, *Biochemistry*, 2013, **52**, 2461-2471.
55. D. E. Sutherland and M. J. Stillman, *Biochem. Biophys. Res. Commun.*, 2008, **372**, 840-844.
56. T. Gan, A. Munoz, C. F. Shaw and D. H. Petering, *J. Biol. Chem.*, 1995, **270**, 5339-5345.

57. J. Pande, C. Pande, D. Gilg, M. Vasak, R. Callender and J. Kägi, *Biochemistry*, 1986, **25**, 5526-5532.
58. M. Good and M. Vasak, *Biochemistry*, 1986, **25**, 3328-3334.
59. J. Ejnik, J. Robinson, J. Zhu, H. Försterling, C. F. Shaw and D. H. Petering, *J. Inorg. Biochem.*, 2002, **88**, 144-152.
60. D. L. Pountney and M. VAŠÁK, *Eur. J. Biochem.*, 1992, **209**, 335-341.
61. S.-H. Chen and D. H. Russell, *Biochemistry*, 2015.
62. P. Palumaa, E. Eriste, O. Njunkova, L. Pokras, H. Jörnvall and R. Sillard, *Biochemistry*, 2002, **41**, 6158-6163.
63. A. Kręzel and W. Maret, *J. Am. Chem. Soc.*, 2007, **129**, 10911-10921.
64. J. Zaia, D. Fabris, D. Wei, R. L. Karpel and C. Fenselau, *Protein Sci.*, 1998, **7**, 2398-2404.
65. G. W. Irvine, T. B. Pinter and M. J. Stillman, *Metallomics*, 2016.
66. J. Kleinman, W. Brown, R. Ware and J. Schwartz, *Am. J. Physiol. Renal. Physiol.*, 1980, **239**, F440-F444.
67. N. Demaurex, *Physiology*, 2002, **17**, 1-5.

Chapter 4

4 Structural changes of MT1a during the arsenic metalation reaction: folding under typically denaturing conditions³

4.1 Introduction

Metallothionein (MT) has long been known to be a major player in cellular metal homeostasis and since its first isolation in 1957, has been shown to affect many cellular processes¹. It is a uniquely structured protein with cysteine accounting for approximately 30% of its total residues with a mass of approximately 6-10 kDa, depending on the isoform. The X-ray determined structure of the fully metalated MT resembles that of a dumbbell with two metal binding domains (α and β), separated by a short linker sequence²⁻³. The formal structure of MT is based almost entirely on the changes induced by metal coordination and the formation of the metal clusters⁴⁻⁵. MT binds a wide variety of metals including Zn^{2+} , Cu^+ , Cd^{2+} and the metalloid As^{3+} .⁶ However, the structure of the partially metalated protein is unknown, yet is important as an intermediate in vital cellular metalation chemistries. In this chapter, experimental evidence of As-MT coordination geometry and stoichiometry as well as partially metalated MT structure will be examined.

MT is a multi functional protein acting as a source of reducing -SH groups in redox reactions, detoxifying heavy metals and regulating cellular zinc and copper concentrations.⁷ The importance of MT to cellular metal homeostasis is highlighted by its ubiquitous nature; nearly all organisms have some type of MT or MT-like protein

³ A version of this chapter has been published:

Reproduced with permission from: Irvine, Gordon W., Kelly L. Summers, and Martin J. Stillman. "Cysteine accessibility during As^{3+} metalation of the α - and β -domains of recombinant human MT1a." *Biochemical and biophysical research communications* 433.4 (2013): 477-483. and Irvine, Gordon W., and Martin J. Stillman. "Topographical analysis of As-induced folding of α -MT1a." *Biochemical and biophysical research communications* 441.1 (2013): 208-213.

Copyright 2013 Elsevier

coded for in their genomes.⁸ In addition to the regular functions of MT, it has emerged that MT can play a role in cancer progression and drug resistance in tumors.⁹⁻¹⁰ With many cancer treatments relying on metal based drugs that may induce expression of MTs, it is important to determine the mechanism by which MT metalates and the structure of the apo- and partially metalated forms of MT that are the predominant species present in the cellular environment.¹ By studying the structure of the metal-free protein and its partially metalated intermediates, predictions about metalation with a wide variety of metals and metal complexes can be made. This may prove useful in designing drugs to combat tumours that have shown resistance to traditional therapies and in determining how MT carries out its many biological functions.

Partially metalated MT (that is MT with fewer metals bound than its maximum capacity) is vital to metal-based cellular chemistry because this species is likely to be the dominant form of cellular MT. It has been considered that apo-MT does not have structure in the traditional sense but rather it adopts a more randomly coiled and ill-defined conformation¹¹. However, more recent studies have suggested that apo-MT may have a loosely defined, but structurally significant conformation at neutral pH that is only lost under denaturing conditions¹²⁻¹³. Metalation of apo-MT can lead to the formation of fully metalated protein. However, due to the concentrations of metals found in a cell, it would be expected that partially metalated species would predominate¹⁴. Unfortunately the only solved structures of MT are fully metalated forms^{2-3, 15-16}. Significantly, structures of both the partially metalated MT and apo-MT remain elusive.

In this chapter, we use the differential rate of the modification of the free cysteines in the α -metal-binding fragment to probe the spatial distribution of cysteines not involved in metal binding as a function of metalation status. We also use this method to quantify free thiols in MT as well as to assess the relative accessibilities of cysteines in the alpha and beta domains of MT. The reaction profile of Bq with up to 11 cysteines in α -MT provides a clear indication of the metal-dependant nature of apo- or partially-metalated MT folding. This reaction is dependent on the variable accessibility of the unbound cysteines. We confirm a stoichiometry of As_3 - α MT and As_3 - β MT and binding mode of terminal cysteine coordination with discrete units of $As(Cys)_3$ as opposed to clustered structures.

Overall, the reaction profile of Bq provides a unique description of the topological distribution of free cysteine residues, conformations adopted in the partially metalated protein and confirms predicted binding motifs of As_x-MT.

4.2 Methods

4.2.1 Protein preparation

Methods for expression and purification of the alpha domain fragment have been previously reported in more detail ¹⁷. In brief, the α -domain of recombinant human MT isoform 1a (α -rhMT 1a) was used having the follow sequence: GSMGKAAAAC CSCCPMSCAK CAQGCVCKGA SEKCSCKKA AAA. The expression of the recombinant protein was carried out in *E. coli* strain BL21 using the recombinant α -rhMT 1a sequence inserted into a pET29a plasmid. The plasmid also coded for an N-terminal S-tag with the sequence MKETAAAKFE RQHMDSPDLG TLVPRGS. The inclusion of an S-tag into the recombinant protein is done to stabilize the protein during purification steps and was removed via a Thrombin CleanCleave™ kit (Sigma).

To limit oxidation of the cysteinyl thiols, all solutions used were saturated with argon and evacuated before use. In addition, all solutions used in the purification process were chilled to maintain the integrity of the protein and prevent degradation. Protein solutions were stored at -20°C in sealed vials that had been thoroughly evacuated.

Demetalation of the protein was achieved by buffer exchange with a 10 mM solution of ammonium formate, pH adjusted to 2.8. The solutions were buffer-exchanged by centrifuge in an Amicon Ultra Centrifugal Filter Tube (Millipore) with a 3 kDA MW filter. This ensured complete demetalation and maintained high concentrations of the protein.

4.2.2 Solution preparation and titrations

Solutions of 150 mM para-benzoquinone (Bq, Fisher Scientific) were prepared by dissolution in 100% methanol (Caledon) and diluted to a final concentration of 15 mM in deionized water. These solutions were prepared just before they were to be used, bubbled

with argon for at least 20 minutes, evacuated and kept on ice shielded from light until use. Solutions of 2 mM As^{3+} were prepared by dissolving As_2O_3 in conc. HCl and diluting with deionized water. The final pH of the solution was adjusted to 2.8 using NH_4OH . The solution was then saturated with argon and evacuated before use.

MT concentrations were determined by metalation of 100 μL aliquots of the apo-MT with Cd^{2+} and examination of the absorption spectrum, specifically the peak at 250 nm. The 250 nm peak corresponds to the ligand-to-metal charge transfer transition of the Cd-thiolate bond ($\epsilon_{\alpha,250\text{ nm}} = 45,000\text{ M}^{-1}\text{ cm}^{-1}$). Concentrations of α -rhMT 1a ranged from 30-60 μM in order to ensure a strong mass spectral signal for all 27 species that are formed during metalation and modification of apo- α -rhMT 1a, that is the set of $\text{As}_n\text{Bq}_x\alpha$ -rhMT ($n=0-2$, $x=0-11$) that will be simultaneously measured.

Titration of MT with As^{3+} was carried out by adding approximately 0.5 molar equivalents of As^{3+} to the protein solution. The reaction of MT with As^{3+} is much slower than with metals such as Cd^{2+} or Zn^{2+} , so the reaction vials were put in an evacuator for 1 hour to equilibrate. Once the system came to equilibrium, the speciation of the α -MT was checked by ESI-MS to ensure that it had been partially-metalated and a distribution of apo-, As_1 - and As_2 - α -rhMT existed in solution, Figure 4-1A. Sequential addition of Bq to the protein solution was performed and mass spectra acquired until all the species had been fully modified (ie. no free cysteinyl thiols remained in any of the partially metalated species). Titrations were performed at pH 2.8.

Mass spectra were measured with a microTOF II electrospray ionization time-of-flight mass spectrometer (Bruker Daltonics, Canada) in the positive ion mode. The settings of the instrument that were used have been previously described¹⁷. The mass spectra were analyzed using the Bruker Daltonics analysis software.

4.3 Results

4.3.1 Metalation of α and β MT with As^{3+}

Figure 4-1A shows the ESI-MS data recorded for the metal free, apo- α MT with mass 4,081.8 Da. Figure 4-1B shows the ESI-MS data after 1 hour equilibration following the

addition of 0.75 molar equivalents of As^{3+} . The data show that there are 3 species of α MT present: apo- α MT, As_1 - α MT and As_2 - α MT (in order of decreasing abundance). These data confirm the non-cooperativity of the As^{3+} metalation reaction because very little As_3 - α MT forms, which is the final product of the metalation reaction. An excess amount of Bq (40 molar equivalents) was added to the reaction vial to ensure complete reaction with any available cysteinyl thiols and the ESI mass spectra were recorded. The number of Bq that reacted was dependant on the number of free cysteines available in each of the species. Figure 4-1C shows ESI-MS data after the excess addition of Bq to the solution measured in Figure 4-1B. All 11 cysteine residues of apo- α MT were modified by binding 11 Bq resulting in a mass of 5,258.9 Da. Similarly, As_1 - α MT had 8 cysteines modified for a final mass of 5,008.7 Da, and As_2 - α MT had 5 cysteines modified for a mass of 4,760.6 Da. There was a very small amount of the As_3 - α -rhMT species present, the two free cysteines were modified by binding 2 Bq resulting in a mass of 4,513.5 Da. The mass spectral data accounted for all the cysteines in each domain.

In a separate experiment, 2.5 mole equivalents of As^{3+} were added to apo- α MT and the solution was equilibrated for 1 h. The spectrum in Figure 4-1D shows that, when compared with the species in Figure 4-1B, the abundance of the apo- α MT and As_1 - α MT species decreased and the proportion of As_2 - α MT and As_3 - α MT increased, with As_3 - α MT being the most abundant as expected with the increased concentration of As^{3+} . In this case, a limiting amount of 2 mole equivalents of Bq were added to the solution after the spectrum in Figure 4-1D was measured to probe the availability and accessibility of the free cysteines. The data in Figure 4-1E illustrate the distribution of the free cysteines. The As_3 - α MT species can be seen without Bq modification and with 1 and 2 Bq molecules bound. The abundances of the modified species for both As_2 - α MT and As_3 - α MT follow an approximately normal distribution. This indicates equal accessibility of the remaining cysteines after metalation with 2 or 3 As^{3+} ions. The mass spectrum for the complete modification of all free cysteines was achieved by adding a 10-fold excess of Bq, Figure 4-1F. The presence of As_3 - α MT with 2 Bq and As_2 - α MT with 5 Bq (4513.4 and 4766.6 Da, respectively) is observed in the mass spectra, as expected for the fully modified protein species. Taken together, the spectra in Figure 4-1 confirm

stoichiometric binding for $\text{As}(\text{Cys})_3$ for each step in the metalation reaction and the presence of two free cysteinyl thiols upon saturation with arsenic.

As- α -rhMT

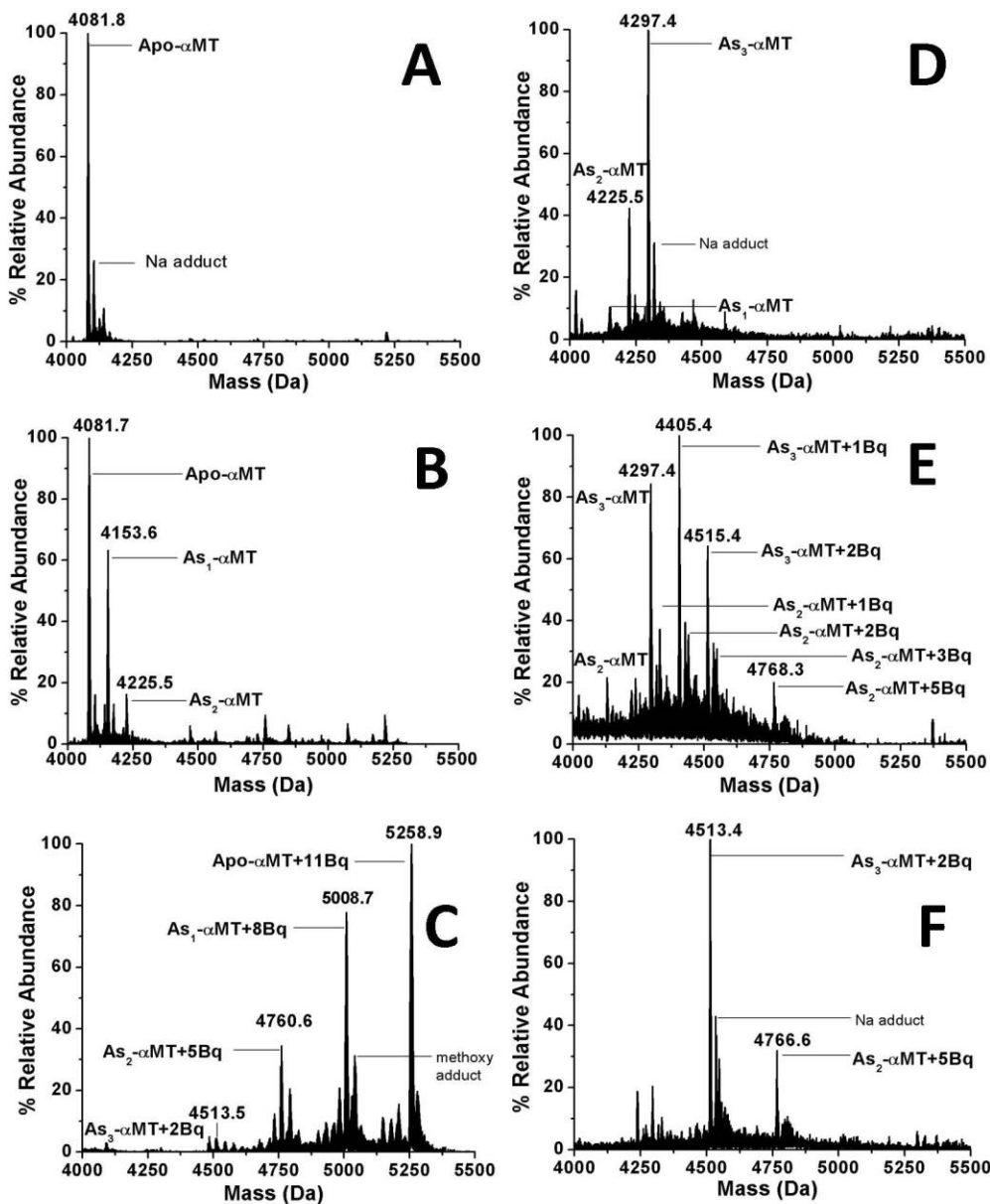


Figure 4-1: ESI mass spectra of α MT1a with increasing As^{3+} loading and cysteine modifications to form As_n - α MT ($n = 1-3$). (A) Metal-free apo- α MT. (B) After 1 h equilibration with 0.75 mole equivalents of As^{3+} added. (C) After 40 mole equivalents of Bq added to the solution in B. (D) After 1 h equilibration with 2.5 mole equivalents As^{3+} added to the apo- α MT solution. (E) After 2 mole equivalents of Bq added to As_n - α MT shown in D. (F) After 10 mole equivalents of Bq added to As_n - α MT species shown in D.

The As^{3+} metalation and Bq reactions of apo- β MT measured by ESI-MS are shown in Figure 4-2. The apo- β MT has a mass of 3752.6 Da (Figure 4-2A). Because As_3 - β MT has no free cysteines, the metalation reaction was quenched after 1 h by addition of 2 mole equivalents of As^{3+} (Figure 4-2B) to ensure that As_1 - and As_2 - β MT were the dominant species and probe Cys accessibility. The mass spectrum shows that the most abundant species were As_2 - β MT (3896.1 Da) and As_1 - β MT (3824.1 Da) with no appreciable amount of apo- β MT or As_3 - β MT. Addition of 10 mole equivalents of Bq resulted in the spectrum shown in Figure 4-2C. Unexpectedly, the excess Bq did not react with all the free cysteines present. Significant fractions of unreacted As_1 - β MT and As_2 - β MT remained, as well as an approximately normal distribution of 1–3 Bq bound to As_2 - β MT and 1–4 Bq bound to As_1 - β MT (Figure 4-2B). Even when excess (40 mol eq) Bq had been added there remained unreacted species (Figure 4-2D). This is likely the result of oxidation since the mass of the unreacted species is less than predicted and decreases by 3 Da, indicating internal Cys-Cys crosslinks had been formed. Despite the oxidation, the Normal distribution pattern can still be deciphered indicating approximately equal access to the remaining cysteine of As_{1-2} - β MT.

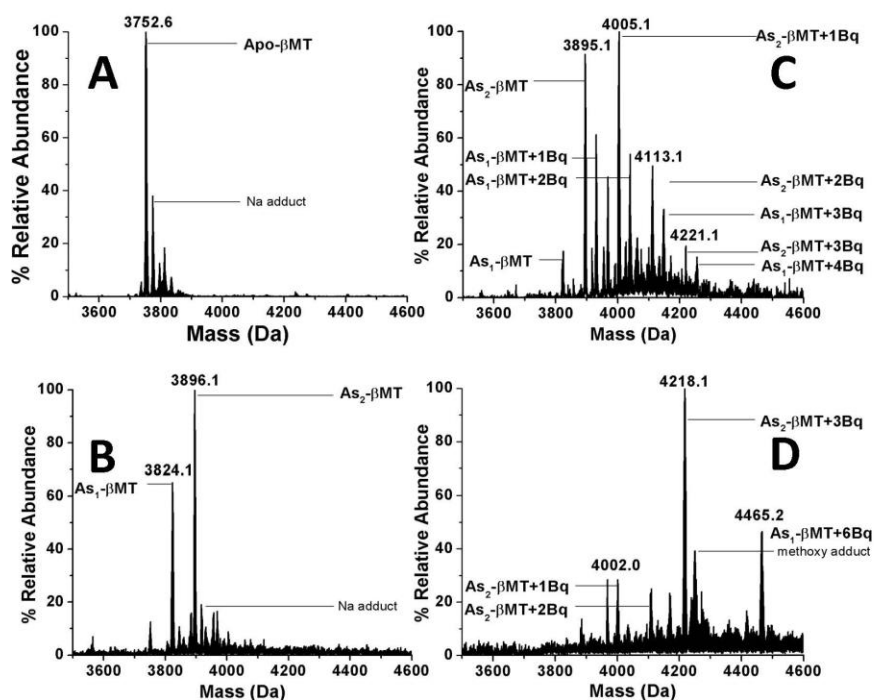
As- β -rhMT

Figure 4-2: ESI mass spectra of β MT1a showing As^{3+} binding and cysteine modification with Bq to form $\text{As}_n\text{-}\beta\text{MT}$ ($n=1\text{--}2$) using Bq. (A) Metal-free apo- β MT. (B) After 2 mole equivalents of As^{3+} added to solution of apo- β MT. (C) After 10 mole equivalents of Bq added to $\text{As}_n\text{-}\beta\text{MT}$ species shown in B. (D) After 40 mole equivalents of Bq added to $\text{As}_n\text{-}\beta\text{MT}$ species shown in B.

4.3.2 Cysteine modification of As_n-αMT with Bq

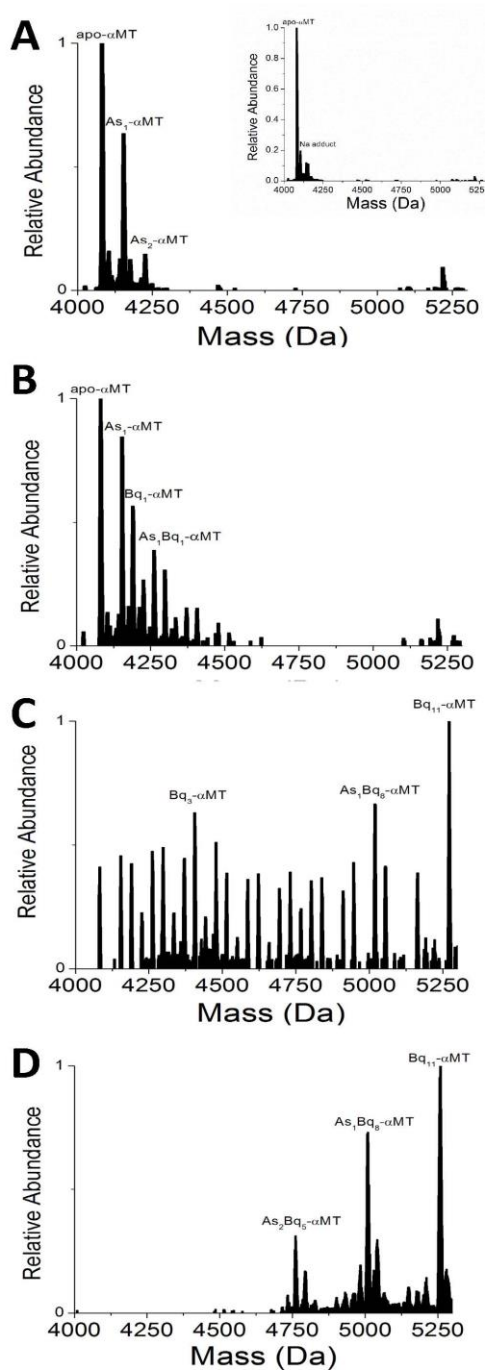


Figure 4-3: Deconvoluted ESI-MS data showing the binding of As³⁺ to apo-αMT and the subsequent titration of the protein solution with Bq. (A) Distribution of species upon reaction of 0.5 mol. eq. of As³⁺ and inset in the top right is the mass spectrum of the starting apo- solution. The spectra show the Bq titration at approx. 1 (B), 5 (C) and 10 (D) mol. eq. of Bq reacted with the protein solution.

The deconvoluted mass spectrum of the apo- α MT is shown in the inset of Figure 4-3A. The reaction with As^{3+} resulted in a distribution of species: apo-, As_1 - and As_2 - α MT with apo- being the most abundant, As_1 at approximately 65% and As_2 at approximately 15% relative abundance. After As-binding was completed, 1 mol eq of Bq was reacted with the solution shown in Figure 4-3A to form the spectrum in Figure 4-3B. In this early stage of the Bq titration, both modified and unmodified species are clearly present in solution. When further mol eqs of Bq are added, a more complicated mass spectrum is recorded, Figure 4-3C, with 27 individual species (more clearly delineated in Figure 4-4). This is the midpoint in the reaction, with the mass spectral data complicated by the presence of both metalated and apo species each having varying degrees of cysteine modification. The identification of all 27 species is shown in Figure 4-4. This spectrum beautifully illustrates the power of ESI-MS in providing exquisite detail for the progress of complicated, multifaceted reactions. Finally, the addition of excess Bq results in all free cysteinyl thiols being modified, greatly simplifying the spectrum (Figure 4-3D). Now just three species are observed: the apo-Bq₁₁-MT, singly metalated As_1 -Bq₈-MT and the doubly metalated As_2 -Bq₅-MT. Thus, Figure 4-3D shows the completed reaction with all the starting species' cysteines being fully modified by Bq.

This complete modification rules out oxidation as a cause of the unusual patterns seen in Figure 4-3C. When MT is oxidized, Cys-Cys bridges are formed and, therefore, are unreactive towards Bq. If there was oxidation in the protein solution the endpoint in the Bq titration would be changed for some proportion of the protein that had been oxidized. For example, instead of Bq₁₁- α MT being an endpoint for the titration of the apo-protein, there would be a distribution of endpoints with Bq₁₁, Bq₉ and Bq₇- α MT being present depending on the extent of protein oxidation. In addition the recorded masses would differ from the expected masses by 2 Da per mole of Cys-Cys oxidation. No such distribution is observed so it can be concluded that the free thiols were not cross-linked but all forms covalent bonds with Bq.

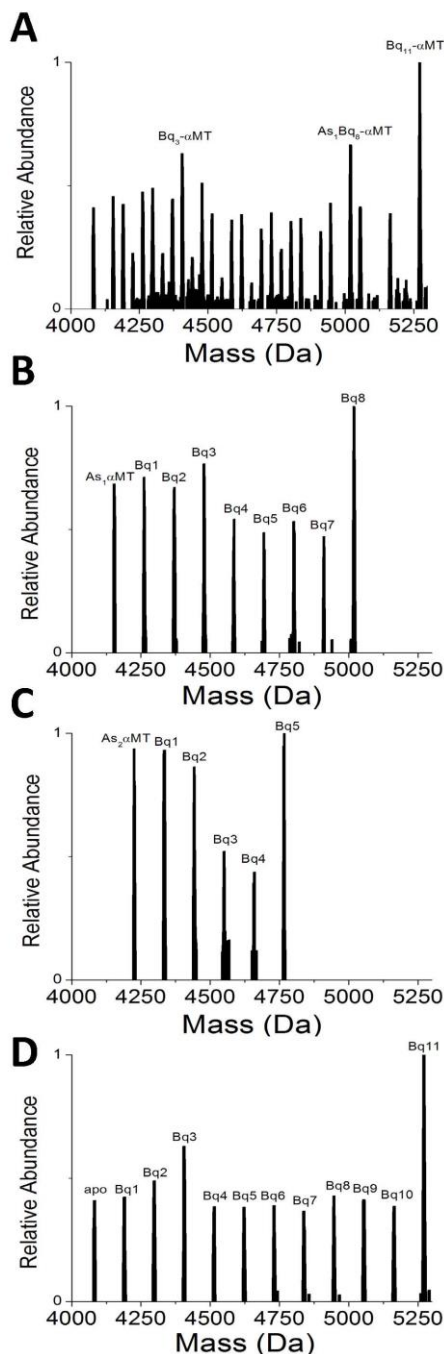


Figure 4-4: Deconvoluted ESI-MS data showing the 27 individual species of intermediate and fully modified MT (A). Peaks are isolated by parent species (ie. apo, As₁ or As₂) and shown on separate axes for clarity. Shown are the reaction profiles for the As₁ (B), As₂ (C) and apo-αMT species (D).

Figure 4-4A shows the ESI-mass spectrum at the midpoint of the titration (taken from

Figure 4-3C). This is mass spectral data that include a combination of the spectra of the

apo-, As₁- and As₂-species variably modified by Bq. Figures 4-4B, C and D separate out the three key species, namely As₂-αMT, As₁-αMT, apo-αMT and their respective cysteine-modified intermediates. We note that insufficient Bq has been added at this stage to fully modify all cysteines in the protein (that saturation point is shown in Figure 4-3D). In all, there are 27 individual MT species shown in this single mass spectrum. This kind of accuracy and resolution of spectral lines is unique to ESI-MS as other spectroscopic techniques would not be able to distinguish with the same detail the abundance of species present in solution. To simplify the data analysis, the spectra of the separately metalated species, along with their intermediate and final products, are isolated and are shown in Figure 4-4B (As₂-α-MT + up to 5 Bq), C (As₁-α-MT + up to 8 Bq) and D (apo-α-MT + up to 11 Bq). Key in this series of spectra is that the As³⁺ can react in single steps from 1 to 3 and that it uses 3 cysteine thiols to bind. So from the 11 cysteines of apo-αMT, there are 8 left free for As₁-, 5 left free for As₂-, and 2 left free in As₃-αMT. When saturated with Bq, all of these free cysteines are modified (Figure 4-3D) but when insufficient Bq is added the reaction stops mid-flight providing a snapshot of the relative accessibility of the free cysteines because the reaction progress is governed by the kinetics of the modification.

In the experiment carried out here the dynamic structure of the protein is controlled by the metalation status (0, 1, 2, or 3 As³⁺). The distribution profile of the Bq-modified cysteines depends on the relative accessibility between all 4 protein species (i.e. apo-, As_n, n=1-3).

The profile for Bq reacting with the five free cysteines in As₂-αMT is complicated.

Although the Bq modification pattern reported for the apo-αMT, namely a Normal

distribution at low pH¹³ is expected to be disrupted by the metalation there are no previous data to suggest what the effect of the metalation will be. Metal-induced folding has been discussed for MT for many years¹⁸⁻²⁰ and it is to be expected that with 2 As³⁺ bound that the peptide will fold and the cysteines could then be buried. The model of As₂-αMT in Figure 4-5C shows this possibility. The data in Figure 4-4B suggest that the five free cysteines in the As₁ species have different steric hindrance with respect to reaction with the incoming Bq. The profiles in Figure 4-4 does not exhibit a Normal distribution rather the profile indicates that some cysteine residues are buried even under denaturing conditions upon metalation with As³⁺.

4.3.3 Modeling the As-MT metalation reaction

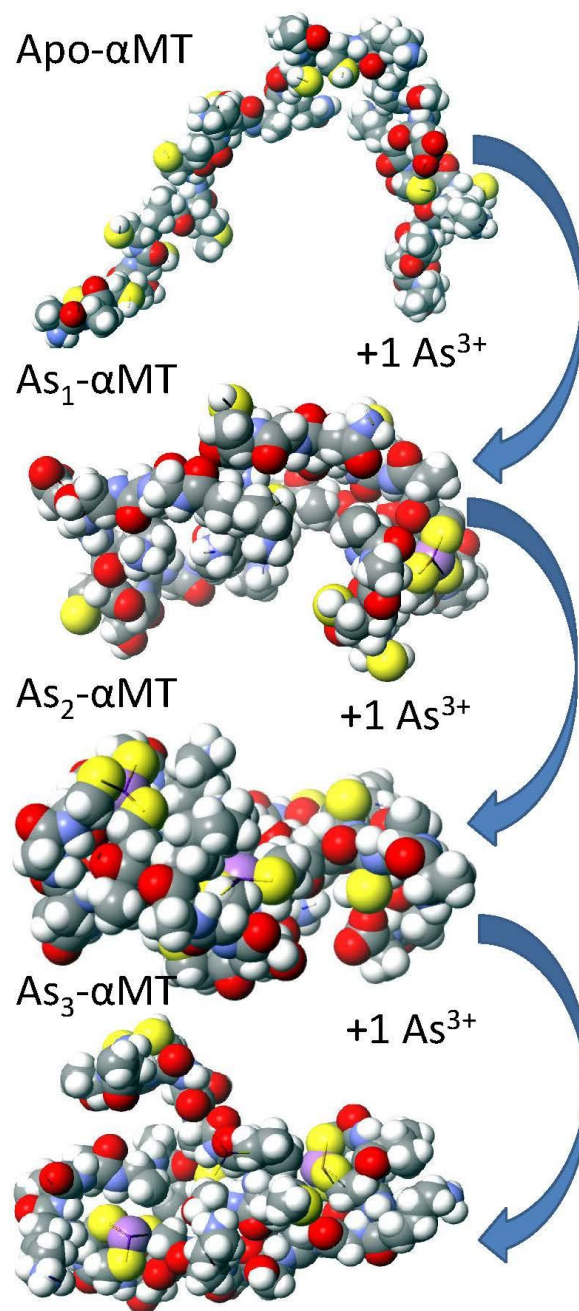


Figure 4-5: Scigress models (MM3/MMD) of the structure of Apo-αMT (A), As₁-αMT (B), As₂-αMT (C) and As₃-αMT (D) using space filling models to visualize the extent of folding in each species. The MD calculations were carried out at 500 K for 500 ps. The As³⁺ ions are shown in purple.

4.4 Discussion

Metal-induced folding is a well studied process in the field of bioinorganic chemistry and particularly important for metals that play a structural role for metalloproteins.²¹⁻²³ MT does not fit nicely into traditional categorization of a catalytic or structural metalloprotein, but instead coordinates metals in a flexible manner as a metallochaperone. The ability to accommodate a large number of metal ions per peptide in a functional homeostatic role makes investigations of metal-induced folding of MT difficult. In addition, the lack of structural features in the random coil, apo-MT further complicates structural investigations. Thus, a new technique of cysteine modification to probe the global reactivity of cysteine-rich MT was used to probe the metal-induced folding and metalation properties of As_x -MTs under denaturing conditions.

The reaction profile for the reaction of Bq with all 11 free cysteines of the apo- α MT is unlike that expected based on the low pH conditions. Based on our previous studies¹³, it was expected that MT would not have a defined structure capable of interfering with the Bq cysteine modification reaction. At pH 2.8, where these titrations were carried out, it was expected that the MT would exist in a denatured form, as a random, loosely defined structure, as depicted by the model in Figure 4-5A. As such, all cysteine residues would be expected to exhibit a similar degree of steric hindrance. This would result in a Normal distribution of the modifications with an increasing manifold maximum from apo- to the fully modified Bq₁₁ species (see Figure 1-5A for an example of a Normal distribution pattern)¹³. This was clearly not the case in the reaction profile of the apo- and As_{1-2} - α MT species studied here. The presence of As^{3+} changed the reaction mechanism for each species and gave non-Normal reaction profiles.

For the As_{1-2} - α MT species, the metal-induced folding likely creates an environment where cysteines not directly involved in metal coordination are shielded by backbone which is now anchored by the metal coordination. For partially-metalated species, the metals are still labile, unable to produce sharp signals in NMR spectra.²⁴ The lability of the metals may bring other so-called "free" cysteines into transient association with the metal ions, shielding them from reaction with Bq at the exterior of the protein surface.

While the reaction profiles for As_1 - α MT and As_2 - α MT are relatively straightforward to explain, the reaction profile of the apo-species in the presence of the As-bound protein is much more difficult to interpret. At pH 2.8 it is unlikely that the apo- α MT adopts a compact conformation that should interfere or modify the accessibilities of the free cysteinyl thiols of the protein. All other studies which modified apo-MTs in isolation at low pH resulted in a Normal distribution of modified species.²⁵⁻²⁷ In previous metalation studies, fully metalated As-MT species have been shown to transfer As^{3+} to apo-species through protein-protein interactions.²⁸ Many other studies have demonstrated MT donating metals such as Zn and Cu to other metalloenzymes through direct interaction with each other.²⁹

The pattern is not likely a result of Bq aggregation or some other property of the cysteine-Bq reaction because the pattern is not replicated in the absence of a bound metal. In solutions only containing apo-MT this phenomenon is not seen.¹³ The presence of metal induced structure at pH 2.8 indicates that H-bonding may not be an important factor in determining As-MT structure. The pattern shown in Figure 4-4D is very similar to the one in 4-4C. It is likely the interaction and transfer from the As_1 - species to the apo-species is causing the altered reaction profile of Bq.

The models were calculated using MM3/MD techniques at a nominal MD temperature of 500 K temperature to simulate a low pH environment with the H-bonds disrupted. The models suggest that the apo- species is indeed the most open conformation of the protein and that when bound to arsenic, the protein adopts a more compact, globular structure. As described previously, even though apo-MT may have an open conformation at low pH, protein-protein interaction with partially metalated species may account for the Bq reaction profile resembling that of a more compact conformer. We suggest that the metalated species and apo-species interact with each other shielding the cysteine residues that are on the surface of both species. The transfer of arsenic most likely occurs by a process of coordination of the As^{3+} by exposed cysteinyl thiols on the surface of an apo-protein.²⁸ This would explain the drastic change in reaction profile, since under metal-free conditions those most exposed residues would be the ones most likely to react with an incoming Bq molecule. The inter-protein exchange maintains a pool of apo- and

minimally-modified species by shielding the residues that, under metal-free low pH conditions, would be the first to be modified. It should be noted that the most exposed residues at such a low pH would likely be closer to the ends of the peptide and have less shielding from the backbone on one side when compared to the cysteine residues in the middle of the sequence.

In addition to information gained about the conformations adopted by the MT species in solution, the stoichiometry was successfully confirmed. Discrete units of $\text{As}(\text{Cys})_3$ form until all cysteine residues are occupied in the β -domain and all but two are involved in coordinated in the α -domain. Unlike for the apo- and As_{1-2} - species the remaining free cysteine residues $\text{As}_{2/3}$ -species were equally accessible, giving rise to a Normal distribution of modified species (Figures 4-1 and 4-2). This is likely the result of significant compaction of the protein structure as more metals are coordinated. For Cd^{2+} metalation it was shown through IM-MS that the number of conformers converged as metalation proceeded and resulted in a more rigid and compact structure.³⁰ It is likely that arsenic metalation mirrors this process, although it is surprising that the convergence on a narrower set of compact conformers is possible even under typically denaturing conditions.

4.5 Conclusions

In this chapter we have demonstrated the multifaceted usefulness of our cysteine modification approach. We were able to confirm the stoichiometry of arsenic binding predicted through first principles of inorganic chemistry and that the binding mode is the same for all levels of arsenic saturation of MT. In addition, information pertaining to protein conformation and possible protein-protein interactions was obtained through the analysis of modification profiles. The deviance from Normal distribution under denaturing conditions is surprising and highlights the importance of metal coordination to the folding of MTs.

4.6 References

1. D. H. Petering, J. Zhu, S. Krezoski, J. Meeusen, C. Kiekenbush, S. Krull, T. Specher and M. Dughish, *Exp. Biol. Med.*, 2006, **231**, 1528-1534.
2. W. Braun, M. Vasak, A. H. Robbins, C. D. Stout, G. Wagner, J. H. Kagi and K. Wuthrich, *Proc. Natl. Acad. Sci. U.S.A.*, 1992, **89**, 10124-10128.
3. A. H. Robbins, D. E. McRee, M. Williamson, S. A. Collett, N. H. Xuong, W. F. Furey, B. C. Wang and C. D. Stout, *J. Mol. Biol.*, 1991, **221**, 1269-1293.
4. K. E. Rigby-Duncan and M. J. Stillman, *J. Inorg. Biochem.*, 2006, **100**, 2101-2107.
5. M. Capdevila, R. Bofill, O. Palacios and S. Atrian, *Coord. Chem. Rev.*, 2012, **256**, 46-62.
6. G. Jiang, Z. Gong, X.-F. Li, W. R. Cullen and X. C. Le, *Chem. Res. Toxicol.*, 2003, **16**, 873-880.
7. T. Fukada, S. Yamasaki, K. Nishida, M. Murakami and T. Hirano, *J. Biol. Inorg. Chem.*, 2011, **16**, 1123-1134.
8. M. J. Stillman, *Coordination Chemistry Reviews*, 1995, **144**, 461-511.
9. J. An, Y. Pan, Z. Yan, W. Li, J. Cui, Y. Jiao, L. Tian, R. Xing and Y. Lu, *J. Cell. Biochem.*, 2013.
10. T. Otsuka, A. Hamada, K. Iguchi, S. Usui and K. Hirano, *Biodmed. Rep.*, 2013, **1**, 614-618.
11. M. Vašák, *J. Trace Elements Med. Biol.*, 2005, **19**, 13-17.
12. K. E. Rigby and M. J. Stillman, *Biochem. Biophys. Res. Commun.*, 2004, **325**, 1271-1278.
13. K. L. Summers, A. K. Mahrok, M. D. M. Dryden and M. J. Stillman, *Biochem. Biophys. Res. Commun.*, 2012, **425**, 485-492.
14. D. H. Petering, J. Zhu, S. K. Krezoski, J. Meeusen, C. Kiekenbush, S. Krull, T. Specher and M. Dughish, *Exp. Biol. Med.*, 2006, **231**, 1528-1534.
15. A. Arseniev, P. Schultze, E. Woergoetter, W. Braun, G. Wagner, M. Vasak, J. H. R. Kaegi and K. Wuthrich, *J. Mol. Biol.*, 1988, **201**, 637-657.
16. D. A. Fowle and M. J. Stillman, *J. Biomol. Struct. Dyn.*, 1997, **14**, 393-406.

17. D. E. K. Sutherland, M. J. Willans and M. J. Stillman, *Biochemistry*, 2010, **49**, 3593-3601.
18. K. L. Bren, V. L. Pecoraro and H. B. Gray, *Inorg. Chem.*, 2004, **43**, 7894-7896.
19. K. E. R. Duncan and M. J. Stillman, *FEBS J.*, 2007, **274**, 2253-2261.
20. M. E. Merrifield, J. Chaseley, P. Kille and M. J. Stillman, *Chem. Res. Toxicol.*, 2006, **19**, 365-375.
21. O. A. Kharenko and M. Y. Ogawa, *J. Inorg. Biochem.*, 2004, **98**, 1971-1974.
22. R. Reid, J. Garipey, A. Saund and R. Hodges, *J. Biol. Chem.*, 1981, **256**, 2742-2751.
23. K. E. Rigby-Duncan and M. J. Stillman, *Journal of Inorganic Biochemistry*, 2006, **100**, 2101-2107.
24. M. Good, R. Hollenstein, P. J. Sadler and M. Vasak, *Biochemistry*, 1988, **27**, 7163-7166.
25. K. L. Summers, A. K. Mahrok, M. D. Dryden and M. J. Stillman, *Biochem. Biophys. Res. Commun.*, 2012, **425**, 485-492.
26. G. W. Irvine, M. Santolini and M. J. Stillman, *Protein Sci.*, 2017.
27. G. W. Irvine, K. E. Duncan, M. Gullons and M. J. Stillman, *Chemistry—A European Journal*, 2015, **21**, 1269-1279.
28. T. T. Ngu, M. D. Dryden and M. J. Stillman, *Biochem. Biophys. Res. Commun.*, 2010, **401**, 69-74.
29. T. B. Pinter and M. J. Stillman, *Biochemistry*, 2014, **53**, 6276-6285.
30. S.-H. Chen, L. Chen and D. H. Russell, *J. Am. Chem. Soc.*, 2014, **136**, 9499-9508.

Chapter 5

5 Selective cysteine modification of metal-free human metallothionein 1a and its isolated domain fragments: Solution structural properties revealed via ESI-MS⁴

5.1 Introduction

Since their discovery in 1957¹, metallothioneins (MTs) have been of interest due to their many unique structural and metal binding properties. These special properties include binding of up to 7 Zn²⁺ and Cd²⁺, forming two metal-thiolate clustered domains (the α and β -domains) that are joined by a short linker sequence.²⁻³ While the biological function(s) of this family of proteins are still debated, it is generally agreed that their functions are connected with zinc and copper homeostasis⁴⁻⁷, redox signalling⁸⁻¹⁰ and toxic metal sequestration.¹¹⁻¹⁵ Despite these many proposed functions, and their capacity to bind so many metals,¹⁶⁻¹⁷ MTs are surprisingly small, flexible proteins that lack typical optically active structural features. This lack of formal secondary and tertiary structure in the absence of bound metal ions precludes traditional structural analysis via spectroscopic methods.¹⁸⁻¹⁹ In addition, the dynamic nature of the coordinated metals in the metal-binding sites makes characterization even more difficult for metalation states other than the fully saturated protein.^{2, 20}

The structures of metallated metallothioneins have been probed with a wide range of methods, including fluorescent resonance energy transfer (FRET)²¹, ion-mobility mass-spectrometry (IMS)²² and, following cysteine modification, electrospray ionization mass spectrometry (ESI-MS) analysis.²³⁻²⁵ Traditional ESI-MS studies have resulted in a large number of mass spectrometric data being reported that clearly distinguish between

⁴ A version of this chapter has been published

Reproduced with permission from: Irvine, Gordon W., Melissa Santolini, and Martin J. Stillman. "Selective cysteine modification of metal- free human metallothionein 1a and its isolated domain fragments: solution structural properties revealed via ESI- MS." *Protein Science* (2017). DOI: 10.1002/pro.3139

Copyright 2017 Wiley

metalation states present in solution. Through the semi-quantitative properties of ESI-MS, the distribution of those species can be analyzed.²⁶ In addition to the extent of metal-saturation, ESI-mass spectral data can also determine the relative concentrations of the many differentially modified protein species simultaneously.²⁴ The abundance of easily modifiable cysteine residues (20 in human MTs) offers an opportunity to exploit this reactivity to obtain information on the solution structure of MTs based on the relative reactivity of individual cysteinyl thiols.^{25, 27-28} This experiment is similar to the use of H/D exchange in identifying regions of proteins that are more or less exposed to the solvent.²⁹⁻³⁰ Analysis of charge state distributions³¹ and ion drift in IMS gives additional information about the overall folded state of the protein.³²

ESI-mass spectral data have been used to determine structural properties of apo-MT²⁵ and MT partially metalated with As³⁺²⁴ and Cd²⁺^{28, 33}. ESI-MS data can also be used to determine quantitative biochemical parameters as recently demonstrated in the determination of arsenic metalation kinetics³⁴, cadmium and zinc equilibrium and kinetic constants^{28, 35-36} and copper binding affinity.³⁷ The key to these semi-quantitative data is the assumption that apo-MTs and those with different numbers of metals coordinated exhibit very similar ionization efficiencies; this assumption has been supported by the literature, especially for metalation of metallothioneins.³⁸ While it is true that the different MT-isoforms will have slightly varying ionization efficiencies,³⁹ when analyzing modifications of the same isoform, the behavior of all species in solution has been demonstrated to be predictable and the metal-binding parameters determined align closely with those determined by other methods.^{36, 40-41}

Previous studies using cysteine modification agents to probe the solution structure and metal binding properties of MTs have focused on one modifier at a time, leading us to question whether there was a bias based on the size and relative solvation properties of the modifying molecule.

In this chapter, we use three cysteine modification agents of varying size and hydrophobicity, p-benzoquinone (Bq), N-ethylmaleimide (NEM) and iodoacetamide (IAM), to probe MT solution structure as a function of the accessibility of its cysteine

residues. We carried out the reactions of the full-length human MT1a and its isolated α - and β -domains under native and denaturing conditions. By analyzing the characteristic modification profiles of folded and unfolded MTs (obtained at neutral and low pH) as well as changes in charge state distribution, we describe the modification properties of the folded, globular apo-metallothionein structure under native conditions and compare it under denaturing conditions. The ESI-mass spectral data provide modification profiles and charge state distributions that we use to determine the relative accessibility of the cysteinyl thiols to the modifiers, which leads to conclusions about the overall compactness of the proteins.

5.2 Methods

5.2.1 Protein preparation

Recombinant human metallothionein 1a ($\beta\alpha$: MGKAAAACSC ATGGSTCTG SCKCKECKCN SCKKCC SCCPMSCAKC AQGCVCKGAS EKCSCCK KA, α : GSMGKCCSC CPMSCAKCAQGCVC KGASEKCSCKKAAAA, β : GSMGKAAAA CSCATGGSTCTGSC KCKECKNSCKKAAAA) was expressed with an S-tag in BL21 *E. coli* cells which has been described in detail elsewhere.⁴² In brief, cells containing the plasmid constructs for the full protein ($\beta\alpha$ -MT1a) and for the isolated domains (β -MT1a and α -MT1a) were plated on to growth media containing kanamycin from a stock culture stored at -80°C and grown for 16 hours at 37°C . The cells were then transferred into 1L broth cultures enriched with $50\ \mu\text{L}$ of 1 M cadmium and incubated in a shaker for 4 hours until OD 600 absorbance was between 0.6-0.8. Isopropyl β -D-1-thiogalactopyranoside (IPTG) was then added to induce expression of MT and 30 minutes later $150\ \mu\text{L}$ of 1 M cadmium sulfate was added. The cells were collected 3.5 hours after induction, centrifuged and stored at -80°C .

The recombinant cells were lysed using a cell disruptor (Constant Systems, UK) at 20K psi. The cell lysate was centrifuged for 1h to remove cellular debris. The supernatant was filtered and loaded on to an SP ion exchange column (GE Healthcare) with a total volume of 10 mL. The columns were washed with pH 7.4 10 mM Tris (tris-hydroxymethylaminomethane) buffer for approximately 2h to remove loosely bound

proteins and other organic materials. MT was eluted using an increasing gradient of 1 M NaCl + 10 mM Tris buffer at pH 7.4. The eluted MT was concentrated down to <20 mL and the S-tag cleaved using a Thrombin Clean-Cleave kit as per the manufacturers' instructions (Sigma-Aldrich). The S-tag was separated using an ion-exchange column since the S-tag does not bind as strongly as MT and thus elutes at lower salt concentrations. The eluted, cut Cd-MT was concentrated to approximately 120 μM and stored at -20°C . In this chapter, we refer to the recombinant human liver MT1a isoform as "MT", but all other isoforms are referred to with their complete isoform and subisoform descriptors.

To prepare MT for the modification experiments, aliquots were first demetalated and desalted using centrifugal filter tubes with a 3 kDa membrane (Millipore) and a 10 mM pH 2.8 ammonium formate buffer. The low pH solutions contained 1 mM dithiothreitol (DTT) to prevent oxidation of the free thiols in MT. The pH was raised by buffer exchange with argon saturated, pH 7.0 10 mM ammonium formate solutions that did not contain reductant. The final concentration of the protein solutions were determined by remetalation of a small aliquot with cadmium using the metal-to-ligand charge transfer band at 250 nm ($\epsilon_{250} = 89,000 \text{ Lmol}^{-1} \text{ cm}^{-1}$). The solutions were also monitored for oxidation using UV-visible absorption spectroscopy to monitor absorption corresponding to 280 nm from oxidized disulfide. Once demetalated and desalted, the MT concentration was determined, all concentrations were between 40-90 μM to ensure good signal to noise ratios In the ESI-MS experiment.

In addition to demetalating MT in the presence of DTT, the solutions were vacuum degassed and bubbled with Argon to displace any dissolved oxygen. This was also carried out for the 10 mM 1,4-benzoquinone (Bq), N-ethylmaleimide (NEM) and iodoacetamide (IAM) solutions and the 0.5% NH_4OH and 0.5% formic acid solutions as well to ensure no oxygen was introduced into the system during the modification reaction or pH adjustment. Great care was taken to reduce the possibility of oxidation of the protein especially at neutral pH. All modification agents were obtained from Sigma-Aldrich (USA).

5.2.2 ESI-mass spectra collection

Mass spectra were measured with a micrOTOF II electrospray-ionization time-of-flight mass spectrometer (Bruker Daltonics) in the positive ion mode. NaI was used as the mass calibrant. The scan conditions for the spectrometer were: end plate offset, -500 V; capillary, $+4200$ V; nebulizer, 2.0 bar; dry gas flow, 8.0 L min^{-1} ; dry temperature, 30 °C; capillary exit, 180 V; skimmer 1, 22.0 V; hexapole 1, 22.5 V; hexapole RF, 600 Vpp; skimmer 2, 22 V; lens 1 transfer, 88 μs ; lens 1 pre-pulse storage, 23 μs . The mass range was 500.0–3000.0 m/z . Spectra were assembled and deconvoluted using the Bruker Compass data analysis software package. ESI-mass spectrometry was used to monitor all stages of the modification reaction. Approximately 1 molar equivalent of the modifying agent (Bq, NEM or IAM) was added stepwise and a spectrum recorded after each addition. The ESI-mass spectra were recorded and averaged over 2 minutes.

5.2.3 Molecular models

MM3/MD calculations were carried out using Scigress Software (Fujitsu, Poland) and parametrized using the modified force field described by Chan *et al.*⁴² with the dielectric constant of 78 for water to obtain energy minimized structures of the Cu-bound protein. The original apo-MT1a structure was obtained from Rigby *et al.*¹⁹ A cycle of MM3 minimizations followed by MD calculations gave energy-minimized apo-MT structures reported here. The structures were first energy minimized using the MM3 calculation followed by an MD simulation at 500 K for 10 ps and then another MD simulation at the same temperature for 1000 ps. Structures with closed, intermediate and open configurations were selected from energy minima as representations of the multiple conformations apo-MT adopts in solution.

5.3 Results

5.3.1 Modification of the isolated α - and β -domain fragments of metallothionein

The isolated α - and β -domain fragments of MT were reacted with each of the three cysteine modifying agents to probe the compactness of their structures at neutral (native conditions) and low pH (denaturing conditions). The fragments were studied separately

from the full-length protein to test whether cysteinyl thiols would be buried to a different extent within the smaller volumes of the individual fragments, especially the small β -domain. Figure 5-1 shows the reaction profile of the β -domain fragment (N-terminus fragment) with p-benzoquinone (Bq). The data show the distinct cysteine access differences between the unfolded state of the fragment at low pH, and the folded, native state at pH 6.8. At low pH the modifications follow a systematic and stochastic trend as the number of equivalents of Bq molecules added increases. At pH 6.8, the pattern is very different, with both the unmodified (0 Bq) apo-fragment and the fully modified (9 Bq) fragment coexisting. While some adducts are present in the low pH spectra, they did not add to the shielding and a Normal distribution of modifications is seen.

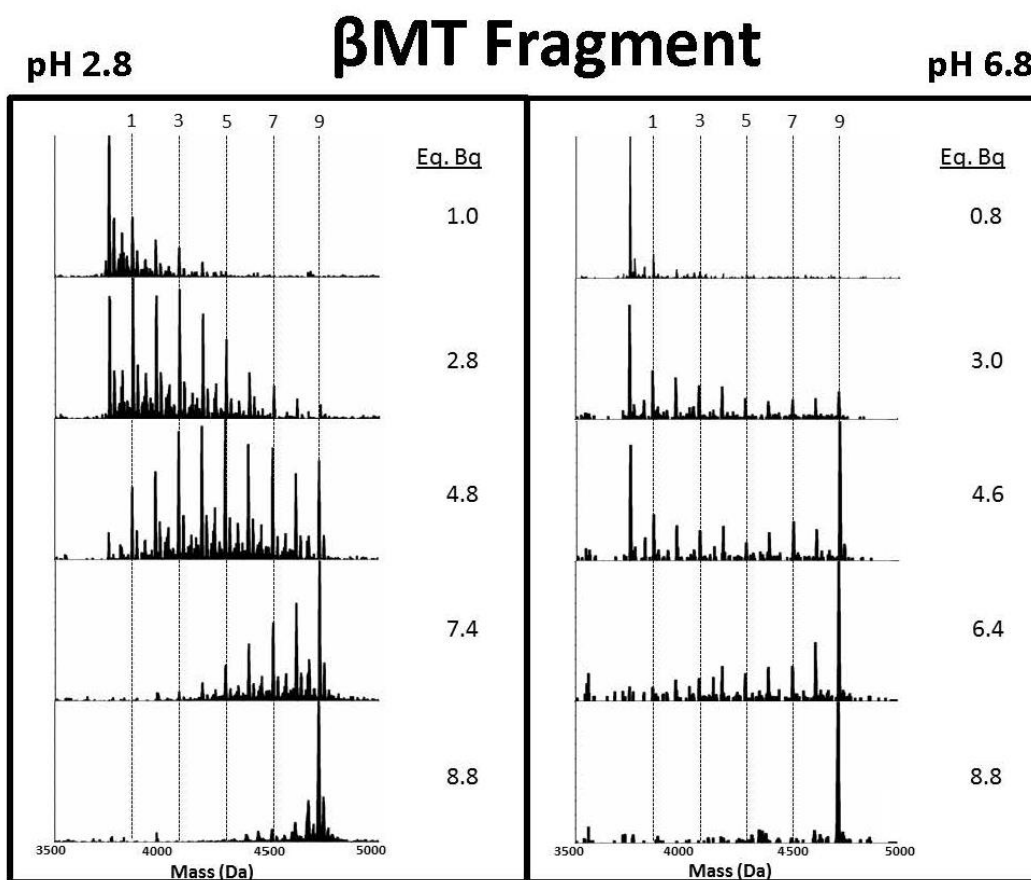


Figure 5-1: Representative deconvoluted ESI-MS spectra from the modification of the β -domain fragment of MT1a with p-benzoquinone (Bq). The reaction at pH 2.8 (left panel) and 6.7 (right panel) gave markedly different reaction products labelled with vertical lines for the 1, 3, 5, and 9 Bq bound masses. Note that the apo-fragment is not indicated, its mass lies to the left of the “1” line. The fully modified fragment is indicated

by the “9” line.. The number of molar equivalents of Bq added in the stepwise titration is listed to the right of each panel up to 8.8.

In the second test, the more hydrophobic and slightly larger modifier, NEM, was used. The reaction profile of the β -domain fragment with NEM is shown in Figure 5-2 under native and denaturing conditions. At low pH, the data show the incremental increase in modification as the mol. eq. of NEM are increased. At pH 7.4 NEM modified fragments from apo-(0) to fully modified (9) are present until the end; a stark departure from the pattern than observed at low pH and remarkably similar to the Bq modification pattern. At all points during the reaction either apo- or Bq₉- β MT are the most abundant species.

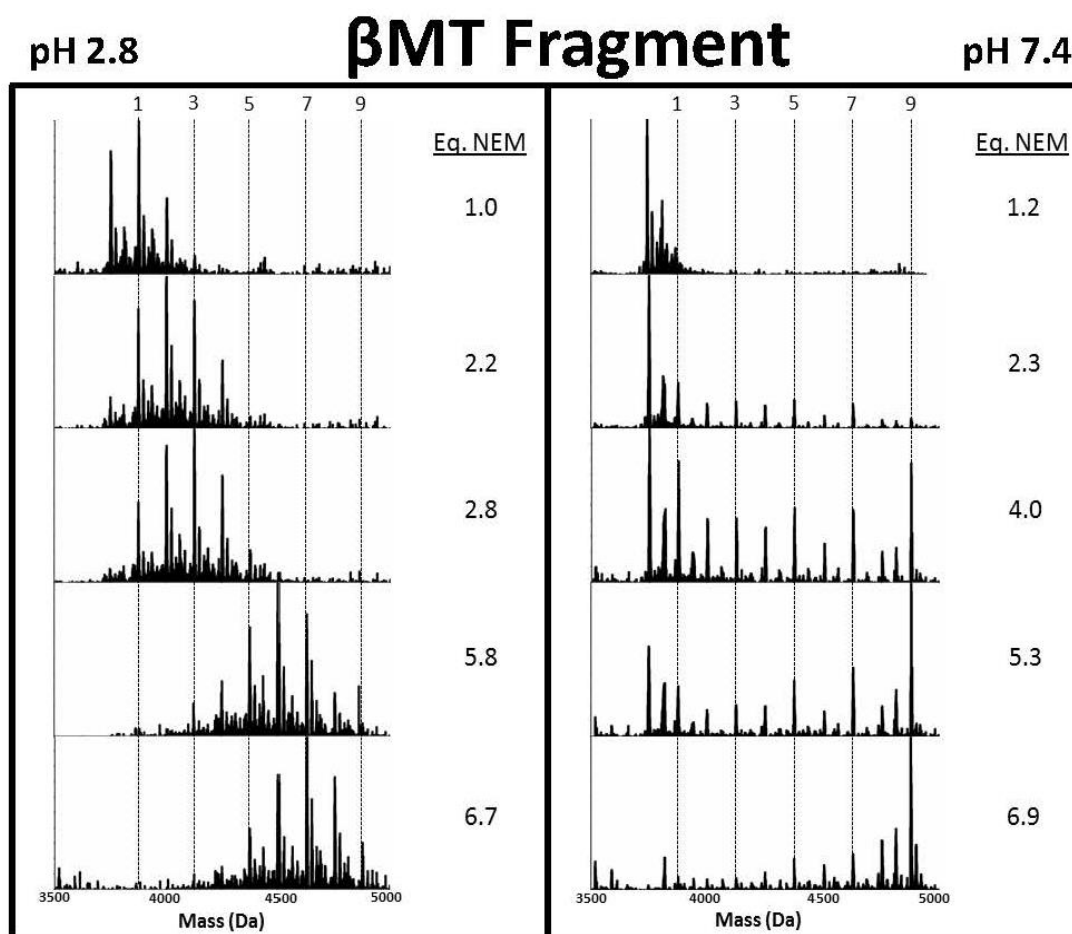


Figure 5-2: Representative deconvoluted ESI-MS spectra from the stepwise modification of the β MT fragment by NEM. The extent of the modification in terms of number of covalent NEM modifications on the MT is shown by the vertical lines for the 1, 3, 5, and 9 NEM bound masses. Note that the apo-fragment is not indicated, its mass lies to the left of the “1” line. The fully modified fragment is indicated by the “9” line..

The number of molar equivalents of NEM added in the stepwise titration is listed to the right of each panel up to 8.8. The NEM was added stepwise with the mol eq as shown to the right of each panel at pH 2.8 (left panel) and pH 7.4 (right panel).

The reaction profiles for the NEM and Bq modification reactions of the β -domain fragment of MT1a (Figs 1 and 2) are strikingly similar at low pH. Both exhibit a stochastic, Normal distribution of intermediate species under these denaturing conditions. Under more native conditions for both modifiers the starting apo- β MT and end product, Mod₉ β MT are the two dominant species in solution with minor abundance of intermediate species. It appears that the modification of the β -domain fragment leads to the protein unfolding, promoting subsequent modification reactions due to the disruption of native structure and exposure of previously buried Cys residues to the solvent. The series of spectra show that throughout the stepwise addition, the native and the fully modified “9” species are the most abundant. The extent of the modifications is seen clearly near the 4.0 NEM mol. eq. point where the differences between neutral and low pH spectra are most dramatic. To further understand the properties of this metal-free, native, folded state of MT under these conditions, the charge state distributions were analyzed.

The charge states of the isolated domain fragments were similar following complete modification with both Bq and NEM. The charge state distributions for the NEM modifications of the β -domain fragment are shown in Figure 5-2. In each of the 6 panels, the charge state average shifts higher following the Cys modification reaction, indicating an increase in surface area. The weighted average charge state shifts only slightly for the apo-proteins between native and denaturing conditions before modification reactions. For $\beta\alpha$ MT the native condition average charge state is 5.2 and increases marginally to 5.5 when the pH is lowered (Left spectra 3A and B). There is a more dramatic shift in charge states upon modification in all cases. The largest differences in average charge state occurs under native conditions in the $\beta\alpha$ - and α -MT modification reactions (3A and E). While the appearance of new charge states indicates unfolding, the effect in the small MT-protein and the even smaller fragments is more subtle than in classic studies, such as that for myoglobin unfolding. Thus it is difficult to make conclusions about the folded

state of MT from charge states alone. However, when combined with the ESI-MS data for the modification reaction patterns the conformational picture of MT becomes clearer.

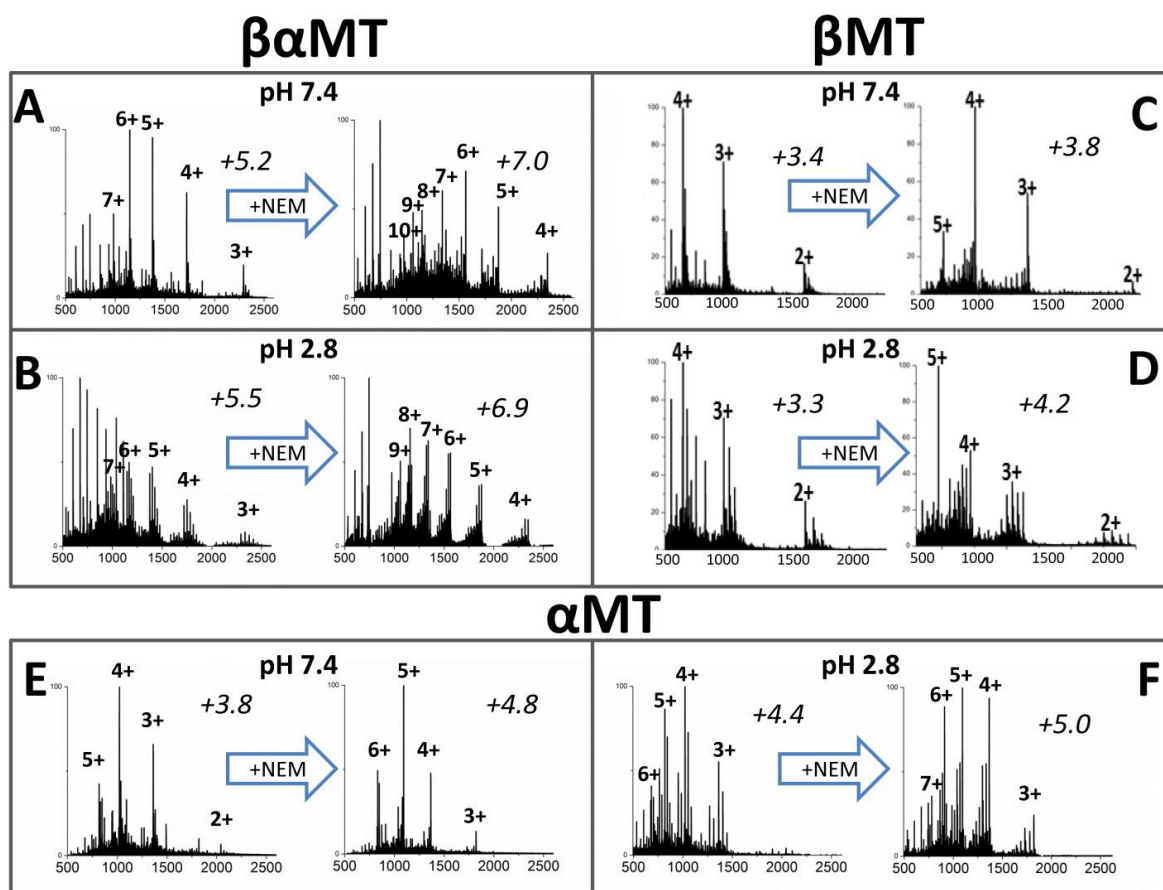


Figure 5-3: Representative ESI-MS charge state manifolds measured during cysteine modification of $\beta\alpha$ MT1a and its isolated fragments. Spectra at approx. 1.6 mol. eq. of NEM added are shown on the left side of each panel and those near the end of the titration on the right side. The weighted average charged state is shown above each spectrum in italics.

The α -domain fragment reacted in a very similar manner when modified with both Bq and NEM. The data for the reaction of the α -domain fragment of MT1a with Bq has been published previously,²⁵. The stepwise NEM modification reaction of the α -domain fragment under native and denaturing conditions is shown in Figure 5-4.

The reaction at pH 2.8 follows the trend for the β -domain fragment and also the previously reported modification of the α -domain fragment by Bq.²⁵ Under denaturing conditions, where the peptide is expected to be unfolded, modification follows a

stochastic, Normal distribution of modified intermediates. As above for the β -domain fragment, at neutral pH it can be seen that the α -domain fragment modification by NEM results in very low abundance of the partially-modified intermediates ($NEM_{1-10}\alpha MT$) when compared with the β -domain reaction. The series of spectra in Figure 5-4 (right) indicate that the initial modification of the apo-fragment is initially sterically unfavorable compared with the low pH reactions. However, once modification has begun, those peptides unfold allowing the subsequent modification to proceed rapidly, culminating in the growing presence of the fully modified $NEM_{11}\alpha$ -fragment. The throttling effect of the initial steric hindrance to modification by NEM results in the very low abundances of the partial modified fragment. The implication is that for the α -domain fragment under native conditions, the folded native peptide is resistant to modification.

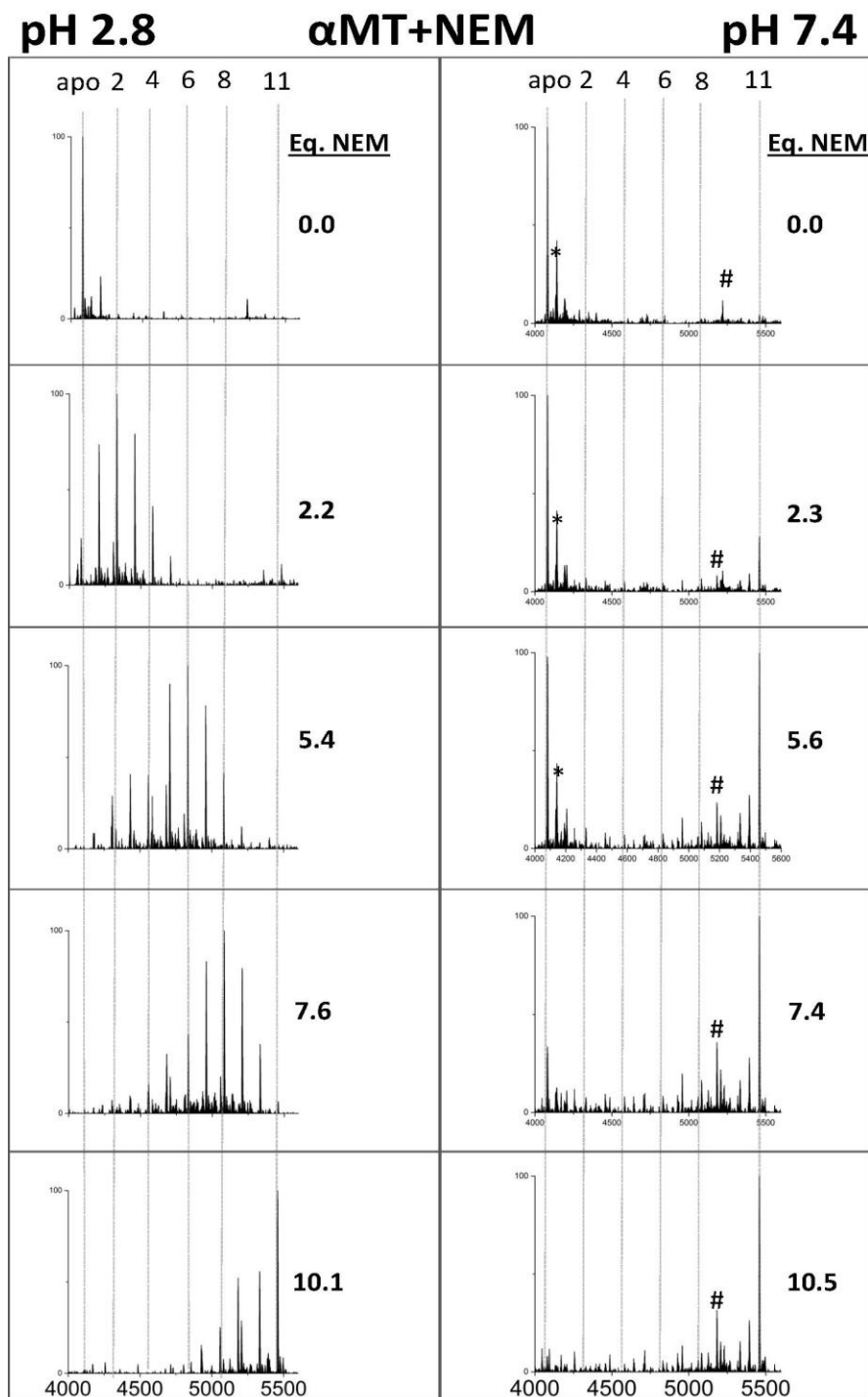


Figure 5-4: Representative deconvoluted ESI-MS spectra of the modification of α MT fragment with NEM. The extent of the covalent NEM modification (0 -11) is shown by vertical lines (apo (0), 2, 4, 6, 8, and 11). NEM was added stepwise, with the molar equivalents added shown to the right of each panel, at pH 7.4 (left panel) and 2.8 (right panel). *-+60 Da adduct, #-unknown contaminant at 5183 Da not corresponding to MT or any modified species.

5.3.2 Modification of the full-length protein ($\beta\alpha$ MT)

The full length protein, $\beta\alpha$ MT, consists of the two isolated domain fragments discussed in the previous sections, joined by a short linker sequence. The protein is much larger with 20 cys in the sequence. Much like the isolated domain fragments, the full protein exhibits a stochastic, Normal distribution of modification intermediates (NEM/Bq₁₋₁₉ $\beta\alpha$ MT) under denaturing conditions as can be seen in Figure 5-5. Both NEM and Bq modifiers exhibit nearly identical patterns and this is consistent across all three peptides studied. Despite the differences in size and hydrophobicity, both NEM and Bq reactions cause similar changes to the structure of the proteins under native conditions.

The results of the modification reactions at pH 7.4 are substantially different when compared with the isolated domains fragments. In particular, the charge state distribution significantly changes during the modification reaction at pH 7.4, which can be seen in Figure 5-3 (left panel). Two new charge states (+9 and +8) emerge for the fully modified protein (NEM₂₀ $\beta\alpha$ MT) compared with only a slight shift in charge state abundance for the modified isolated α - and β -domain fragments. This can be explained by a larger number of covalent modifications, resulting in a much larger peptide that also has a very different electrostatic surface and by the more drastic surface area difference between the folded and unfolded states.

Despite having different properties, it is clear that in the case of the full MT protein at denaturing pH (2.8), cysteine modification with Bq and NEM follows a similar pathway, resulting in largely the same type of reaction profile. In order to contrast the reactions of these hydrophobic molecules, we also used iodoacetamide (IAM) to covalently modify the cysteine residues of the full MT protein. The full length protein was chosen for IAM modification because of the more dramatic changes in charge state and reaction pattern expected. IAM is much smaller, more hydrophilic and reacts via a different mechanism than the NEM and Bq cysteine modifiers described above.

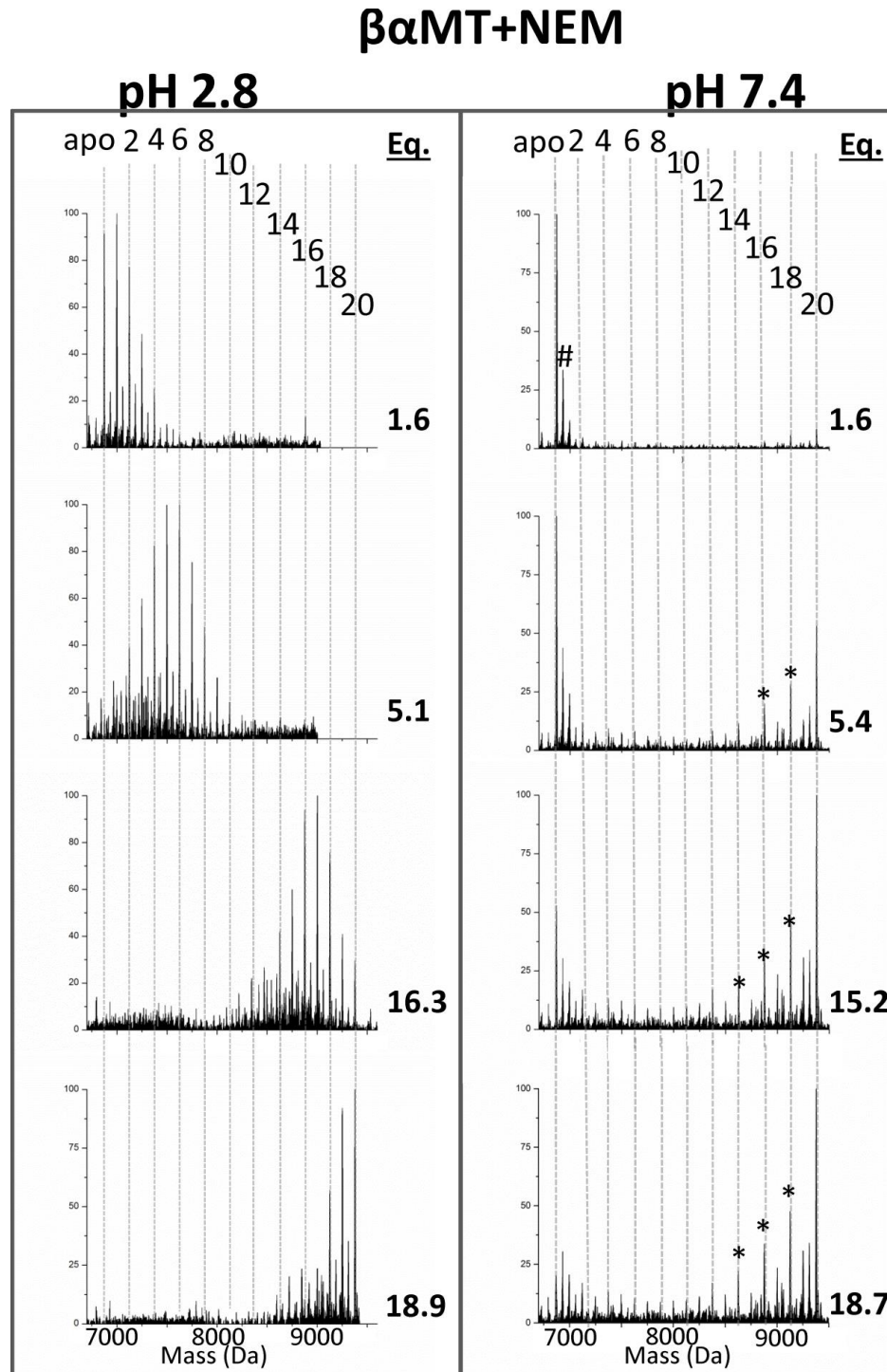


Figure 5-5: Deconvoluted mass spectra of NEM modifications of $\beta\alpha$ MT under native (pH 7.4, right) and denaturing (pH 2.8, left) conditions. The masses and numbers of the covalent modifications are shown by the vertical lines 0 (apo)-20. The mol. eq. of NEM reacted are shown to the right of each spectrum. *-indicates the presence of partially oxidized MT species #+60 Da adduct.

Figure 5-6 shows the results of the IAM modification experiment. Under both denaturing (7, left panel) and native (7, right panel) conditions, IAM results in a Normal distribution of modified MT species, although the distribution is wider under the native, pH 7.4 conditions. At low pH, the modification reaction is much slower than for the other two modifiers tested and excess IAM was reacted with the apo-MT solution overnight. However, even with a large excess of IAM, after 24 h only 5.8 molar equivalents of IAM had reacted but the general pattern of modification is apparent and matches that of the other modifiers. It is also similar to the neutral pH reaction in terms of modification profile and distribution of modified species, although a smaller range of modified species are present at any given time. The IAM modification did not result in the cooperative modification patterns indicative of structure disruption in the full length protein.

5.4 Discussion

The challenges of investigating the structure of apo-metallothioneins are numerous. The fluxional nature of a disorganized peptide and the lack of good chromophores make traditional methods of structure determination difficult or impossible. Proton NMR showed a disordered structure for apo-human, horse and bovine MT2a, however, the chemical shifts were similar to the zinc and cadmium analogues.⁴³ FRET studies have shown that the overall volumes of the full protein, as well as its isolated domains, are largely unchanged between the metal-free and metal-saturated states.^{21, 44-45} Ion-mobility mass-spectrometry has confirmed the presence of a range of conformations in the apo-protein and the fluxionality inherent before metal binding occurs.²² In previous reports, we have begun to probe the structure via global reactivity towards cysteine modifying agents.^{24-25, 27, 31} Other groups have also probed the reactivity of the fully metalated protein towards NEM to investigate properties of demetalation and stability of cadmium-MT clusters.³³

In this study we sought to probe the metal-free solution structures of $\beta\alpha$ MT and its isolated domain fragments using three different commonly used cysteine modifiers and analyze the reaction profiles using ESI-MS. Our report here includes the reaction profiles for modification of the isolated domain fragments and contrasts those differential modification data with the reactivity of the full length protein. The isolated domains being smaller, having less overall volume and a smaller surface area than the full protein were predicted to exhibit a smaller change in average charge state and this is observed in Figure 5-3. Although the charge states only changed slightly in the isolated domain fragments (α increased 1.0 and 0.6 and β 0.4 and 0.9 at high and low pH respectively), reaction profiles for NEM and Bq followed a cooperative pathway under native conditions at neutral pH (Figures 5-1, 5-2 and 5-4).

We have previously described the cooperative pattern arising from unequal solvent access of the cysteines in apo-MTs.²⁵ The modification proceeds rapidly once the compact conformation initially proposed many years ago from early molecular dynamics calculations¹⁹ is unfolded by the initial modifications. This indicates that both isolated

fragments are capable of adopting a more folded conformation to shield cysteine residues from the solvent despite their small size (3.7 and 4.08 kDa).

In Figures 5-1, 5-2 and 5-4, it is clear that during the reaction of both apo- α and apo- β , the unmodified apo-fragments coexist with the fully modified protein during the step-wise addition of the modifier. This is counter-intuitive for a protein with 9 or 11 cysteinyl thiols that remain unreacted while other individual MT molecules, with only a few free cysteines, react to become fully modified. This can be explained by the compact conformers adopted by the full length protein at neutral pH (6.8 – 7.4) making the cysteines sterically inaccessible. Conceptually, it can be understood that modifiers of any size or of hydrophobicity should be at least somewhat hindered in their reaction. The data we have measured are essentially “snapshots” of the reaction, the progress reports that would be observed if excess modifier were added and ultra-high speed spectra recorded. Instead we use a step-wise addition where we run out of modifier and the distribution of modified species is recorded at each point. The modification status is governed by the relative kinetics of the reaction to modify each cysteine. The reaction kinetics are governed by two major factors: the intrinsic rate of the chemical modification of the cysteine and the inhibition effect of the steric hindrance of the surrounding protein structure. Since the reactions are irreversible, the reverse equilibrium reaction has no effect on the distribution of the products.

Under denaturing conditions at low pH, all three modifiers (NEM, Bq and IAM) followed pathways that resulted in a stochastic, Normal distribution of species that summed to the mol. eq. of modifier added. Under these conditions the protein adopts a more extended conformation and it is reasonable to conclude that all cysteines are essentially equally exposed to the solvent and incoming modifier molecules. This results in a purely statistical reaction pathway where individual MT molecules with more unreacted cysteinyl thiols are more likely to be modified than those with more modifications already present.

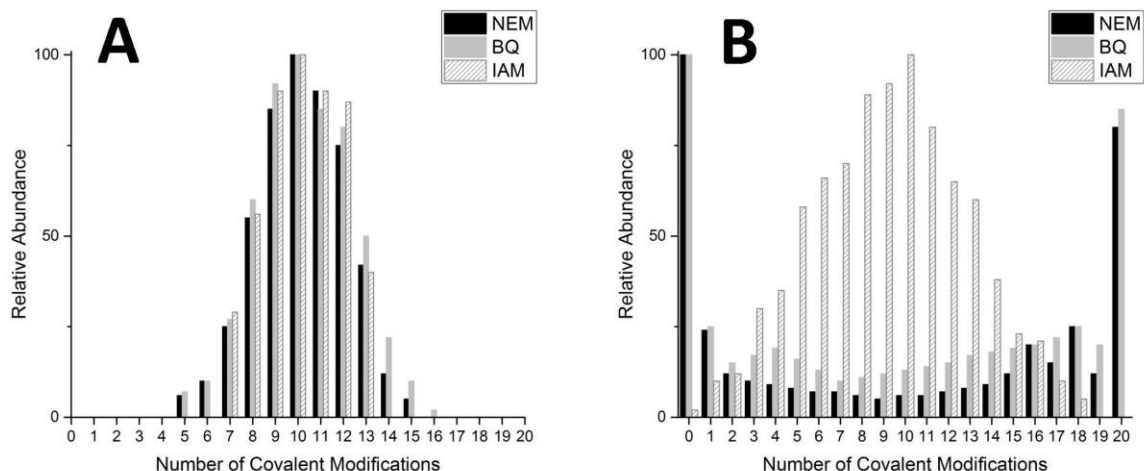


Figure 5-7: Comparison of the reaction profiles shown by the relative abundances of each modified β MT-species at approximately the half way point, for the three cysteine modifiers used. (A) Relative abundances under denaturing conditions at pH 2.8-3.0 and (B) relative abundances under native conditions at pH 6.8-7.4. The relative abundances shown in this Figure were extracted from raw deconvoluted ESI-MS data at approximately 10 mol. eq. of each modifier.

A very different picture emerges during modification under native conditions at neutral pH. The larger, more hydrophobic modifiers (NEM and Bq) give rise to a cooperative-like pattern. Under native conditions, the more compact conformations shield most of the cysteinyl thiols, allowing only a fraction of the apo-protein to react, becoming increasingly unfolded as modifications proceed. Russell and co-workers showed a small fraction of apo-MT2a exists as a more disordered and open conformer, at least in the gas phase for the +5 charge state.²² These conformers are likely more accessible for modification and are the ones that fully react, leaving the more compact conformers of apo-MT with unmodified thiols. To visualize the equilibrium between apo-MT conformers, molecular dynamics simulations were used to generate a range of possible structures (Figure 5-8). Because the reaction with the modifiers is controlled by access to the cysteinyl thiols, the thiols in the more compact conformers remain less reactive than those species whose structure has been disrupted by modification. This results in a large fraction of unreacted apo-MT, small amounts of partially modified protein and the accumulation of the fully modified protein as seen in Fig 8B for NEM and Bq modifications.

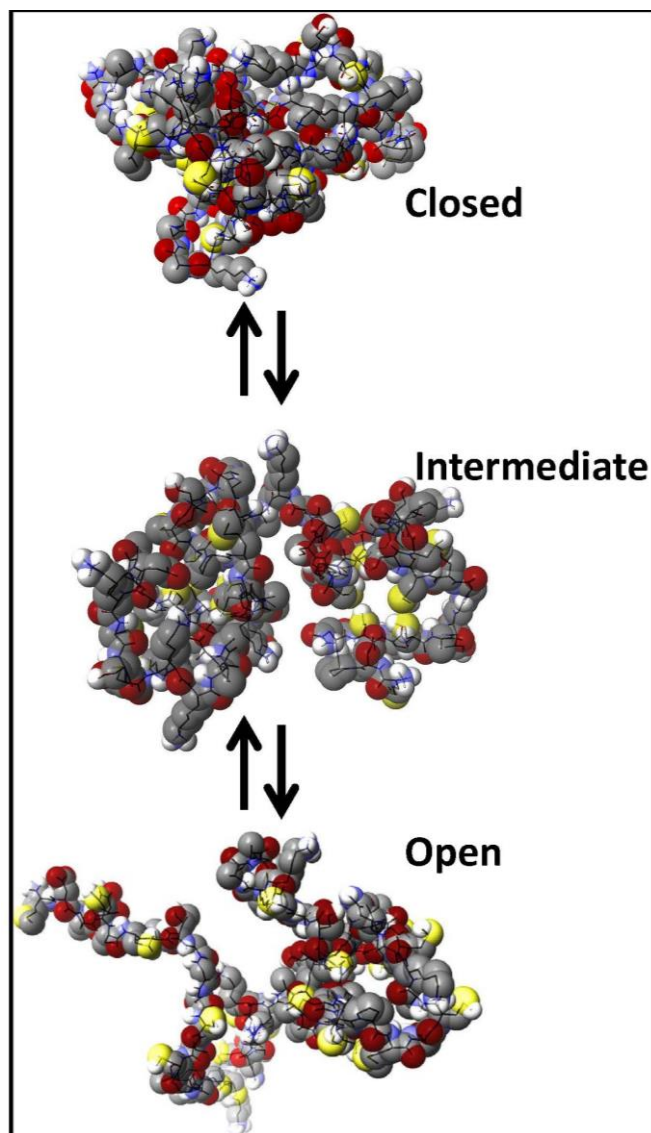


Figure 5-8: Molecular dynamics simulated structures of apoMT under native conditions. The "closed" structure is one where the Cys residues are more buried within the interior of a bundled protein, "intermediate" where there is more access to the Cys residues and "open" where there is the most unhindered access.

It is interesting that this cooperative-like pattern is not observed in the mass spectral data from the reaction of the smaller and more hydrophilic IAM modifier. Instead, a wider stochastic distribution is observed and the width of the distribution of the IAM reaction profile is compared in Figure 5-9C. The wider distribution is likely due to the unequal solvent accessibility of the cysteinyl thiols in the folded configuration. IAM is less disruptive to the compact conformers of MT than the larger and more hydrophobic Bq and NEM modifiers. This has implications for the choice of modifier when examining

properties of cysteine-rich proteins like MTs. IAM may be more suitable if native structure needs to remain largely intact, whereas Bq and NEM are better in producing a more dramatic change in reaction profile depending on the protein conformation. In addition, NEM is able to be used over a wide range of pH, 2.8-7.4 tested here, where IAM is unreliable at low pH (<4) and Bq unreliable at basic pH (>7) ranges.

Figure 5-9 compares the reaction profiles at the halfway point (10 mol. eq.) under native (neutral pH) and denaturing (acidic pH) conditions. The Bq and NEM reaction profiles show how the reactivity of apo-MT has been dramatically changed by the switch between compact and extended conformers at neutral and low pH respectively. However, these profiles are contrasted by the reaction profile of the IAM species, Fig 10C, where the profiles follow stochastic distributions under both denaturing and native conditions, although the low pH distribution is much narrower. This may be a function of slow kinetics of the reaction under these conditions or may speak toward the equal accessibility of the cysteines and even less interference by the surrounding peptide due to the small size of the IAM molecule.

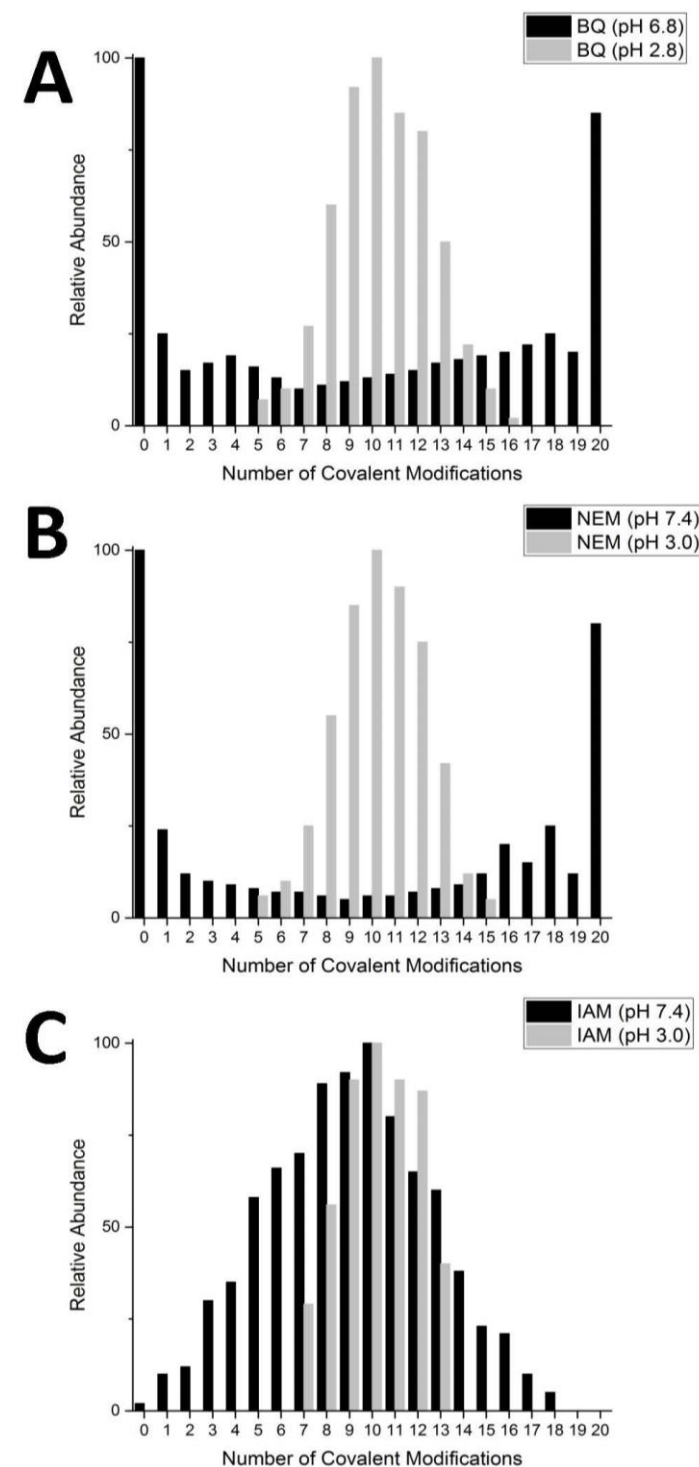


Figure 5-9: Extracted ESI-MS reaction profiles for all three cysteine modifiers used. In this Figure, the relative abundances of each of the $\beta\alpha$ MT-species are compared after 10 mol. eq. of each modifier has been reacted under native (neutral pH) and denaturing (low pH) conditions. (A) Comparison of the BQ, (B) NEM and (C) IAM reaction at low (grey bars) and neutral pH (black bars).

Our systematic approach in probing the structures of $\beta\alpha$ MT and its isolated domains have provided further evidence for the adoption of a bundled or compact structure by the metal-free protein. These data summarized in Table 5-1, indicate that even the smaller, isolated fragments behave in the same fashion. To completely understand the metalation mechanisms of MT, a starting point must be established which up until recently was a poorly defined apo-structure.

The biological significance of apo-metallothioneins remains a source of controversy within the community. Some have indicated that apo-MT comprises a significant portion of the cellular MT pool⁴⁶. Regardless, upon ribosomal translation the nascent MT will be in its apo-form and it remains a mystery how specificity and quantity of MT metalation occurs. The redox properties of MT have also been a source of controversy. While it is clear glutathione is the major source of reducing thiols in the cell,⁴⁷⁻⁴⁸ it is unclear to what extent MTs also play a role.⁴⁹⁻⁵¹ The "hidden" nature of most of the thiols in MT demonstrated in this chapter may cast doubt on how integral a role MT1a plays in cellular redox chemistry.

Table 5-1: Summary of reaction profiles following reaction of three cysteine modifiers with the full protein and the two isolated fragments under native and denaturing conditions

Protein construct	Modifier	Native reaction profile	Denatured reaction profile
$\beta\alpha$ MT1a	NEM	Cooperative	Non-cooperative, stochastic
	Bq ³¹	Cooperative	Non-cooperative, stochastic
	IAM	Non-cooperative, stochastic, wide distribution	Non-cooperative, stochastic, narrow distribution
α MT1a	NEM	Cooperative	Non-cooperative, stochastic
	Bq ²⁵	Cooperative	Non-cooperative, stochastic
	IAM	Non-cooperative, stochastic	Non-cooperative stochastic
β MT1a	NEM	Cooperative	Non-cooperative, stochastic
	Bq	Cooperative	Non-cooperative, stochastic
	IAM	Non-cooperative, stochastic	Non-cooperative, stochastic

5.5 Conclusion

In this chapter we describe the cysteine modification reactions of metallothionein and its isolated domain fragments with well known modification reagents (Table 5-1). All three peptides (α - and β -domain as well as the full $\beta\alpha$ MT) gave similar reaction profiles under native and denaturing conditions, indicating all three fold into a tightly wrapped structure, burying selective cysteine residues. The larger modifiers, Bq and NEM, showed the most drastic difference between conditions, going from a stochastic non-cooperative pattern when denatured to a cooperative one under native conditions. The smaller IAM only showed a broader distribution of modified cysteine residues under native conditions but the overall pattern was similar to the denatured conditions. The larger modifiers were better able to probe the ill-defined structure of apo-MT as they caused larger disruptions to the native fold. This highlights a new way probe intrinsically disordered, or "less ordered", protein structure by monitoring residue modification by ESI-MS.

5.6 References

1. M. Margoshes and B. L. Vallee, *J. Am. Chem. Soc.*, 1957, **79**, 4813-4814.
2. Y. Boulanger, I. Armitage, K. Miklossy and D. Winge, *J. Biol. Chem.*, 1982, **257**, 13717-13719.
3. W. Braun, M. Vasak, A. Robbins, C. Stout, G. Wagner, J. Kägi and K. Wüthrich, *Proc. Natl. Acad. Sci. U. S. A.*, 1992, **89**, 10124-10128.
4. T. Miyayama, Y. Ishizuka, T. Iijima, D. Hiraoka and Y. Ogra, *Metallomics*, 2011, **3**, 693-701.
5. T. Fukada, S. Yamasaki, K. Nishida, M. Murakami and T. Hirano, *J. Biol. Inorg. Chem.*, 2011, **16**, 1123-1134.
6. W. Maret, *The Journal of nutrition*, 2000, **130**, 1455S-1458S.
7. W. Maret, *BioMetals*, 2011, **24**, 411-418.
8. W. Maret, *The Journal of nutrition*, 2003, **133**, 1460S-1462S.
9. Y. J. Kang, *Exp. Biol. Med.*, 2006, **231**, 1459-1467.
10. H. Gonzalez-Iglesias, L. Alvarez, M. García, C. Petrash, A. Sanz-Medel and M. Coca-Prados, *Metallomics*, 2014, **6**, 201-208.

11. R. J. Person, N. N. O. Ngalame, N. L. Makia, M. W. Bell, M. P. Waalkes and E. J. Tokar, *Toxicol. Appl. Pharmacol.*, 2015, **286**, 36-43.
12. W. Qu and M. P. Waalkes, *Toxicol. Appl. Pharmacol.*, 2015, **282**, 267-274.
13. G. Nordberg, R. Goyer and M. Nordberg, *Arch. Pathol.*, 1975, **99**, 192-197.
14. C. Dorian, V. H. Gattone and C. D. Klaasen, *Toxicol. Appl. Pharmacol.*, 1992, **114**, 173-181.
15. S. Satarug, J. Baker, P. E. Reilly, M. Moore and D. Williams, *Hum. Exp. Toxicol.*, 2001, **20**, 205-213.
16. D. E. Sutherland and M. J. Stillman, *Metallomics*, 2011, **3**, 444-463.
17. D. E. Sutherland and M. J. Stillman, *Metallomics*, 2014, **6**, 702-728.
18. R. W. Olafson, W. D. McCubbin and C. Kay, *Biochem. J.*, 1988, **251**, 691-699.
19. K. E. Rigby and M. J. Stillman, *Biochem. Biophys. Res. Commun.*, 2004, **325**, 1271-1278.
20. K. E. R. Duncan and M. J. Stillman, *J. Inorg. Biochem.*, 2006, **100**, 2101-2107.
21. S.-H. Hong, Q. Hao and W. Maret, *Protein Eng. Des. Sel.*, 2005, **18**, 255-263.
22. S.-H. Chen, L. Chen and D. H. Russell, *J. Am. Chem. Soc.*, 2014, **136**, 9499-9508.
23. X. Yu, Z. Wu and C. Fenselau, *Biochemistry*, 1995, **34**, 3377-3385.
24. G. W. Irvine and M. J. Stillman, *Biochem. Biophys. Res. Commun.*, 2013, **441**, 208-213.
25. G. W. Irvine, K. E. Duncan, M. Gullons and M. J. Stillman, *Chem.--Eur. J.*, 2015, **21**, 1269-1279.
26. P. Palumaa, I. Tammiste, K. Kruusel, L. Kangur, H. Jörnvall and R. Sillard, *Biochimica et Biophysica Acta (BBA)-Proteins and Proteomics*, 2005, **1747**, 205-211.
27. G. W. Irvine, K. L. Summers and M. J. Stillman, *Biochem. Biophys. Res. Commun.*, 2013, **433**, 477-483.
28. S.-H. Chen and D. H. Russell, *Biochemistry*, 2015, **54**, 6021-6028.
29. L. Konermann, J. Pan and Y.-H. Liu, *Chem. Soc. Rev.*, 2011, **40**, 1224-1234.
30. S. W. Englander, L. Mayne, Z.-Y. Kan and W. Hu, *Annual review of biophysics*, 2016.

31. K. L. Summers, A. K. Mahrok, M. D. Dryden and M. J. Stillman, *Biochem. Biophys. Res. Commun.*, 2012, **425**, 485-492.
32. C. E. Bartman, H. Metwally and L. Konermann, *Anal. Chem.*, 2016, **88**, 6905-6913.
33. S.-H. Chen, W. K. Russell and D. H. Russell, *Anal. Chem.*, 2013, **85**, 3229-3237.
34. T. T. Ngu, A. Easton and M. J. Stillman, *J. Am. Chem. Soc.*, 2008, **130**, 17016-17028.
35. T. B. Pinter, G. W. Irvine and M. J. Stillman, *Biochemistry*, 2015, **54**, 5006-5016.
36. T. B. Pinter and M. Stillman, *Biochem. J.*, 2015, BJ20150676.
37. L. Banci, I. Bertini, S. Ciofi-Baffoni, T. Kozyreva, K. Zovo and P. Palumaa, *Nature*, 2010, **465**, 645-648.
38. J. Zaia, D. Fabris, D. Wei, R. L. Karpel and C. Fenselau, *Protein Sci.*, 1998, **7**, 2398-2404.
39. S. Pérez-Rafael, S. Atrian, M. Capdevila and Ò. Palacios, *Talanta*, 2011, **83**, 1057-1061.
40. Y. Hathout, D. Fabris and C. Fenselau, *Int. J. Mass Spectrom.*, 2001, **204**, 1-6.
41. X. Yu, M. Wojciechowski and C. Fenselau, *Anal. Chem.*, 1993, **65**, 1355-1359.
42. J. Chan, Z. Huang, I. Watt, P. Kille and M. J. Stillman, *Can. J. Chem.*, 2007, **85**, 898-912.
43. M. Vasak, A. Galdes, H. A. O. Hill, J. H. Kaegi, I. Bremner and B. W. Young, *Biochemistry*, 1980, **19**, 416-425.
44. S.-H. Hong and W. Maret, *Proceedings of the National Academy of Sciences*, 2003, **100**, 2255-2260.
45. W. Maret, *J. Chromatogr. B*, 2009, **877**, 3378-3383.
46. D. H. Petering, J. Zhu, S. Krezoski, J. Meeusen, C. Kiekenbush, S. Krull, T. Specher and M. Dughish, *Exp. Biol. Med.*, 2006, **231**, 1528-1534.
47. L. E. Hernández, J. Sobrino-Plata, M. B. Montero-Palmero, S. Carrasco-Gil, M. L. Flores-Cáceres, C. Ortega-Villasante and C. Escobar, *J. Exp. Bot.*, 2015, **66**, 2901-2911.
48. E. B. Maryon, S. A. Molloy and J. H. Kaplan, *Am. J. Physiol. Cell. Physiol.*, 2013, **304**, C768-C779.

49. M. A. Lynes, J. Hidalgo, Y. Manso, L. Devisscher, D. Laukens and D. A. Lawrence, *Cell Stress Chaperones*, 2014, **19**, 605-611.
50. W. Maret and A. Krężel, *Mol. Med.*, 2007, **13**, 371.
51. L.-J. Jiang, W. Maret and B. L. Vallee, *Proceedings of the National Academy of Sciences*, 1998, **95**, 3483-3488.

Chapter 6

6 Metalation kinetics of the human α -metallothionein 1a Fragment is dependent on the fluxional structure of the apo-protein⁵

6.1 Introduction

One-third of all proteins require a metal cofactor in a functional or structural capacity to perform their respective function.⁵² These cofactors are commonly d-block metal ions such as Fe, Cu, Zn or Mo, termed essential metals, which have been selected evolutionarily for their physicochemical properties and environmental availability⁵³. Despite this efficient use of metal ions by biological machinery, other metal ions present in the surrounding environment can be highly toxic, even at very low levels of exposure.⁵⁴⁻⁵⁶ These toxic metals, which include As, Cd, Hg, and Pb, often replace essential metals in key metalloproteins, resulting in inactivation of enzymatic function and inhibition of critical cellular processes.⁵⁷ Fortunately, the cell has natural defences to protect against inevitable toxic metal exposure by sustaining significant quantities of biological ligands that act to sequester the metal ions.⁵⁸⁻⁵⁹ Examples of these molecules include the tri-peptide glutathione and the small, two-domain protein, metallothionein.⁶⁰⁻⁶¹

Metallothionein (MT) is a small, cysteine-rich, metal-binding protein. The mammalian forms adopt a two-domain structure when saturated with divalent metals⁶². In the fully metalated, two-domain protein, metal binding is organized into two metal-thiolate clusters with stoichiometries of: M_4S_{11} (α domain) and M_3S_9 (β domain) where these divalent, d^{10} metals are tetrahedrally coordinated by a combination of terminal and

⁵ A version of this chapter has been published

Reproduced with permission from: Irvine, Gordon W., et al. "Metalation Kinetics of the Human α - Metallothionein 1a Fragment Is Dependent on the Fluxional Structure of the apo- Protein." *Chemistry– A European Journal* 21.3 (2015): 1269-1279.

Copyright Wiley 2014

bridging thiolate ligands of the 20 cysteines.⁶³ Under normal cellular conditions, in the absence of toxic metal exposure, MT coordinates Zn^{2+} and Cu^+ ions⁶⁴. In this state, MT is considered to act as a metallochaperone or storage protein, able to shuttle essential metals to apometalloenzymes⁶⁵⁻⁶⁷. This homeostatic or metal buffering role is a critical role for metallothioneins, especially for Zn^{2+} and Cu^+ ⁶⁸⁻⁶⁹, however, following exposure to toxic metals, such as Cd^{2+} , MT adopts a more protective role by actively sequestering these metal ions^{63, 70}. Because of the central role of MT in cellular metal regulation, dysfunction in gene coding for metallothioneins or modifications to their native structures can lead to serious disease and increased toxic metal sensitivity⁷¹⁻⁷⁵. Previous studies have shown that *de novo* transcription of MT mRNA can be induced by both Cd^{2+} and Zn^{2+} ⁷⁶⁻⁷⁸. Consequently, two potential mechanisms are possible by which MT can act to sequester the toxic Cd^{2+} ions: (1) metal substitution in which Cd^{2+} replaces Zn^{2+} in pre-existing Zn-MT, or (2) coordination of Cd^{2+} to *de novo*-synthesized apo-MT.

While MT is ubiquitous across all kingdoms and in all organs in mammals, the actual metalation mechanism of the apo-MT is poorly understood. The mechanism leads to selectivity between different metals in the metal-saturated proteins⁷⁹⁻⁸⁰. Although many studies have investigated metal substitution reactions of Zn-MT with Cd^{2+} or exchange between Zn-MT and Cd-MT⁸¹⁻⁸⁸, few studies have investigated the details of the metalation reaction of the metal-free or apo-MT. This is due to the technical difficulties working with a sulfhydryl-rich protein that is highly sensitive to oxidation, lacks a formal 2^o or 3^o structure which precludes CD spectroscopic analysis, and is chromophorically silent due to the d¹⁰ metals typically bound *in vivo*. The structure of a metal-free protein can usually be used to provide detailed information about metalation pathways from the changes that take place as metalation proceeds⁸⁹. But for metallothioneins, it has been generally considered that apo-MT has no formal structure⁹⁰ and only after metalation does MT gain a more organized structure^{79, 90-92}. The topology of the partially-metalated-As_x-MT species have recently been probed experimentally^{24, 27} and it was shown that the differential rate of the covalent modification of cysteine residues on MT is an effective probe of solution structures.

The question then arises whether these conformations, which can be identified by modification with Bq, influence the metalation mechanism. Biologically, this is important because tumors are known to have a much lower pH ($5.8 \leq$) than normal cells as a result of the anoxic environment in which they are found⁹³. In this context, apo-MT may adopt an altered conformation and, therefore, might interact with metal-based drugs differently due to the structural changes induced by the lower pH. Thus, understanding the conformational dependence of metalation of apo-MT is of great importance in determining the poorly known but vitally important mechanistic details of metalation.

The lack of an intrinsic probe in apo-MT makes it difficult to monitor structural changes due to metalation or change in environment. Previous studies have overcome this limitation using FRET-labeled-MT to monitor changes in overall dimensions of the protein⁹⁴. These studies have shown that FRET emissions only change slightly when MT was demetalated, suggesting that the apo-MT fragment dimensions remains somewhat compact⁹⁴⁻⁹⁵. This retention of compact dimensions in the α - and β -domains may indicate that despite the lack of formal structural features, the globular structure of the apo-MT may be important to its metal binding properties.

In this study, we investigated the dependence of the rate of the metalation reaction with Cd^{2+} on the extremes of the folded state of apo- α MT1a. To reduce the complexity of the two-domain, 7-metal binding protein we chose to study the α fragment that contains only the four-metal α domain.

Figure 6-1 shows the α -fragment's four-metal-binding domain structure of the Cd_4 - α MT1a and the arrangement of the metals both within the peptide folded structure and with the thiolates of the Cd_4 -S(Cys)₁₁ cluster⁹⁶. Since high concentrations of denaturant are not compatible with ESI-MS studies, we used low pH to model the denaturing effects of the guanadinium hydrochloride denaturant and used the modification reaction profiles of the 11 cysteines by benzoquinone as a way of probing the solution structure of the apo-MT under two extremes of conformation: folded and unfolded. Our objective was to determine whether the conformation of the apo-MT affected the metalation reaction.

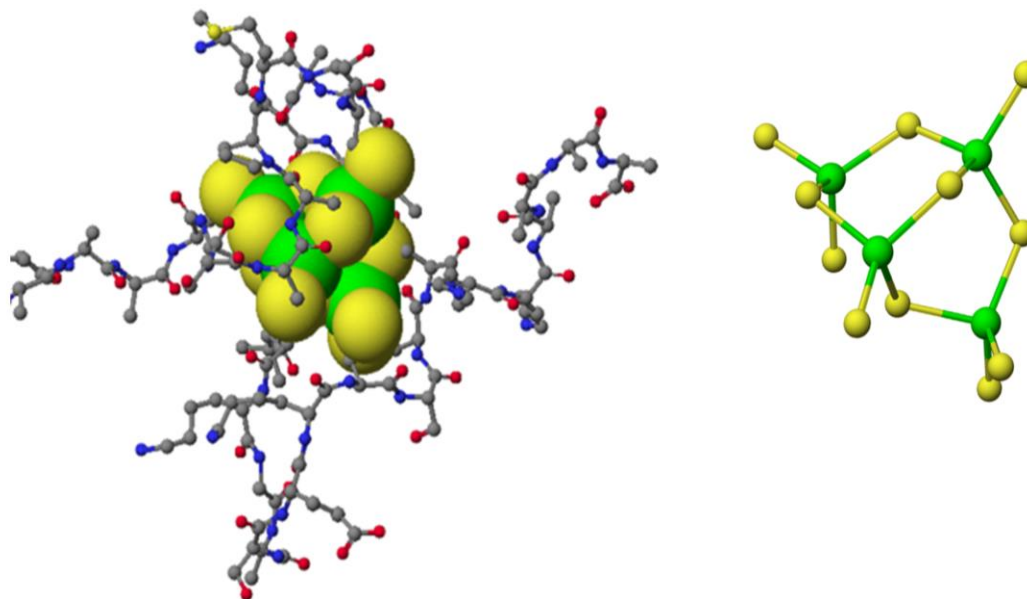


Figure 6-1: The structure of the α -fragment of hMT1a. (Left) The $\text{Cd}_4\text{SCYS-11}$ cluster structure showing the wrapping of the peptide chain. (Right) The connectivity between the 11 Cys and the 4 Cd^{2+} in the α -binding domain showing the mixture of terminal and bridging S from the 11 Cys. Structures adapted from the model of Chan et al.²⁴. The NMR structure of $\text{Cd}_4\text{-MT2}$ was originally reported by Messerle et al.⁹⁷ The sequence of α -rhMT1a is provided in the Experimental Procedures section.

The molecular probe chosen was benzoquinone (Bq) due to its reactivity towards cysteine residues. Previously, MT cysteines have been modified by iodoacetamide to determine the extent of free cysteine and the extent of disulfide bridge formation⁹⁸. Bq is a larger molecule than modifiers like iodoacetamide and, therefore, is likely more affected by steric hindrance in the vicinity of the thiol reaction site. This provides a more sensitive marker of the steric hindrance of the cysteines introduced by the conformational changes introduced by folding. Therefore, the differential accessibility of each of the cysteinyl thiols is a probe of the extent of shielding of the cysteines. Bq also reacts more quickly than alkylating reagents at the pH range used in this study⁹⁹. The chemistry of Bq with respect to thiols is attractive because the reaction with quinones is fast and quantitative at pH below 7.5¹⁰⁰.

Our results clearly show that there are structural differences in the conformational families of apo-MT under native and denaturing conditions and that there is a significant metalation rate dependence on those conformations.

6.2 Methods

6.2.1 Metallothionein preparation

The recombinant α domain of human metallothionein 1a (MGKAAAACCSCCPMSCAKCA QGCVCKGASE KCSCCKKAAA) was produced by over-expression in *E. coli* BL21(DE3) cells as described in detail elsewhere¹⁰¹. Briefly, the cells were grown in the presence of CdSO₄ and the Cd-containing α -domain was isolated and purified as an S-tag fusion protein using an SP ion exchange column and superfine G-25 Sephadex size exclusion column equilibrated with 10 mM Tris-HCl (pH 7.4). The N-terminal S-tag (MKETAAAKFE RQHMDSPDLG TLVPRGS) was subsequently cleaved from the concentrated protein fraction using a Thrombin CleanCleave™ Kit (Sigma) as per the manufacturer's instructions.

Metal-free or apo- α MT was prepared by eluting the thrombin-cleaved Cd-bound protein from a G-25 size exclusion column equilibrated with 10 mM Tris-HCl pH 2.7. Elution of the protein with a low pH eluent effectively removes the metal ions from the protein, which separate from the protein band on the G25 size-exclusion column. Since MT is devoid of aromatic amino acids, the metal-free protein fractions were detected by the UV absorption at 220 nm, which corresponds to the electronic transitions generated by the polypeptide backbone. Protein concentrations were determined by remetalation with Cd²⁺ and examination of the UV absorption spectrum at 250 nm, which corresponds to the ligand-to-metal charge transfer transition generated by the metal-thiolate bond ($\epsilon_{\alpha 250} = 45,000 \text{ M}^{-1}\text{cm}^{-1}$);¹⁰². For ESI-MS studies the pH of the protein solutions was adjusted using NH₄OH (Caledon Laboratory Chemicals) and HCOOH (Caledon Laboratory Chemicals).

Solutions of 500 mM parabenzoquinone (Bq; Fisher Scientific) were prepared in 100% methanol (Caledon Laboratory Chemicals) and diluted to 50 mM in >16 M Ω ·cm deionized water (Barnstead Nanopure Infinity). Bq solutions were bubbled extensively with argon. The reaction of benzoquinone with thiols has been previously described¹⁰³. Reactions were carried out in 10 mM ammonium formate buffer at pH 2.8 and 6.7 with

MT concentrations ranging between 20-40 μM . The neutral pH data set was collected at pH 6.7 and the low pH data set at pH 2.8.

6.2.2 ESI-MS of proteins with modified cysteines

Mass spectra were collected on a micrOTOF II electrospray-ionization time-of-flight mass spectrometer (Bruker Daltonics, Toronto, Ontario, Canada) in the positive ion mode. NaI was used as the mass calibrant. The scan conditions for the spectrometer were: end plate offset, -500V; capillary, +4200 V; nebulizer, 2.0 bar; dry gas flow, 8.0 L/min; dry temperature, 30°C; capillary exit, 180 V; skimmer 1, 22.0 V; hexapole 1, 22.5 V; hexapole RF, 600 Vpp; skimmer 2, 22 V; lens 1 transfer, 88 μs ; lens 1 pre puls storage 23 μs . The mass range was 500.0–3000.0 m/z. Spectra were constructed and deconvoluted using the Bruker Compass DataAnalysis software package.

6.2.3 ESI-MS data analysis and reaction modeling

The relative rate constant values (k_n) of each of the 11 reactions of apo- α -MT with Bq were estimated using ReactLab software (Jplus Consulting Pty Ltd, Australia) and those values were used in the simulation program HYSS (Hyperquad, UK). The set of 11 k_n 's were slightly modified in HYSS to fit the mass spectral data points measured for reactions at both neutral and low pH (6.7 and 2.8). The relative rate constants were determined using an integrated second-order bimolecular reaction expression:

$$\ln[B_t/A_t] = \ln[B_0/A_0] + k[B_0 - A_0]t$$

Where B is in excess relative to A, ie in this equation B would represent Bq and A the MT species. It is solved as a series of 11 consecutive reactions where the k is the rate constant and the reactions are coupled to each other. HYSS allows coupling of multiple expressions in a single model and tuning of the k-values to minimize the difference between model and experimental results. In this way 11 k-values were obtained.

6.2.4 Molecular modeling of apo- α MT and cysteine modifications

Molecular modeling calculations for Figure 6-6 were carried out using Scigress Version 3.0.0 (Fujitsu Poland Ltd.). The calculations for Figure 6-1 was carried out using Cache

Version 6.1 (Fujitsu, America). Allinger's MM3 Force Field augmented for metals was used with the modified force field from Chan et al.⁹⁶. Modeling parameters and sequence information have been previously described by Rigby and Stillman¹⁹.

6.2.5 Kinetic measurements of cadmium binding to α MT

Separate solutions of apo- α -rhMT 1a at pH 2.0 were prepared for the kinetic study containing 237.5 mM KCl and 2.0, 3.0, 4.0, 5.0, 6.0, or 7.0 M guanidinium chloride (GdmCl). The concentrations of the apo- α MT 1a ranged from 9.5-17.2 μ M. Cadmium solutions were prepared as the sulfate salt at a concentration of 52 mM in 10 mM Tris/HCl buffer (pH 7.4) with 200 mM KCl. The metalation kinetics of apo- α -MT1a in the presence of GdmCl were measured under stoichiometric Cd^{2+} conditions equating to 4.0 molar equivalents of Cd^{2+} per mole of apo- α MT 1a. The metalation reaction was carried out at 10°C using a BioLogic SFM-300 stopped-flow instrument (BioLogic Science Instruments, Claix, France) powered by a MPS-52 unit (BioLogic) and coupled to a MOS-250 light source (BioLogic). The low pH protein solution of apo- α MT1a was neutralized by mixing with 1% NH_4OH in the mixing chamber of the stopped-flow instrument immediately prior to mixing with Cd^{2+} . Metalation was monitored by detecting the change in UV absorbance at 250 nm corresponding to Cd-thiolate bond formation. The dead time for this mixing sequence was 2 ms. Data points were collected every 2 ms for 8 s, every 1 ms for 6 s, or every 500 μ s for 0.5 s followed by every 2 ms for 7 s depending on the rate of the reaction. The reported kinetic data are an average of at least four independent kinetic traces. The kinetic traces of the metalation reaction of MT with Cd^{2+} were fit using the Gepasi v. 3.0 (Virginia Polytechnic Institute, Blacksburg, VA (6-7)) simulation program as a single bimolecular reaction such as that shown in Equation 4, Scheme 1.



Scheme 6-1: The four, sequential, bimolecular reaction steps that lead to complete metalation of the apo- α MT1a

To check that the reaction rate was not dependent on the increasing viscosity of the solution, apo- α MT1a was prepared with 237.5 mM KCl and 0.34 M sucrose. The sucrose was prepared by adding 0.582 g of sucrose to 5 mL of protein in 10 mM Tris-HCl pH 7.4. A solution of Cd₄- α MT1a in the presence of 5 M Cl⁻ was also prepared. The kinetic analyses (not shown) were then carried out in the presence of high sucrose and high salt concentrations. In neither case were the kinetic results were changed.

6.3 Results

6.3.1 Metallothionein cysteine modification using p-benzoquinone (Bq)

We have previously described the reaction of Bq with the cysteines of apo-MT and the successful use of this method to probe for changes in surface topography as a function of As³⁺ metalation²⁷. We further demonstrated that a single Bq molecule reacts stoichiometrically with each cysteine residue in MT for a total of 11 Bq reacting with the 11 cysteine residues in α -rhMT1a¹⁰⁴. In the current study, aliquots of the Bq solution were added to the solution of apo- α MT. ESI-MS was used to determine the extent of Bq modification of cysteine side chain residues upon sequential addition of Bq to the MT solution (Figure 6-2). The reactivity of Bq towards free cysteine residues is determined by two main factors: (1) the intrinsic nature of the chemistry of covalent bond formation between Bq and the thiol and (2) the steric hindrance of the access to the cysteinyl thiol introduced by the folding of the protein structure surrounding the thiol^{27, 104}. Therefore, the differential rate of the reaction between the 11 cysteines of the apo- α MT1a is will

depend of the relative accessibility of the thiol and presence or absence of surrounding structure.

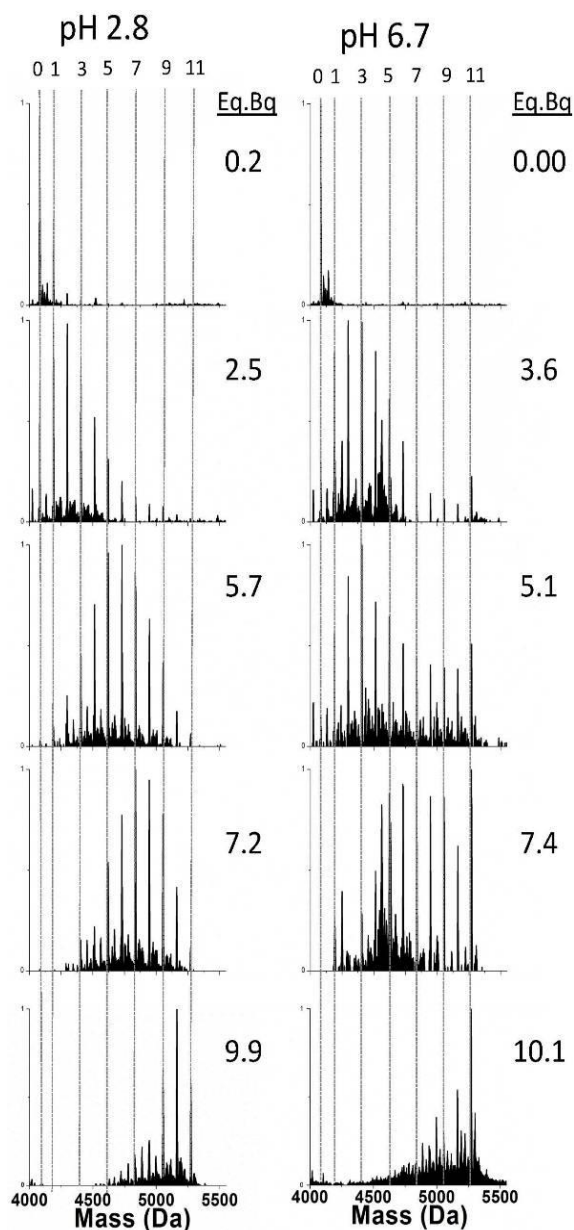


Figure 6-2: ESI mass spectral data recorded for the stepwise modification of the 11 Cys in apo- α MT1a with para-benzoquinone (Bq). The number of Bq bound to the protein is shown by the vertical lines from 0 to 11. The Bq was added stepwise with mol eq as shown.

Figure 6-2 shows a partial set of the experimental ESI mass spectral data for titrations of apo- α MT under denaturing (i) and native(ii) conditions: (i) at pH 2.8 and (ii) at pH 6.7.

Many more steps were recorded than shown here. Of importance in these two data sets is the difference in the distribution of the Bq modified species. The denatured or unfolded (pH 2.8) peptide was modified in the expected manner; that is, a Normal distribution of modifications was observed as a function of the mol eqs of Bq added. The maxima of the Normal distribution progresses in an approximately linear fashion as a function of increasing Bq addition.

Under native or folded conditions (at pH 6.7) the data show an important and significant change to this trend: the additions of Bq do not result in a linear and progressive increase in the Normal distribution maximum. Rather the relative abundance of modified species lags behind the profile of the low pH traces and exhibits a tailing pattern that dips significantly, then the relative abundance sharply increases for the fully modified species, Bq11 (Figure 6-2, right). The reaction profile at pH 6.7 becomes so irregular that a significant fraction of the completely modified apo- α MT, with 11 Bq, is clearly present even with just 3.6 eq Bq added, in complete contrast to the profile of the reaction carried out at pH 2.8. By the 7.4-Bq-added point, the 11-Bq species dominates. This nonlinear behaviour contrasts sharply the stochastic pattern of the low pH reaction.

The variance in range of modified species is due to residues in the unfolded protein having similar accessibilities. In the folded protein the accessibilities vary and broaden the range of species present at any given point. The presence of a folded apo-MT under native conditions also introduces another process: the unfolding of the native structure due to Bq modification, further explored in the Discussion section.

6.3.2 Determination of relative rate constants

The key to the interpretation of the difference in the reaction profiles of the Bq modification reactions at low and neutral pH is found in the differences in the 11 relative rate constants for the two conditions. The 11 k_n 's of the reaction of Bq with each of the cysteines at both neutral and low pH were determined by modeling the 11 sequential bimolecular reactions using the computer program HYSS. HYSS allows for the tuning of each of the 11 separate k_n 's involved in the complete modification reaction of apo- α MT. As a result of the large number of sequential reactions involved in the complete

modification of the cysteines in apo- α MT it is unlikely that selection of a series of incorrect k_n values could give a reaction profile that fits the observed ESI mass spectral data as closely as here. In Figure 6-3A, the reaction profile of all 11 species at low pH is plotted with insets that show the predicted mass spectral relative abundance data at two stages in the reaction: namely at 3 and 7 equivalents of Bq reacted. The distribution of modified species closely matches the experimental ESI mass spectral data shown in Figure 6-2 at the same point in the Bq additions (Figure 5).

Figure 6-3B shows the modeled reaction profile for the Bq titration at neutral pH. This profile clearly differs from that in Figure 6-3A in that the MT(Bq₁₀) and MT(Bq₁₁) species appear much earlier in the titration at pH 6.7. The green line in Figure 6-3B (which represents the relative abundance of MT(Bq₁₁)) is the most prominent of the 11 species by the 6-Bq point compared with only dominating at the 10-Bq point at pH 2.8. The insets show the relative abundance of MT species at the stages where 3 and 7 equivalents of Bq have reacted with the apo-MT illustrating the same tailing pattern at the beginning of the titration as seen in the ESI mass spectral data. At 7 Bq equivalents the MT(Bq₁₁) species is the most abundant in solution which mirrors the experimental mass spectral data, Figure 6-2. The modeled data show that the differences in the experimental plots are due largely to the differential k_n values of each of the 11 separate MT-Bq reactions.

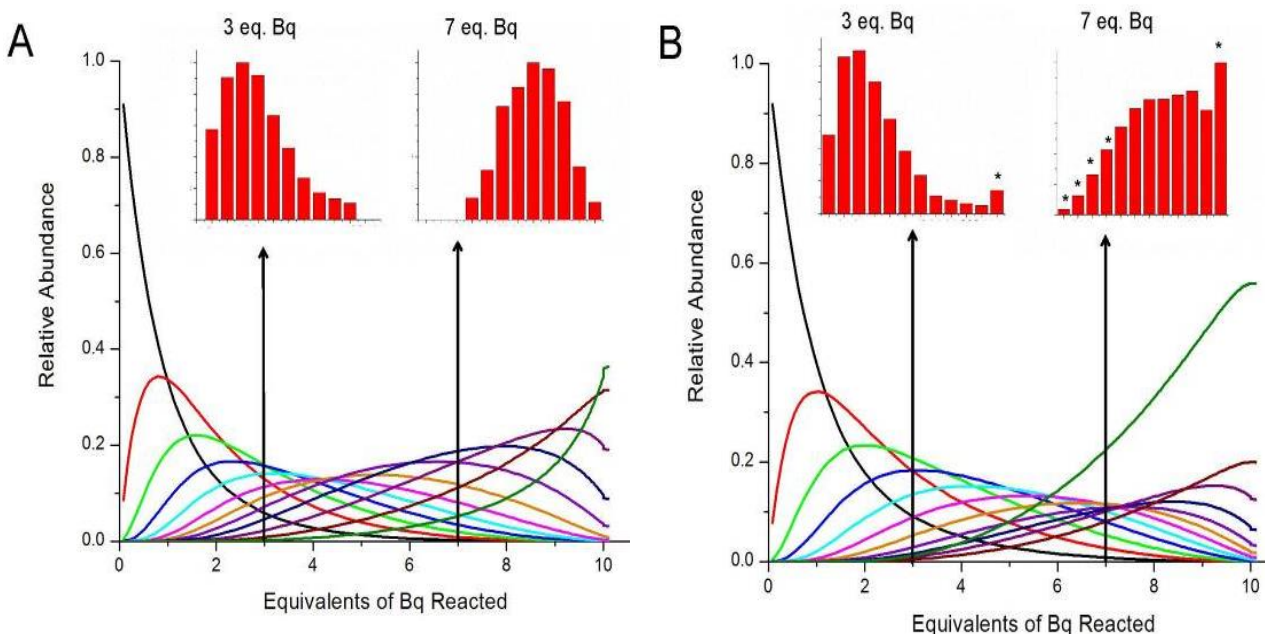


Figure 6-3: Simulations of the protein speciation when 11 mol eq Bq react over time with apo- α MT at (A) pH 2.8 and (B) pH 6.7. Each species of $(\text{Bq})_n\text{-}\alpha\text{MT}$ ($n=0\text{-}11$) is shown as it forms then is replaced by the $n+1$ Bq modified species: apo (black), Bq1 (red), Bq2 (green), Bq3 (blue), Bq4 (teal), Bq5 (pink), Bq6 (orange), Bq7 (purple), Bq8 (dark blue), Bq9 (fuchsia), Bq10 (brown) and Bq11 (dark green). In both simulations, the relative abundance of each species, as would be observed in ESI-MS data, is shown at 3 and 7 molar equivalents of Bq reacted in bar graph format. The insets model the ESI-MS data actually measured and shown in detail in Figure 6-2. The * indicates where the abundance of particular species differs between conformations. k_n 's used: pH 2.8: 3.76, 3.59, 3.46, 3.40, 3.38, 3.37, 3.29, 3.26, 3.13, 3.01, 2.87 and for the neutral pH: 4.14, 4.04, 3.98, 3.92, 3.89, 3.85, 3.84, 3.79, 3.80, 3.78, 3.99. It is estimated that the error in these values is $\pm 10\%$ the same as from the original ESI-MS data.

Figure 6-4 assembles the experimental data (black) and simulated data (red) as a function of the relative abundance of the Bq-modified species for the titrations carried out at pH 2.8 (left) and 6.7 (right). The simulated ESI-MS relative abundance data were obtained by extracting slices at each Bq-addition point based on the 11 k_n values used in Figure 6-3. This Figure provides a direct comparison between the experimental data and the model with its simulated spectra. The model matches the experimental data remarkably well, particularly reproducing all the specific features of the experimental data at both low and neutral pH closely.

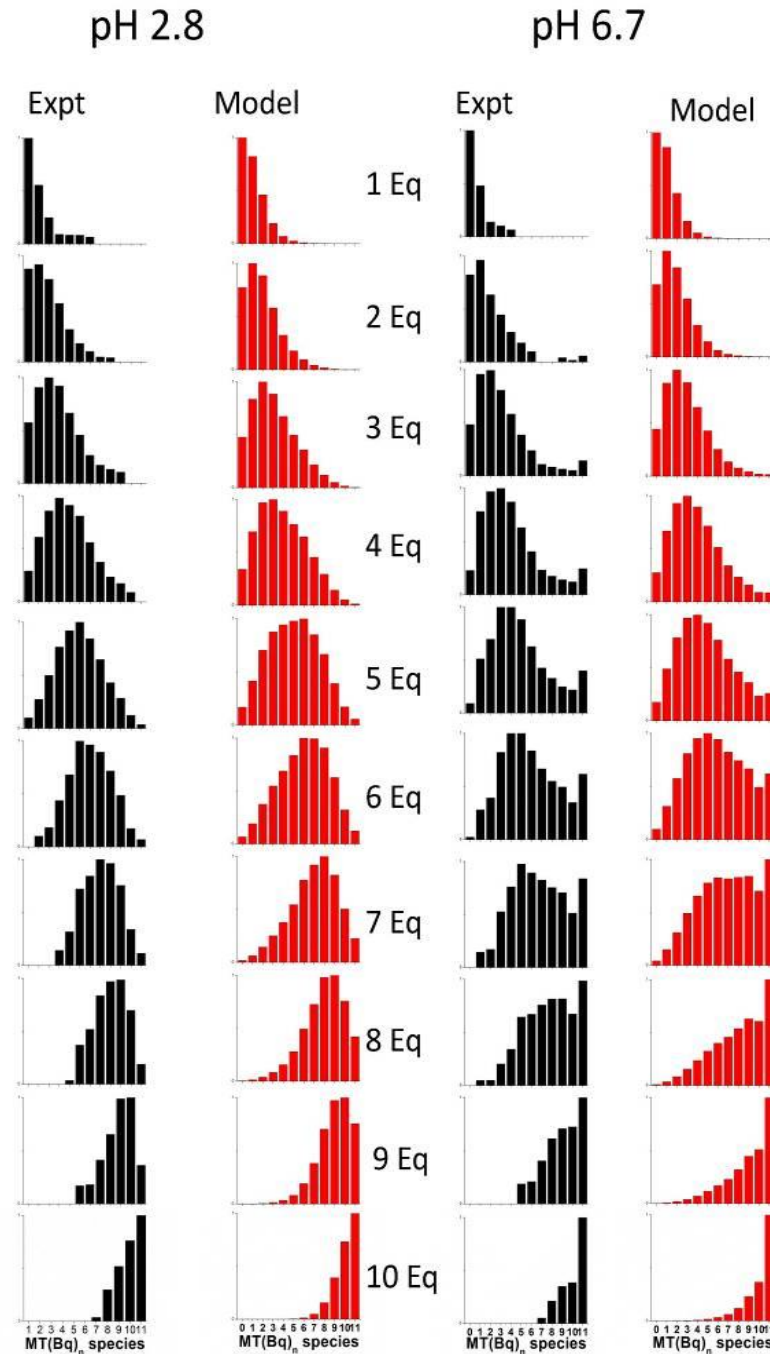


Figure 6-4: Comparison between the experimental data (black) and the simulated model data (red) for stepwise modification of apo- α MT by Bq at low pH (Left) and neutral pH (Right). The black bars show the experimental ESI-MS spectra recorded at the specified Bq addition point. The simulated model data at each pH are taken from a single calculation that requires all 11 kn's to be used.

6.3.3 Comparison of the k_n Values Used in Generating the Model Reaction Profile

The values of the 22 k_n 's (11 for each pH) were compared by normalizing the k_n 's of the first 10 reactions to the final reaction k_n ($\text{MT}(\text{Bq}_{10}) + \text{Bq} \rightarrow \text{MT}(\text{Bq}_{11})$) for both data sets. Our argument for this approach is that it is likely that once 10 cysteine residues have been modified by Bq, any specific structure present prior to the reaction will have been disrupted. Because we consider that the $\text{MT}(\text{Bq}_{10})$ structure is similar under both conditions, we consider that the reaction rates of this final modification step, $\text{MT}(\text{Bq}_{10}) + \text{Bq} \rightarrow \text{MT}(\text{Bq}_{11})$, at both neutral and low pH will be similar. In Figure 6-5 it can be readily seen that the normalized ratios of each k_n are much higher in the low pH data set (black) than the neutral pH data set (red); also, the range of the values are very different, ~5% variance at neutral pH versus ~33% variance at low pH.

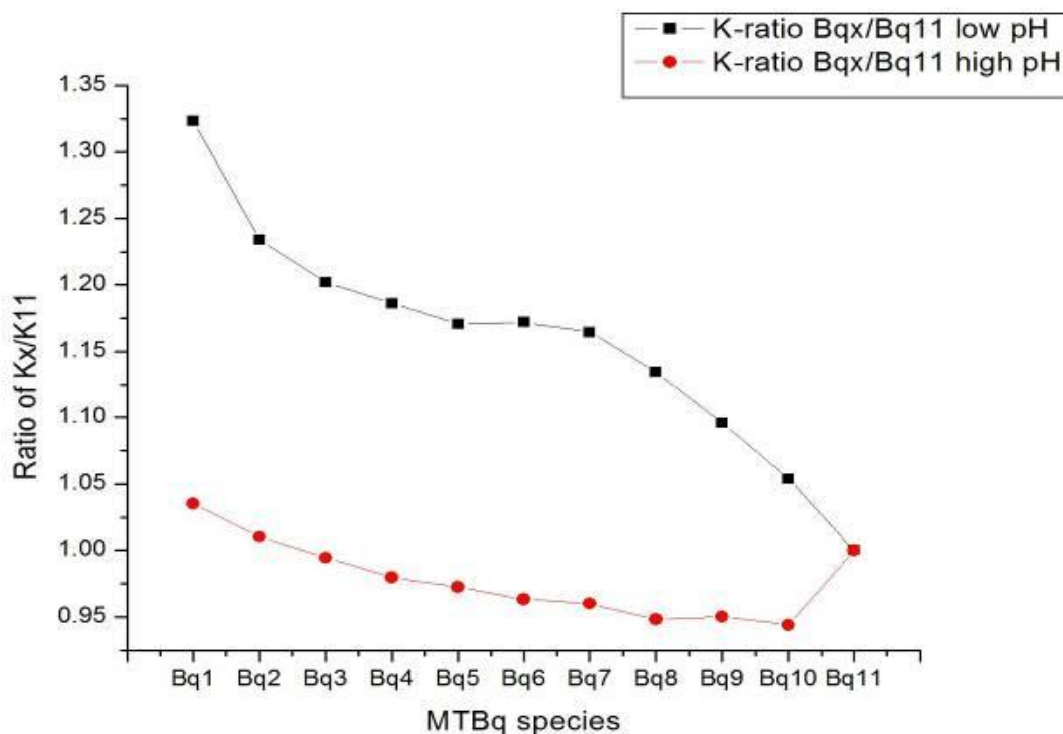


Figure 6-5: Normalized relative rate constants (k_n) for each of the 11 cysteine modification reactions at each pH (2.8 and 6.7). The ratios for the low pH k_n s are shown in black and the high pH k_n ratios are shown in red. The k_n were determined through simulation of the data in the program HYSS. The k_n s are normalized to the k_n for the last modification reaction: $\text{apo- } \alpha\text{MT}(\text{Bq})_{10} + \text{Bq} \rightarrow \text{apo- } \alpha\text{MT}(\text{Bq})_{11}$.

The accuracy of the simulation using the HYSS-determined k_n values can be seen in Figure 6-4 where the simulation and the actual data points from the ESI-MS are plotted on adjacent axes. It can be seen that the simulation tracks the data points remarkably closely. The errors in the ESI-MS data are estimated to be 10%¹⁰⁵. The simulation models 11 separate reactions in one calculation; any error in an individual k_n value will affect the distribution of all species in the simulation. The close alignment of the simulation and the experimental data for the 11 simultaneous bimolecular reactions is challenging and the fact that the alignment is so close points to the reasonableness of the analytical approach.

6.3.4 Molecular dynamics models

Molecular dynamics calculations were used to obtain representative structures of the apo- α MT and the cysteine modified apo- α MT for the native and denatured protein (Figure 6-6). To mimic the effects of denaturation, the temperature setting was increased from 200 K to 500 K, a nominal temperature, that results in a much more open structure in the MD calculations. In Figure 6-6A, the native protein model, results in a structure that is globular making it possible for the cysteine residues to be shielded from the solvent in the interior of the globular structure. This structure closely resembles that reported previously by Rigby, et al.¹⁹. The denatured model, in Figure 6-6C, shows a structure that is much more string-like where the cysteine residues are not shielded and, therefore, will be far more accessible to both the solvent and the incoming Bq molecules. The native and denatured models of apo- α MT agree with previous experiments by Liu et al.¹⁰⁶ that showed a decrease in effective diameter of the protein when folding. The effects of the Bq modification of all 11 cysteine residues on the native and denatured structures are shown in Figure 6-6B and D. The Bq modifications have the effect of disrupting the globular structure in the native model opening the structure so that it resembles the denatured structure. This provides some support for our proposal that the effect of the protein structure on the $MT(Bq_{10}) + Bq \rightarrow MT(Bq_{11})$ reaction is practically the same at high and low pH.

This is the origin of the reaction profile of the native structure. The modification provides a continuum of increasingly unfolded structures when starting with a folded protein.

When the initial structure is already unfolded, there is no such continuum and the tailing reaction profile is not observed, but rather a profile that exhibits a stochastic pattern mirroring a Normal distribution.

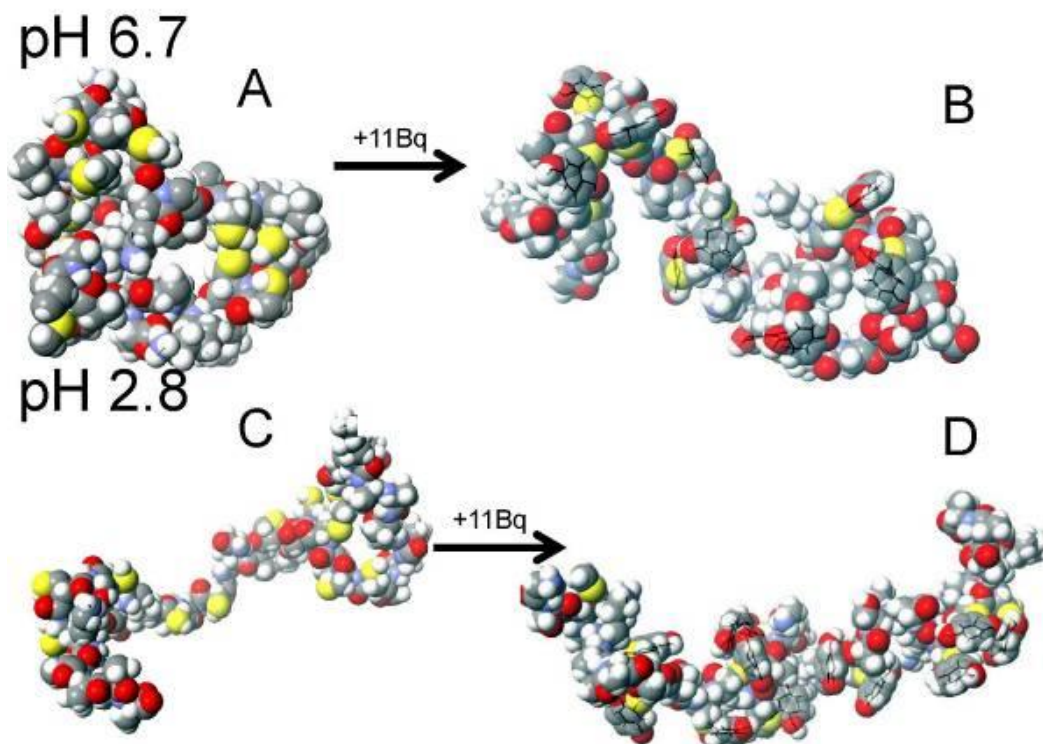


Figure 6-6: Molecular dynamics (MM3/MD) calculated structures at the energy minima for each of the key structures. Representations of (A) native apo- α MT at neutral pH with H- bonding properties intact and (C) denatured apo- α MT. The structure of apo- α MT with 11 Bq modified cysteine residues in native conditions (B) and under denaturing conditions (D).

6.3.5 Cadmium metalation kinetics of α MT in the presence of a chemical denaturant

The ESI-MS Bq modification data indicated the presence of two families of conformers: open at low pH and closed or folded at neutral pH. However, while metalation at neutral pH is possible with both Zn^{2+} and Cd^{2+} it is not possible to use low pH to study the metalation of the unfolded structure. To obtain the unfolded conformers we used an increasing concentration of a protein denaturant. Specifically, guanidinium chloride (GdmCl) was used as the chemical denaturant as it disrupts hydrogen bonds that may be

stabilizing the protein backbone as predicted from the previous modeling studies¹⁹. The binding of four divalent metals to the α -domain has been proposed to occur as four sequential bimolecular reactions¹⁰⁷ corresponding to the addition of each of the four metal ions to the protein to form the fully metallated Cd_4 species in much the same way as the three As^{3+} ions bind sequentially to apo- α MT¹⁰⁸.

CD spectra were recorded at increasing GdmCl concentrations to ensure that the presence of GdmCl did not interfere directly with the metalation reaction causing the product of the reaction to be altered. Figure 6-7A shows that the effect of increasing [GdmCl] added to already folded Cd_4 - α MT is a slight blue shift of approximately 1-2 nm. This is likely a solvent effect due to the interaction of increasing amounts of GdmCl with the exterior of the protein, it did not effect the overall envelope shape. From this we can conclude that the metal core remains intact because we still see the exciton effect from the Cd_4S_{11} cluster. The UV-Vis spectrum remained essentially unchanged (S. Fig 13). To ensure the GdmCl did not directly interfere with the metal-induced folding in the presence of 6M GdmCl, Cd_4 - α MT. was demetalated by reduction of pH and remetalated by bringing the pH back to 7. The demetalation causes a loss of CD intensity in the S to Cd^{2+} charge transfer region (Figure 6-7B, blue line), which is regained when the pH is returned to neutral (Figure 6-7B, green line). The spectra of Cd_4 - α MT metalated in the presence of GdmCl matched that of the already folded Cd_4 - α MT.

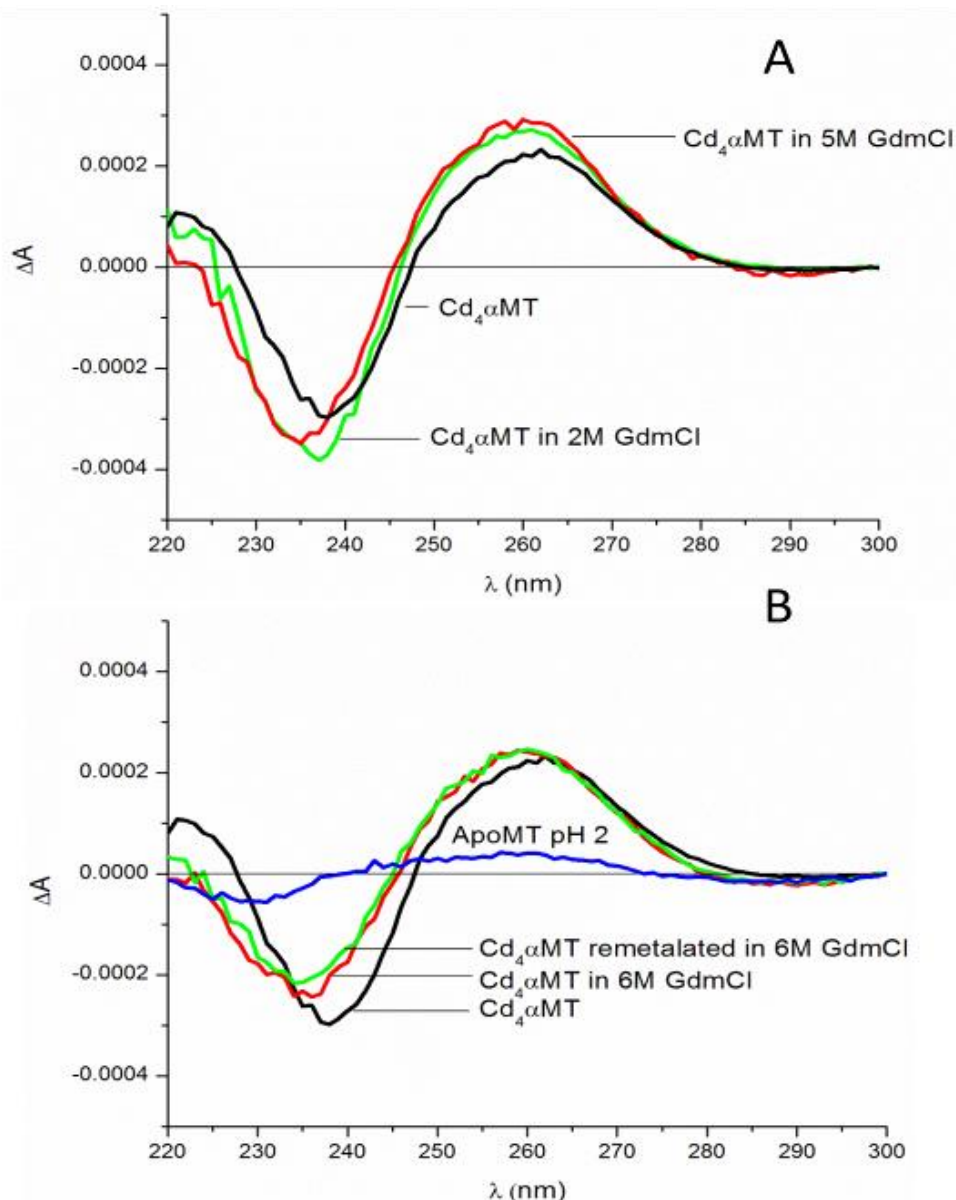


Figure 6-7: Circular dichroism spectra of $Cd_4\alpha$ -MT in 10mM ammonium formate (black lines). (A) Effect on the CD spectrum of the presence of increasing GdmCl concentrations. (B) Effect on the CD spectrum of demetalation, followed by re-metalation in the presence of increasing GdmCl concentrations. (B) Effect on the CD spectrum of demetalation, followed by re-metalation in the presence of 6M GdmCl.

Figure 6-8 shows representative kinetic traces (in black) obtained for the metalation reaction in the presence of 2.0, 4.0 and 7.0 M GdmCl at 10 °C. A slowing of the metalation kinetics is apparent by visual inspection of the kinetic traces where the time required to reach an absorption plateau, thus signaling the end of the metalation reaction, increases from less than 0.2 s in the presences of 2 M GdmCl to greater than 4 s in the

presence of 7 M GdmCl. The kinetic data were fit using the Gepasi simulation program as a single bimolecular reaction (red traces) to obtain the observed rate constants (k_{obs}). A single bimolecular reaction was used because it resulted in the best fit of the kinetic data suggesting that the final bimolecular reaction in the series of four bimolecular reactions (one for each addition of the four metal ions) is the rate-limiting step and thus the only observable reaction at 250 nm. This final reaction results in formation of the cluster structure and is, therefore, expected to be the slowest step of the 4-step reaction.

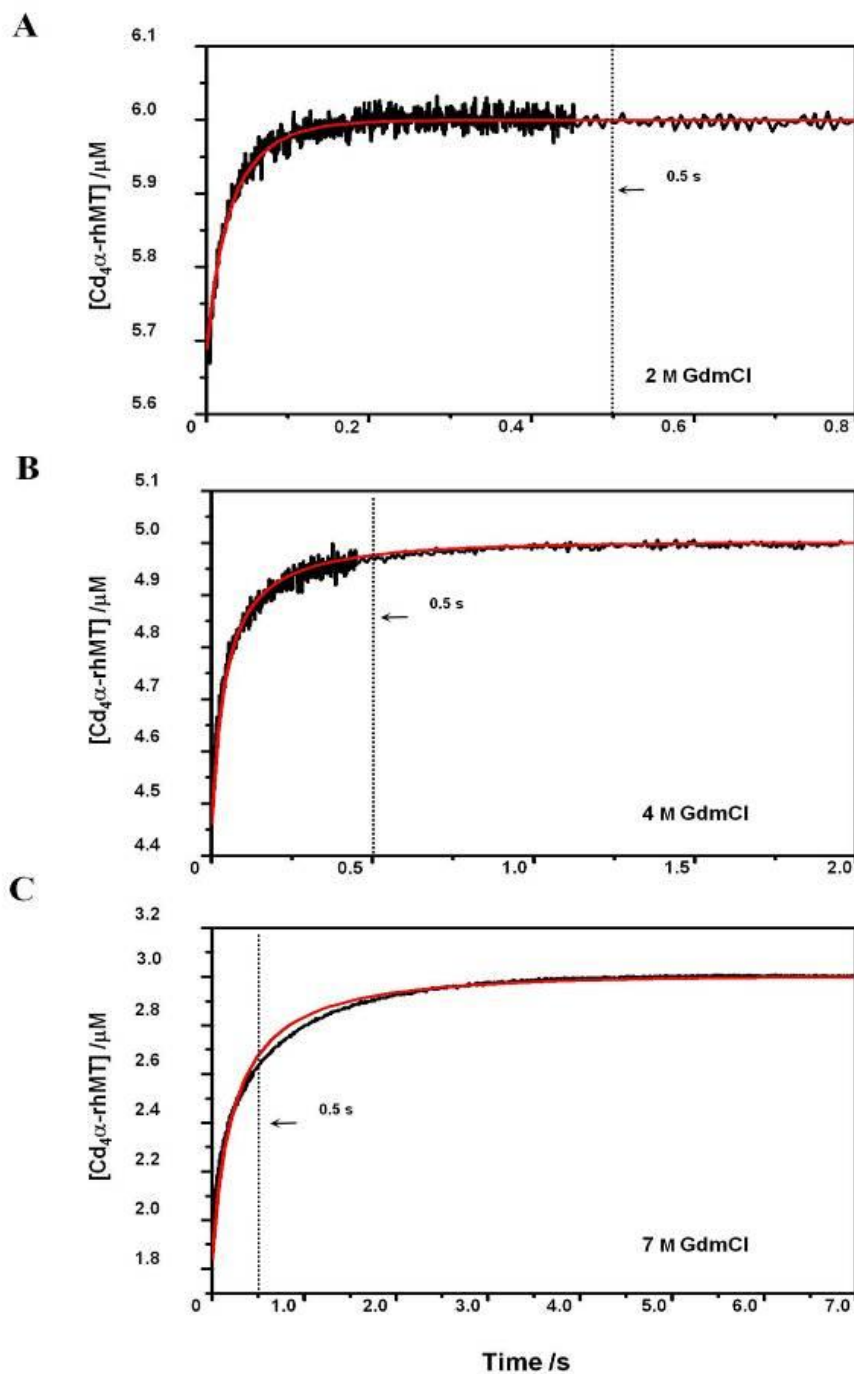


Figure 6-8: Time dependence of the metalation reaction of apo- α MT with Cd^{2+} as a function of an increasing concentration of GdmCl. The red line indicates the fit generated by the program Gepasi. Each trace has a different X- axis range for (A) 0 - 0.8 s; (B) 0 - 2.0 s; (C) 0 - 7.0 s). A line marks 0.5 s in each trace to illustrate the reduction in the rate as a function of increased GdmCl concentration. The absorbance was monitored at 250 nm.

The observed k values plotted in Figure 6-9 were fit with a sigmoidal curve emphasizing the significant reduction in the second-order rate constant over the narrow range of 3 – 5 M GdmCl. From these data, it can be reported that > 4 M GdmCl results in complete denaturation of the metal-free protein and no further rate reduction is observed. The noise varies in the plots shown due to the faster reactions being completed close to the dead time of the stopped flow mixer, requiring a much shorter integration time. The final concentrations of protein differ from the initial due to dilution when mixing with the Cd^{2+} and basic buffer solution but the rate constants have been normalized for concentration.

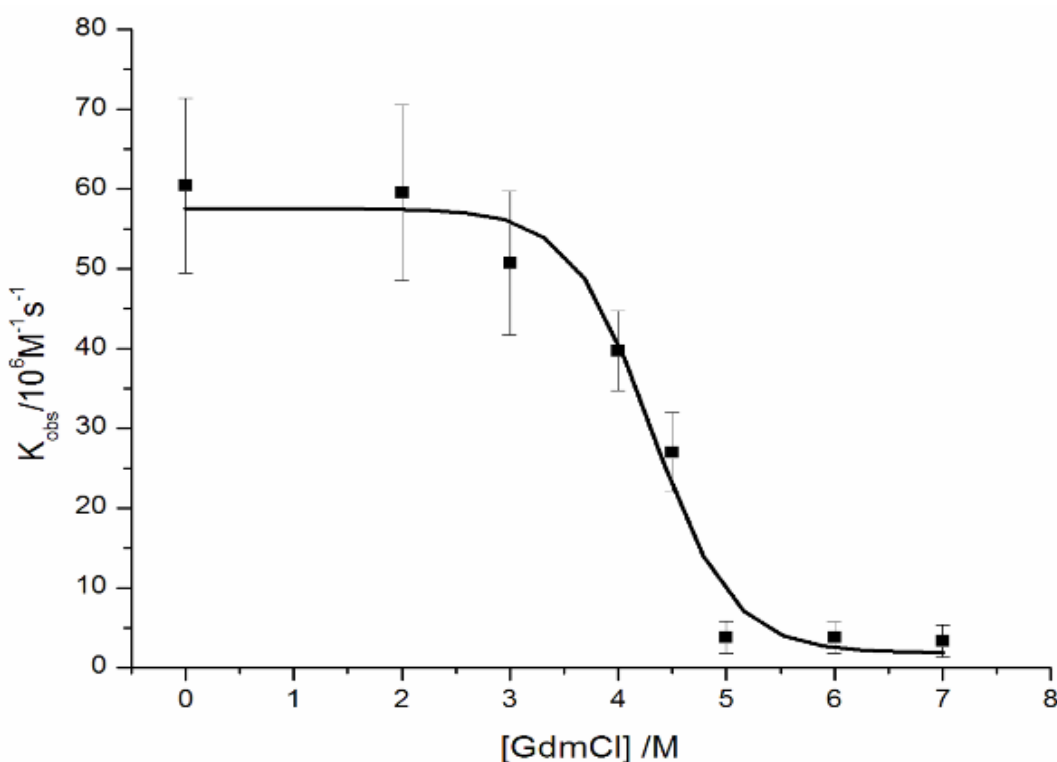


Figure 6-9: The observed rate constant (k_{obs}) for the metalation of apo- α -MT with Cd^{2+} as a function of GdmCl concentration. k_{obs} sharply decreases between 3 and 5 M GdmCl as a result of loss of protein structure. The error in the measurement is higher with higher k_{obs} due to the limitations of the stopped flow device and dead time. The mean k_{obs} values are: 60.4 ± 10.3 , 57.8 ± 10.1 , 50.7 ± 9.8 , 39.7 ± 4.8 , 27.0 ± 5.3 , 3.80 ± 2.9 , 3.74 ± 1.8 , 3.32 ± 1.9 $10^6 \text{ M}^{-1} \text{ s}^{-1}$.

6.4 Discussion

The metal-saturated structure of mammalian metallothioneins is dominated by cysteine-metal bond formation. These structures have been studied extensively by NMR, EXAFS

and XANES methods^{96, 101, 109-112}. Despite this extensive literature, the details of the stepwise metalation mechanism by which the 7 Zn²⁺ or Cd²⁺ ions bind to the apo-MT is very poorly understood. However, it is clear that the metalation reaction follows a distinct pathway because in the case of both Cu⁺^{64, 113} and As³⁺^{105, 108} kinetic data have been reported that are metal-status dependent. By this we mean that the time dependent data recorded during these metalation reactions are sensitive to the metal loading between 0 metals bound and being fully saturated.

So, stepping back from the structures of the fully metalated MT previously reported, takes us to the question of the dependence of metalation on the structure or conformation of the metal-free, apo-MT. There are few techniques that can give information about this hard-to-characterize protein. Particularly, the conformation of the metal-free, apo-MT, because of its fluxional nature¹¹⁰ has not been described extensively. FRET experiments provided evidence that at neutral pH both α and β MT fragments retained their compact structure upon demetalation⁹⁴⁻⁹⁵ and molecular models¹¹⁴ and ESI-MS data¹¹⁵ support this conclusion. However, it is important to understand the dependence of metalation on the conformation of the apo-MT in order to determine metalation mechanism and the directors for metal specificity. Moving forward through the metalation process brings us to the important role of the partially metalated protein. This role is directly related to the buffering or homeostatic role of MTs. In that role, the bound metals will shuttle in and out of the MT's binding sites. The conformation of the partially metalated protein then becomes the launching point for delivery of a metal to a metal-dependent enzyme or the receiving point for uptake of metals from metal-chaperones. This process has been recently discussed for Zn-MT¹¹⁶. The structural determinants for this process are unknown. However, elucidation of the metalation and folding mechanisms is critical for characterizing the functional role or roles of MT *in vivo*. The challenge is in understanding the conformational dependences of the stepwise metalation of apo-MT.

The metal-induced folding of apo- α MT is driven by the stepwise formation of the metal-thiolate cluster within the core of the domain¹¹⁷. To study the structural properties of the apo- α MT starting point we used cysteine modification with Bq, and exploited the observed differential reaction rate of the Bq with the cysteinyl thiols to provide

information on the ease of the modification of the cysteine thiols and, therefore, the relative exposure of the thiols to the reactive Bq.

The Bq reaction profiles with apo- α MT are interpreted as being due to random binding at low pH giving a Normal distribution of Bq modifications with an increasing manifold maximum. At neutral pH a highly selective modification profile was observed and can be explained by the differential shielding of the cysteinyl thiols by the globular structure. It is the reaction profile showing all 11 modification reactions that is the key result of this experiment: at neutral pH, the MT(Bq₁₁) species is observed after the reaction of only 2-3 equivalents of Bq. If the reaction were solely due to probability of the 11 free thiols of the apo- α MT reacting with the Bq then only a relatively narrow band of cysteine modifications should be present at any given point in the reaction. The observation of the MT(Bq₁₁) species with only a small amount of Bq reacted indicates very unusual reaction properties that are uniquely present at neutral pH but not at low pH (Figure 6-2). This unusual reactivity at neutral pH can be explained by the cysteinyl thiols in apo- α MT being shielded by the compact, folded structure of the apoprotein. However, as increasing numbers of Bq molecules react with the cysteine residues in the protein, the protein becomes more and more unfolded, exposing the remaining free thiols to the solvent and to the incoming Bq. In other words, as the protein is modified, it adopts more open sets of conformations which promote Cys-Bq reactivity.

In Figure 6-5, at neutral pH, we can understand the trend in k_n 's as a function of Bq added is a composite of two opposing trends: (i) the k_n 's decline as in the low pH reaction and in keeping with the statistical loss of reaction sites as a function of increasing Bq and (ii) the k_n 's increase as the peptide unfolds due to structural changes induced by Bq modification, exposing remaining free thiols to the solvent. The starting k_n is depressed significantly due to the effects of steric shielding, so the span in k_1 to k_{11} is essentially zero. The claim that the protein is being unwound by cysteine modifications is supported by molecular dynamics models where the native protein under the same conditions but having been modified by Bq appears as a string-like structure instead of having a globular structure (Figure 6-6).

In contrast, during the low pH reaction, there is no structure to shield the cysteinyl thiols and this unusual reaction pattern does not occur. At low pH the first k_n is much higher than in the final reaction because there are 11 thiols that are all equally accessible. These k_n values follow the trend reported by Ngu et al.¹⁰⁵ for the rate constants for 6 As^{3+} binding to apo- $\beta\alpha$ -MT in which the rate constants diminished linearly as a function of remaining sites for the As^{3+} to bind to the apoprotein. However, even at low pH we observe a pause in the reduction of k_n that we interpret as being due to an unfolding of any residual structure as a result of the Bq loading at the 5-Bq point. So, the values of the k_n for Bq 5, 6 and 7 do not diminish, but then the statistical dependence of the remaining Cys dominates the k_n value to the last reaction that forms apo- α MT(Bq₁₁)

6.4.1 Metalation of the α -domain with Cd^{2+} : Testing the Two Conformational Classes

Only one report has been published on the kinetics of the metal binding reaction of metal-free MT with Cd^{2+} . This report showed that the metalation of the two-domain rabbit liver MT2a proceeded at a rate that was immeasurable by stopped-flow techniques at room temperature in that the reaction was complete within the 4 ms dead time of the instrument.⁹¹ Indeed, that report was somewhat surprising in that the reaction was found to proceed at a rate much faster than what might be predicted but this fast rate is confirmed in this present study.

A more recent study on the metalation of the individual domains of human MT1a with As^{3+} showed a metalation reaction that proceeded several orders of magnitude slower than that observed for Cd^{2+} , with observed rate constants in the range of $0.8 - 6.3 \text{ M}^{-1}\text{s}^{-1}$.¹⁰⁸ The slow metal binding kinetics permitted the use of selective mass spectrometric techniques to monitor the relative formation of the individual domain intermediates in the metalation pathway. This report showed that the metal binding mechanism of As^{3+} to MT followed a series of sequential bimolecular reactions, in which the observed second-order rate constants decreased for the successive steps in the reaction scheme. This is consistent with a non-cooperative mechanism of metal binding to the each of the domains of human MT1a.¹⁰⁷ In the experiments described here, the Bq modification data pointed to the presence of different conformational families, a native form at neutral pH

and a denatured form at low pH. This terminology is not really useful for metallothioneins because the conformation of the metal-free, apo-MT does not appear to be rigid at either pH; rather at neutral pH the structure is more globular and bundled whereas at low pH it is more linear. It is the metalation of the protein that introduces the rigid structure¹¹⁷⁻¹¹⁸. However, it is clear from the experimental and computational data that the neutral pH apo-MT structure is more folded and certainly the data described here show that it exists in a form that shields the cysteines far more than the conformations adopted at low pH do.

The metalation experiment could not use acidity to change the conformation because that would alter the metalation reaction itself, rather we used a reversible chemical denaturant added in increasing concentrations to the metal-free protein solution to provide a gradually unfolded structure. A significant result of this work is that the more compact, globular conformation metalated significantly faster than the denatured protein. The fit of the data to a single bimolecular reaction suggests that the rate-limiting step is the final addition of the 4th Cd^{2+} to form the metal-thiolate cluster. This folding step requires the rearrangement of the partially metalated $\text{Cd}_3\text{-}\alpha\text{MT}$ peptide backbone to allow for formation of the $\text{Cd}_4\text{-}\alpha\text{MT}$ cluster. This rearrangement of the coordinating cysteinyl thiols involves the movement of the bridging and terminal cysteine ligands to the correct orientation (Figure 6-1). It is likely that in the globular conformation, the cysteine residues are pre-arranged to have to the correct orientation for cluster formation and therefore, this final rearrangement step is fast. The denatured protein may be able to bind the first two metals more quickly in a bead-like structure previously reported¹¹⁶, but once bridging cysteines are required for the cluster structure, the necessary structural rearrangement is much slower. Although one might expect the open, string-like conformation to metalate more rapidly due to the increased accessibility of cysteine residues compared to the globular state, the results of the metalation experiment with Cd^{2+} show unambiguously that the opposite is true. These data suggest that the cluster formation must be the rate limiting step and that the globular structure of apo- $\alpha\text{-MT}$ allows for a more rapid formation of this clustered core.

The presence of the two-conformational families as descriptions of the structure of apo- α -MT accounts for both the metalation kinetics and the Bq reactivity data. A template-structured apo- α MT retains a globular structure upon demetalation and this globular structure accounts for the increased rate of metalation when compared to the unfolded protein. The randomly structured protein is thought to resemble the nascent apo- α -MT at a post-translational state prior to initial metalation. This structure, although present for only a short period of time in the cell, may play a relevant role in the redox status, signalling and metal homeostasis of the cellular environment¹¹⁹. Our final consideration concerns the metalation mechanism of apo-MT for Zn^{2+} , Cd^{2+} and Cu^+ . The conformation of the apo-MT is pH dependent and the pH of the cellular environment would be able to confer structural effectors that may favour binding of a specific metal species or change the way in which MT interacts with other metal chaperones and metalloenzymes.

6.5 Conclusions

The conformation of apo- α MT has been shown to have a direct bearing on the rate of the metalation reaction with Cd^{2+} . The cysteine modifier benzoquinone was used to probe the surface structure of the apo- α MT in globular (neutral pH) and unwound (low pH) conformations. The rate constants of the metalation reactions were directly related to the folded state of the apo- α MT. The conformation of the protein was assessed by using low pH conditions to unfold the protein and then by comparing the modification reaction profiles as up to 11 Bq molecules modified the cysteinyl thiols. The significant difference in reaction profiles for the modification of the 11 cysteines at neutral and low pH was interpreted in terms of a globular conformation with restricted access to the thiols at neutral pH compared with a much more open structure with essentially unimpeded access to the thiols at low pH. Molecular modeling provided structures that illustrated the two extremes. The arrangement of coordinating cysteine residues is a main driver of the metalation kinetic rates and the close proximity of the cysteines in the folded, or native conformation allows for rapid formation of the Cd-thiol core. This may be important in mechanisms of MT-mediated metal detoxification by *de novo* synthesized MT and displacement of other bound metals.

6.6 References

1. M. Margoshes and B. L. Vallee, *J. Am. Chem. Soc.*, 1957, **79**, 4813-4814.
2. Y. Boulanger, I. Armitage, K. Miklossy and D. Winge, *J. Biol. Chem.*, 1982, **257**, 13717-13719.
3. W. Braun, M. Vasak, A. Robbins, C. Stout, G. Wagner, J. Kägi and K. Wüthrich, *Proc. Natl. Acad. Sci. U. S. A.*, 1992, **89**, 10124-10128.
4. T. Miyayama, Y. Ishizuka, T. Iijima, D. Hiraoka and Y. Ogra, *Metallomics*, 2011, **3**, 693-701.
5. T. Fukada, S. Yamasaki, K. Nishida, M. Murakami and T. Hirano, *J. Biol. Inorg. Chem.*, 2011, **16**, 1123-1134.
6. W. Maret, *The Journal of nutrition*, 2000, **130**, 1455S-1458S.
7. W. Maret, *BioMetals*, 2011, **24**, 411-418.
8. W. Maret, *The Journal of nutrition*, 2003, **133**, 1460S-1462S.
9. Y. J. Kang, *Exp. Biol. Med.*, 2006, **231**, 1459-1467.
10. H. Gonzalez-Iglesias, L. Alvarez, M. García, C. Petrash, A. Sanz-Medel and M. Coca-Prados, *Metallomics*, 2014, **6**, 201-208.
11. R. J. Person, N. N. O. Ngalame, N. L. Makia, M. W. Bell, M. P. Waalkes and E. J. Tokar, *Toxicol. Appl. Pharmacol.*, 2015, **286**, 36-43.
12. W. Qu and M. P. Waalkes, *Toxicol. Appl. Pharmacol.*, 2015, **282**, 267-274.
13. G. Nordberg, R. Goyer and M. Nordberg, *Arch. Pathol.*, 1975, **99**, 192-197.
14. C. Dorian, V. H. Gattone and C. D. Klaasen, *Toxicol. Appl. Pharmacol.*, 1992, **114**, 173-181.
15. S. Satarug, J. Baker, P. E. Reilly, M. Moore and D. Williams, *Hum. Exp. Toxicol.*, 2001, **20**, 205-213.
16. D. E. Sutherland and M. J. Stillman, *Metallomics*, 2011, **3**, 444-463.
17. D. E. Sutherland and M. J. Stillman, *Metallomics*, 2014, **6**, 702-728.
18. R. W. Olafson, W. D. McCubbin and C. Kay, *Biochem. J.*, 1988, **251**, 691-699.
19. K. E. Rigby and M. J. Stillman, *Biochem. Biophys. Res. Commun.*, 2004, **325**, 1271-1278.
20. K. E. R. Duncan and M. J. Stillman, *J. Inorg. Biochem.*, 2006, **100**, 2101-2107.
21. S.-H. Hong, Q. Hao and W. Maret, *Protein Eng. Des. Sel.*, 2005, **18**, 255-263.
22. S.-H. Chen, L. Chen and D. H. Russell, *J. Am. Chem. Soc.*, 2014, **136**, 9499-9508.
23. X. Yu, Z. Wu and C. Fenselau, *Biochemistry*, 1995, **34**, 3377-3385.
24. G. W. Irvine and M. J. Stillman, *Biochem. Biophys. Res. Commun.*, 2013, **441**, 208-213.
25. G. W. Irvine, K. E. Duncan, M. Gullons and M. J. Stillman, *Chem.--Eur. J.*, 2015, **21**, 1269-1279.
26. P. Palumaa, I. Tammiste, K. Kruusel, L. Kangur, H. Jörnvall and R. Sillard, *Biochimica et Biophysica Acta (BBA)-Proteins and Proteomics*, 2005, **1747**, 205-211.
27. G. W. Irvine, K. L. Summers and M. J. Stillman, *Biochem. Biophys. Res. Commun.*, 2013, **433**, 477-483.
28. S.-H. Chen and D. H. Russell, *Biochemistry*, 2015, **54**, 6021-6028.
29. L. Konermann, J. Pan and Y.-H. Liu, *Chem. Soc. Rev.*, 2011, **40**, 1224-1234.
30. S. W. Englander, L. Mayne, Z.-Y. Kan and W. Hu, *Annual review of biophysics*, 2016.

31. K. L. Summers, A. K. Mahrok, M. D. Dryden and M. J. Stillman, *Biochem. Biophys. Res. Commun.*, 2012, **425**, 485-492.
32. C. E. Bartman, H. Metwally and L. Konermann, *Anal. Chem.*, 2016, **88**, 6905-6913.
33. S.-H. Chen, W. K. Russell and D. H. Russell, *Anal. Chem.*, 2013, **85**, 3229-3237.
34. T. T. Ngu, A. Easton and M. J. Stillman, *J. Am. Chem. Soc.*, 2008, **130**, 17016-17028.
35. T. B. Pinter, G. W. Irvine and M. J. Stillman, *Biochemistry*, 2015, **54**, 5006-5016.
36. T. B. Pinter and M. Stillman, *Biochem. J.*, 2015, BJ20150676.
37. L. Banci, I. Bertini, S. Ciofi-Baffoni, T. Kozyreva, K. Zovo and P. Palumaa, *Nature*, 2010, **465**, 645-648.
38. J. Zaia, D. Fabris, D. Wei, R. L. Karpel and C. Fenselau, *Protein Sci.*, 1998, **7**, 2398-2404.
39. S. Pérez-Rafael, S. Atrian, M. Capdevila and Ò. Palacios, *Talanta*, 2011, **83**, 1057-1061.
40. Y. Hathout, D. Fabris and C. Fenselau, *Int. J. Mass Spectrom.*, 2001, **204**, 1-6.
41. X. Yu, M. Wojciechowski and C. Fenselau, *Anal. Chem.*, 1993, **65**, 1355-1359.
42. J. Chan, Z. Huang, I. Watt, P. Kille and M. J. Stillman, *Can. J. Chem.*, 2007, **85**, 898-912.
43. M. Vasak, A. Galdes, H. A. O. Hill, J. H. Kaegi, I. Bremner and B. W. Young, *Biochemistry*, 1980, **19**, 416-425.
44. S.-H. Hong and W. Maret, *Proceedings of the National Academy of Sciences*, 2003, **100**, 2255-2260.
45. W. Maret, *J. Chromatogr. B*, 2009, **877**, 3378-3383.
46. D. H. Petering, J. Zhu, S. Krezoski, J. Meeusen, C. Kiekenbush, S. Krull, T. Specher and M. Dughish, *Exp. Biol. Med.*, 2006, **231**, 1528-1534.
47. L. E. Hernández, J. Sobrino-Plata, M. B. Montero-Palmero, S. Carrasco-Gil, M. L. Flores-Cáceres, C. Ortega-Villasante and C. Escobar, *J. Exp. Bot.*, 2015, **66**, 2901-2911.
48. E. B. Maryon, S. A. Molloy and J. H. Kaplan, *Am. J. Physiol. Cell. Physiol.*, 2013, **304**, C768-C779.
49. M. A. Lynes, J. Hidalgo, Y. Manso, L. Devisscher, D. Laukens and D. A. Lawrence, *Cell Stress Chaperones*, 2014, **19**, 605-611.
50. W. Maret and A. Krężel, *Mol. Med.*, 2007, **13**, 371.
51. L.-J. Jiang, W. Maret and B. L. Vallee, *Proceedings of the National Academy of Sciences*, 1998, **95**, 3483-3488.
52. K. L. Bren, V. L. Pecoraro and H. B. Gray, *Inorg. Chem.*, 2004, **43**, 7894-7896.
53. C. M. Palmer and M. L. Guerinot, *Nat. Chem. Biol.*, 2009, **5**, 333-340.
54. L. Järup and A. Åkesson, *Toxicol. Appl. Pharmacol.*, 2009, **238**, 201-208.
55. J. J. Wirth and R. S. Mijal, *Syst. Biol. Reprod. Med.*, 2010, **56**, 147-167.
56. S. Clemens, *Biochimie*, 2006, **88**, 1707-1719.
57. A. Hartwig, M. Asmuss, H. Blessing, S. Hoffmann, G. Jahnke, S. Khandelwal, A. Pelzer and A. Burkle, *Food Chem. Toxicol.*, 2002, **40**, 1179-1184.
58. S. S. Sharma and K.-J. Dietz, *Trends Plant Sci.*, 2009, **14**, 7.
59. L. R. Perez and K. J. Franz, *Dalton Trans.*, 2010, **39**, 10.
60. D. E. K. Sutherland and M. J. Stillman, *Metallomics*, 2011, **3**, 444-463.

61. D. E. K. Sutherland and M. J. Stillman, in *Brain Diseases and Metalloproteins*, ed. D. Brown, Pan Stanford Publishing Pte. Ltd. , Editon edn., 2013, p. 58.
62. Y. Boulanger, I. M. Armitage, K.-A. Miklossy and D. R. Winge, *J. Biol. Chem.*, 1982, **257**, 13717-13719.
63. P. Babula, M. Masarik, V. Adam, T. Eckschlager, M. Stiborova, L. Trnkova, H. Skutkova, I. Provaznik, J. Hubalek and R. Kizek, *Metallomics*, 2012, **4**, 739-750.
64. A. Presta, A. R. Green, A. Zelazowski and M. J. Stillman, *Eur. J. Biochem.*, 1995, **227**, 226-240.
65. T. Miyayama, Y. Ishizuka, T. Iijima, D. Hiraoka and Y. Ogra, *Metallomics*, 2011, **3**, 8.
66. S. Atrian and M. Capdevila, *Biomol. concepts*, 2013, **4**, 143-160.
67. K. J. Waldron and N. J. Robinson, *Nature Rev.*, 2009, **6**, 25.
68. C. A. Blindauer, M. D. Harrison, J. A. Parkinson, A. K. Robinson, J. S. Cavet, N. J. Robinson and P. J. Sadler, *Proc. Natl. Acad. Sci. USA*, 2001, **98**, 9593-9598.
69. R. A. Colvin, W. R. Holmes, C. P. Fontaine and W. Maret, *Metallomics*, 2010, **2**, 306-317.
70. C. D. Klaassen, J. Liu and B. A. Diwan, *Toxicol. Appl. Pharmacol.*, 2009, **238**, 5.
71. Y. Manso, P. A. Adlard, J. Carrasco, M. Vasak and J. Hidalgo, *J. Biol. Inorg. Chem.*, 2011, **16**, 1103-1113.
72. Y. Manso, J. Carrasco, G. Comes, G. Meloni, P. A. Adlard, A. I. Bush, M. Vašák and J. Hidalgo, *Cell. Mol. Life Sci.*, 2012, **69**, 3683-3700.
73. S. Sauge-Merle, C. Lecomte-Pradines, P. Carrier, S. Cuiné and M. DuBow, *Chemosphere*, 2012, **88**, 918-924.
74. M. Namdarghanbari, W. Wobig, S. Krezoski, N. M. Tabatabai and D. H. Petering, *J. Biol. Inorg. Chem.*, 2011, **16**, 1087-1101.
75. A. Torreggiani, C. Chatgialiloglu, C. Ferreri, M. Melchiorre, S. Atrian and M. Capdevila, *J. Proteomics*, 2013.
76. V. Rodilla, A. T. Miles, W. Jenner and G. M. Hawksworth, *Chem.-Biol. Interact.*, 1998, **115**, 71-83.
77. M. J. Bebianno and W. J. Langston, *Mar. Biol.*, 1991, **108**, 91-96.
78. M. Karin, A. Haslinger, H. Holtgreve, R. I. Richards, P. Krauter, H. M. Westphal and M. Beato, *Nature*, 1984.
79. O. I. Leszczyszyn, C. R. J. White and C. A. Blindauer, *Mol. BioSyst.*, 2010, **6**, 1592-1603.
80. Ò. Palacios, A. Pagani, S. Pérez-Rafael, M. Egg, M. Höckner, A. Brandstätter, M. Capdevila, S. Atrian and R. Dallinger, *BMC Biol.*, 2011, **9**, 4.
81. J. Ejnik, C. F. Shaw and D. H. Petering, *Inorg. Chem.*, 2010, **49**, 6525-6534.
82. A. E. Funk, F. A. Day and F. O. Brady, *Fed. Proc.*, 1983, **42**, 1897-1897.
83. A. E. Funk, F. A. Day and F. O. Brady, *Comp Biochem Physiol*, 1987, **86**, 1-6.
84. J. Ejnik, A. Muñoz, T. Gan, C. F. Shaw Iii and D. H. Petering, *J. Biol. Inorg. Chem.*, 1999, **4**, 784-790.
85. K. Połec Pawlak, Ò. Palacios, M. Capdevila, P. González-Duarte and R. Łobiński, *Talanta*, 2002, **57**, 1011-1017.
86. M. Huang, C. F. Shaw Iii and D. H. Petering, *J. Inorg. Biochem.*, 2004, **98**, 639-648.

87. M. J. Stillman, W. Cai and A. J. Zelazowski, *J. Biol. Chem.*, 1987, **262**, 4538-4548.
88. M. J. Stillman and A. Zelazowski, *J. Biol. Chem.*, 1988, **263**, 6128-6133.
89. A. Hörnberg, D. T. Logan, S. L. Marklund and M. Oliveberg, *J. Mol. Biol.*, 2007, **365**, 333-342.
90. M. Vasak, *J. Trace Elem. Med. Biol.*, 2005, **19**, 13-17.
91. J. Ejniak, J. Robinson, J. Zhu, H. Forsterling, C. F. Shaw, III and D. H. Petering, *J. Inorg. Biochem.*, 2002, **88**, 144-152.
92. D. Ghosh and V. L. Pecoraro, *Inorg. Chem.*, 2004, **43**, 7902-7915.
93. R. van Sluis, Z. M. Bhujwalla, N. Raghunand, P. Ballesteros, J. Alvarez, S. Cerdan, J.-P. Galons and R. J. Gillies, *Magn Reson Med*, 1999, **41**, 743-750.
94. S.-H. Hong and W. Maret, *Proc. Natl. Acad. Sci. USA*, 2003, **100**, 2255-2260.
95. S.-H. Hong, Q. Hao and W. Maret, *Protein Eng. Des. Sel.*, 2005, **18**, 255-263.
96. J. Chan, M. E. Merrifield, A. V. Soldatov and M. J. Stillman, *Inorg. Chem.*, 2005, **44**, 4923-4933.
97. B. A. Messerle, A. Schaffer, M. Vasak, J. H. R. Kagi and K. Wuthrich, *J. Mol. Biol.*, 1990, **214**, 765-779.
98. W. Feng, F. W. Benz, J. Cai, W. M. Pierce and Y. J. Kang, *J. Biol. Chem.*, 2006, **281**, 681-687.
99. W. R. Bernhard, M. Vasak and J. H. Kagi, *Biochemistry*, 1986, **25**, 1975-1980.
100. W.-W. Li, J. Heinze and W. Haehnel, *J. Am. Chem. Soc.*, 2005, **127**, 6140-6141.
101. D. E. K. Sutherland, M. J. Willans and M. J. Stillman, *Biochemistry*, 2010, **49**, 3593-3601.
102. J. Chan, M. E. Merrifield, A. V. Soldatov and M. J. Stillman, *Inorg. Chem.*, 2005, **44**, 4923-4933.
103. J. M. Snell and A. Weissberger, *J. Am. Chem. Soc.*, 1939, **61**, 450-453.
104. K. L. Summers, A. K. Mahrok, M. D. M. Dryden and M. J. Stillman, *Biochem. Biophys. Res. Commun.*, 2012, **425**, 485-492.
105. T. T. Ngu, A. Easton and M. J. Stillman, *J. Am. Chem. Soc.*, 2008, **130**, 17016-17028.
106. Y.-L. Liu, H.-T. Lee, C.-C. Chang and L.-S. Kan, *Biochem. Biophys. Res. Commun.*, 2003, **306**, 59-63.
107. K. E. R. Duncan and M. J. Stillman, *FEBS J.*, 2007, **274**, 2253-2261.
108. T. T. Ngu and M. J. Stillman, *J. Am. Chem. Soc.*, 2006, **128**, 12473-12483.
109. W. Lu, M. Kasrai, G. M. Bancroft, M. J. Stillman and K. H. Tan, *Inorg. Chem.*, 1990, **29**, 2561-2563.
110. A. Galdes, M. Vasak, H. A. O.Hill and J. H. R. Kagi, *FEBS Lett.*, 1978, **92**, 17-21.
111. R. Riek, B. Precheur, Y. Wang, E. A. Mackay, G. Wider, P. Guntert, A. Liu, J. H. R. Kagi and K. Wuthrich, *J. Mol. Biol.*, 1999, **291**, 417-428.
112. I. Bertini, C. Luchinat, L. Messori and M. Vasak, *J. Am. Chem. Soc.*, 1989, **111**, 7296-7300.
113. M. T. Salgado and M. J. Stillman, *Biochem. Biophys. Res. Commun.*, 2004, **318**, 73-80.
114. K. E. Rigby, J. Chan, J. Mackie and M. J. Stillman, *Proteins Struct. Funct. Bioinf.*, 2006, **62**, 159-172.

115. K. L. Summers, A. K. Mahrok, M. D. M. Dryden and M. J. Stillman, *Biochem. Biophys. Res. Commun.*, 2012, **425**, 485-492.
116. K. L. Summers, D. E. K. Sutherland and M. J. Stillman, *Biochemistry*, 2013, **52**, 2461-2471.
117. K. E. Rigby-Duncan and M. J. Stillman, *J. Inorg. Biochem.*, 2006, **100**, 2101-2107.
118. T. E. Creighton, *Proteins: Structures and molecular properties 2nd ed.*, W.H. Freeman and Co, New York, 1993.
119. A. Krezel and W. Maret, *J. Am. Chem. Soc.*, 2007, **129**, 10911-10921.

Chapter 7

7 A Simple Metallothionein-Based Biosensor for Enhanced Detection of Arsenic and Mercury⁶

7.1 Introduction

Many toxic metals are found naturally in the earth's crust at a very wide range of concentrations and are present in many environments. The inherent toxicity of these metals and their bioavailability influence the extent to which they pose problems for human health as well as to plant and animal life. Two species with significant effects on human health are As^{3+} and Hg^{2+} .¹⁻² Mercury contamination, which has been well documented in Japan, as well as in other countries including Canada, has caused thousands of cases of Minamata disease.³ Clearly, contamination from industry, agriculture and natural deposition must be monitored in a cost-effective and rapid method to prevent future cases.⁴ Hg^{2+} is the most common speciation of mercury in aquatic systems owing to its solubility and interaction with organic species.⁵ MT has been shown to bind Hg with a high affinity and form stable complexes with a variety of Hg species.⁶⁻⁹ However, MT does not bind specifically to any one metal due to its fluxional nature and lack of defined binding sites that would discriminate against certain metal co-factors.¹⁰⁻¹¹

Arsenic, in particular As^{3+} , is present at chronic as well as acute levels in drinking water in many parts of the world but is not evenly distributed among sources.¹² Therefore detection and quantification of arsenic in potable water and even water used for irrigation that can bioaccumulate in crops, is vital in assessing the safety of various water sources.

13-14

⁶ A version of this chapter has been published

Reproduced with permission from: Irvine, G.W.; Tan, S.N.; Stillman, M.J. A Simple Metallothionein-Based Biosensor for Enhanced Detection of Arsenic and Mercury. *Biosensors* **2017**, *7*, 14.

Copyright 2017 MDPI

Areas that are affected by significant arsenic contamination tend to be poor and have limited access to expensive and centrally located testing facilities.¹⁵⁻¹⁶ A cheap, portable, reliable and easy-to-use method to detect arsenic would help in monitoring contamination levels in poor, rural areas of South and Southeast Asia. The method must have a low detection limit due to the high toxicity of arsenic and mercury. Even small concentrations (<50ppb) of arsenic can have serious chronic effects.¹⁷⁻¹⁸ Biosensors are a broad category of sensors based on biological materials that may meet these criteria.

Biosensors containing DNA, enzymes and metal-binding proteins offer promising tools with which to obtain real-time, in-situ data for heavy metal contamination.¹⁹⁻²⁰

Metallothioneins (MTs) are a family of cysteine-rich, metal-binding proteins that bind soft metals like mercury with particularly high affinity.²¹⁻²³ Hg²⁺ has been shown to have higher affinity for MTs than other Hg-species.²⁴⁻²⁵

At low pH, MTs are able to bind strongly to As³⁺ although the reaction is slower than with native metals (zinc or copper) at neutral pH.^{7, 26-27} Cd and ZnMT demetalate below pH 3.5²⁸ leaving the metal-free apo-MT available for the coordination of arsenic species.²⁹ The unique properties of MT make it an excellent candidate for increasing the sensitivity of electrochemical sensor and efforts have been made to create MT-modified electrodes for metal sensing.³⁰⁻³³ The success of many of these devices is limited due to the time consuming preparation and expense required for other essential components, such as MT-specific antibodies³⁴ or reducing agents.³⁵ In this study our goal was to develop a low-cost, environmentally friendly biosensor using MT adsorbed onto paper discs and placed on screen printed carbon electrodes (SPCEs) for the detection of arsenic and mercury.

7.2 Methods

7.2.1 Reagents and instrumentation

All reagents used were of analytical grade. Electrochemical characterizations and measurements were performed using a four-channel system (eDAQ QuadStat, e-Corder 8 and Echem software, eDAQ Europe, Warsaw, Poland). SPCEs (DRP-110) and the boxed connector for SPEs (DRP-DSC) were purchased from DropSens (Asturias, Spain). The

working electrode was carbon while the reference and counter electrodes were Ag/AgCl and a carbon ring, respectively. Circular paper discs were cut from Grade 1 filter paper (Whatman Asia Pacific Pte Ltd., Singapore, Singapore). Standard solutions of 1000 ppm As^{3+} and Hg^{2+} were diluted with 18 M Ω ultrapure water obtained from a Millipore Alpha-Q water system (Bedford, MA, USA) to final concentrations ranging from 1 ppm to 5 ppb. Data were plotted on Microsoft Excel and refined using ORIGIN (Northhampton, MA, USA).

7.2.2 Recombinant protein preparation

Recombinant human metallothionein 1a (MGKAAAACSC ATGGSCCTCTG SCKCKECKCN SCKKCC SCCPMSCAKC AQGCVCKGAS EKCSCCK KAA AA) was expressed with an S-tag in BL21 E. coli cells, as described in detail elsewhere [36]. In brief, cells containing the plasmid for the full protein ($\beta\alpha$ -MT1a) were plated on to growth media containing kanamycin from a stock culture stored at $-80\text{ }^{\circ}\text{C}$ and grown for 16 h at $37\text{ }^{\circ}\text{C}$. The grown cells were then inoculated into $4 \times 1\text{ L}$ broth cultures enriched with $50\text{ }\mu\text{L}$ of 1 M cadmium sulfate and incubated in a shaker for 4 h until the OD600 absorbance was 0.8. Isopropyl β -D-1-thiogalactopyranoside (IPTG) was then added to induce expression of MT and 30 min later $150\text{ }\mu\text{L}$ of 1 M cadmium sulfate solution was added to the broth. The cells were collected 3.5 h after induction, centrifuged and stored at $-80\text{ }^{\circ}\text{C}$.

The recombinant cells were lysed using a cell disruptor (Constant Systems, Daventry, UK) shot at 20 k psi. From there, the cell lysate was centrifuged for 1 h to pellet out cellular debris. The supernatant was filtered and loaded on to a GE healthcare SP ion exchange column with a total volume of 10 mL. The columns were washed with pH 7.4 10 mM Tris(tris-hydroxymethyl-aminomethane) buffer for approximately 2 h to remove loosely bound proteins and other organic compounds. MT was eluted using an increasing gradient of 1 M NaCl + 10 mM Tris buffer at pH 7.4. The eluted MT was concentrated down to $<20\text{ mL}$ and the S-tag cleaved using a Thrombin Clean-Cleave kit as per the manufacturers' instructions (Sigma-Aldrich). The mixture was then diluted, desalted and placed on another SP ion exchange column. The S-tag does not bind as strongly as MT and thus elutes at low salt concentrations. The protein and S-tag were separated in this

fashion. The eluted MT was concentrated to a total volume of 10 mL and lyophilized for storage and transport.

The lyophilized MT was reconstituted in 10 mM ammonium formate buffer and buffer exchanged to remove excess salt. The MT solution was checked for oxidation using UV-Vis spectroscopy and ESI mass spectrometry to ensure the lyophilisation process did not cause oxidation of the MT thiols or loss of bound metals.

7.2.3 Disc preparation and electrochemical measurements

Filter paper was cut into discs of approximately 8 mm using a hole puncher and 20 μL of 40 μM reconstituted MT solution was added to the discs. The discs were kept in the fridge and allowed to dry under nitrogen to prevent oxidation. Once dry, the discs were placed on a DropSens electrode. The integration of the protein laden disc and SPCE has been described in detail elsewhere.³⁶ For the Hg^{2+} experiments measurements were taken with an incubation time of 2 minutes to allow for equilibration.

For the As^{3+} experiments, HCl was added to the metal solutions to adjust the pH to 2.0. This was done to remove and Zn^{2+} or Cd^{2+} still bound to MT adsorbed onto the paper disc. The equilibration time was longer, up to 30 minutes to allow for complete reaction as the kinetics of As^{3+} -MT binding is known to be slow at room temperature.²⁶

Anodic stripping voltammetry (ASV) measurement parameters for both metal detection experiments were as follows: deposition potential -350 mV; deposition time 150 s; scanning range between -0.2 and +0.3 V; scanning rate 100 mV/s; step W 20 ms; step H 2 mV; eChem stripping linear mode.

7.3 Results

7.3.1 Biosensor preparation

The quality of the MT protein adsorbed on to the paper discs was checked first by ESI-MS prior to and after lyophilization to ensure purity. The protein was examined again prior to disc preparation by far UV absorption spectroscopy to monitor for oxidation of the thiols. UV spectroscopy is a fast, non-destructive technique for determining MT

quality and concentration. The ligand-to-metal charge transfer (LMCT) absorption at 250 nm was used to calculate protein concentration. For use in the biosensor, it was crucial that there was little (<0.15 abs) absorbance at 280 nm which would indicate the presence of oxidized thiols (Figure 7-1).

In the preparation of the MT-loaded discs, it was determined that solutions of 40 μM gave the best signal response (Figure 7-2). Adsorption of additional aliquots of MT solution did not increase the signal response significantly, nor did the addition of higher concentrations of MT. This addition of 40 μM concentration of MT to the paper discs results in approximately 8 μg of protein being loaded in total. It should be noted that MT contains 20 cysteine residues and is stored bound to Cd^{2+} so the thiol and Cd^{2+} concentration loaded on to the disc is 20 and 7 times larger, respectively.

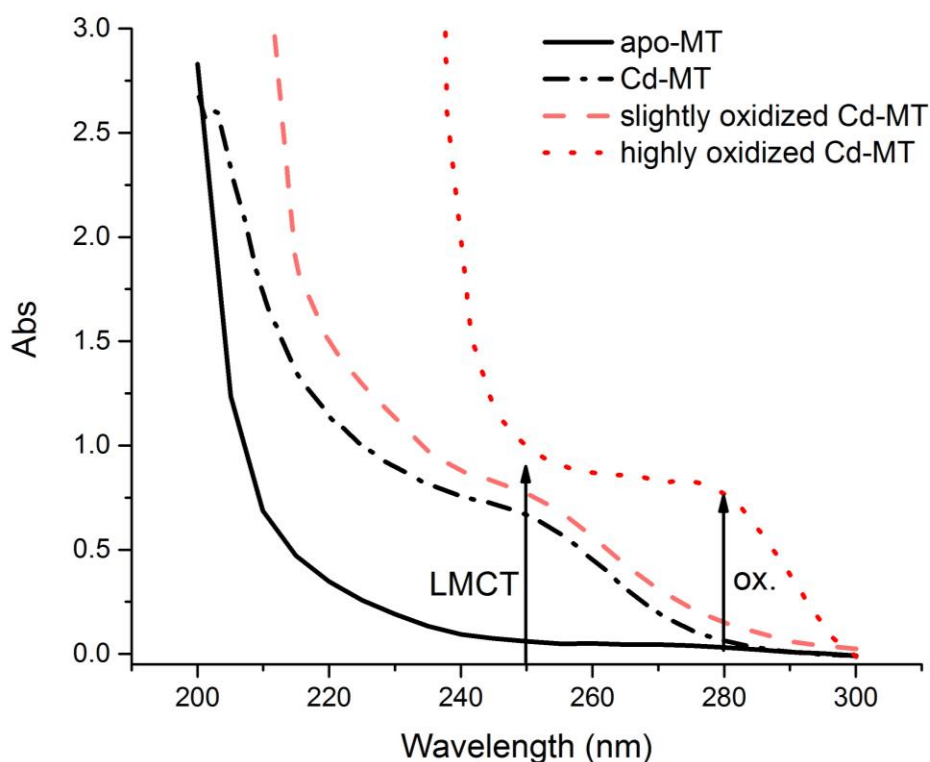


Figure 7-1: Far UV spectra of metallothionein (MT) used to monitor oxidation of thiols. Apo-MT (solid black line), Cd-MT (dashed black line) are both fully reduced with no thiol oxidation. Aerated MT solutions are shown to illustrate the oxidation: minimal oxidation (dashed pink line) and significant oxidation (dotted red line). The ligand-to-metal charge transfer (LMCT) band and the oxidized thiol absorbance are highlighted with arrows.

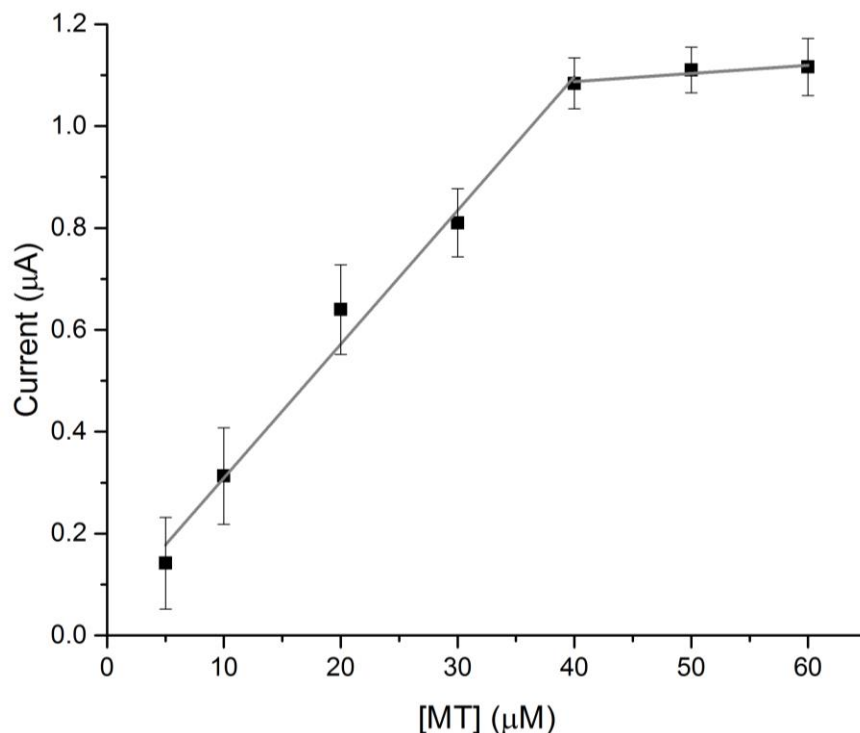


Figure 7-2: Influence of paper disc MT-loading on the peak heights of the SCys responses at +0.22 V in the electrochemical scans. The MT concentrations of each of the 20 μL aliquots added to the paper discs are plotted on the x-axis ($n=3$).

The blank discs on the SPCEs did not show any signals in the scans performed. The MT-adsorbed discs gave signals slightly above +200mV in both ASV and CV scans, likely due to the presence of free thiols in the protein. There was also a reduction peak around -50mV in the CV scan which corresponds to the cysteinyl thiols in MT. The heights of the peaks are relatively small and this is due to the presence of Zn/Cd²⁺ in the isolated, lyophilized protein masking the thiol signal. The presence of these bound metals is essential to the stability of the protein for longer periods of storage, as apo-MT degrades more rapidly and is prone to oxidation.³⁷ Compared to apo-MT, Cd/Zn-MT can be stored as a frozen solution or lyophilized and reconstituted after 2-4 years of storage without significant degradation.

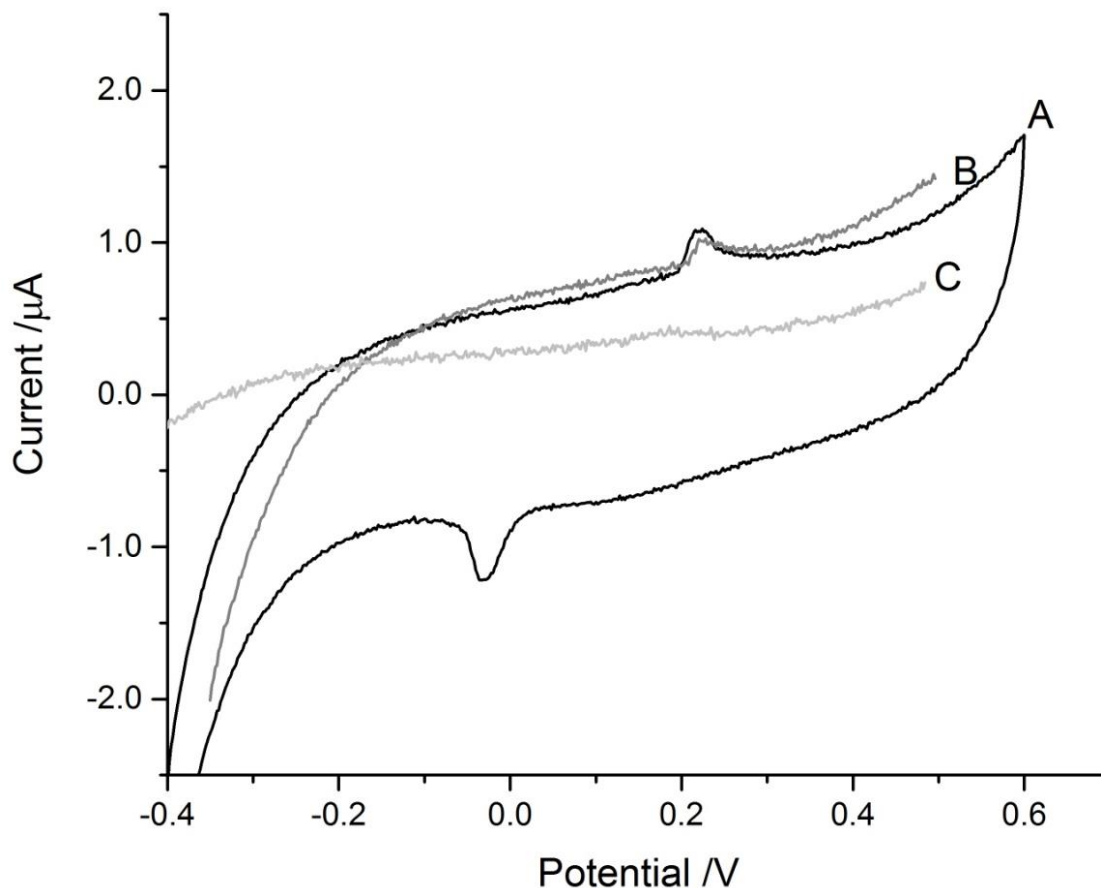


Figure 7-3: Representative electrochemical measurements of MT-loaded and blank-paper discs on SPCEs with 25 μL of deionized water added. (A) Cyclic voltammetry (CV) scan of MT-adsorbed disc; (B) anodic stripping voltammetry (ASV) scan on MT-adsorbed disc; and (C) ASV scan of blank paper disc. The ASV and CV scans of the blank paper disc were similar and showed no distinct peaks.

7.3.2 Arsenic detection using anodic stripping voltammetry (ASV)

The paper discs on the SPCE connected to the DropSens device, coupled with the eChem software was able to detect As^{3+} reasonably well in the control experiments, achieving a strong signal down to a concentration of 100 ppb. The limit of detection (LOD) (3S/N) calculated for the control paper disc on the SPCE was 69 ppb. For reference, the WHO recommended limit for arsenic in drinking water is 10 ppb. When the MT was physically adsorbed on to the paper discs placed over the SPCEs, the sensitivity was increased and the signal intensity amplified greatly. This can be seen in Figures 7-4 and 7-5, where the MT disc achieved a three-fold signal enhancement, which results in a detection limit

below 20 ppb As^{3+} . LOD ($3S/N$) was calculated to be 13 ppb for the MT-adsorbed discs on the SPCEs.

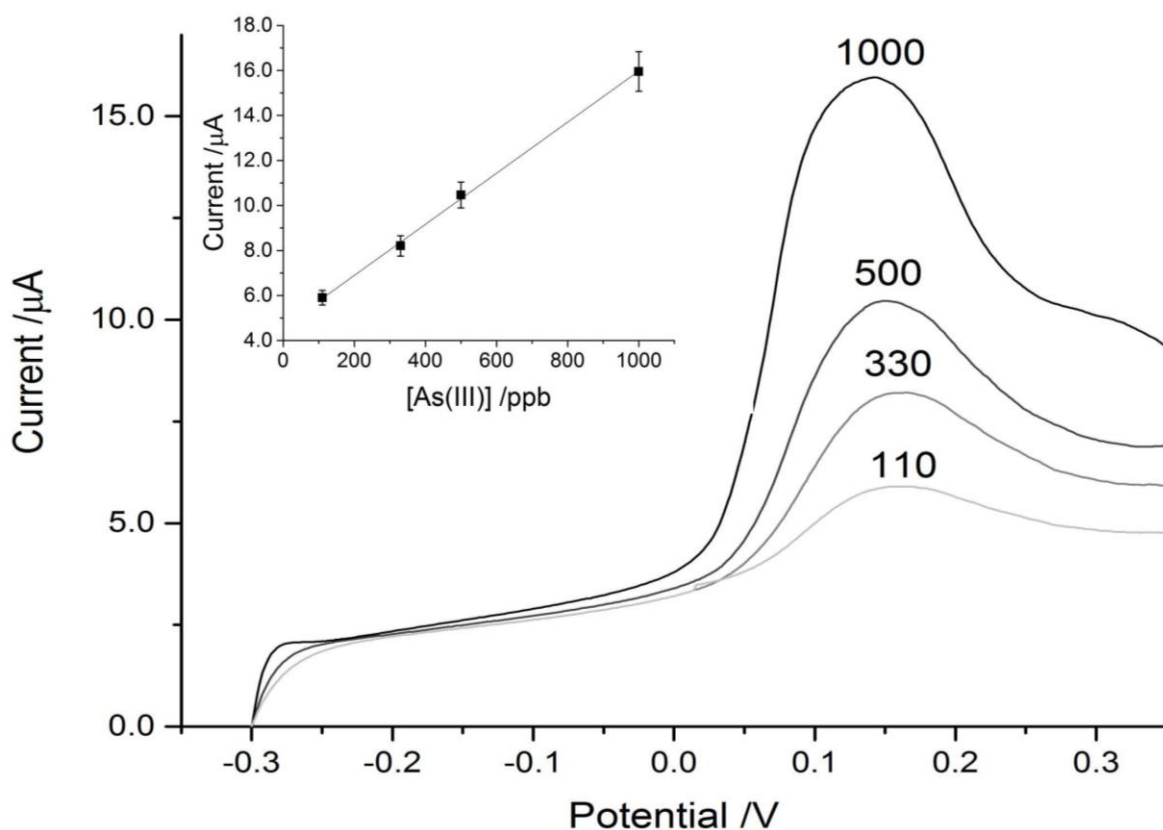


Figure 7-4: Typical ASV scans using blank paper discs on screen-printed carbon electrodes (SPCEs) with 25 μL of arsenic solutions of varying concentration added. The arsenic concentrations are indicated above their respective trace. Inset in the top left is the linear response curve for the blank disc set-up.

While this is still higher than the recommended limit for drinking water, it is low enough to potentially be useful in screening for arsenic contamination in high risk areas. For example, the Cambodian recommended limit is 50 ppb with some wells having concentrations as high as 3.5 ppm (to emphasize the danger, 3500 ppb).³⁸ In Bangladesh, 43% of wells have concentrations exceeding 50 ppb.¹⁷ The incorporation of the cysteine-rich metallothionein pushed the LOD to concentrations below that typically found in areas of concern.

In addition to an increase in signal intensity, the interactions between the arsenic and MT-disc shifted the peak intensity to a more negative potential. The control disc with no MT adsorbed showed As(III)-dependent peaks at approximately +160 mV (Figure 7-3) which is very similar to that reported in the literature with more sensitive electrodes.³⁹⁻⁴¹ The potential of As³⁺-stripping in the MT-modified disc scans was shifted to approximately -60 mV and this type of shift is consistent with coordination by thiol⁴² and protein modified electrodes.⁴³

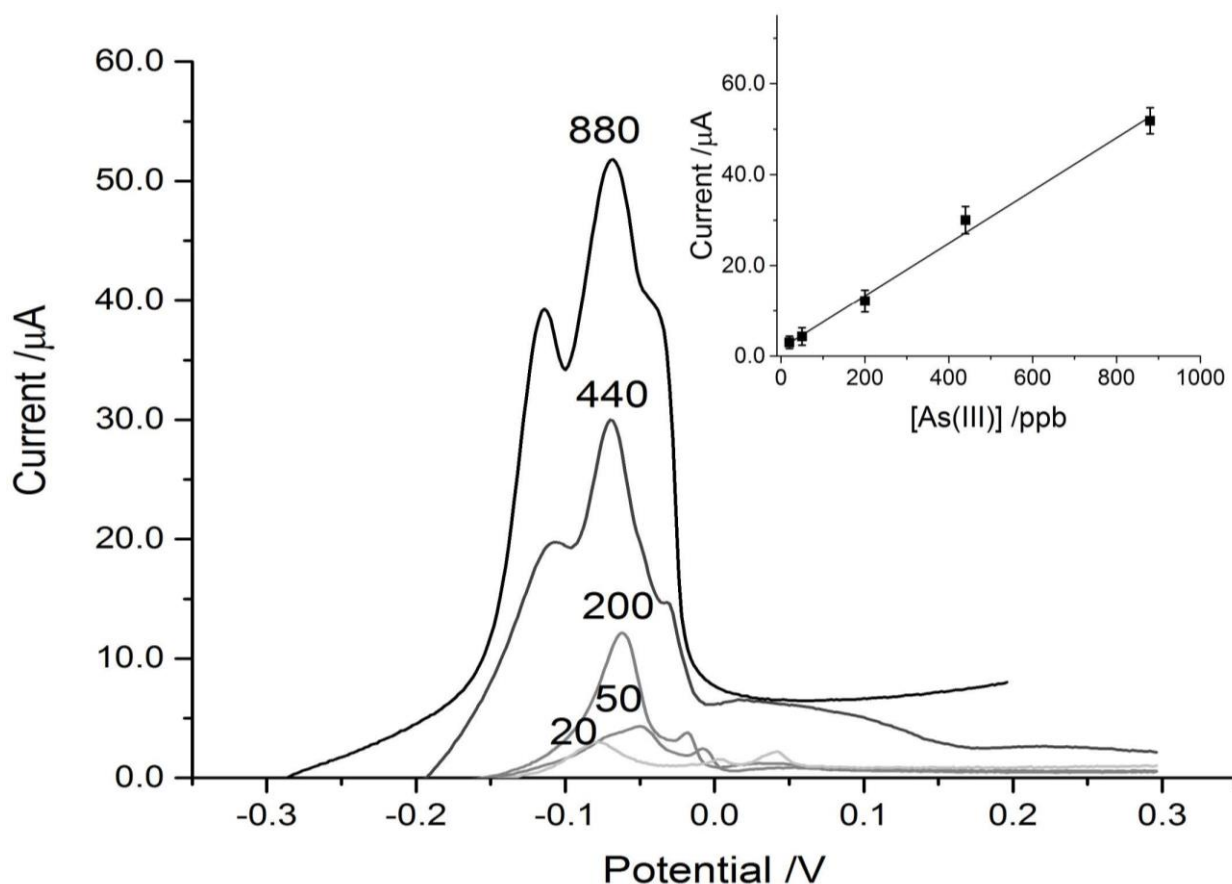


Figure 7-5: Representative ASV scans of MT-adsorbed paper discs with 25 μL droplets of varying arsenic concentrations added. The concentrations are labeled above their respective traces. Inset in the top right is the linear response curve for the MT-disc set-up.

7.3.3 Mercury detection using ASV

In addition to As³⁺ which selectively binds to MT at low pH, we sought to leverage the higher affinity that MT generally has for Hg²⁺ over Zn²⁺ and Cd²⁺, as similar strategies

have been previously tested for MT-based metal detection ⁴⁴. Since the affinity for Hg^{2+} is higher than that of the native metals bound to MT, Hg^{2+} will displace these metals ⁴⁵. In addition, both zinc and cadmium require more negative plating potentials than were applied during this experiment, limiting their interference in this device. Upon lowering the pH for arsenic detection or the displacement by mercury, the interferent (Cd/Zn) concentration is approximately 280 μM .

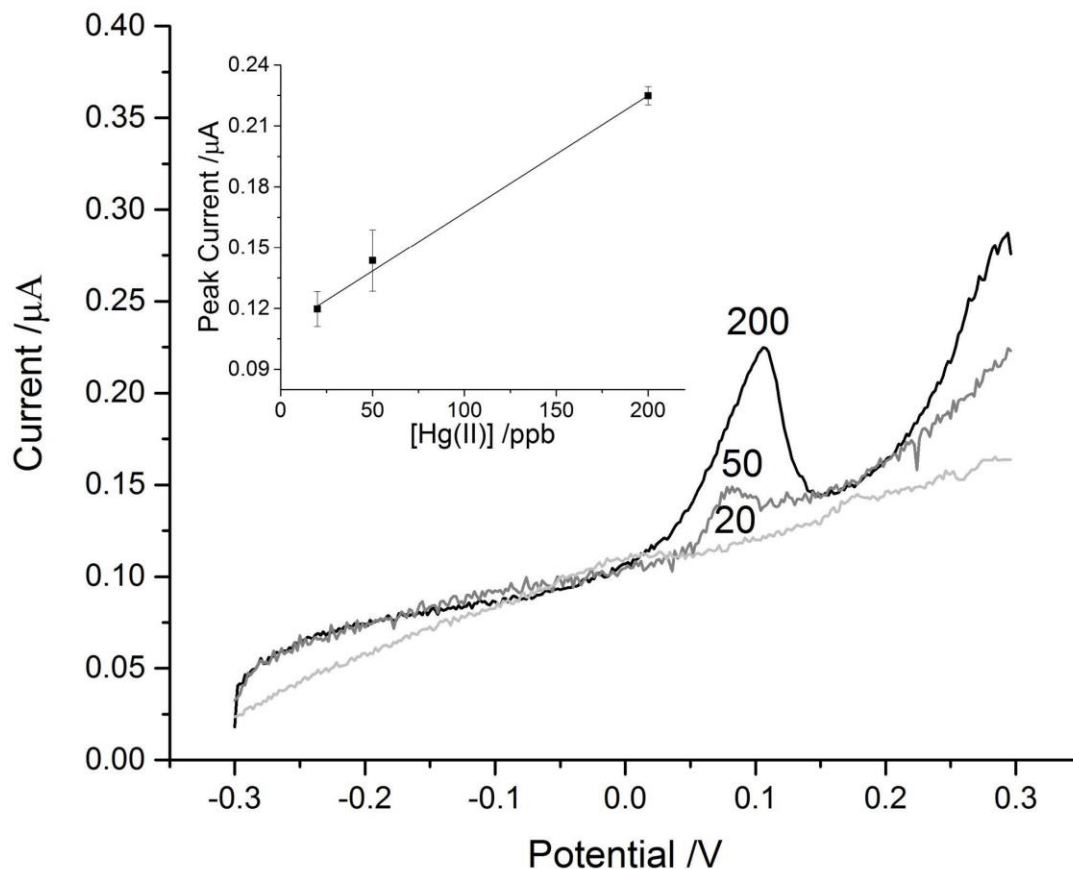


Figure 7-6: Representative ASV scans of blank paper discs on SPCEs with 25 μL aliquots of Hg^{2+} solutions of concentrations 20, 50 and 200 ppb. The concentration corresponding to each trace is labeled near the peaks at +0.1 V. Inset in the top left corner is the linear fit of the control data (n=3).

Below 20 ppb detection of Hg^{2+} became impossible even with the enhancement from the MT-adsorbed discs. A comparison of Figures 7-6 and 7-7 show the approximately three-fold enhancement of the peak current achieved by the MT-disc. The WHO guideline upper limit for mercury in drinking water is six parts per billion, meaning the device is

not achieving the sensitivity required to detect such low concentrations, especially in more natural samples with organic interferents. However, it may be more useful in monitoring area suspected of contamination which typically have higher concentrations than the recommended limit ⁴⁶. The LOD (3S/N) for the MT-modified paper disc was 45 ppb and 120 ppb for the blank paper disc.

The peak current for the Hg^{2+} signals was shifted to a more negative potential (Figure 7-7) similar to the shift in the As^{3+} signal seen in Figures 7-4 and 7-5. The peak seen around +200 mV in the experimental trace is from the thiols in the protein and was also observed in the control tests where deionized water was added to the MT-discs (Figure 7-3).

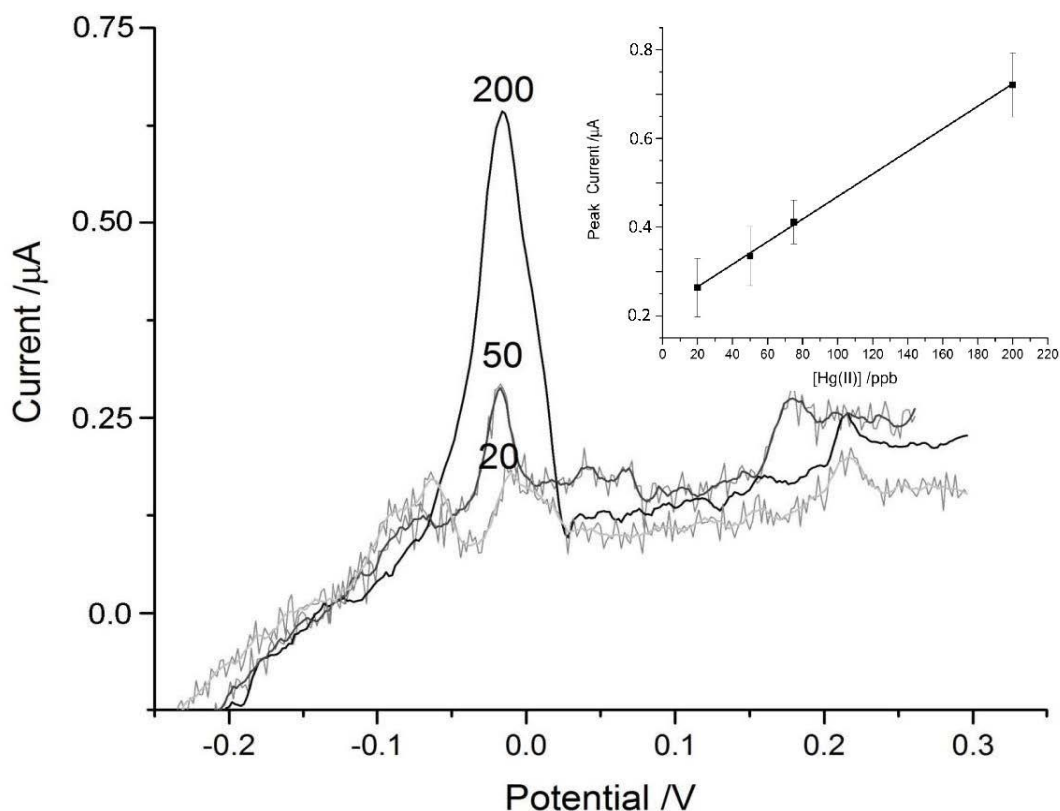


Figure 7-7: Representative ASV scans for MT-loaded discs with 25 μL drops of diluted Hg^{2+} standards with concentrations of 20, 50 and 200 ppb. The concentration is indicated on the graph near the Hg^{2+} peaks around -0.02 V. The peaks near $+0.2$ V correspond to the thiols of metallothionein. Inset in the top right corner is the linear fit of the data ($n = 3$).

The linearity over the range of mercury concentrations typically found in water contaminated by industry is adequate since even polluted waters have concentrations up to 200 ppb⁴⁶⁻⁴⁸. While the sensitivity of the device is not ideal for sensing lower concentrations of Hg²⁺ typical of non-industrially polluted waters, we have demonstrated the versatility in our approach in incorporating a protein known to interact with many soft metals and metalloids that cause environmental health problems. MT is able to enhance the signal of both metals tested due to its promiscuity of metal binding and lack of discriminatory metal binding sites.

7.4 Discussion

7.4.1 MT biosensors

The potential of MT-incorporated devices for sensing a wide range of metals is summarized in Table 2, which lists examples of various metallothioneins being used to enhance detection methods. The advantage of this strategy is that MT can enhance methods with specific advantages such as specificity, low detection limit, portability or low-cost. In our paper disc/SPCE sensor, we enhance a 'green' paper matrix with MT to produce a more sensitive As³⁺/Hg²⁺ sensor. The low-cost and environmentally friendly design of the sensor is greatly enhanced with the protein modification because the detection limit pre-MT adsorption is much higher than what would be considered acceptable.

By modifying the conditions under which the ASV scans are run, we can use MT as an effective and selective pre-concentration agent for both As³⁺ and Hg²⁺. Thus, the same device could be used for different assays depending on the type of contamination suspected in the given area. Table 2 shows a summary of the different metals sensed by a number of MT-based biosensors. It is likely a simple MT biosensor would be able to measure all the metals listed in Table 2, but slightly different strategies or configurations might have to be used. By using different MT isoforms⁴⁹ or a rational design approach⁵⁰⁻⁵¹ to increase the binding affinity for certain metals, a device could be customized for any soft metal.

Table 7-1: Summary of MT incorporated biosensors

Metal	Method/Electrode Type	Modifiers and Extra Components	Detection Limit	Reference
Cd, Zn, Ni	SPR	MT on carboxymethylated chips	1–2.25 ppm	[21]
Cd, Zn	HDME	TCEP	5.6 ppb	[41]
Cd	Fluorescence	Zn-Chelex resin, Rh-labelled MT	50 ppb	[36]
Pt (cisplatin)	HDME	TCEP	10 ppb	[23]
Ag	Carbon paste	anti MT-antibodies	0.05 ppb	[25]
Pd	HDME	TCEP	10 ppb	[42]
As	Paper disc/SPCE	MT-adsorption	13 ppb	This work
Hg	Paper disc/SPCE	MT-adsorption	45 ppb	This work
Hg, Cu, Zn, Cd	Modified gold electrode	Coupling agents, bacterial MT, continuous flow set-up	1×10^{-15} M	[43]

Another strategy would be to incorporate apo-MT to eliminate the need for the sensed metal to have a much higher affinity than the endogenous metals (Cd/Zn). This would pose additional engineering constraints due to the high oxygen sensitivity of metal-free metallothionein and would require more extensive sample preparation to remove dissolved oxygen⁵²⁻⁵⁴.

7.5 Conclusions

Adsorbing the cysteine-rich protein metallothionein on to paper discs provided a simple, specific, sensitive and inexpensive sensor for the toxic metals As^{3+} and Hg^{2+} . Metallothionein incorporation allowed the SPCE/paper disc system to sense As^{3+} at low enough concentrations to be potentially useful in environmental monitoring. This signal enhancement is likely due to pre-concentration effects of the MT-metal coordination. Our work shows that even simple physical adsorption of the protein onto an inexpensive SPCE/paper disc can dramatically increase the signal associated with a metal of interest without the need for costly coupling reagents or expensive and complicated set-ups.

7.6 References

1. K. Phan, S. Phan, S. Heng, L. Huoy and K.-W. Kim, *Environ. Pollut.*, 2014, **185**, 84-89.
2. G. A. Wasserman, X. Liu, N. J. LoIacono, J. Kline, P. Factor-Litvak, A. van Geen, J. L. Mey, D. Levy, R. Abramson and A. Schwartz, *Environ. Health*, 2014, **13**, 1.
3. A. Kudo and S. Miyahara, *Water Sci. Technol.*, 1991, **23**, 283-290.
4. Q. Wang, D. Kim, D. D. Dionysiou, G. A. Sorial and D. Timberlake, *Environ. Pollut.*, 2004, **131**, 323-336.
5. N. T. Loux, *Chem. Speciat. Bioavailab.*, 1998, **10**, 127-136.
6. W. Lu and M. J. Stillman, *J. Am. Chem. Soc.*, 1993, **115**, 3291-3299.
7. M. J. Stillman, D. Thomas, C. Trevithick, X. Guo and M. Siu, *J. Inorg. Biochem.*, 2000, **79**, 11-19.
8. R. Chen, H. Ganther and W. Hoekstra, *Biochem. Biophys. Res. Commun.*, 1973, **51**, 383-390.
9. J. Piotrowski, B. Trojanowska, J. Wiśniewska-Knypl and W. Bolanowska, *Toxicol. Appl. Pharmacol.*, 1974, **27**, 11-19.
10. G. W. Irvine, K. E. Duncan, M. Gullons and M. J. Stillman, *Chem.--Eur. J.*, 2015, **21**, 1269-1279.
11. S.-H. Chen, L. Chen and D. H. Russell, *J. Am. Chem. Soc.*, 2014, **136**, 9499-9508.
12. D. A. Polya, A. G. Gault, N. J. Bourne, P. R. Lythgoe and D. A. Cooke, *Plasma source mass spectrometry: Applications and emerging technologies*, 2003, **288**, 127-140.
13. G. Duan, W. Liu, X. Chen, Y. Hu and Y. Zhu, *Metallomics*, 2013, **5**, 784-792.
14. T. Murphy, M. Sampson, C. Le, K. Irvine, R. Gerads, L. Smith, T. Parr, K. Irvine, T. Murphy and S. Vermette, *Water resources and development in Southeast Asia*, 2010, 57-88.
15. M. Berg, C. Stengel, P. T. K. Trang, P. H. Viet, M. L. Sampson, M. Leng, S. Samreth and D. Fredericks, *Sci. Total Environ.*, 2007, **372**, 413-425.

16. 16. M. Sampson, B. Bostick, H. Chiew, J. Hagan and A. Shantz, *Appl. Geochem.*, 2008, **23**, 2977-2986.
17. 17. A. H. Smith, E. O. Lingas and M. Rahman, *Bull. W.H.O*, 2000, **78**, 1093-1103.
18. 18. A. K. Mitra, B. K. Bose, H. Kabir, B. K. Das and M. Hussain, *Journal of Health, Population and Nutrition*, 2002, 198-204.
19. 19. S. Babkina and N. Ulakhovich, *Anal. Chem.*, 2005, **77**, 5678-5685.
20. 20. N. Verma and M. Singh, *BioMetals*, 2005, **18**, 121-129.
21. 21. J. M. Wiśniewska, B. Trojanowska, J. Piotrowski and M. Jakubowski, *Toxicol. Appl. Pharmacol.*, 1970, **16**, 754-763.
22. 22. M. P. Waalkes, M. J. Harvey and C. D. Klaassen, *Toxicol. Lett.*, 1984, **20**, 33-39.
23. 23. A. E. Funk, F. A. Day and F. O. Brady, *Comparative Biochemistry and Physiology Part C: Comparative Pharmacology*, 1987, **86**, 1-6.
24. 24. M. Xu, L. Yang and Q. Wang, *Metallomics*, 2013, **5**, 855-860.
25. 25. W. Cai and M. J. Stillman, *J. Am. Chem. Soc.*, 1988, **110**, 7872-7873.
26. 26. T. T. Ngu, A. Easton and M. J. Stillman, *J. Am. Chem. Soc.*, 2008, **130**, 17016-17028.
27. 27. G. W. Irvine and M. J. Stillman, *Biochem. Biophys. Res. Commun.*, 2013, **441**, 208-213.
28. 28. E. Freisinger and M. Vašák, in *Cadmium: From Toxicity to Essentiality*, Springer, Editon edn., 2013, pp. 339-371.
29. 29. G. Jiang, Z. Gong, X.-F. Li, W. R. Cullen and X. C. Le, *Chem. Res. Toxicol.*, 2003, **16**, 873-880.
30. 30. C.-M. Wu and L.-Y. Lin, *Biosens. Bioelectron.*, 2004, **20**, 864-871.
31. 31. F. Amaro, A. P. Turkewitz, A. Martín- González and J. C. Gutiérrez, *Microbial biotechnology*, 2011, **4**, 513-522.
32. 32. J. Petrlova, D. Potesil, J. Zehnalek, B. Sures, V. Adam, L. Trnkova and R. Kizek, *Electrochim. Acta*, 2006, **51**, 5169-5173.
33. 33. S. Hu, B. Ye, X. Yi, Z. Cao, D. Wu, C. Shen and J. Wang, *Talanta*, 2016, **155**, 272-277.
34. 34. L. Trnkova, S. Krizkova, V. Adam, J. Hubalek and R. Kizek, *Biosens. Bioelectron.*, 2011, **26**, 2201-2207.
35. 35. S. Krizkova, D. Huska, M. Beklova, J. Hubalek, V. Adam, L. Trnkova and R. Kizek, *Environ. Toxicol. Chem.*, 2010, **29**, 492-496.
36. 36. N. C. Sekar, L. Ge, S. A. M. Shaegh, S. H. Ng and S. N. Tan, *Sensors and Actuators B: Chemical*, 2015, **210**, 336-342.
37. 37. C. D. Klaassen, S. Choudhuri, J. M. McKim Jr, L. D. Lehman-McKeeman and W. C. Kershaw, *Environ. Health Perspect.*, 1994, **102**, 141.
38. 38. D. A. Polya, M. Berg, A. G. Gault and Y. Takahashi, *Appl. Geochem.*, 2008, **23**, 2968-2976.
39. 39. M. Kopanica and L. Novotný, *Anal. Chim. Acta*, 1998, **368**, 211-218.
40. 40. L. Xiao, G. G. Wildgoose and R. G. Compton, *Anal. Chim. Acta*, 2008, **620**, 44-49.
41. 41. X. Dai, O. Nekrassova, M. E. Hyde and R. G. Compton, *Anal. Chem.*, 2004, **76**, 5924-5929.

42. 42. D. Li, J. Li, X. Jia, Y. Han and E. Wang, *Anal. Chim. Acta*, 2012, **733**, 23-27.
43. 43. X. Fuku, F. Iftikar, E. Hess, E. Iwuoha and P. Baker, *Anal. Chim. Acta*, 2012, **730**, 49-59.
44. 44. A. Varriale, M. Staiano, M. Rossi and S. D'Auria, *Anal. Chem.*, 2007, **79**, 5760-5762.
45. 45. À. Leiva- Presa, M. Capdevila and P. González- Duarte, *Eur. J. Biochem.*, 2004, **271**, 4872-4880.
46. 46. P. Li, X. Feng, G. Qiu, L. Shang and Z. Li, *J. Hazard. Mater.*, 2009, **168**, 591-601.
47. 47. G. Zhang, C.-Q. Liu, P. Wu and Y. Yang, *Appl. Geochem.*, 2004, **19**, 1735-1744.
48. 48. X. Feng, Q. Dai, G. Qiu, G. Li, L. He and D. Wang, *Appl. Geochem.*, 2006, **21**, 1955-1968.
49. 49. R. Bofill, R. Orihuela, M. Romagosa, J. Domenech, S. Atrian and M. Capdevila, *FEBS J.*, 2009, **276**, 7040-7056.
50. 50. C. S. Mocny and V. L. Pecoraro, *Acc. Chem. Res.*, 2015, **48**, 2388-2396.
51. 51. L. Zhou, M. Bosscher, C. Zhang, S. Özçubukçu, L. Zhang, W. Zhang, C. J. Li, J. Liu, M. P. Jensen and L. Lai, *Nature Chem.*, 2014, **6**, 236-241.
52. 52. W. Maret, *Proceedings of the National Academy of Sciences*, 1994, **91**, 237-241.
53. 53. D. Minkel, K. Poulsen, S. Wielgus, C. Shaw and D. Petering, *Biochem. J.*, 1980, **191**, 475-485.
54. 54. R. Kassim, C. Ramseyer and M. Enescu, *J. Biol. Inorg. Chem.*, 2013, **18**, 333-342.
- 55.

Chapter 8

8 Conclusion⁷

8.1 Metal binding mechanisms of MT

Metallothioneins (MTs) were initially isolated through repeated enrichment of cadmium-containing fractions of horse kidney cortex.¹ As a result the main function of MTs was originally thought to be heavy metal detoxification. While this remains true, a number of other functions have since been proposed for MTs including maintenance of zinc and copper homeostasis and significant contribution to cellular redox chemistry due to its abundance thiols which are easily oxidized.² The capacity to bind up to 7 zinc or cadmium ions and up to 20 monovalent metals, such as copper and silver has confounded the determination of the metalation mechanisms. The number of structural conformations, coordination modes and isoforms of MTs has prevented agreement on an overarching binding mechanism. This diversity of metalated structures and coordination geometries does not even begin to include the ambiguities introduced by mixed metal species.

There has been considerable debate surrounding the nature of the zinc and cadmium binding mechanism of MT, specifically the long studied cadmium mechanism. Cadmium was historically used as a proxy for the more biologically relevant zinc due to its amenability to investigation by absorption and CD spectroscopy, as well as ^{111,113}Cd NMR.³⁻⁶ With the advent of ESI-MS, more detailed metalation studies could be performed but conflicting results only appeared to add to the confusion surrounding the true mechanism.⁷⁻⁹

⁷ A version of this chapter has been published:

Irvine, G.W. and Stillman, M.J. (2017) Residue modification and mass spectrometry for the investigation of structural and metalation properties of metallothionein and cysteine-rich proteins. *Int. J. Mol. Sci.* **2017**, *18*(5), 913 doi:10.3390/ijms18050913

Copyright 2017 MDPI

One of the main focuses of this thesis was to investigate the binding mechanisms of zinc, cadmium and arsenic using ESI-MS techniques to determine the binding mechanisms associated with their coordination and more importantly establish the binding constants that govern the reaction.

8.1.1 A non-cooperative mechanism?

The non-cooperative mechanism for Cd^{2+} determined via ESI-MS was first reported in 2007¹⁰ and then confirmed by Sutherland and coworkers one year later for MT1a.⁷ but subsequent studies using the same method with MT2a showed a more cooperative binding mechanism.⁹ Although the authors described the mechanism as cooperative, significant amounts of intermediate species were formed making this description only partially accurate. The mechanism for MT2a clearly favoured the formation of Cd_4 - and Cd_7 -MT clusters which could be accurately described as a mixed mechanism. These studies highlighted potential isoform specific differences in binding mechanism.

A single NMR study from 1988 indicated a pH dependence in the cadmium cluster formation of rabbit liver metallothionein.¹¹ The stability of the cluster allowed for sharp NMR signals from the α -domain below neutral pH, whereas a broad indistinguishable signal was observed at higher pH.¹¹ While cluster formation refers more to the structure formed by MT and not the mechanism, the two are inexorably linked and this was demonstrated in Chapters 2 and 3. The data presented in these two Chapters show that both cooperative and non-cooperative binding mechanisms are possible for MT1a binding of zinc and cadmium. This is likely true for all mammalian isoforms as their sequence and binding properties are very similar.

Chapter 2 highlighted the differences between cadmium and zinc binding, while both were pH dependent, zinc binding was only semi-cooperative at low pH around 5.0 whereas cadmium binding was fully cooperative at that pH and remained at least semi-cooperative until neutral pH. We were able to specifically measure the pH at which the binding mechanism changed, and this switch occurred rapidly.

The lack of information with regard to location of the metals within the protein was a limitation of the experiments chronicled in Chapter 2. In Chapter 3, the isolated domains were investigated for pH dependence of cadmium binding and it was found that the α -domain followed the pH dependence of the full-length protein closely although the binding mechanism of the isolated β -domain was also pH dependent. The specific crossover point which we termed the " pK_{cluster} " was 7.0 for the α -domain and 5.8 for the β -domain. Chapters 2 and 3 were able to reconcile years of conflicting reports on the binding mechanism and showed that both can be correct depending on pH conditions.

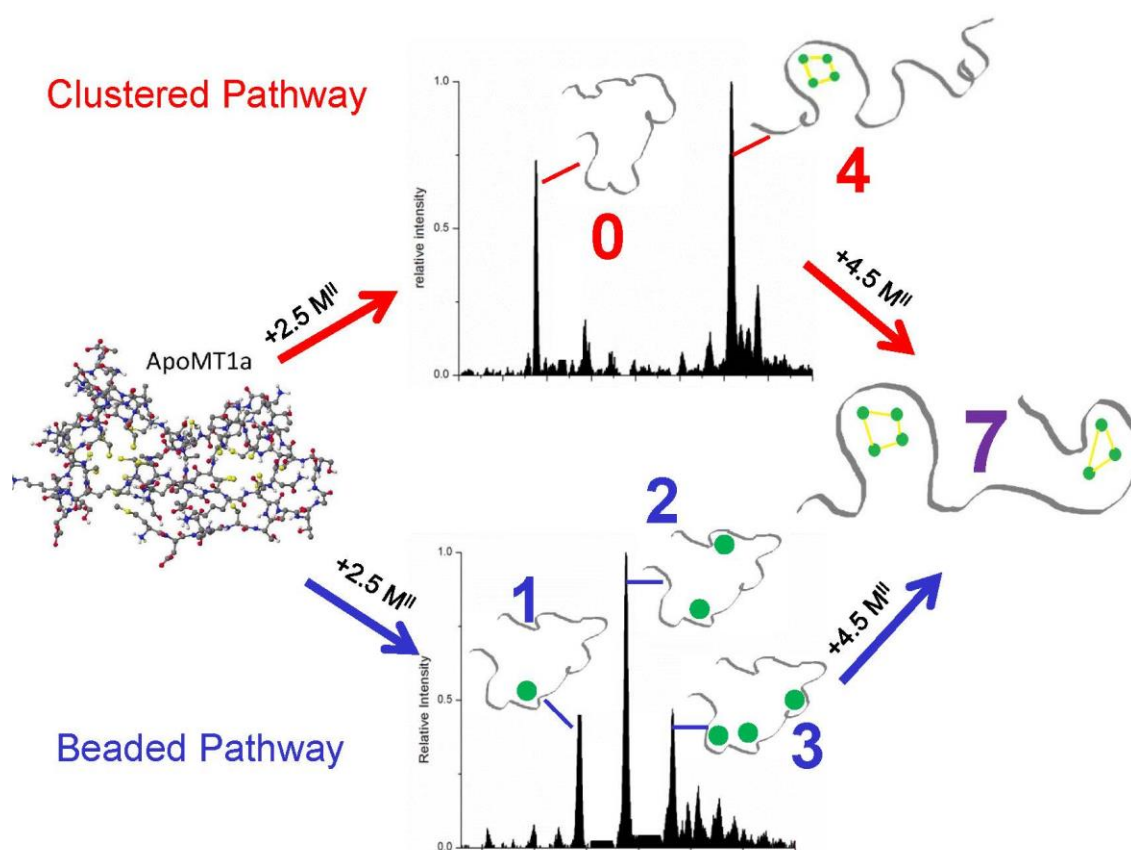


Figure 8-1: Potential metalation pathways and subsequent deconvoluted mass spectra.

Significant progress had been made in determining the arsenic binding mechanism prior to the work reported in this thesis, with the establishment of kinetic and thermodynamic parameters associated with As^{3+} binding to MT.¹² New information regarding the binding mechanism was presented in Chapter 4 which reinforced the strong evidence of only non-

cooperative binding modes for As^{3+} binding. We are not aware of any reports indicating the opposite. More specifically, at all points in the step-wise metalation 3 cysteine residues are involved in the coordination of each arsenic ion, allowing the accommodation of 3 As^{3+} per domain. In the α -domain 2 cysteine residues are not involved in As^{3+} coordination and remain free under arsenic saturation conditions.

8.2 Cysteine alkylation

In Chapter 4 we introduced the method of cysteine modification through reaction with the alkylating reagent p-benzoquinone (Bq) for structural studies of MTs. First investigated for the ability to "count cysteines", this method proved to be useful for more than just detecting the presence of uncoordinated, free thiols.

First of all any oxidation of the thiols in MT can be detected upon complete reaction since the end point of the reaction will be 2 modifiers less or more depending on the extent of the oxidation. Extent of Cys-Cys bridges formed in the peptides in solution can be measured directly. More interesting is the reaction profiles of cysteine modifiers that can inform on the solution structure of MTs due to reaction differences between conformers. Both of these applications are explored in Chapter 4, with surprising results concerning the non-Normal distribution of modified species under denaturing conditions. As^{3+} is able to bind to MT under low pH conditions and causes considerable metal-induced folding, indicating metal binding anchors the structure of partially metalated MTs and is a more important factor than H-bonding.

Due to concerns over these patterns being specific to the Bq modifier, other cysteine alkylating reagents were tested in Chapter 5, N-ethylmaleimide (NEM) and iodoacetamide (IAM). These three modifiers have different sizes, hydrophobicities and reaction mechanisms that are well characterized.¹³⁻¹⁵

From these tests it was clear that larger and more hydrophobic modifiers like Bq and NEM resulted in cooperative-like modification profiles, whereas the smaller, more hydrophilic IAM resulted in Normal distributions of varying width. This is explained by the more disturbing nature of Bq and NEM to the compact, native conformers of apo-

MTs. These studies underscore the importance in choice of alkylating reagent depending on the experiment. To probe structure, a noticeable change must occur and for these studies larger modifiers are more suited. For studies where protein conformations must be preserved, IAM is more suited, provided the studies are being done within the effective pH range of the reagent. The pH ranges were also reported, with NEM being the most robust, effective over the entire range tested (2.8-7.4) whereas IAM binding kinetics were prohibitively slow below a pH of 5 and Bq ineffective above neutral pH.

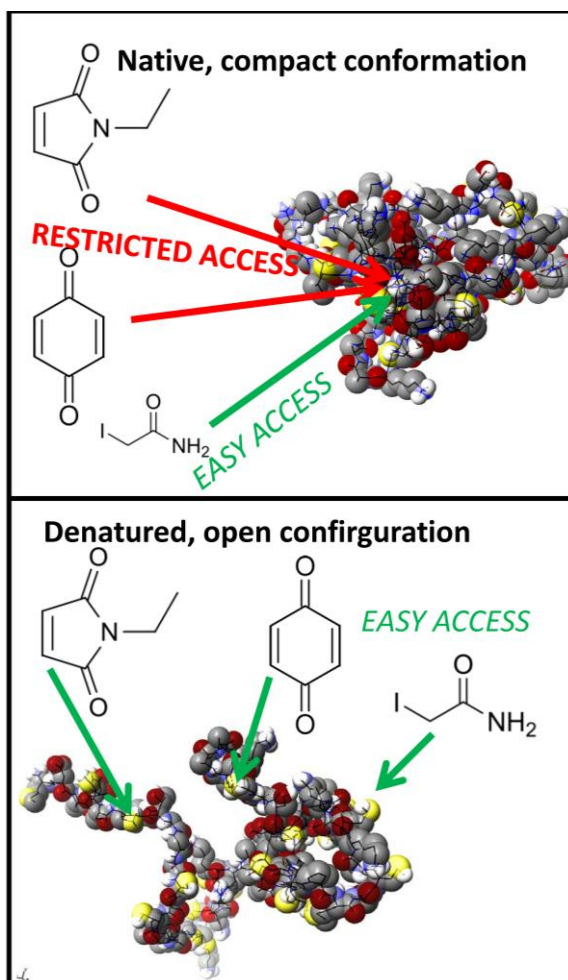


Figure 8-2: Cysteine alkylating reagent accessibility to the compact and open conformers of apo-MT

8.3 Importance of the structure of apo-MT

The conformation adopted by MT is one that is fluxional and ill-defined but we have shown in Chapter 6 it is essential for metalation kinetics. This is somewhat counter-

intuitive, since a more open conformer where the cysteine residues are most exposed to the solvent and incoming metal ions might be expected to metalate faster. However, key to the metalation mechanism of MTs, especially when binding cadmium, is the formation of cadmium-thiolate clusters which involve both bridging and terminal cysteine residues.⁵ The more compact conformer(s) found under native conditions, while it may not represent all conformers found under these conditions,¹⁶ likely orients the cysteine residues in a way that is "primed" for metal binding and cluster formation. That is, the cysteine residues are aligned so that the bridging cysteines are in, or close to, the optimal position to form a bridging bond between two cadmium ions. Once formed, the cadmium-thiolate cluster is known for its stability and amenability to determination by ¹¹³Cd NMR and other methods.^{4, 17-19}

To better understand the origin of these differential modification patterns, the reaction was modeled using a series of sequential, bi-molecular reactions which gave simulated mass spectral data that included species abundances at different points in the reaction. When the modeled Ks of the reaction reproduce the experimental mass spectra to a high degree of similarity, the relative values of the Ks can be compared and conclusions drawn. In the data presented in Chapter 6, the Ks revealed a series of declining values under denaturing conditions which is expected as the loss of binding sites as the reaction proceeds results in the statistical decrease of binding constants. Under native conditions, the relative constants do not decrease but increase slightly. This can be explained by the opening or denaturation of the compact conformers by the modification of cysteinyl thiols by the bulky Bq molecule. There are two major factors in addition to the intrinsic chemical nature of the reaction that govern the rate at which cysteine residues are modified:

(1) The statistical availability of free thiols

During the early stages of the modification of a peptide, the abundance of free thiols makes a reaction more likely since there are more "binding sites" for the modification reagents. Since there are more places on the protein that are capable of reaction, a successful collision between a free cysteine and an alkylation reagent is more likely. As

the cysteine residues are modified, the likelihood of a successful collision decreases due to the increasingly rare potential reaction sites on the protein.

(2) The steric accessibility of free thiols

It is well-known that the semi-hydrophobic nature of cysteine allows for marked differences in solvent accessibility depending on the folded state of the protein.²⁰⁻²³ The more solvent accessible of these residues react at a much faster rate.²⁰ During the modification reaction of MTs, the compact conformer extends, exposing previously buried residues and increasing their solvent accessibility and therefore, the rate of modification. This is likely the origin of the semi-cooperative nature of the modification reaction of MTs under native conditions.

8.4 Insight into potential metal sensing applications

The intimate knowledge of the arsenic binding properties of MT allowed us to design a simple, "green", electrochemical MT-biosensor. The adsorption onto paper discs provided a simple and "green" platform for electrochemical detection using anodic stripping voltammetry and carbon paste electrodes. This was achieved without the need for complicated and expensive coupling reagents or electrodes.

The set-up leveraged the unique binding properties of both arsenic and mercury to MT. As^{3+} is one of only a few ions that can strongly bind to MT at low pH (<4) so by adding HCl to the sample, the device was rendered selective for As^{3+} and removed interference from $\text{Cd}^{2+}/\text{Zn}^{2+}$ that the MT is co-purified with. Mercury has a much higher binding affinity to MT than most other metals and is able to displace bound $\text{Cd}^{2+}/\text{Zn}^{2+}$.

Signal enhancement of arsenic and mercury was 3-fold for each metal and was likely due to the preconcentration effects of MT. This signal amplification allowed the limit of detection to be pushed down to a level where the simple device could potentially be used for arsenic contamination monitoring. We also demonstrated that with slight changes in protocol the MT-based biosensor was able to detect and amplify the signal of multiple metals of concern. This application could likely be extended to other metals that have been successfully tested with other, more complicated MT-biosensors.²⁴

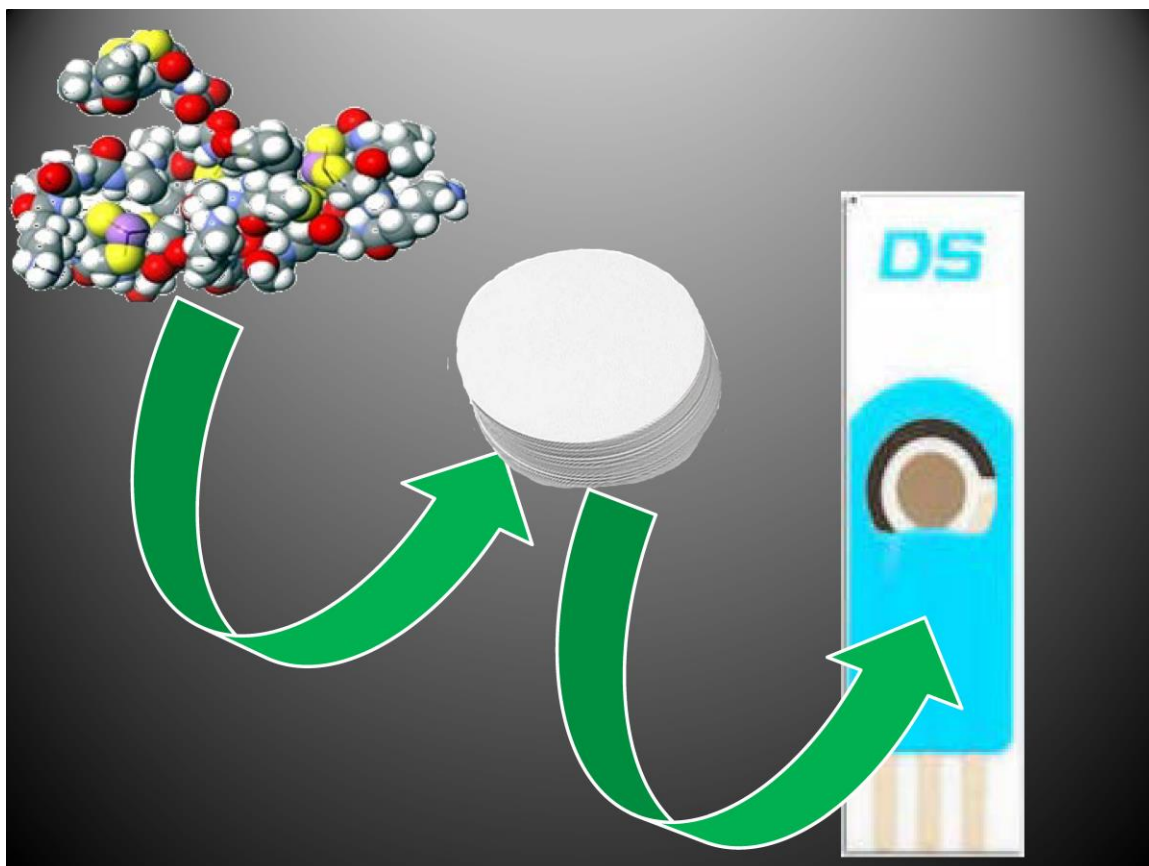


Figure 8-3: Schematic of the MT-biosensor preparation

8.5 Biological relevance of MT structure and metalation

With the data presented in the preceding Chapters, it is worthwhile to put all of it into context. How do these findings impact our understanding of MT's role in a biological context?

With respect to the pH dependence of the metal binding mechanism, it is clear that zinc binding is a non-cooperative process in a biological environment. This makes sense in the context of MT's role as a homeostatic zinc buffer, requiring constant metal coordination and release. Also the propensity to form terminally coordinated structures as opposed to metal-thiolate clusters allows for more precise control of metal release with the lability of individual metal ions disconnected from the others coordinated within the protein.

For cadmium binding, only slightly acidic conditions are required for cluster formation and these are found in many sub-cellular compartments, including those involved in facilitating protein folding and the breakdown of wastes and toxic products.²⁵ It is also known that clustered Cd-MTs are resistant to degradation and MTs partially-metalated with cadmium will be digested until the metals are shuffled into one domain and form a resistant cluster. The high toxicity of Cd-MTs in the renal proximal tubules is a major problem in kidney disease and these species are very long lived.²⁶⁻²⁷ Cells in the renal proximal tubules are known to vary widely and but have intracellular pH well below 7.4 due to the constant transport of $\text{HCO}_3^-/\text{H}^+$.²⁸⁻²⁹ Clustering in the α -domain of Cd-MTs may be the source of the longevity of these toxic species.

Accessibility of cysteinyl thiols is also biologically relevant due to the major role MT is thought to play in cellular redox chemistry.^{2, 30-31} The potential shielding of these thiols may lessen the potential impact that apo-MTs have on the redox chemistry of the cell, especially when in competition with smaller reducing agents such as glutathione.

8.6 Final remarks

The data presented in this thesis provide reconciliation of previously conflicting reports on the metal binding mechanisms of MT. Both cooperative and non-cooperative mechanisms can accurately describe the binding of cadmium to MTs, depending on pH conditions. This is also true for zinc binding, but in a biologically relevant range above pH 5.5, the most truthful description is that of a non-cooperative mechanism. The power of ESI-MS for resolving a multitude of species in solution was essential in the determination of the true binding mechanism and in the insights gained into apo- and partially metalated MT structure.

The novel method of covalent modification of cysteine residues applied to MTs proved to be useful in probing many aspects of the structure/function of the protein. Not only were we able to "count" the free cysteines to propose an unambiguous binding mechanism for As^{3+} but also we were able to visualize conformational preferences and protein-protein interactions through the reaction profiles of the cysteine modifiers. The lack of description of apo-MT structure over the many years of study of this protein emphasizes

the difficulty and lack of techniques with which to probe the structures of hard-to-characterize proteins. The powerful resolution of ESI-MS coupled with the lower resolution cysteine probe allowed a reasonable description of conformational preferences of apo-MT and highlighted the necessity of even loosely defined structure in the kinetics of metal binding. The work in this thesis highlights the need for multi-method analysis in the description and characterization of disordered proteins.

8.7 References

1. M. Margoshes and B. L. Vallee, *J. Am. Chem. Soc.*, 1957, **79**, 4813-4814.
2. W. Maret and A. Krężel, *Molecular Medicine*, 2007, **13**, 371.
3. H. Li and J. D. Otvos, *Biochemistry*, 1996, **35**, 13929-13936.
4. Y. Boulanger, I. Armitage, K. Miklossy and D. Winge, *Journal of Biological Chemistry*, 1982, **257**, 13717-13719.
5. K. Zangger, G. ÖZ, I. M. Armitage and J. D. Otvos, *Protein Sci.*, 1999, **8**, 2630-2638.
6. J. D. Otvos, H. R. Engeseth and S. Wehrli, *Biochemistry*, 1985, **24**, 6735-6740.
7. D. E. Sutherland and M. J. Stillman, *Biochemical and Biophysical Research Communications*, 2008, **372**, 840-844.
8. M. Vaheer, N. Romero-Isart, M. Vašák and P. Palumaa, *Journal of Inorganic Biochemistry*, 2001, **83**, 1-6.
9. S.-H. Chen, W. K. Russell and D. H. Russell, *Anal. Chem.*, 2013, **85**, 3229-3237.
10. K. E. Duncan and M. J. Stillman, *FEBS Journal*, 2007, **274**, 2253-2261.
11. M. Good, R. Hollenstein, P. J. Sadler and M. Vasak, *Biochemistry*, 1988, **27**, 7163-7166.
12. T. T. Ngu, A. Easton and M. J. Stillman, *J. Am. Chem. Soc.*, 2008, **130**, 17016-17028.
13. Y. Li, S. Jongberg, M. L. Andersen, M. J. Davies and M. N. Lund, *Free Radic. Biol. Med.*, 2016, **97**, 148-157.

14. P. M. Cal, G. J. Bernardes and P. M. Gois, *Angewandte Chemie International Edition*, 2014, **53**, 10585-10587.
15. C. Smythe, *J. Biol. Chem.*, 1936, **114**, 601-612.
16. S.-H. Chen, L. Chen and D. H. Russell, *J. Am. Chem. Soc.*, 2014, **136**, 9499-9508.
17. N. Cols, N. Romero-Isart, M. Capdevila, B. Oliva, P. González-Duarte, R. González-Duarte and S. Atrian, *Journal of Inorganic Biochemistry*, 1997, **68**, 157-166.
18. J. Pande, C. Pande, D. Gilg, M. Vasak, R. Callender and J. Kägi, *Biochemistry*, 1986, **25**, 5526-5532.
19. M. J. Stillman and A. Zelazowski, *Journal of Biological Chemistry*, 1988, **263**, 6128-6133.
20. S. K. Jha and J. B. Udgaonkar, *J. Biol. Chem.*, 2007, **282**, 37479-37491.
21. N. S. Gould, P. Evans, P. Martínez-Acedo, S. M. Marino, V. N. Gladyshev, K. S. Carroll and H. Ischiropoulos, *Chem. Biol.*, 2015, **22**, 965-975.
22. B. Wiggins, L. Liu- Shin, H. Yamaguchi and G. Ratnaswamy, *J. Pharm. Sci.*, 2015, **104**, 1362-1372.
23. J. Alegre-Cebollada, P. Kosuri, D. Giganti, E. Eckels, J. A. Rivas-Pardo, N. Hamdani, C. M. Warren, R. J. Solaro, W. A. Linke and J. M. Fernández, *Cell*, 2014, **156**, 1235-1246.
24. L. Trnkova, S. Krizkova, V. Adam, J. Hubalek and R. Kizek, *Biosens. Bioelectron.*, 2011, **26**, 2201-2207.
25. N. Demaurex, *Physiology*, 2002, **17**, 1-5.
26. W. Tang, S. Sadovic and Z. A. Shaikh, *Toxicol. Appl. Pharmacol.*, 1998, **151**, 276-282.
27. J. Godt, F. Scheidig, C. Grosse-Siestrup, V. Esche, P. Brandenburg, A. Reich and D. A. Groneberg, *J. Occup. Med. Toxicol.*, 2006, **1**, 22.
28. K. Yoshitomi and E. Frömter, *Pflügers Archiv European Journal of Physiology*, 1984, **402**, 300-305.
29. R. Krapf and R. J. Alpern, *J. Membr. Biol.*, 1993, **131**, 1-10.
30. D. H. Petering, J. Zhu, S. Krezoski, J. Meeusen, C. Kiekenbush, S. Krull, T. Specher and M. Dughish, *Experimental Biology and Medicine*, 2006, **231**, 1528-1534.

31. H. Gonzalez-Iglesias, L. Alvarez, M. García, C. Petrash, A. Sanz-Medel and M. Coca-Prados, *Metallomics*, 2014, **6**, 201-208.

Curriculum Vitae

Name: Gordon W. Irvine

Post-secondary Education and Degrees: Brock University
St. Catharines, Ontario, Canada
2008-2012 B.Sc.
Honours Double Major in Biology and Chemistry

The University of Western Ontario
London, Ontario, Canada
2012-2017 Ph.D.
Bioinorganic Chemistry

Publications:

1. **Irvine, G.W.** and Stillman, M.J. (2017) Residue modification and mass spectrometry for the investigation of structural and metalation properties of metallothionein and cysteine-rich proteins. *Int. J. Mol. Sci.* **2017**, 18(5), 913 doi:10.3390/ijms18050913
2. Scheller, J., **Irvine, G.W.**, Wong, D.L. and Stillman, M.J. (2017) Stepwise copper(I) binding to metallothionein: A mixed cooperative and non-cooperative mechanism. *Metallomics*. DOI: 10.1039/C7MT00041C
3. **Irvine, G.W.**, Tan, S.N. and Stillman, M.J. (2017) A Simple Metallothionein Based Biosensor for Enhanced Detection of Arsenic and Mercury. *Biosensors*. 7(1),14 DOI:10.3390/bios7010014
4. **Irvine, G.W.**, Santolini, M. and Stillman, M.J. (2017) Selective cysteine modification of metal-free human metallothionein 1a and its isolated domains: structural properties revealed via ESI-MS. *Prot. Sci.* DOI: 10.1002/pro.3139
5. **Irvine, G.W.** and Stillman, M.J. (2016) Cadmium binding mechanisms of isolated domains of human MT1a: Non-cooperative terminal sites and cooperative cluster sites. *J. Inorg. Biochem.*, 158: 115-121

6. **Irvine, G.W.**, Pinter, T.B.J. and Stillman, M.J (2016) Redefining the metal binding pathways of human metallothionein 1a: balancing zinc availability and cadmium seclusion. *Metallomics* 8(1): 71-81 *****Highlighted in the January issue and selected for the back-cover and a top 20 download of 2016**
7. Pinter, T.B.J., **Irvine, G.W.** and Stillman, M.J. (2015) Domain selection in metallothionein 1A: Affinity controlled mechanisms of zinc binding and cadmium exchange. *Biochemistry* 54(32): 5006-5016
8. **Irvine, G.W.**, Rigby-Duncan, K.E., Gullons, M. and Stillman, M.J. (2015). Metalation kinetics of the α -metallothionein fragment is dependent on the structure of the apo-protein. *Chem Eur J.* 21(3): 1269-1279
9. **Irvine, G.W.** and Stillman, M.J. (2013) Topographical analysis of As-induced folding of α -MT1a. *Biochem. Biophys. Res. Commun.* 441(1), 208-213
10. **Irvine, G. W.**, Summers, K. L., and Stillman, M. J. (2013) Cysteine accessibility during As^{3+} metalation of the α - and β -domains of recombinant human MT1a, *Biochem. Biophys. Res. Commun.* 433(4): 477-483

Conference Presentations:

1. **Irvine, G.W.** and Stillman, M.J. "*Structural determination of hMT1a and implications for metal binding mechanisms*" Bioinorganic Chemistry- Gordon Research Seminar, January 26-29, 2017, Ventura, CA. Poster presentation by G.W. Irvine (Ph.D International)
2. **Irvine, G.W.** and Stillman, M.J. "*Unraveling the structure of apo-metallothionein using ESI-MS and selective cysteine modification*" 34th Chemistry Graduate Student Symposium, May 16-18, 2016 Buffalo, NY. Oral presentation by G.W. Irvine. (Ph.D International)
3. **Irvine, G.W.** and Stillman, M.J. "*Metalation pathways of human metallothionein 1a and its isolated domains*" Pure and Applied Chemistry Conference (PACCON 2016), February 9-11, 2016, Bangkok, Thailand. Poster presentation by G.W. Irvine. (Ph.D International)

International)

4. **Irvine, G.W.**, Pinter, T.B.J. and Stillman, M.J. "*Metallothionein metalation pathways: Zinc beads and cadmium clusters*" 17th International Conference on Biological Inorganic Chemistry, July 20-24, 2015, Beijing, China. Poster presentation by G.W. Irvine (PhD International)

5. **Irvine, G.W.**, Pinter, T.B.J and Stillman, M.J. "*Origin of metallothionein versatility: zinc availability, cadmium sequestration and redefining the binding mechanism*" May 19-23rd, 2015, Parry Sound, Canada. Oral Presentation by G.W. Irvine (PhD International)

6. **Irvine, G.W.** and Stillman, M.J. "*Exploring the conformations of partially metalated and apo-metallothioneins using covalent labelling*" Metals in Biology Gordon Research Conference, January 25-30th, 2015, Venutra, CA. Poster Presentation by G.W. Irvine. (Ph.D International)

7. **Irvine, G.W.** and Stillman, M.J. "*Unlocking the secrets of metal induced folding in metallothioneins from ESI-MS studies of the stepwise metallation of arsenic and topographical analysis using cysteine modification*" 97th Canadian Chemistry Conference, June 1-5th, 2014, Vancouver, British Columbia. Oral Presentation by G.W. Irvine. (Ph.D National)

8. **Irvine, G.W.**, and Stillman, M.J. "*Analyzing the structure of apo-metallothionein using ESI-MS and covalent labeling*" 32nd Chemistry Graduate Student Symposium, University at Buffalo, Buffalo, NY, May 19-21, 2014. Oral Presentation by G.W. Irvine. (Ph.D International)

9. **Irvine, G.W.**, Rigby-Duncan, K.E. and M.J. Stillman, "*Conformational analysis of apo-metallothionein using ESI-MS and molecular probes*" International Symposium on Applied Bioinorganic Chemistry 12, Sun Yat-sen University, Guangzhou, China, December 3-6, 2013. Oral presentation by M.J. Stillman (Ph.D International)

10. **Irvine, G.W.**, Rigby-Duncan, K.E. and M.J. Stillman. "*Ordered structure in apo- α MT controls kinetics of Cd^{2+} binding*" Inorganic Discussion Weekend, York University, Toronto, ON, Nov 8-10, 2013. Oral presentation by Gordon Irvine (Ph.D Provincial)

11. **Irvine, G.W.** and M.J. Stillman. "*Probing the surface topography of partially metalated metallothionein*" 4th International Georgian Bay Conference on Bioinorganic Chemistry, Parry Sound, ON, May 21-25, 2013. Poster presented by Gordon Irvine (MSc. International).

Honours and Awards:

NSERC- Michael Smith Foreign Study Supplement Award	2016
Lipson-Baines Award	2015
NSERC-Canada Graduate Scholarship	2014-2017
Ontario Graduate Scholarship	2013-2014
Distinguished Graduating Student Award	2012
Society of Chemical Industry Merit Award	2012
Scholler Foundation Award	2011
NSERC- Undergraduate Student Research Award	2011
Brock University Entrance Scholarship	2008-2012

Research Experience:

The University of Western Ontario Graduate Researcher; Supervisor: Martin J. Stillman Structural properties and metal binding mechanisms of apo-metlothionein	London, ON 2012-present
Nanyang Technological University - National Institute of Education Visiting Graduate Researcher; Supervisor: Swee Ngin Tan A simple metallothionein-based biosensor	Singapore 2016
Brock University Undergraduate Researcher; Supervisor: Michael J. Bidochka Upregulation of genes involved in induced systemic	St. Catharines, ON 2011-2012

resistance pathway in *Glycine Max* by *Metarhizium robertsii*

Related Professional Experience:

Third year Bioinorganic chemistry guest lecturer (CHEM 3391)	02-2017
Society of Graduate Students- Chemistry Councillor	2015-2016
Volunteer chaperone and advisor for students from Nanyang Technological University-Singapore on their trip to Upstate New York for water quality analysis	06-2015
Organizing committee for the 5th International Georgian Bay Conference on Bioinorganic Chemistry	05-2015
Teaching Assistant- EnvrSust 9014A	2015-2016
Teaching Assistant- Calculus 1000	2013-2014
Member of the U.W.O Biosafety Committee	2014-2017
Chemistry Outreach Volunteer	2013-2014
Prospective graduate student welcoming tour and lunch volunteer	2013-2014
Organizational volunteer in charge of computer networks, presentation set-up and volunteer coordination for the 4th International Georgian Bay Conference on Bioinorganic Chemistry in Parry Sound, ON	05-2013
U.W.O Dept. of Chemistry March break open house volunteer	03-2013
U.W.O Dept. of Chemistry fall preview day volunteer	10-2012
Teaching Assistant- Chem 1000, Chem 2213, Chem 2211	2012-2013
Chemistry, biology and math tutor	2008-2016